

Dynamic organization of human brain function and its relevance for psychosis vulnerability.

Thèse N° 7516

Présentée le 20 septembre 2019

à la Faculté des sciences et techniques de l'ingénieur
Laboratoire de traitement d'images médicales
Programme doctoral en génie électrique

pour l'obtention du grade de Docteur ès Sciences

par

Daniela Maria ZÖLLER

Acceptée sur proposition du jury

Prof. J.-Ph. Thiran, président du jury
Prof. D. N. A. Van De Ville, Prof. M. Schaer, directeurs de thèse
Prof. D. S. Bassett, rapporteuse
Dr D. Garrett, rapporteur
Prof. O. Blanke, rapporteur

2019

Abstract

The brain is the substrate of a complex dynamic system providing a remarkably varied range of functionalities, going from simple perception to higher-level cognition. Disturbances in its complex dynamics can cause an equally vast variety of mental disorders. One such brain disorder is schizophrenia, a neurodevelopmental disease characterized by abnormal perception of reality that manifests in symptoms like hallucinations or delusions. Even though the brain is known to be affected in schizophrenia, the exact pathophysiology underlying its developmental course is still mostly unknown. In this thesis, we develop and apply methods to look into ongoing brain function measured through magnetic resonance imaging (MRI) and evaluate the potential of these approaches for improving our understanding of psychosis vulnerability and schizophrenia. We focus on patients with chromosome 22q11.2 deletion syndrome (22q11DS), a genetic disorder that comes with a 30fold increased risk for developing schizophrenia, thus enabling the study of developmental alterations and risk factors that precede the onset of full-blown psychosis.

We first examine temporal variability of the blood oxygenation level dependent (BOLD) signal, a voxelwise measure of dynamic fluctuations. As static functional connectivity (sFC) is scaled for variance, we also compare BOLD signal variability with altered sFC. The broad pattern of altered BOLD signal variability in 22q11DS partly, but not entirely, overlaps with altered sFC, suggesting a complex non-linear relationship between the two measures. Further, testing for altered BOLD signal variability in patients with higher psychotic symptoms, we find reduced values in the dorsal anterior cingulate cortex (dACC), a central node of the salience network (SN).

Going beyond a voxel-wise measure of brain dynamics, we next look into aberrant dynamics of large-scale functional brain networks. We use innovation-driven co-activation patterns (iCAPs), an approach that stands out by its ability to recover spatial and temporal overlap of functional brain networks. As in the original iCAPs framework such spatial overlap can introduce spurious temporal activations, we propose a novel spatio-temporal regression framework that relies on transient-based constraints to overcome this limitation. With this improved scheme, we probe into clinical risk factors of psychosis in 22q11DS and find aberrant activation and coupling of functional brain networks, again implicating the SN, as well as the amygdala and hippocampus.

Finally, we explore the implications of structural network topology on functional dynamics, by combining iCAPs with network control theory, an approach that relies on a dynamic model to predict the energy required for controlling the brain's state given its structural connectivity.

Abstract

We find that the brain operates in an energetically optimal way, spending less time in brain states that require higher control energy. In patients with 22q11DS, this relationship is less pronounced, suggesting less efficient functional brain dynamics in these patients.

In summary, our results confirm that the dynamic nature of brain function contains essential information and warrants further attention for the development of clinically relevant imaging markers for psychosis vulnerability. Moreover, we provide initial evidence for aberrant relationship between brain function and structure in patients with 22q11DS that merits further exploration.

Keywords: brain imaging, functional MRI, diffusion weighted MRI, schizophrenia, 22q11.2 deletion syndrome, BOLD signal variability, large-scale brain network dynamics, network control theory, salience network

Résumé

Le cerveau est un système dynamique complexe qui génère une palette de fonctionnalités remarquablement variées, passant de la simple perception, à des processus cognitifs de plus haut niveau. Des perturbations de ces dynamiques complexes peuvent mener à une multitude de maladies psychiatriques tout aussi variées. La schizophrénie, par exemple, est une maladie neurodéveloppementale qui s'accompagne d'une perception anormale de la réalité s'exprimant par des symptômes comme des hallucinations ou des délires. Bien qu'on sache que le cerveau est affecté dans la schizophrénie, la pathophysiologie exacte de sa trajectoire développementale n'est pas encore bien comprise. Dans cette thèse, nous développons et appliquons des méthodes d'analyse de la fonction cérébrale dynamique mesurée par l'imagerie par résonance magnétique (IRM) et évaluons leur potentiel pour améliorer notre connaissance de la schizophrénie. Nous investiguons des patients avec une microdélétion 22q11.2 (MD22q11), une maladie génétique associée à un risque de schizophrénie 30 fois plus élevé, nous permettant d'étudier des altérations développementales et des facteurs de risque qui précèdent la psychose.

D'abord nous examinons la variabilité du signal BOLD (de l'anglais « blood oxygenation level dependent »), une mesure de fluctuations dynamiques par voxel. La comparaison entre cette variabilité et la connectivité fonctionnelle statique (CFs) nous montre que les multiples altérations de ces deux mesures sont partiellement, mais pas entièrement superposées, ce qui suggère une relation non-linéaire complexe. De plus, chez les patients avec plus de symptômes psychotiques nous trouvons des réductions de variabilité dans le cortex cingulaire antérieur dorsal, un nœud central du réseau de saillance (RS).

Par la suite, nous étudions des dynamiques des réseaux cérébraux fonctionnels. Nous utilisons la méthode d'iCAPs (de l'anglais « innovation-driven co-activation patterns ») qui permet d'extraire des réseaux qui peuvent se superposer spatialement et temporellement. Avec la méthode originale, une telle superposition spatiale peut introduire de fausses activations. Nous proposons donc une nouvelle approche de régression spatio-temporelle qui surmonte cette limitation. Avec cette méthode améliorée, nous analysons des facteurs de risque cliniques de psychose chez les patients avec MD22q11 et trouvons des altérations d'activité et d'interaction de réseaux cérébraux, dont à nouveau le RS, mais aussi l'amygdale et l'hippocampe.

Enfin, nous explorons l'implication de la topologie de réseaux structurels sur la fonction dynamique en combinant les iCAPs et la théorie de contrôle de réseaux, une approche qui se base sur un modèle dynamique pour prédire l'énergie nécessaire pour contrôler l'état du

Résumé

cerveau sachant sa connectivité structurelle. Nous trouvons que le cerveau fonctionne de façon optimale en passant moins de temps dans des états qui demandent plus d'énergie de contrôle. Chez les patients avec MD22q11 cette relation est moins prononcée ce qui suggère une fonctionnalité cérébrale moins efficace.

En somme, nos résultats confirment que la nature dynamique de la fonction cérébrale contient des informations essentielles qui sont importantes à considérer dans la recherche de marqueurs de vulnérabilité pour la psychose. De plus, nous présentons la preuve d'une relation aberrante entre structure et fonction du cerveau chez les patients avec MD22q11 qui mérite d'être explorée plus profondément.

Mots clés : imagerie du cerveau, IRM fonctionnelle, IRM pondérée en diffusion, schizophrénie, microdélétion 22q11.2, variabilité du signal BOLD, dynamique de réseaux cérébraux, théorie de control de réseaux, réseau de saillance

Every mountain top is within reach,
if you just keep climbing.
— Barry Finlay

Für Ruth und Peter.

Acknowledgements

First, I am deeply thankful to my advisor Dimitri. Thank you for your kindness, for always making the time to discuss science and at the same time being so supportive in handling the sometimes-stressful PhD life. You are a great mentor and inspiration in your way to always see the bigger picture and think outside the box. Thank you for making MIP:lab such a happy place and for this opportunity to take part in your research during these last years.

Je tiens aussi à remercier ma co-superviseuse Marie. Merci de m'avoir introduit aux enjeux de la recherche clinique et pour ta patience à l'époque où je ne reconnaissais pas une seule région cérébrale. Merci pour ton soutien, tes visions positives des choses lorsque j'avais l'impression que plus rien n'allait, et pour ton retour toujours positif à mon travail.

Un grand merci à Stephan, d'abord pour m'avoir donné l'opportunité de travailler sur ce dataset clinique tellement rare et unique, ainsi que pour tes conseils dans mes choix et réflexions sur mon futur professionnel et finalement pour l'immense liberté que tu m'as laissé me permettant d'explorer mes propres questions scientifiques.

I also sincerely thank Dani, for your openness and spontaneity in readily welcoming me to your lab for a short research stay. It has been an inspiration and great experience to work with you and your lab.

I would like to thank all members of my thesis committee, Dani, Douglas, Olaf and Jean-Philippe, for the time that you have invested in the evaluation of my dissertation and in the participation in my defense. Thank you all sincerely for your insightful feedback, for the interesting discussions and for your positive assessment of my work.

Thanks to all my colleagues and friends in my two amazing labs: Thank you to all the members of DIPlab who I have worked with during these past years, for the friendly environment and your patience in helping me out with pretty basic clinical questions. Especially, I would like to thank the clinical team for your continued effort and hard work in establishing this unique dataset without which my work would not have been possible. Thank you Marica and Elisa for your kind introduction to the lab, your support, availability and help during the first part of my thesis. A special thanks to Corrado for sharing your tremendous clinical knowledge with me, and for being my go-to person in all questions about psychiatry and interpretations of results. Also a big thank you to all the MIP:labers who I have crossed (in more or less chronological order) Manuela, Giulia, Zafer, Hamid, Thomas, Yury, Djalel, Kirsten, Valeria, Naghmeh, Rotem, Isik, Elvira, Lo, Anji, Stefano, Nico, Nawal, Younes, Serafeim, Miljan, Giuli, Silvia, Raph, Van and Laura. Thank you so much for being the most awesome lab I could ever imagine, for the countless moments of fun and adventures, the travels and activities, the

Acknowledgements

many coffee breaks, countless cakes and discussions about science, life or sometimes just berries. Especially thank you Lo, Giulia, Laura, Van and Raph for your help with proofreading and useful tips for the thesis.

Ich danke meinen Eltern dafür, dass ihr mich schon mein ganzes Leben lang so unterstützt. Danke Mama, dass Du immer ein offenes Ohr für mich hast und Papa für Deinen immer nützlichen Rat zu allen Facetten des Lebens. Danke an Christiane, mein größtes Vorbild seit ich denken kann. Und vielen Dank Jan, für Deine Geduld und Unterstützung, Deinen immer guten Rat und ehrliche Kritik. Danke Tani, für Deine jahrelange Freundschaft und endlose Telefonate. And thanks to my friends in Geneva – Magali, Mario, Sam, Dani, Amanda – and those all over the world – Mia, Andi, Anne, Annika, Marina – for your friendship that doesn't depend on geographical distance and for being the amazing people you are.

I am grateful to have all these inspiring people around me without whom these last four years would not have been possible.

Contents

Abstract	iii
Résumé	v
Acknowledgements	ix
Lists of abbreviations	xv
1 Introduction	1
1.1 Motivation	1
1.2 Organization and contributions	2
2 Background	7
2.1 Mapping of brain dynamics through MRI	7
2.1.1 Resting-state functional MRI	8
2.1.2 Diffusion weighted MRI	11
2.2 Schizophrenia and 22q11.2 deletion syndrome	13
2.2.1 Schizophrenia	13
2.2.2 22q11.2 deletion syndrome	16
2.3 Brain dynamics in psychosis vulnerability	18
2.3.1 Brain dynamics in schizophrenia and individuals at clinical high risk . .	18
2.3.2 Brain mapping in 22q11DS	20
3 BOLD signal variability to analyze dynamic brain function	23
3.1 Journal Article: Disentangling BOLD variability and PCC functional connectivity	24
3.1.1 Introduction	25
3.1.2 Methods	27
3.1.3 Results	32
3.1.4 Discussion	38
3.1.5 Methodological considerations	42
3.1.6 Conclusions and outlook	42
3.2 Journal Article: BOLD variability in patients with 22q11DS with psychotic symptoms	44
3.2.1 Introduction	45
3.2.2 Methods	46
	xi

Contents

3.2.3	Results	50
3.2.4	Discussion	53
3.2.5	Conclusions and limitations	55
3.3	Summary and outlook	57
4	Large-scale brain network dynamics	59
4.1	Journal Article: Robust recovery of temporal overlap between network activity.	60
4.1.1	Introduction	60
4.1.2	Methods	62
4.1.3	Data description	69
4.1.4	Results	70
4.1.5	Discussion	74
4.1.6	Conclusions and future directions	79
4.2	Journal Article: Dynamics of large-scale brain networks in 22q11DS.	80
4.2.1	Introduction	80
4.2.2	Methods and materials	83
4.2.3	Results	86
4.2.4	Discussion	91
4.3	Summary and outlook	95
5	Control energy to probe into dynamics of structural brain networks	97
5.1	Journal Article: Control energy of functional brain states	99
5.1.1	Introduction	100
5.1.2	Materials and methods	102
5.1.3	Results	107
5.1.4	Discussion	110
5.1.5	Conclusion	113
5.2	Summary and outlook	115
6	Summary and perspectives	117
6.1	Summary	117
6.2	Future research directions	118
A	Supplementary material for chapter 3	123
A.1	Supplementary material for section 3.1	123
A.2	Supplementary material for section 3.2	130
A.2.1	Subjects already included in previous studies.	130
A.2.2	Summary on subject exclusion criteria.	130
A.2.3	Analysis of motion effects.	130
B	Supplementary material for chapter 4	137
B.1	Supplementary material for section 4.1	137
B.1.1	Supplementary tables	137
B.1.2	Supplementary figures	139

B.1.3	Supplementary results	143
B.2	Supplementary material for section 4.2	145
B.2.1	Supplementary methods	145
B.2.2	Supplementary results & discussion	148
B.2.3	Supplementary figures	150
B.2.4	Supplementary tables	154
C	Supplementary material for chapter 5	169
C.1	Supplementary material for section 5.1	169
C.1.1	Supplementary tables	169
C.1.2	Supplementary figures	170
Bibliography		173
Curriculum Vitæ		207

Lists of abbreviations

Brain regions and networks

ACC	anterior cingulate cortex.
aDMN	anterior DMN.
aIN	anterior insula.
AMY/HIP	amygdala / hippocampus.
AUD/SM	auditory / sensorimotor.
CAU	caudate.
CEN	central executive network.
dACC	dorsal anterior cingulate cortex.
dACC/dlPFC	dorsal anterior cingulate cortex / dorsolateral prefrontal cortex.
dlPFC	dorso-lateral prefrontal cortex.
DMN	default mode network.
FPN	fronto-parietal network.
IPC	inferior parietal cortex.
iTEMP/FUS	inferior temporal / fusiform.
LAN	language network.
MFC	middle frontal cortex.
mPFC	medial prefrontal cortex.
OFC	orbitofrontal cortex.
PCC	posterior cingulate cortex.
pDMN	posterior DMN.
PFC	prefrontal cortex.
PREC/vDMN	precuneus / ventral DMN.
PrimVIS1	primary visual 1.
PrimVIS2	primary visual 2.
REC	gyrus rectus.
SecVIS	secondary visual.
sFC	superior frontal cortex.

General acronyms

SM	sensorimotor.
SN	saliency network.
STG	superior temporal gyrus.
THA	thalamus.
TPO	temporal poles.
V2	secondary visual cortex.
VSN	visuospatial network.

General acronyms

22q11DS	chromosome 22q11.2 deletion syndrome.
ABCL	adult behavioral checklist.
ADHD	attention deficit hyperactivity disorder.
ALFF	amplitude of low-frequency fluctuations.
AUC	area under the curve.
BIC	Bayesian information criterion.
BOLD	blood oxygenation level dependent.
CAP	co-activation pattern.
CBCL	child behavioral checklist.
CDF	cumulative distribution function.
CHR	clinical high-risk.
CorrComp	correlation component.
CSF	cerebrospinal fluid.
DARTEL	diffeomorphic anatomical registration.
DCR	dynamic connectivity regression.
dFC	dynamic functional connectivity.
dMRI	diffusion weighted magnetic resonance imaging.
DPARF	data processing assistant for resting-state fMRI.
DSM-V	diagnostic statistical manual.
DTI	diffusion tensor imaging.
EEG	electroencephalography.
FC	functional connectivity.
FD	framewise displacement.
FDR	false discovery rate.
fMRI	functional magnetic resonance imaging.
FWHM	full width half maximum.
GLM	general linear model.
HC	healthy control.

HRF	hemodynamic response function.
IBASPM	individual brain atlases using statistical parametric mapping.
IC	independent component.
ICA	independent component analysis.
iCAP	innovation-driven co-activation pattern.
IQ	intelligence quotient.
LV	latent variable.
MEG	magnetoencephalography.
MNI	Montreal Neurological Institute.
MRI	magnetic resonance imaging.
PCA	principal component analysis.
PE	persistence control energy.
PLS	partial least squares.
PLSC	partial least squares correlation.
PPA	point process analysis.
RMSE	root mean squared error.
ROI	region of interest.
rs-fMRI	resting-state functional magnetic resonance imaging.
RSN	resting-state network.
SD _{BOLD}	BOLD signal standard deviation.
sFC	static functional connectivity.
SIFT	spherical-deconvolution informed filtering of tractograms.
SIPS	structured interview of prodromal symptoms.
SPM12	statistical parametric mapping.
SVD	singular value decomposition.
TA	total activation.
WM	white matter.

1 Introduction

1.1 Motivation

Schizophrenia is a common mental disorder that is strongly debilitating for affected individuals and poses a heavy burden for society (Owen et al., 2016). It is characterized by an aberrant perception of reality, which manifests in positive psychotic symptoms like hallucinations and delusions, negative symptoms like social withdrawal and lack of motivation, thought disorders like disorganized speech and thinking, as well as cognitive impairments. Even though the brain is known to be affected, the exact pathophysiology that underlies schizophrenia remains mostly unknown (Insel, 2010) and thus, the clinical management is nowadays entirely based on clinical observation of symptoms. Magnetic resonance imaging (MRI) is a unique and powerful tool to non-invasively provide images of brain structure and function and is thus ideal to investigate the substrate of mental disorders such as schizophrenia. Indeed, imaging markers are promising tools to delineate aberrant brain mechanisms in the progression towards psychosis and schizophrenia (Kapur et al., 2012). A more precise biomarker-informed staging of patients at high clinical risk for psychosis, that is, of patients with clinical symptoms that precede the onset of full-blown schizophrenia, could complement existing clinical diagnostic tools and allow more targeted and consequently more successful treatment strategies (Insel, 2010; Kapur et al., 2012; Millan et al., 2016). Chromosome 22q11.2 deletion syndrome (22q11DS) is a neurodevelopmental disorder coming with a 30 % to 40 % prevalence of schizophrenia (Schneider et al., 2014). As patients with 22q11DS are usually already diagnosed during childhood, this genetic disorder provides the unique opportunity to study markers related to the development of psychosis even before the onset of full-blown schizophrenia (Insel, 2010).

Importantly, thanks to resting-state functional MRI (rs-fMRI) it has become evident in recent years that even during rest the brain activates in a highly organized way (Damoiseaux et al., 2006). Specifically, it dynamically fluctuates between multiple large-scale brain states characterized by coherent activation of distributed sets of brain regions (Chang and Glover, 2010). Furthermore, the brain can be modeled as a complex dynamic system whose intrinsic structural architecture – measured using diffusion weighted magnetic resonance imaging (dMRI) – determines its functional organization; i.e., its ability to move between different, but well defined functional states (Gu et al., 2015; Honey et al., 2009). Delineating how this

dynamic activity is altered in individuals at high risk for psychosis is a promising step towards the goal of imaging markers that could improve clinical management of schizophrenia.

Although approaches to study brain dynamics through functional magnetic resonance imaging (fMRI) are still in their infancy, they have already given promising insights in aberrant brain function in patients with schizophrenia (Van Den Heuvel and Fornito, 2014; Damaraju et al., 2014). Studies in 22q11DS, however, have mainly focused on brain morphology and static properties of brain function. In this dissertation, I am bridging this gap by developing and applying methods to look into features of dynamic brain function in 22q11DS. First, I use multivariate pattern analysis techniques to analyze alterations and age-relationship of blood oxygenation level dependent (BOLD) signal variability – a summary measure of voxel-wise dynamism. Second, I move towards dynamics of large-scale functional brain states, where I propose a methodological contribution to improve the robust recovery of temporally and spatially overlapping large-scale functional brain states¹ coactivating during rest. Then I use this improved method to investigate temporal activation of functional brain states in patients with 22q11DS. Finally, I use concepts of network control theory (Gu et al., 2015) to investigate how the brain's structural backbone may support the observed dynamic brain function.

1.2 Organization and contributions

This thesis is organized as a compilation of four published articles and one manuscript in preparation for submission. Chapter 2 provides the background for the studies included in this thesis. It gives an introduction and overview on techniques and processing approaches for brain mapping with MRI, followed by a presentation of the clinical picture of schizophrenia and 22q11DS, and ending with an overview on current knowledge on brain dynamics in schizophrenia and 22q11DS. Four published articles are reproduced in chapters 3 and 4, and chapter 5 contains an unpublished manuscript in preparation. Finally, chapter 6 summarizes the results and provides propositions for future research directions.

The following paragraphs will summarize main objectives and contributions of each article, briefly summarized also in figure 1.1. In all included articles, I contributed to the initial idea, performed data processing, methods' development and statistical analyses, wrote the manuscript and performed revisions. As all of the articles were obviously collaborative work of all authors, I will use the personal form "we" throughout the following summary.

¹ A note on terminology: In the field of brain image analysis, there is an ambiguity in the utilization of the term 'network'. In the mathematical sense, a network is defined by a number of nodes (brain regions) that are connected by a number of edges (connectivity). In structural connectivity analyses this is the predominant view. In the context of fMRI analysis on the other hand, the term 'network' is often used to describe sets of coherently activating brain regions, such as for example the default mode *network* or salience *network*. This term was initially chosen because activity in regions of such a brain state is highly correlated, which allows to construct a 'functional network' in which edges are defined by values of functional connectivity between regions. In this thesis, however, I use the term 'brain state' in the context of functional activation patterns and the term 'brain network' to describe networks in the mathematical sense (nodes and edges). For brain states that have widely accepted names that incorporate the term 'network' (e.g. the 'default mode network'), these standard names will be used to ensure coherence with existing literature.

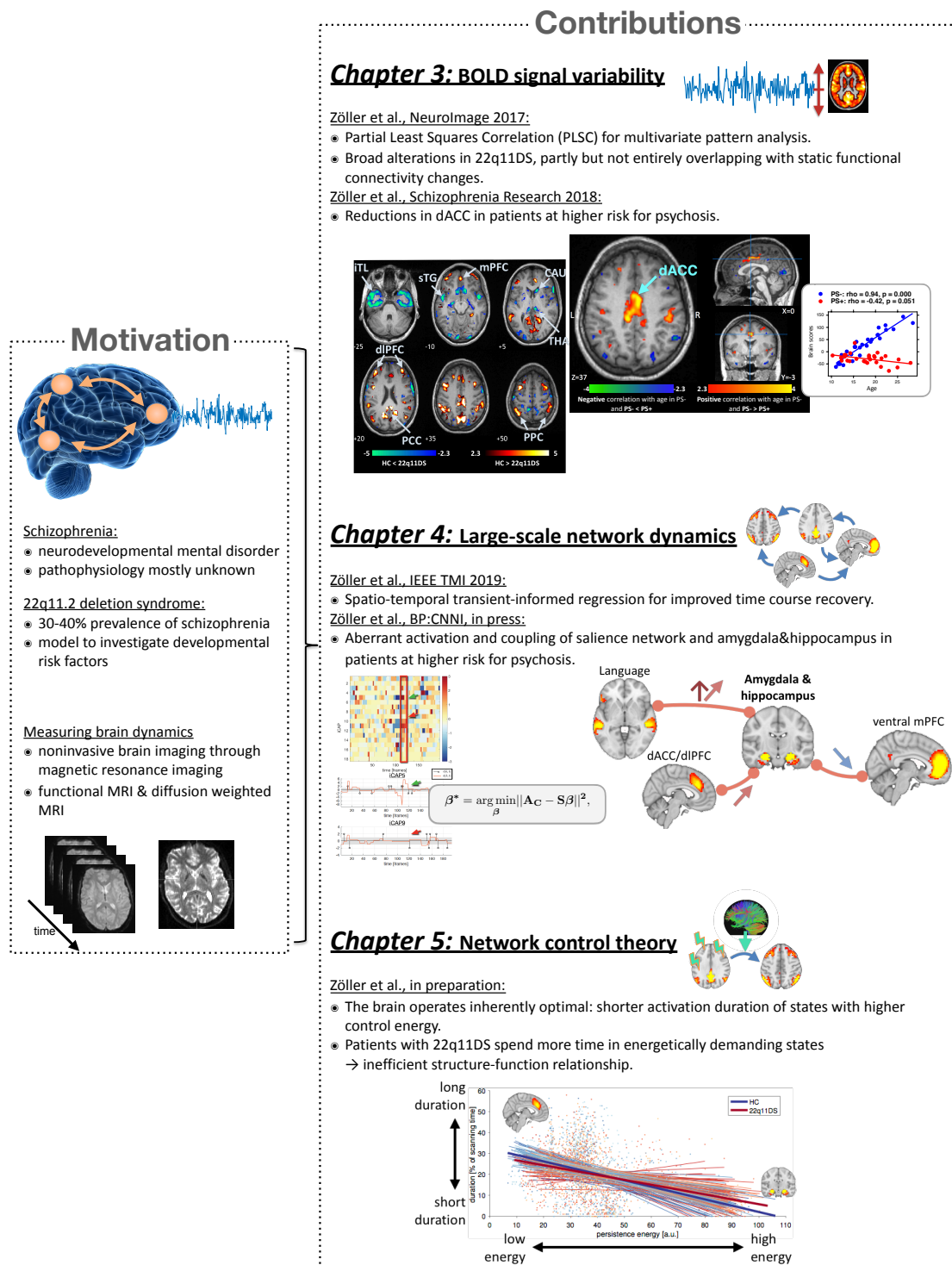


Figure 1.1 – Overview of this thesis on brain dynamics in 22q11.2 deletion syndrome.

Chapter 3: Mapping brain dynamics through BOLD signal variability

To the best of our knowledge, no-one so far has looked into dynamic brain function in 22q11DS. In this chapter, we therefore investigate functional brain dynamics in terms of the voxel-wise measure of BOLD signal variability and evaluate its potential to give insights into psychosis vulnerability in the syndrome.

Section 3.2: Disentangling BOLD signal variability and static functional connectivity

How is BOLD signal variability altered in 22q11DS?

How do alterations of BOLD signal variability relate to static functional connectivity?

Moment-to-moment BOLD signal variability; e.g., estimated by calculating the standard deviation of voxel-wise BOLD signals, provides a summary measure of ‘dynamism’ over the entire fMRI scanning duration. Higher BOLD variability may be beneficial for higher flexibility of brain function (Deco et al., 2011) and has been found to change with age (Grady and Garrett, 2014). It may thus present a potentially valuable measure of dynamic brain function in health and disease. BOLD signal variability is necessarily related to static functional connectivity (sFC), the probably still most commonly used approach for resting-state fMRI analysis, as variance appears in the denominator of Pearson correlation.

In this first study, we present a multivariate partial least squares correlation (PLSC)-based approach to investigate alterations and age-relationship of BOLD signal variability in 22q11DS. Further, we study how alterations of BOLD signal variability relate to alterations of sFC in the default mode network (DMN). We find that BOLD signal variability is broadly altered in patients with 22q11DS and replicate findings on aberrant DMN functional connectivity. Alterations of BOLD signal variability and sFC are overlapping in part, but not entirely, suggesting a complex non-linear relationship that relies on different functional mechanisms.

Section 3.2: Altered BOLD signal variability in psychosis vulnerability

Is altered BOLD signal variability a potential imaging marker for psychosis vulnerability?

Building on the promising findings on broadly altered BOLD signal variability in patients with 22q11DS, we further explore its potential in tracking aberrant brain function related to increased psychosis vulnerability. To this aim, we investigate BOLD signal variability in patients who have high prodromal positive psychotic symptoms and are thus at clinically elevated risk for developing schizophrenia. Indeed, reports on aberrant BOLD signal variability in schizophrenia underline its potential to detect clinically meaningful alterations of dynamic brain function (Xu et al., 2015).

Using again the multivariate PLSC based approach from the previous study, we discover reduced BOLD signal variability in the dorsal anterior cingulate cortex (dACC) that is caused by altered development in patients with higher positive psychotic symptoms. This finding supports previously reported alterations of the dACC in increased psychotic symptoms in 22q11DS (Padula et al., 2018). Indeed, the dACC is a central node of the salience network (SN), which is intriguing as disrupted salience processing has been suggested as a mechanism for the emergence of positive psychotic symptoms (Kapur, 2003).

Chapter 4: Mapping brain dynamics through large-scale brain state activation

To go beyond a voxel-wise measure of dynamic brain function, we continue by investigating dynamics of large-scale functional brain states.

Section 4.1: Recovering temporal overlap of spatially dependent brain states

How can we recover unadulterated temporal overlap of spatially overlapping brain states?

Among the multiple approaches to retrieve and analyze large-scale functional brain states and their temporal dynamic properties, the innovation-driven co-activation patterns (iCAPs) framework (Karahanoğlu et al., 2015) stands out as it allows for spatial *and* temporal overlap of brain states. In other words, one brain region can be part of multiple brain states and many brain states can be active at the same time.

In this first part of chapter 4, we show that in the original framework, spatial overlap of brain states can introduce spurious temporal activation. We then present a novel approach for the recovery of brain state time courses that overcomes this limitation and allows the robust recovery of temporal overlap unhindered by spatial overlap. This new method incorporates spatio-temporal constraints that use temporal information on timing of transitioning activity, as well as information on the brain states' spatial distribution. We demonstrate the performance of our technique both on simulated and experimental data.

Section 4.2: Altered large-scale brain state activation in psychosis vulnerability

How is large-scale brain state activation altered in 22q11DS?

Is altered brain state activation a potential imaging marker for psychosis vulnerability?

The methodological improvement of the iCAPs framework now allows to recover reliable information on large-scale brain states and their temporal properties, which are potentially valuable to improve our understanding of psychosis vulnerability. Indeed, dynamic activation of functional brain states has been reported to be altered in patients with schizophrenia and at clinical high risk for psychosis and points towards alterations of the SN and DMN (Pelletier-Baldelli et al., 2018; Du et al., 2018). In 22q11DS, functional dynamics of large-scale brain networks have not been studied so far.

We use the improved iCAPs framework to recover large-scale brain networks in 22q11DS and probe into alterations related to clinical risk factors for psychosis, namely prodromal positive psychotic symptoms and elevated levels of anxiety. We again observe aberrant activation of the cingulo-prefrontal SN (which includes dACC) in patients with higher levels of prodromal positive psychotic symptoms, as well as an implication of activation of the amygdala and hippocampus for higher levels of anxiety. Further, the iCAPs framework allows to look into network interactions. Looking into coupling of the amygdala and hippocampus, we uncover differential roles of more dorsal and more ventral frontal brain regions, with higher levels of anxiety in patients with stronger coupling to dorsal frontal regions and lower levels of anxiety in patients with stronger coupling to ventral frontal regions. This first study using iCAPs in a clinical population underlines the framework's potential to detect complex functional brain dynamics that are relevant to better understand brain disorders such as psychosis.

Chapter 5: Mapping dynamic structure-function relation through network control theory

Notably, dynamic brain function such as observed so far, takes place on the anatomical substrate of structural connections in the brain. However, how alterations in these anatomical connections constrain or facilitate dynamic function remains an open question.

Section 5.1: Control energy of functional brain states in psychosis vulnerability

How does altered structural connectivity translate into aberrant energy consumption?

How does altered control energy relate to functional activation?

Structural network architecture measured through dMRI is known to be altered in schizophrenia and 22q11DS. How these alterations relate to aberrant functional activation remains an open question that comes with important methodological challenges. Network control theory is an approach that relies on a dynamic model of brain function to explore the implications of structural network topology on the energy required to control the brain's state.

In this final study, we combine iCAPs analysis with network control theory to investigate how the underlying structural connectivity of functional brain states influences their controllability properties. We uncover that the brain functions in an inherently optimal way, spending less activation time (measured with fMRI) in brain states that are energetically more demanding (based on their structural connectivity measured with dMRI). In patients with 22q11DS this relationship is less pronounced, suggesting inefficient functional brain dynamics. In summary, we provide initial evidence for aberrant relationship of brain function and structure in patients with 22q11DS that deserves further investigation.

2 Background

NONINVASIVE brain imaging through magnetic resonance imaging (MRI) has been a young but rapidly growing field, which has had also considerable influence on research in schizophrenia as it allowed for the first time to noninvasively test hypotheses on the underlying mechanisms of the disease. In the following, I will give a brief overview on the background of this thesis, presenting principles and processing techniques for functional and structural MRI, followed by an introduction on the clinical characteristics of schizophrenia and chromosome 22q11.2 deletion syndrome (22q11DS), and ending with a summary on current brain imaging findings in schizophrenia. As the main goal of this thesis was the evaluation of dynamic features of brain function and structure, there will be a specific focus on dynamic methods and findings in all parts.

2.1 Mapping of brain dynamics through MRI

MRI is a relatively young imaging modality, but has become one of the most commonly used medical imaging techniques since its introduction in 1973 (Lauterbur, 1973) and the first images of the human body in 1977 (Damadian et al., 1977). The tomographic technique is unique in its ability to provide high-resolution volumetric images of tissue in a non-invasive way and without the necessity for the injection of contrast agents or exposition to X-ray radiation. Nowadays, a multiplicity of MRI sequences exist, allowing to map brain morphology through structural imaging, white matter connectivity through diffusion imaging, blood perfusion through arterial spin labeling, and brain function through the indirect measure of blood-oxygenation levels that change with neural activity (Viallon et al., 2015; Huettel et al., 2014). Along with the discovery and development of MRI recording methods came new challenges for the analysis of these images (Soares et al., 2016). While initial studies mostly investigated anatomical and static properties of the brain, recent findings and developments during the last decade have led to an increasing focus on *dynamic* properties of the brain (Prete et al., 2017). In the following subsections, the principles of the two modalities used in this thesis – resting-state functional magnetic resonance imaging (fMRI) and diffusion weighted magnetic resonance imaging (dMRI) – will be outlined in more detail, including an overview on developments in the analysis of dynamic features for each of them.

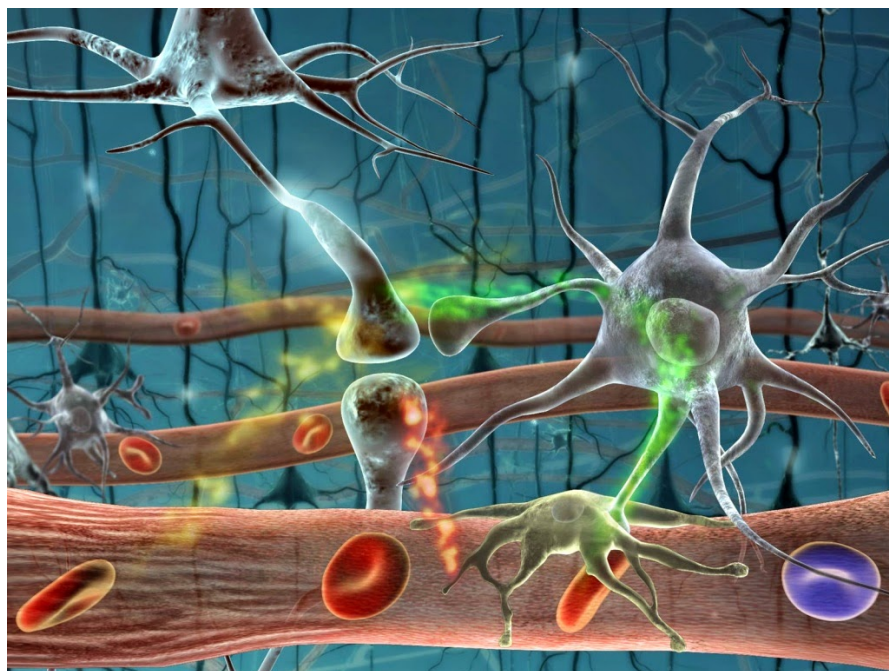


Figure 2.1 – Neurovascular coupling. The electric activity of synapses requires energy, which is provided through increased blood flow and higher supply of oxygenated hemoglobin in the surrounding blood vessels. Reproduced from Toga and Mazziotta (2002).

2.1.1 Resting-state functional MRI

fMRI was first introduced in the late 1980s, when Ogawa and colleagues discovered that cerebral activity can be estimated through blood oxygenation level dependent (BOLD) signals (Ogawa et al., 1990). Briefly, neural activity in the gray matter leads to an increase in blood flow and a higher concentration of oxygenated hemoglobin in the blood in order to sustain the metabolism in the microvascular bed that is surrounding the neurons (see figure 2.1). As it is, the magnetic properties of hemoglobin change with its level of oxygenation: while oxygenated hemoglobin is diamagnetic, deoxygenated hemoglobin is paramagnetic and therefore has a higher magnetic susceptibility. When inserted into a magnetic field, higher magnetic susceptibility caused by lower levels of oxygenation leads to a reduction of transverse magnetization, which can be measured with a T_2^* -weighted MRI contrast (Huettel et al., 2014). Of note, changes in oxygenation level that are measureable with fMRI are much slower than neural activity itself and follow a typical response function, the hemodynamic response function (HRF), starting with a lag of 1 s to 2 s, peaking after 4 s to 6 s and slowly decreasing afterwards. fMRI scans are typically characterized by a spatial resolution of $1 \times 1 \times 1 \text{ mm}^3$ to $3 \times 3 \times 3 \text{ mm}^3$. Temporal resolution usually lays between 1 s to 3 s, but has been pushed below 1 s in more recent multiband acquisitions (e.g., in the publicly available data of the Human Connectome Project at a temporal resolution of 0.72 s; humanconnectome.org).

After its introduction, studies using fMRI first relied on task-based paradigms, during which subjects were asked to execute a specific task during certain periods (or “blocks”)

followed by control blocks. Then, the statistical comparison between the BOLD activity during task and control conditions, identifies brain regions that activate or de-activate in response to the task (Friston and Frith, 1995). Years of research using such paradigms have given us an extensive map of the brain's localized functionality, which nowadays can be explored through online meta-analytic tools such as brainmap.org (Fox and Lancaster, 2002) or neurosynth.org (Yarkoni et al., 2011). In 1995, Biswal and colleagues showed in a seminal work that even during rest, brain activity in the motor cortex is highly structured and correlated across hemispheres, even in absence of any motor task (Biswal et al., 1995), see figure 2.2. Further research has led to the consensus that brain activity during rest can be described in terms of activation and fluctuation of distinct brain states; i.e., sets of brain regions that are coherently activating (Fox et al., 2005; Damoiseaux et al., 2006), see figure 2.2. For clinical neuroscience, the resting condition has the great advantage that it does not require the capacity to conduct a specific task. Therefore, it is particularly well suited for children and adolescents or populations with cognitive disabilities, such as patients with 22q11DS. Further, it allows the comparison and pooling of data recorded across multiple sites without the consideration of variability in the task design.

Static analysis of resting state fMRI In the resting state, there is no prior information on the timing of spontaneous changes in brain activity, and thus different methods than in task-based fMRI are required for its analysis. Classically, resting-state fMRI has been analyzed in terms of **static functional connectivity (sFC)**, that is, the temporal correlation over the entire scanning duration either between the activity of a seed and the rest of the brain, or between region of interests (ROIs) defined by a brain atlas (Biswal et al., 1995; Lee et al., 2013). Such approaches have led to the discovery of several resting-state brain states, including, e.g., visual and auditory states, as well as the famous default mode network (DMN) (Hart et al., 2017), see figure 2.2. Alternatively to seed- or ROI-based sFC approaches, another widely-used method for the extraction of brain states and their static connectivity has been **independent component analysis (ICA)** (McKeown et al., 1998; Calhoun et al., 2001). By assuming spatial or temporal independence, the resting-state fMRI data is decomposed into a set of spatial patterns and their temporal activation. Then, these independent components (or brain states) can be investigated in terms of within- and between-state correlations. In fact, the resting-state brain states extracted with ICA correspond well to the states that were discovered already previously using seed-based approaches, but with the advantage that no specific seed needs to be specified.

Dynamic analysis of resting state fMRI While these static approaches are still most commonly used for resting-state analysis, it has been shown that functional connectivity (FC) is indeed variable over time (Chang and Glover, 2010) and that dynamic properties of resting-state activity contain potentially valuable information (Hutchison et al., 2013a; Christoff et al., 2016).

A relatively simple measure of brain dynamics is **BOLD variability**, which is most commonly computed as the temporal standard deviation of the BOLD signal at each voxel (McIntosh et al., 2010). Variability exists on all scales from the cellular level up to the whole-body and

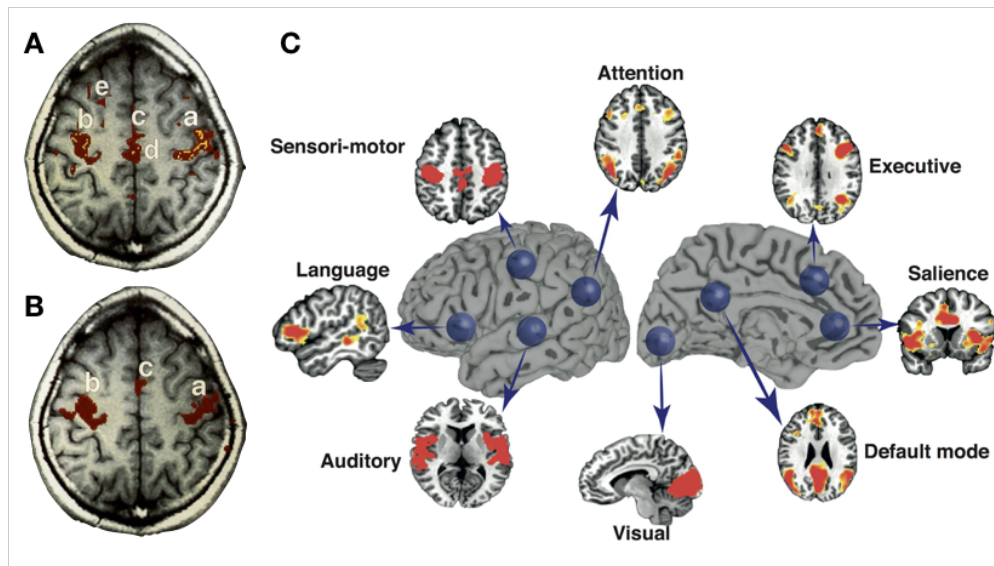


Figure 2.2 – Even during rest, the correlation map of a single voxel in the left motor cortex (A) resembles task-induced activity during bilateral finger movement (B), reproduced with permission from Biswal et al. (1995). Seed correlation analysis has led to the discovery of several resting-state brain states that were previously known from task-based fMRI studies. Reproduced with permission from Hart et al. (2017).

higher levels of variability may be beneficial for systems stability and dynamic range (Faisal et al., 2008; Deco et al., 2011). Even though the exact mechanisms and implications of BOLD variability are not known yet, recent research has confirmed its relevance for development and cognitive performance, as well as its potential for clinical applications (reviewed in Garrett et al., 2013b). Chapter 3 of this thesis is dedicated to an investigation of BOLD variability in terms of its relationship to sFC (section 3.1), as well as its potential as marker for psychosis vulnerability in 22q11DS (section 3.2).

While BOLD variability measures dynamics of *activity*, other increasingly popular approaches focus on **brain state dynamics**, or in other words on dynamics of *connectivity*. The initial discovery that FC varies when computed inside a short temporal window that is slid over the scanning time (Chang and Glover, 2010; Sakoglu et al., 2010) has motivated a multiplicity of methodological developments to retrieve and analyze dynamic properties of brain states (reviewed in Preti et al., 2017 and Hutchison et al., 2013b). Such sliding window approaches have been used in combination with seed-based analysis (Kang et al., 2011) and applied on time-courses of independent components retrieved with ICA (Sakoglu et al., 2010; Allen et al., 2014). For the further analysis of the derived time-dependent connectivity matrices, many approaches have been proposed. Connectivity dynamics can be assessed in terms of simple measures of variation, such as e.g. the standard deviation (Kucyi et al., 2013). Further, several approaches have been proposed to further decompose dynamic functional connectivity (dFC) timecourses into dynamic meta-states; e.g. using principal component analysis

(PCA) (Leonardi et al., 2013), k-means clustering (Allen et al., 2014) or hidden Markov models (Vidaurre et al., 2016).

Window-based dFC methods are however limited by the selection of the size of the window as too short windows can introduce spurious fluctuations (Leonardi and Van De Ville, 2015; Zalesky and Breakspear, 2015), but too long windows miss faster changes in connectivity. In a parallel development, Tagliazucchi et al. (2012) switched the attention from windows to the analysis of single frames, and discovered that only a fraction of the time-frames, selected by thresholding the time course of a seed region, was sufficient to reproduce seed-based sFC patterns. Their so-called point process analysis (PPA) approach was then further extended by Liu and Duyn (2013) who applied temporal clustering on selected frames to obtain multiple co-activation patterns (CAPs). Chapter 4 of this thesis covers yet another approach, which is motivated by these CAPs, but instead of temporally clustering on *activation*, we apply clustering on activation *changes*, allowing for the exploration of brain dynamics without the employment of sliding windows. The so deduced innovation-driven co-activation patterns (iCAPs) represent brain states that are simultaneously changing, which allows the recovery of spatial *and* temporal overlap at the same time (Karahanoglu et al., 2015). In section 4.1 we introduce a novel method for the robust recovery of temporal overlap of these brain states and in section 4.2 we use iCAPs to investigate aberrant brain state dynamics in patients at risk for psychosis.

2.1.2 Diffusion weighted MRI

DMRI for the brain was developed based on the discovery that water diffusion in the human body can be measured by adding magnetic pulse gradients to the MRI sequence (Le Bihan and Johansen-Berg, 2012; Le Bihan and Lima, 2015). Such field gradient pulses encode the movement of water molecules along one direction, where higher diffusion results in an attenuated MR signal. The white matter of the brain is composed of millions of axons that interconnect different areas of the brain. In order to minimize electrical transmission energy, these axons are wrapped in a layer of myelin, which constrains the main water diffusion direction. In such anisotropic tissue, the main diffusion direction can be reconstructed from diffusion weighted images by measuring diffusivity in multiple different gradient directions. In diffusion tensor imaging (DTI), which was first introduced by Basser et al. (1994), a tensor encoding the main direction is reconstructed for every voxel from the multiple directions. Nowadays, diffusion-weighted images typically have a spatial resolution in the order of millimeters (Le Bihan and Lima, 2015). Since its first introduction in the 1990s, multiple methodological developments for the analysis of diffusion weighted images. A widely-used approach is the direct investigation of voxel-wise diffusivity measures such as axial diffusivity, which measures the diffusivity along the fibres, or radial diffusivity reflecting perpendicular diffusivity through the cell membranes. Finally, fractional anisotropy is a summary measure of anisotropy in each voxel (Armitage and Bastin, 2000).

Alternatively to voxel-wise anisotropy measures, **fibre tracking** (or **tractography**) algorithms reconstruct white matter tracts by propagating streamlines into the main diffusion directions (Catani et al., 2002; Jbabdi et al., 2015). From the reconstructed streamlines it is

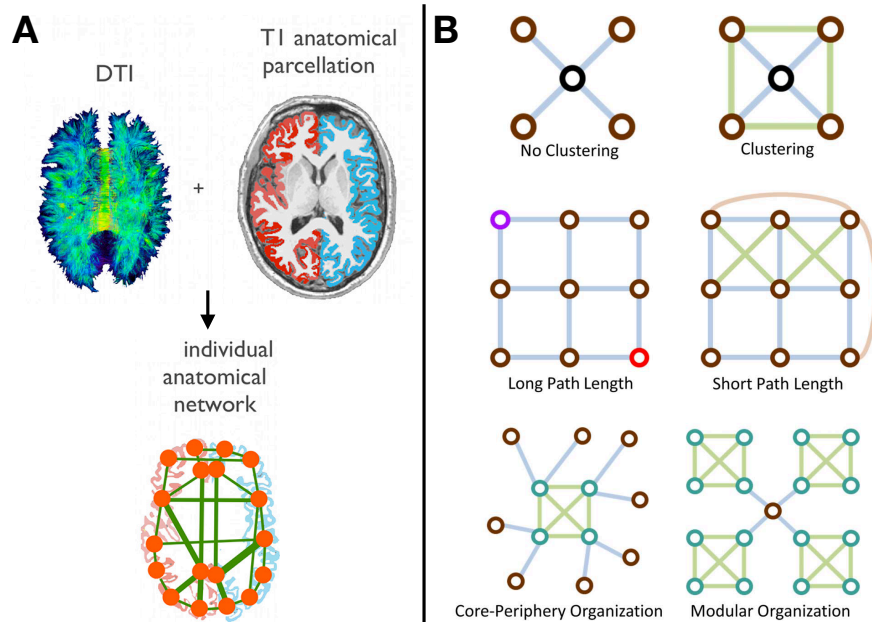


Figure 2.3 – A) Structural networks can be reconstructed from DTI connectivity data by counting streamlines that are connecting brain regions of an anatomical atlas. Network node corresponds to a brain regions, and network edges correspond to the connectivity strength between regions. Adapted with permission from van den Heuvel and Sporns (2011). B) Structural brain networks can be analyzed using graph theory measures such as clustering, shortest path length, and modularity structure. Reproduced with permission from Medaglia et al. (2015).

then possible to represent the brain's structural connectivity as a network, in which each brain region is a node and their connectivity in terms of streamline counts (or other measures of structural connectivity) are edges that interconnect the nodes (Bullmore and Bassett, 2011) (see figure 2.3). Modeling the brain in this way then allows to use tools from network science and **graph theory** to derive local and global measures of topology and wiring properties (Bullmore and Sporns, 2009; Bassett and Sporns, 2017). In particular, the human brain is characterized by high levels of 'small-worldness', that is the combination of high clustering and low path lengths (Bassett and Bullmore, 2017). Further, brain networks are highly modular and the different modules are interconnected by highly connected nodes, the so-called 'network hubs' (van den Heuvel and Sporns, 2013). These hubs are in turn highly interconnected between themselves, forming a 'rich club' (van den Heuvel and Sporns, 2011).

Dynamic analysis of structural brain networks While most commonly, structural brain networks are still analyzed in terms of their (static) topology, there have been increasing efforts dedicated to the investigation of their dynamic properties (Bassett and Sporns, 2017). Briefly, it can be distinguished between dynamics *of* networks and dynamics *on* networks (Bassett and Sporns, 2017), see figure 2.4. In the context of structural brain networks, dynamics *of* networks have mainly been investigated in terms of changing network configuration over brain development (Betzel et al., 2014; DiMartino et al., 2014), e.g. using multilayer graphs

(Bassett and Sporns, 2017). In the analysis of dynamics *on* networks on the other hand, developments in the field of networks science provide an ideal framework to investigate how brain function is related to its underlying structure (Bassett and Sporns, 2017). First attempts to address this question have demonstrated that functional connectivity can be in part, but not entirely predicted by the underlying structural connectivity (Honey et al., 2009; Goñi et al., 2014). Since these initial investigations, several methodological developments have been suggested to further probe into this structure-function relationship. A promising idea has been to use mechanistic models of brain dynamics to probe into the effect of the brain's particular structure on these dynamics (Braun et al., 2018). In particular, it has been proposed to use principles from network control theory to understand how functional brain states evolve over time on a structural brain graph (Gu et al., 2015, 2017; Betzel et al., 2016). By modeling the brain as a system characterized by a structural brain graph and a model of the system's dynamic behavior, control theory allows to investigate how and where the brain's structure constrains or facilitates the transition between different functional brain states. Since its initial introduction into neuroscience in an application to cognitive control (Gu et al., 2015), network control has provided promising insights into brain development from childhood to adulthood (Tang et al., 2017a), gender differences in executive functions (Cornblath et al., 2019), mild traumatic brain injury (Gu et al., 2017), and bipolar disorder (Jeganathan et al., 2018).

In chapter 5 of this thesis, we use network control theory to characterize the brain's structural architecture that underlies brain states retrieved from fMRI data and to probe into alterations in psychosis vulnerability.

2.2 Schizophrenia and 22q11.2 deletion syndrome

In this thesis, I investigated dynamic brain properties in patients with 22q11DS in order to probe into alterations related to the development of psychosis. The following sections first introduce the current view on schizophrenia as a neurodevelopmental disorder, followed by a description of 22q11DS and its relevance for the study of psychosis risk factors.

2.2.1 Schizophrenia

Schizophrenia is a common mental disorder that is strongly debilitating for affected individuals and poses a heavy burden for society due to high unemployment rates and high costs for treatment and care (Owen et al., 2016; Insel, 2010). It is characterized by a multiplicity of symptoms that can be divided into positive symptoms (hallucinations and delusions), negative symptoms (social withdrawal and lack of motivation), thought disorders (disorganized speech and thinking) and cognitive impairments. Despite great efforts to research the neuroscientific and genetic bases of schizophrenia, its pathophysiology still remains largely unknown (Insel, 2010). Therefore, the current clinical management of the disease is based entirely on clinical observation of symptoms. Diagnoses and treatment choices are made purely based on observations by trained physicians and criteria described in the diagnostic statistical manual (DSM-V) (American Psychiatric Association, 2013).

The increasingly recognized neurodevelopmental hypothesis of schizophrenia suggests

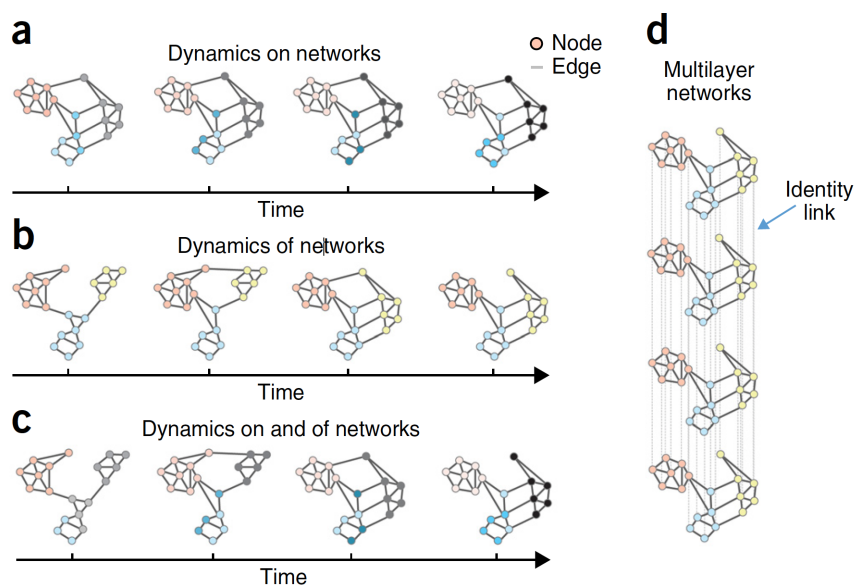


Figure 2.4 – The different views on structural brain networks dynamics include a) dynamics of brain states *on* a structural brain networks, or b) the dynamics of the structural network structure itself. c) There have been efforts to integrate both phenomena. d) Multilayer networks provide a framework to look into dynamics of brain networks. Reproduced with permission from Bassett and Sporns (2017).

that psychosis is only the final stage of a developmental course that starts already many years before the onset of full-blown schizophrenia, which appears usually in early adulthood (Insel, 2010; Fusar-Poli et al., 2013; Rapoport et al., 2012). Further, evidence points towards the existence of sensitive periods during development in which interventions can have long-term consequences (Marín, 2016). In the negative sense, such sensitive periods are moments of higher vulnerability and larger risk for a deterioration that may only appear at a later time. But also in the positive sense, there are periods in which prevention and treatments may be more promising than later on (Marín, 2016). The neurodevelopmental model of schizophrenia has lead to the formulation of a prodromal state, elaborated in the clinical high-risk (CHR) criteria (Fusar-Poli et al., 2013). Figure 2.5 outlines the different phases and criteria of this prodromal period. Individuals diagnosed with CHR state have a strong risk of 30 % to 40 % for transition to psychosis after 4 years of follow-up (Fusar-Poli et al., 2012; Schultze-Lutter et al., 2015), which underlines the potential of such criteria in predicting the development towards psychosis.

However, even though the CHR criteria perform well in the assessment of clinical risk for psychosis in help-seeking populations (Fusar-Poli, 2017b), they are still purely defined based on clinical criteria and are highly heterogeneous (Fusar-Poli, 2017a). Also clinical manifestations of schizophrenia itself are extremely heterogeneous and treatment response is highly variable from one individual to another. The identification of biologically-defined markers for different developmental stages and patients subgroups bares an immense potential to unravel

2.2. Schizophrenia and 22q11.2 deletion syndrome

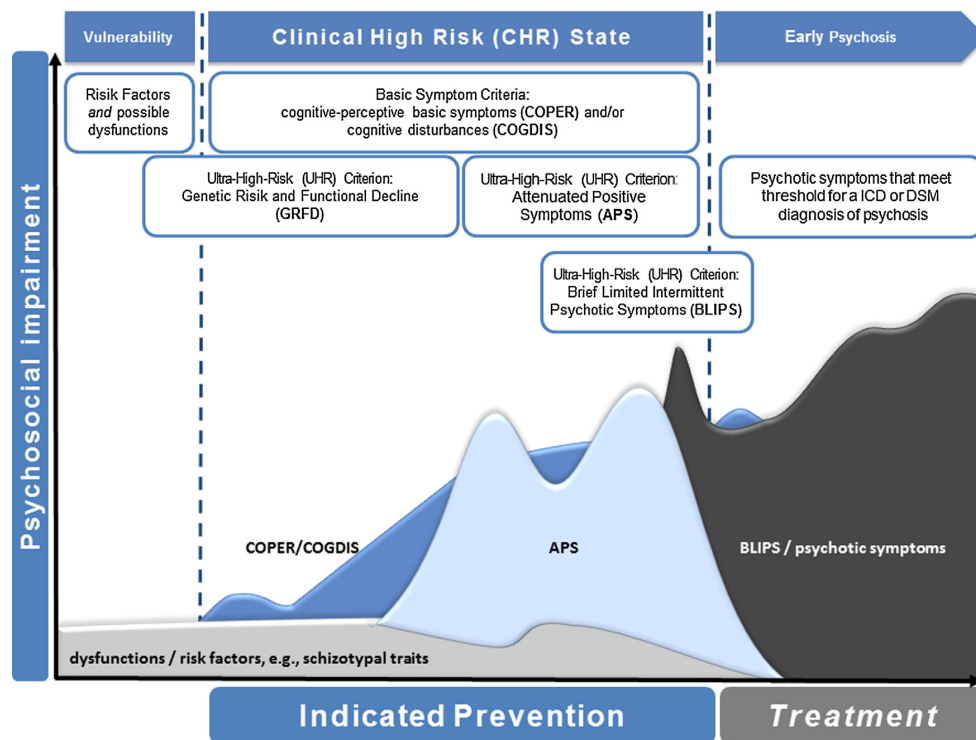


Figure 2.5 – Developmental stages in the course of early psychosis. Reproduced with permission from Schultze-Lutter et al. (2015).

this heterogeneity (Kapur et al., 2012). Studies investigating the neuroscientific bases underlying the aberrant trajectories towards psychosis and schizophrenia will help to obtain a better understanding of the disease. Such a better understanding of the disease is crucial to improve prevention and allow the development of more targeted and effective therapies, which will ultimately lead to better clinical outcomes and improved patients' well-being (Kapur et al., 2012).

In the general population, the investigation of the trajectory toward schizophrenia has the intrinsic limitation that patients are usually only identified after onset of psychotic symptoms (Insel, 2010). At the same time, a growing body of literature suggests that developmental alterations in the brain manifest already much earlier before the appearance of clinical symptoms themselves (Insel, 2010). A unique opportunity to look into developmental alterations before the onset of psychosis is the study of 22q11DS. This genetic disease is caused by a microdeletion on the 22nd chromosome and comes with an extremely elevated risk for schizophrenia (Schneider et al., 2014). In fact, by adulthood 30 % to 40 % of patients with 22q11DS develop a form of schizophrenia that is identical to idiopathic schizophrenia (Schneider et al., 2014; Bassett and Chow, 1999). Due to somatic manifestations, individuals with 22q11DS are usually diagnosed at very early age. Longitudinal studies of individuals with the disorder therefore allow to compare the trajectories of patients who develop schizophrenia with those who don't. In the following section 2.2.2, this genetic model for schizophrenia will be reviewed in more detail.

2.2.2 22q11.2 deletion syndrome

Chromosome 22q11.2 deletion syndrome (22q11DS) – formerly also known as velocardiofacial syndrome, Di George syndrome, or conotruncal anomaly face syndrome – affects approximately 1 per 3000-6000 live births (McDonald-McGinn et al., 2015). In affected individuals, the microdeletions on the 22nd chromosome leads to a variety of clinical manifestations including somatic, cognitive and psychiatric impairments.

Somatic manifestations

Somatic alterations in 22q11DS are varied and can affect a multiplicity of organs and functions (reviewed in McDonald-McGinn et al., 2015). Congenital heart defects are present in approximately 75 % of patients and, as they already manifest in the prenatal or neonatal period, are among the most common indicators that lead to initial diagnosis of 22q11DS at very early age (Van et al., 2017; McDonald-McGinn and Sullivan, 2011). Further common somatic anomalies include palatal abnormalities (~75 % of patients), deficiencies of the immune system (~75 % of patients), hypocalcaemia (~50 % of patients), gastrointestinal problems (~30 % of patients) and genitourinary anomalies (~30 % of patients).

Cognitive manifestations

Right after congenital heart disease, developmental delays are the second most common indicator that leads to initial diagnosis of 22q11DS during childhood (Van et al., 2017). The average intelligence quotient (IQ) in patients lays at 70 with approximately 66 % of individuals having an IQ in the range between 55 and 85. In a large multi-site study that included longitudinal assessments from 411 individuals with 22q11DS, patients who developed a psychotic disorder at a later time had significantly lower IQ at baseline (Gothelf et al., 2013; Vorstman et al., 2015). Further, IQ in children was found to significantly decline over age, particularly affecting verbal competences. This decline in verbal IQ was significantly steeper in individuals who later developed psychosis (Gothelf et al., 2013; Vorstman et al., 2015). Thus, lower IQ and a decline in verbal IQ are considered risk factors for psychosis in 22q11DS.

Psychiatric manifestations

In patients with 22q11DS there is an elevated prevalence of several psychiatric disorders (Schneider et al., 2014; McDonald-McGinn et al., 2015), see figure 2.6. During childhood and adulthood especially rates of autism spectrum disorder and attention deficit hyperactivity disorder (ADHD) are elevated. Mood disorders such as bipolar disorder and major depressive disorders are present with increasing prevalence at higher age, but with comparable rates to the general population (Schneider et al., 2014; Fung et al., 2010; Kessler et al., 2005).

The prevalence of schizophrenia is at least 25-fold increased compared to the general population where the expected prevalence is 1 in 100 (Bassett et al., 2017; Butcher et al., 2018). In 22q11DS prevalence values of up to 40 % have been reported (Schneider et al., 2014), but as they were mostly conducted in psychiatric setting these values might be inflated (Fung et al., 2010). Therefore, more conservative estimates taken from subjects ascertained in non-

2.2. Schizophrenia and 22q11.2 deletion syndrome

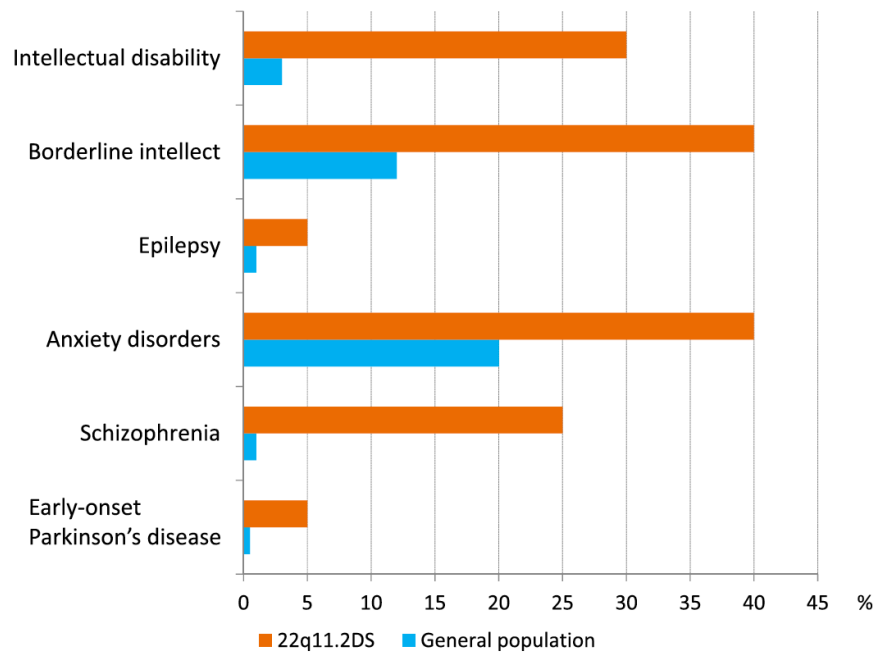


Figure 2.6 – Approximate risk estimates of neuropsychiatric disorders with significantly different prevalence in 22q11DS compared to the general population. Reproduced with permission from Bassett et al. (2017).

psychiatric settings presume a prevalence of approximately 25 % (Fung et al., 2015; Butcher et al., 2018). Patients with 22q11DS and schizophrenia account for 0.5 % to 1 % of individuals with schizophrenia in the entire population and thus, 22q11DS represents the strongest known molecular risk factor for schizophrenia (McDonald-McGinn et al., 2015). The phenotype of schizophrenia in 22q11DS is identical to idiopathic schizophrenia except for the overall lower IQ (Tang et al., 2017b; McDonald-McGinn et al., 2015; Butcher et al., 2018), which makes the disorder a good model to study the neurodevelopmental aspects of schizophrenia in general (Bassett and Chow, 1999; Insel, 2010), see also subsection 2.2.1. In particular, a recent study investigating the CHR criteria found a predictive value of 27.3 % that is comparable to previously reported values in clinical samples (Schneider et al., 2016; Fusar-Poli et al., 2012; Fusar-Poli, 2017b), which points toward a common clinical trajectory with idiopathic schizophrenia.

Finally, also anxiety disorders are more prevalent throughout all ages, but especially during childhood and adolescence (Schneider et al., 2014) and the presence of an anxiety has found to be a strong predictor for developing a psychotic disorder at a later time (Gothelf et al., 2007, 2013; Kates et al., 2015b). A possible factor in this relationship between higher anxiety and the development of psychosis may be the recently discovered elevated stress intolerance of patients with 22q11DS (Tang et al., 2017b; Armando et al., 2018). Armando et al. (2018) found an association of higher stress load with the development of psychosis that was mediated by dysfunctional strategies to cope with stress (Armando et al., 2018). Of note, a similar role

of dysfunctional coping strategies as mediator for the development of psychosis has been reported in the general population (Laloyaux et al., 2016; Ered et al., 2017), which once again suggests a common trajectory towards psychosis in 22q11DS and the general population.

2.3 Brain dynamics in psychosis vulnerability

Conceptualizations of schizophrenia as a disease of broad whole-brain disconnectivity date back to the late 19th century and have been confirmed through neuroimaging after the development of noninvasive MRI techniques (Collin et al., 2016; Friston, 1994). Since the 1990s, large efforts have been made to map alterations in brain anatomy and function in individuals with schizophrenia (Collin et al., 2016). Main findings nowadays include reduced overall gray matter and white matter volume, as well as reduced overall structural connectivity. (for extensive reviews see Van Den Heuvel and Fornito, 2014; Ellison-Wright and Bullmore, 2009). Findings on functional connectivity are more heterogeneous, but point towards mostly reduced connectivity within functional systems, and both reduced and increased connectivity between different functional systems (Dong et al., 2018b). Importantly, a disruption of the structural connectivity affects the dynamic functional organization of the brain and static functional connectivity approaches are limited in capturing such alterations (see section 2.1 for an overview on methodological motivations). Thus, very recently there has been increasing interest in mapping functional dynamics and dynamic implications of structural alterations in schizophrenia to link observed anatomical abnormalities to functional dynamics relevant for the emergence of psychotic symptoms (Preti et al., 2017). The following sections will give an overview on studies that looked into dynamic features of brain function and structure in schizophrenia with a particular focus on populations at high risk for psychosis. In 22q11DS, dynamic brain function and structure has not been studied yet. Therefore, the last subsection will give a brief overview on general findings in MRI studies on the syndrome.

2.3.1 Brain dynamics in schizophrenia and individuals at clinical high risk

Functional MRI Schizophrenia is probably the most studied disease in terms of dynamic brain function. Most relevant dFC studies in schizophrenia have relied on **sliding-window dFC**, either ROI-based or in a combination with ICA (e.g., Damaraju et al., 2014; Du et al., 2016; Dong et al., 2018a; Mennigen et al., 2018; Pelletier-Baldelli et al., 2018). These studies report mostly the existence of patient-specific, more weakly connected dynamic connectivity states (Damaraju et al., 2014; Du et al., 2016, 2018; Sun et al., 2018; Lottman et al., 2017; Sanfratello et al., 2019) and a reduced overall dynamism (Miller et al., 2016), but both increased and decreased variability of functional connectivity in different functional systems, with higher dFC variability in sensory systems (Dong et al., 2018a; Bhinge et al., 2019; Deng et al., 2018), precuneus (Guo et al., 2018) and amygdala (Yue et al., 2018) and lower dFC variability in higher-order functional systems such as DMN and fronto-parietal network (FPN) (Dong et al., 2018a; Bhinge et al., 2019). It is of note that there are discrepancies in the direction of reported results, which may be due to the high variety of applied methods (whole-brain, seed-based, ICA-based and others).

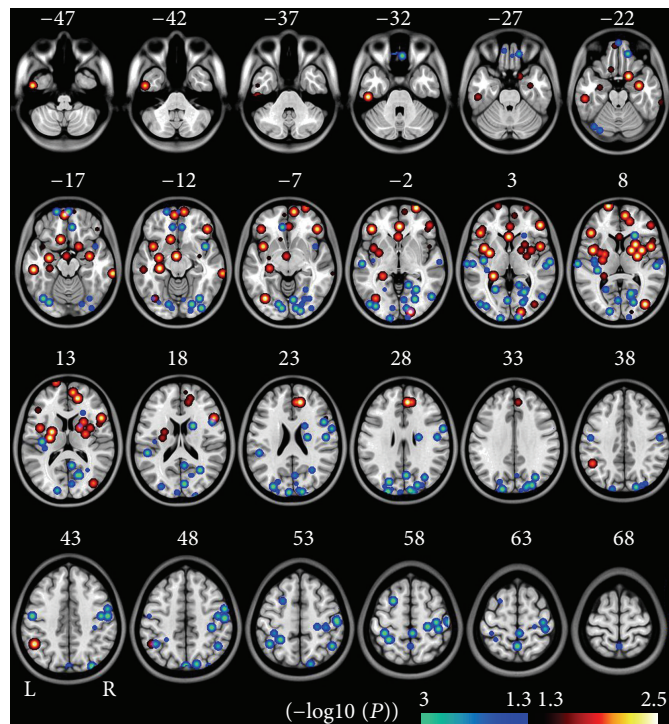


Figure 2.7 – Results from a meta-analysis of BOLD variability in schizophrenia show increased variability levels in frontal and reduced levels in posterior parietal and occipital regions. Reproduced with permission from Xu et al. (2015).

In populations at clinical high risk for schizophrenia, there are only few studies yet looking into dynamic brain function. In a seed-based approach, Pelletier-Baldelli et al. (2018) found decreased variability of dFC between regions in the salience network (SN) and DMN with regions involved in sensory, motor and attention processes in individuals at CHR. Du et al. (2018); Mennigen et al. (2018, 2019) compared patients with early-illness schizophrenia, individuals at CHR and healthy controls and found reduced dynamics in CHR individuals at an intermediate level between healthy control (HC) profiles and reductions in schizophrenic patients, which points towards a shared trajectory towards psychosis.

Schizophrenia has also been studied in terms of dynamic *activity* (as opposed to dynamic *connectivity*), using approaches like the amplitude of low-frequency fluctuations (ALFF) to estimate **BOLD signal variability**. These studies on BOLD variability point towards globally increased BOLD variability in schizophrenia (Yang et al., 2014), which is most pronounced in higher-order functional systems such as the DMN and FPN (Yang et al., 2014, 2015). Xie et al. (2018) further found increased variability in temporal, fusiform and medial prefrontal cortex (PFC) and lower variability in precuneus, posterior cingulate cortex (PCC), lingual and calcarine regions. BOLD variability measured through ALFF is also consistently reported to be increased in medial prefrontal, temporal and basal ganglia, but decreased in posterior parietal and occipital areas (Turner et al., 2013; Xu et al., 2015; Wang et al., 2019b; Alonso-Solís et al., 2017; Salvador et al., 2017; Tang et al., 2019), see figure 2.7.

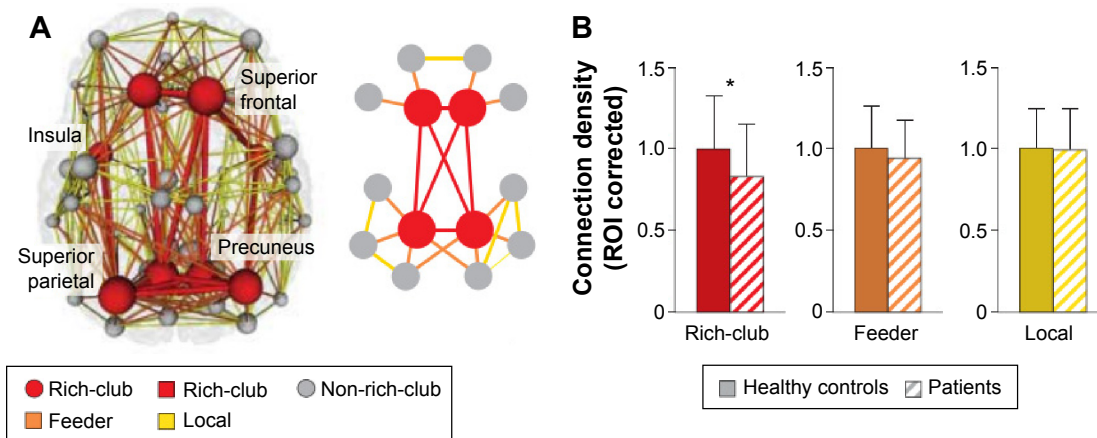


Figure 2.8 – Structural connectivity networks in schizophrenia are characterized by reduced connectivity in the brain's rich club. Reproduced with permission from Cao et al. (2015).

Studies on dynamic activity in terms of BOLD variability in individuals at high risk are again more sparse. Similarly to studies on dynamic connectivity, a study on individuals at clinical high risk reported similar alterations to those observed in schizophrenia, but less pronounced at an intermediate level between HCs and patients with schizophrenia (Fryer et al., 2016). Another recent study on individuals at genetic high risk (with a parent with schizophrenia) found that individuals at genetic high risk were indistinguishable from HCs in terms of ALFF except for increased variability in subcortical areas.

Structural MRI The dynamic implications of structural connectivity alterations in schizophrenia have not yet been investigated. Studies on the general structural network architecture point towards a more segregated structural network organization characterized by elevated clustering, modularity and average path length and lower global efficiency (Van Den Heuvel and Fornito, 2014). Further, the brain's rich-club has found to be less connected in schizophrenia (Van Den Heuvel et al., 2013), see figure 2.8. Structural network investigations in CHR individuals suggest that the disruption of rich-club organization is already present before the onset of schizophrenia (Schmidt et al., 2017). The implication of this aberrant network organization on dynamic brain function have yet to be explored (Bassett et al., 2018).

2.3.2 Brain mapping in 22q11DS

In 22q11DS, neither functional, nor structural network dynamics have been studied so far. Thus, the following summary will give an overview on existing findings on functional and structural connectivity organization aside from dynamic properties.

Functional MRI One of the most replicated finding in resting-state functional magnetic resonance imaging (rs-fMRI) studies in 22q11DS is functional dysconnectivity of the DMN (Padula et al., 2015; Mattiaccio et al., 2016, 2018; Debbané et al., 2012; Schreiner et al., 2014, 2017) and visuospatial network (VSN) (Debbané et al., 2012). Investigations of whole-brain connectivity report mostly alterations of frontal functional connectivity, including dorso-lateral prefrontal

cortex (dlPFC) and anterior cingulate cortex (ACC) (Scariati et al., 2014, 2016b). Also in task-based fMRI studies, patients with 22q11DS show mostly reduced activity, principally in frontal brain areas, across a multiplicity of tasks (Larsen et al., 2018).

Finally, a recent study investigated thalamic and hippocampal seed connectivity and found increased thalamic and decreased hippocampal connectivity with the sensorimotor network and an opposite pattern (lower thalamic connectivity and higher hippocampal connectivity) with the FPN (Schleifer et al., 2018).

Structural MRI White matter architecture and connectivity structure has been extensively studied in 22q11DS. Most studies so far have focused on measures of diffusivity, initially on the whole-brain level (reviewed in Scariati et al. (2016a)) with a recent shift of interest towards tract-based analyses (e.g., Kikinis et al., 2016; Tylee et al., 2017; Olszewski et al., 2017; Roalf et al., 2017). While reported alterations in 22q11DS are not always consistent, affected white-matter bundles seem to mainly include long-range connections of frontal regions such as inferior and superior longitudinal fasciculus, inferior fronto-occipital fasciculus and uncinate fasciculus, as well as the cingulum bundle (Scariati et al., 2016a). Fewer studies have so far relied on region-to-region connectivity and the characterization of whole-brain network properties (Ottet et al., 2013b; Kikinis et al., 2013; Ottet et al., 2013a; Padula et al., 2017a; Váša et al., 2016; Zhan et al., 2018). In line with tract- and voxel-based studies, main ROI-based findings report fronto-temporal, fronto-parietal (Ottet et al., 2013b,a; Zhan et al., 2018) and limbic dysconnectivity (Ottet et al., 2013a; Padula et al., 2015), and altered anterior and posterior midline connectivity in the presence of psychotic symptoms (Scariati et al., 2016a; Padula et al., 2017a). Two studies focused on structural connectivity only between selected brain states and found principally reduced connectivity within and between DMN, FPN, and SN (Padula et al., 2015, 2017b). Váša et al. (2016) used a whole-brain graph theoretical approach and identified an affected core that included frontal, parietal and subcortical regions. Further, the authors uncovered a ‘de-centralization’ in 22q11DS with a rerouting of shortest network paths to circumvent the affected core. Finally, two studies have investigated whole-brain networks in 22q11DS based on structural covariance (Schmitt et al., 2016; Sandini et al., 2017) and reported less robust geographic organization with a particular implication of parietal and occipital lobes (Schmitt et al., 2016), and higher average covariance strength in patients with 22q11DS (Sandini et al., 2017).

3 BOLD signal variability to analyze dynamic brain function

AMONG the measures of brain dynamics, moment-to-moment BOLD signal variability is a relatively simple, but powerful measure. It is nevertheless rarely investigated in clinical MRI studies. Even though its exact underlying mechanisms are not yet entirely understood, we know nowadays that variability (or ‘noise’) exists on all levels of the nervous system, from the cellular to the behavioral level (Faisal et al., 2008). Currently, multiple theories exist on the mechanisms and significance of BOLD variability in the brain (Garrett et al., 2013b). Variability at the right level (not too high and not too low) may be beneficial to allow the detection of weak signals and in this way lead to higher neuronal synchrony (Garrett et al., 2013b; Faisal et al., 2008). It may also reflect a greater dynamic range and complexity, and following higher flexibility in the brain’s function (Deco et al., 2011; McIntosh et al., 2010). In schizophrenia, BOLD variability has been found to be altered in multiple studies (see Xu et al., 2015 for a meta-analysis). It thus represents a potentially valuable measure for abnormal brain dynamics in psychosis vulnerability.

This chapter is dedicated to the analysis of brain dynamics through BOLD signal variability in patients with 22q11DS. In the first article in section 3.1, we compare BOLD signal variability in patients to healthy controls and test how functional connectivity in the default mode network is related to BOLD signal variability. In the second article in section 3.2, we use the approach developed in the first article to test for alterations in BOLD signal variability in patients with prodromal positive psychotic symptoms and evaluate its potential as marker for psychosis vulnerability. In the last section 3.3 follows a summary on findings and conclusions of these two articles and a motivation for our following analyses.

3.1 Journal Article: Disentangling BOLD variability and PCC functional connectivity

Postprint version of the article published in: NeuroImage 2017, 149:85–97, <https://doi.org/10.1016/j.neuroimage.2017.01.064>

Disentangling resting-state BOLD variability and PCC functional connectivity in 22q11.2 deletion syndrome.

Daniela Zöller^{1,2,3}, Marie Schaer³, Elisa Scariati³, Maria Carmela Padula³, Stephan Eliez³, Dimitri Van De Ville^{1,2}

¹Medical Image Processing Laboratory, Institute of Bioengineering, École Polytechnique Fédérale de Lausanne (EPFL), Lausanne, Switzerland; ²Department of Radiology and Medical Informatics, University of Geneva, Geneva, Switzerland; ³Developmental Imaging and Psychopathology Laboratory, Office Médico-Pédagogique, Department of Psychiatry, University of Geneva, Geneva, Switzerland

Although often ignored in functional magnetic resonance imaging (fMRI) studies, moment-to-moment variability of blood oxygenation level dependent (BOLD) signals reveals important information about brain function. Indeed, higher brain signal variability has been associated with better cognitive performance in young adults compared to children and elderly adults. Functional connectivity, a very common approach in resting-state fMRI analysis, is scaled for variance. Thus, alterations might be confounded or driven by BOLD signal variance alterations. Chromosome 22q11.2 deletion syndrome (22q11DS) is a neurodevelopmental disorder that is associated with a vast cognitive and clinical phenotype. To date, several resting-state fMRI studies reported altered functional connectivity in 22q11DS, however BOLD signal variance has not yet been analyzed. Here, we employed partial least squares (PLS) correlation analysis to reveal multivariate patterns of diagnosis-related alterations and age-relationship throughout the cortex of 50 patients between 9 and 25 years old and 50 healthy controls in the same age range. To address how functional connectivity in the default mode network is influenced by BOLD signal fluctuations, we conducted the same analysis on seed-to-voxel connectivity of the posterior cingulate cortex (PCC) and compared resulting brain patterns. BOLD signal variance was lower mainly in regions of the default mode network and in the dorsolateral prefrontal cortex, but higher in large parts of the temporal lobes. In those regions, BOLD signal variance was correlated with age in healthy controls, but not in patients, suggesting deviant developmental trajectories from child- to adulthood. Positive connectivity of the PCC within the default mode network as well as negative connectivity towards the frontoparietal network were weaker in patients with 22q11DS. We furthermore showed that lower functional connectivity of the PCC was not driven by higher BOLD signal variability. Our results confirm the strong implication of BOLD variance in aging and give an initial insight in its relationship with functional connectivity in the default mode network (DMN).

3.1. Journal Article: Disentangling BOLD variability and PCC functional connectivity

3.1.1 Introduction

Inter- and intra-subject variability of resting-state functional magnetic resonance imaging (rs-fMRI), such as between-trial variability (Poldrack et al., 2015; Laumann et al., 2015; Davis et al., 2014), spatial variability between voxels (Davis et al., 2014; Gopal et al., 2016) and moment-to-moment variability of blood oxygenation level dependent (BOLD) signals within every voxel (McIntosh et al., 2010; Deco et al., 2011; Allen et al., 2014) have gained interest in recent literature. Such variability measures are rarely taken into account in conventional rs-fMRI analysis, but their consideration might give a deeper insight into underlying brain processes and their connection to disease-related alterations (McIntosh et al., 2010; Gopal et al., 2016). Even though the exact implications of the latter, moment-to-moment BOLD signal variability, are not clear yet, theoretical work has suggested that spontaneous signal fluctuations are crucial for neural system functions and reflect larger network complexity and dynamic range (Deco et al., 2011; McIntosh et al., 2010). Several studies focusing on the implications of BOLD signal variability on aging and cognitive performance in adults have demonstrated that moment-to-moment variability is not just noise as previously assumed, but is higher in better performing, younger adults compared to lower performing, elderly subjects (Garrett et al., 2013a, 2014; Grady and Garrett, 2014). Findings in other modalities such as electroencephalography (EEG) (McIntosh et al., 2008; Lippé et al., 2009) and magnetoencephalography (MEG) (Misić et al., 2010) support those findings, suggesting lower brain variability in children compared to young adults. Moment-to-moment BOLD signal fluctuations have been shown to be altered in multiple neuropsychiatric disorders such as autism (Di Martino et al., 2014; Lai et al., 2010), Alzheimer's disease (Zhao et al., 2014; Liu et al., 2014; Han et al., 2011; Xi et al., 2012) and attention deficit hyperactivity disorder (Zang et al., 2007), as well as schizophrenia (Yu et al., 2014; Yang et al., 2014; Liu et al., 2016). The strong relationship of BOLD signal variability with age and cognitive performance make this approach especially promising to obtain further insight in the mechanisms driving the development of cognitive and psychiatric disorders.

Rs-fMRI has been widely used in recent years to analyze altered brain function in numerous psychiatric diseases. It is especially advantageous when studying populations with limited abilities to respond to task, such as young children or individuals with impaired cognitive functions and attention deficits. Most rs-fMRI studies focus on stationary functional connectivity, assessed by computing the temporal correlation between the BOLD signals of different brain regions computed over the whole resting-state session. However, conventional functional connectivity is normalized for BOLD signal variance. In other words, the Pearson correlation coefficient is scaled with respect to individual signal standard deviation and BOLD signal variability might even confound results of functional connectivity (Garrett et al., 2013b). For instance, lower functional connectivity might result from higher variance, or oppositely, lower variance might have weakened the effect of functional connectivity reduction.

Chromosome 22q11.2 deletion syndrome (22q11DS) is a neurodevelopmental disorder caused by a microdeletion in chromosome 22. It occurs in approximately 1 out of 4000 live births and comes with a vast phenotype that includes somatic, cognitive and psychiatric features (Oskarsdóttir et al., 2004). Amongst others, patients with 22q11DS suffer from a

Journal Article

wide range of cognitive impairments, including mild mental delay and impaired executive functions (Maeder et al., 2016; Antshel et al., 2008; Niklasson and Gillberg, 2010; Swillen et al., 1997). Furthermore, 22q11DS comes with a very high risk of developing schizophrenia, which occurs in 30 % to 40 % of patients (Lewandowski et al., 2007; Murphy et al., 1999; Schneider et al., 2014). The developmental characteristics of the disease and the high risk of psychotic symptoms makes 22q11DS a unique model for the study of behavioral, clinical and neural markers in schizophrenia in order to improve treatments and prevention (Bassett and Chow, 1999).

In 22q11DS, to date, several studies have analyzed functional connectivity during rest (Debbané et al., 2012; Padula et al., 2015; Scariati et al., 2014; Schreiner et al., 2014; Mattiaccio et al., 2016). They have revealed altered connectivity in multiple resting-state networks (RSNs) such as the visuospatial, sensory-motor and default mode networks. Two of the studies (Padula et al., 2015; Schreiner et al., 2014) specifically focused on connectivity of the default mode network (DMN), a RSN that has been associated with self-referential, autobiographical mental processes and social cognition (Greicius et al., 2003; Fair et al., 2008; Qin and Northoff, 2011). They revealed decreased connectivity in 22q11DS, especially between anterior-posterior regions (Schreiner et al., 2014; Padula et al., 2015). Alterations within the DMN have furthermore been associated with dysfunctional social behavior (Schreiner et al., 2014) as well as psychotic symptoms (Debbané et al., 2012; Mattiaccio et al., 2016).

To our best knowledge, no studies to date have investigated BOLD signal variability in 22q11DS. Given its link to development and cognition, we hypothesize that BOLD signal variability is broadly altered in 22q11DS and that it is increasing during development from child- to adulthood. We used the BOLD signal standard deviation (SD_{BOLD}) to measure brain variability. We then employed multivariate partial least squares (PLS) correlation (Krishnan et al., 2011; McIntosh et al., 2004) in order to identify multivariate brain variability alterations and developmental characteristics in our 22q11DS cohort compared to controls. PLS correlation is better suited for voxelwise brain analysis than mass-univariate approaches, as they assume independence between all voxels (a hypothesis which is obviously wrong in the brain) and are thus very limited by the problem of multiple comparisons. PLS correlation measures multivariate relationship between two sets of variables (here: voxelwise SD_{BOLD} on one side and a combination of subject-specific design variables, i.e. diagnosis, age and age by diagnosis interaction, on the other side). Its second advantage in addition to multivariability of the brain pattern is thus the possibility to investigate the relationship of brain data with multiple external variables at the same time. We secondly hypothesize that conventional functional connectivity analysis might be influenced by BOLD variation, as Pearson correlation is normalized for standard deviation. To obtain an insight on possible links between functional connectivity and brain variability, we selected a seed inside the posterior cingulate cortex (PCC) and analyzed brain-wide seed-to-voxel connectivity. The PCC was selected as it is a central hub inside the DMN, one of the best studied RSN (Greicius et al., 2003; Fair et al., 2008; Menon and Uddin, 2010). It additionally appeared as a region of strongly decreased SD_{BOLD} variability during the first analysis. We used the same PLS approach as before to identify multivariate alterations and age-relationship of PCC functional connectivity. In a last step we

3.1. Journal Article: Disentangling BOLD variability and PCC functional connectivity

identified regions where both functional connectivity and BOLD signal variance were altered in our cohort. In those regions, SD_{BOLD} might confound or even drive functional connectivity alterations. Thus, we compared the direction of alteration of both measures in those regions, in order to obtain a first insight in the relationship between BOLD variability and functional connectivity.

3.1.2 Methods

Participants

Fifty patients with 22q11DS aged between 9 and 25 (M/F = 21/29, mean age = 16.53 ± 4.25 years) were included in the study (see table 3.1). The control group comprised fifty healthy subjects in the same age range (M/F = 22/28, mean age = 16.44 ± 4.20 years). Healthy controls (HCs) were recruited amongst siblings of our patients and through the Geneva state school system.

From our initial sample of 110 patients and 75 HCs between 9 and 25 years old, a total of 85 participants had to be excluded to ensure the good quality of the data. Five subjects (only patients) were excluded because they reported having fallen asleep during the scanning session. Another 34 subjects (5 HCs) had to be excluded due to excessive motion of more than 3 mm in translation or 3° in rotation and the data of 35 more subjects (19 HCs) were not used because parts of the cortex were not captured. From the remaining dataset, 11 more participants (1 HCs) were excluded after motion scrubbing (Power et al. 2012, see paragraph *Preprocessing*) as less than 100 rs-fMRI scans, corresponding to 4 min of scanning time, had a framewise displacement below the threshold of 0.5 mm. Table 3.2 shows a summary of motion data within the two groups.

Written informed consent was received from participants and their parents (for subjects younger than 18 years old). The research protocols were approved by the Institutional Review Board of Geneva University School of Medicine. The cohort is partly overlapping with our previous rs-fMRI studies: 33 subjects (15 HCs) have been also included in Debbané et al. (2012), 52 subjects (27 HCs) in Scariati et al. (2014), and 57 subjects (32 HCs) in Padula et al. (2015).

Image acquisition

Structural and functional MRI data were acquired at the Centre d'Imagerie BioMédicale (CIBM) in Geneva on a Siemens Trio (N = 78) and a Siemens Prisma (N = 22) 3 Tesla scanner. Anatomical images were acquired with a T1-weighted sequence of $0.86 \times 0.86 \times 1.1 \text{ mm}^3$ volumetric resolution (192 slices, TR = 2500 ms, TE = 3 ms, acquisition matrix = 224×256 , field of view = 22 cm^2 , flip angle = 8°), and functional images with a T2-weighted sequence of 8 minutes (voxel size = $1.84 \times 1.84 \times 3.2 \text{ mm}$, 38 slices, TR = 2400 ms, TE = 30 ms, flip angle = 85°). For the rs-fMRI session, participants were asked to fix a cross projected on a screen, let their minds wander while not thinking of anything in particular and not to fall asleep.

Table 3.1 – Demographic information.

	HCS	22q11DS	p value
Number of subjects (M/F)	50 (22/28)	50 (21/29)	0.910
Age mean \pm SD	16.44 \pm 4.20	16.53 \pm 4.25	0.840
(range)	(9.5-24.9)	(9.0-24.8)	
Right handed*	71.43 %	80.95%	
IQ**	109.68 \pm 12.99	68.20 \pm 12.21	<0.001
N. subjects meeting criteria for psychiatric diagnosis	N/A	27 (54 %)	
Anxiety disorder	N/A	8	
Attention deficit hyperactivity disorder	N/A	2	
Mood disorder	N/A	4	
Schizophrenia	N/A	1	
More than one psychiatric disorder	N/A	12	
N. subjects medicated	0	14	
Methylphenidate	0	8	
Antipsychotics	0	2	
Anticonvulsants	0	1	
More than one class of medication	0	3	

* Handedness was measured using the Edinburgh laterality quotient, right handedness was defined by a score of more than 50. ** IQ was measured using the Wechsler Intelligence Scale for Children–III (Wechsler, 1991) for children and the Wechsler Adult Intelligence Scale–III (Wechsler, 1997) for adults.

Preprocessing

Figure 3.1 shows a graphical overview on our complete analysis, including rs-fMRI preprocessing steps. The rs-fMRI scans were preprocessed using statistical parametric mapping (SPM12) (Wellcome Trust Centre for Neuroimaging, London, UK: <http://www.fil.ion.ucl.ac.uk/spm/>). We adapted the pipeline of our previous studies (Richiardi et al., 2012; Scariati et al., 2014) and utilized functions of the data processing assistant for resting-state fMRI (DPARSF) (Yan Chao-gan, 2010) and individual brain atlases using statistical parametric mapping (IBASPM) (Aleman-Gomez et al., 2006) toolboxes. Functional images were realigned and spatially smoothed with an isotropic Gaussian kernel of 6 mm full width half maximum (FWHM). Structural scans were coregistered to the functional mean and segmented with the SPM12 *Segmentation* algorithm (Ashburner and Friston, 2005). A study-specific template was generated using diffeomorphic anatomical registration (DARTEL) (Ashburner, 2007). After initial preprocessing, the voxelwise time series were extracted in individual subject space, excluding

3.1. Journal Article: Disentangling BOLD variability and PCC functional connectivity

Table 3.2 – fMRI – functional magnetic resonance imaging motion parameters. FD – framewise displacement.

		HCS	22q11DS	p value	correlation with age (p value)
Mean translation (mm)	x	0.13±0.13	0.12±0.14	0.7411	0.04 (0.6851)
	y	0.19±0.14	0.18±0.18	0.8446	0.03 (0.7994)
	z	0.31±0.29	0.39±0.34	0.1670	-0.10 (0.3222)
Mean rotation (degree)	r_x	0.34±0.27	0.39±0.30	0.3149	-0.04 (0.7260)
	r_y	0.20±0.17	0.18±0.14	0.6221	-0.14 (0.1661)
	r_z	0.17±0.17	0.19±0.19	0.5786	-0.05 (0.6430)
Mean FD (mm), before scrubbing		0.16±0.10	0.22±0.11	<0.001	-0.20 (0.046)
Mean FD (mm), after scrubbing		0.14±0.05	0.17±0.06	0.002	-0.14 (0.1560)

the first five time points, and the voxelwise time series were filtered with a bandwidth of 0.01 Hz to 0.1 Hz. Then, we applied motion scrubbing (Power et al., 2012) to correct for motion artifacts. Frames with high motion were marked according to the framewise displacement, which was calculated as the sum of the absolute values of the six realignment parameters (Power et al., 2012). Scans with a framewise displacement of more than 0.5 mm, as well as one scan before and two scans after, were excluded from the analysis.

BOLD signal variability

Voxelwise signal variability was determined by calculating the standard deviation (SD_{BOLD}) of preprocessed time series in subject space. According to Parseval's theorem, this approach is equivalent to the frequency-domain computation of the amplitude of low-frequency fluctuations (ALFF) at 0.01 Hz to 0.1 Hz.

Voxelwise BOLD variability maps were z-scored and warped to the study-specific DARTEL template by means of the nonlinear flow fields that were previously generated by the algorithm. We made the choice to apply spatial normalization on the variability maps, rather than the rs-fMRI data beforehand, as in this way voxel-wise measures such as ALFF are less affected by the spatial distortions (Wu et al., 2011).

Seed-based DMN functional connectivity

For DMN connectivity analysis, a seed region of $7 \times 7 \times 11 \text{ mm}^3$ was placed in the PCC at MNI coordinates [0, -56, 26] (Karahanoğlu et al., 2015) and spatially transformed into the common space the study-specific DARTEL template. The seed region was then mapped into individual subject space and seed functional connectivity maps were calculated by computing

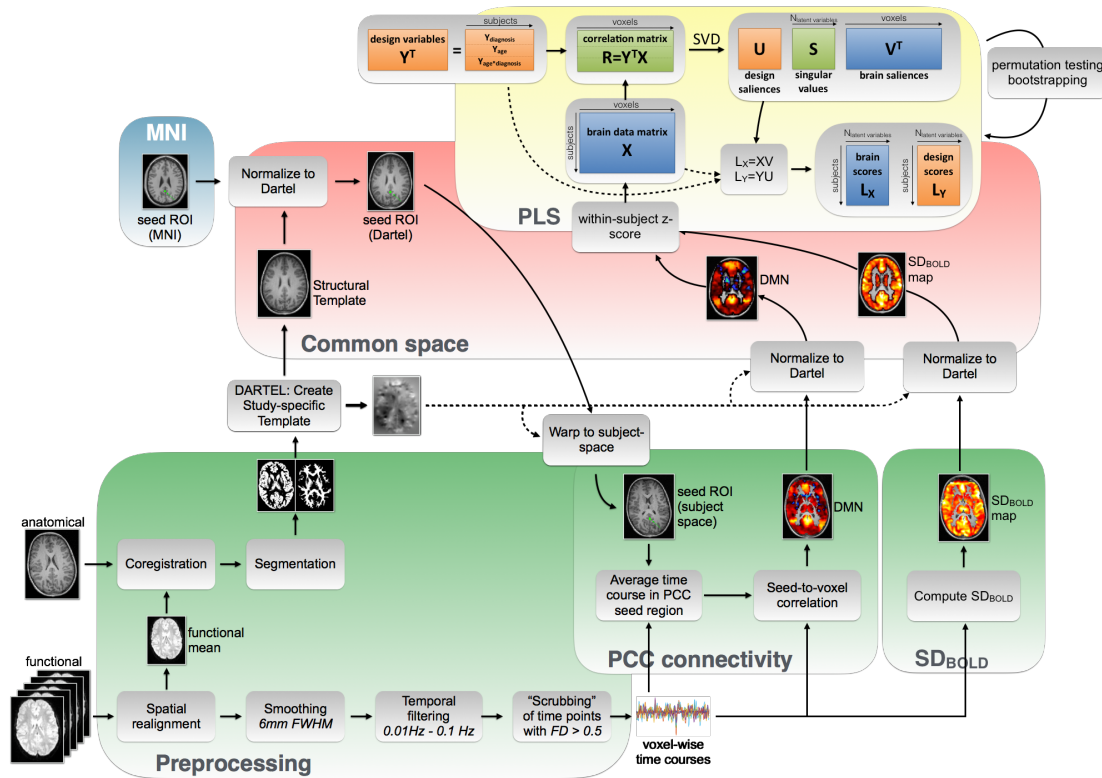


Figure 3.1 – Processing pipeline including preprocessing, computation of SD_{BOLD} and PCC connectivity, spatial normalization to a study-specific template created with DARTEL and PLS correlation analysis.

the Pearson correlation coefficient of every voxel time course with the average time course inside the seed region. Voxelwise seed functional connectivity maps were z-scored for every subject and warped to the study-specific DARTEL template.

PLS correlation analysis

We applied PLS correlation (Krishnan et al., 2011; McIntosh and Lobaugh, 2004) to reveal alterations related to diagnosis and the relationship between brain measures and age. In the following, we are going to refer to subject-specific design variables (see also figure 3.1, yellow box).

For the current study, we included a variable corresponding to diagnosis (1 for HCs, -1 for 22q11DS), age and age by diagnosis interaction as design variables in the PLS correlation analysis. As there were no significant effects of gender and its interaction with diagnosis when included in the analysis, here we only show the results for age and diagnosis. Only voxels with a probability higher than 0.5 of laying inside the gray matter of the study-specific DARTEL template were considered as brain data input. Prior to the application of PLS correlation, subject-specific design variables and voxelwise brain data were z-scored across all subjects, as group information was already included in the first design variable.

3.1. Journal Article: Disentangling BOLD variability and PCC functional connectivity

The first step of PLS correlation is the computation of the correlation matrix $\mathbf{R} = \mathbf{X}^T \mathbf{Y}$ between a matrix of voxel data per subject \mathbf{X} and a number of subject-specific design variables \mathbf{Y} . Here, we included the three design variables diagnosis, age and their interaction. Then, the singular value decomposition (SVD) of $\mathbf{R} = \mathbf{U} \mathbf{S} \mathbf{V}^T$ produced three latent variables (LVs). Every LV is associated with 1) a singular value (diagonal elements of \mathbf{S}) indicating the correlation explained by that LV, 2) a vector of three left singular values \mathbf{U} , also called design saliences, and 3) a vector of right singular values \mathbf{V} , also called brain saliences or voxel saliences. The design saliences \mathbf{U} indicate how strong each one of the three design variables contributes to the brain-design correlation explained by this LV. Similarly, the brain saliences \mathbf{V} express how strong every voxel contributes to the brain-design correlation explained by this LV. Then, the projection of every subject's original brain data (in \mathbf{X}) onto the multivariate brain salience pattern (in \mathbf{V}) produces so-called "brain scores" $\mathbf{L}_X = \mathbf{X} \mathbf{V}$. Those brain scores give a measure on the similarity of a subject's individual brain data with the salient brain pattern. Similarly, so-called "design scores" can be computed by $\mathbf{L}_Y = \mathbf{Y} \mathbf{U}$, which are a projection of every subject's design variables onto the respective design saliences.

In order to determine whether the explained correlation of every LV was significant, we applied permutation testing using 1000 permutations to determine the null distribution of the singular values. We applied Bonferroni correction for multiple comparisons when testing for significance of the three LVs. A LV was considered significant if the singular value was higher than 98.3 % of its null distribution ($p=0.017$). If a LV was significant, we furthermore evaluated the robustness of brain and design saliences using a bootstrapping procedure with 500 random samples with replacement. Brain and design saliences were re-calculated for every bootstrap sample, resulting in a typical bootstrap distributing of the salience values. The division of the mean of this distribution by its standard deviation gives bootstrap scores for every voxel respectively design variable. Those bootstrap scores indicate the robustness of a voxel's response; i.e., its contribution to the voxelwise brain-behavior correlation and can be interpreted similarly to z-scores (Krishnan et al., 2011). In the results, we show the brain patterns of bootstrap scores thresholded at absolute values greater than 3.00, which corresponds to a robustness at a confidence level of approximately 99 % (Garrett et al., 2013a). As there are only three design saliences per LV, a more detailed visualization than for the brain saliences is possible and we show the design salience bootstrap means as bar plots with error bars according to the bootstrap standard deviations.

Group-wise correlation of brain scores with age

In order to provide an alternative visualization of the results captured in the design saliences, we computed the correlation between brain scores and age in every group separately. In the results section, we plot the group-wise brain scores and their age-relationship in addition to the design saliences to facilitate the interpretation of those. P-values of the group-wise correlations were determined within the permutation loop during PLS correlation analysis.

Comparing brain salience patterns

In order to reveal similarities and differences in the patterns of voxel salience bootstrap scores in SD_{BOLD} and PCC connectivity, we computed a joint map according to the magnitude and sign of the two brain maps. All voxels where the root mean square of bootstrap scores in both maps exceeded 3 were included into the joint map. Remaining voxels were colored according to the angle between SD_{BOLD} bootstrap scores and PCC connectivity bootstrap scores. This allowed us to combine the following cases in one single map: 1) Areas where either *only* SD_{BOLD} or *only* PCC connectivity are altered, color-coded according to the direction of that alteration (four cases: only SD_{BOLD} higher/lower, only PCC connectivity higher/lower). 2) Areas where *both* SD_{BOLD} and functional connectivity are altered, color-coded according to the direction of that alteration (four cases: both higher, both lower, SD_{BOLD} higher and PCC connectivity lower, SD_{BOLD} lower and PCC connectivity higher).

3.1.3 Results

PLS correlation analysis of voxelwise SD_{BOLD} resulted in two significant LVs. The first significant LV ($p < 0.001$) captured mainly effects of diagnosis of the SD_{BOLD} -design correlation, the corresponding brain saliences can thus be interpreted similarly to a multivariate contrast between patients and controls. The second significant LV ($p = 0.001$) captured mainly age-effects in the SD_{BOLD} -design relationship and almost no effect of diagnosis. The corresponding brain saliences thus represents voxels which are strongly correlated with age in both groups.

PLS correlation analysis of seed-to-voxel PCC connectivity resulted in only one significant LV ($p < 0.001$) which captured both a strong effect of diagnosis *and* age. The corresponding brain salience pattern shows thus voxels which are different in patients compared to controls, but where PCC connectivity is also correlated with age in both groups.

In the following section, we show the PLS correlation results for SD_{BOLD} and PCC connectivity in more detail. The first subsection describes results obtained in SD_{BOLD} , the second subsection describes results obtained in PCC connectivity and in the third subsection, we provide a comparison of the two previous results by showing an overview on the similarities and differences between the brain salience patterns of the first (mainly diagnosis-related) LV of SD_{BOLD} and the first (both diagnosis- and age-related) LV of PCC connectivity.

SD_{BOLD}

In this subsection, we first show the average SD_{BOLD} maps in our cohort, then describe the first (mainly diagnosis-related) significant LV that results from the PLS correlation analysis of SD_{BOLD} , and conclude with a description of the second (mainly age-related) significant LV.

SD_{BOLD} : average across all subjects Figure 3.2 shows the average SD_{BOLD} across all subjects. SD_{BOLD} is very strong in medial regions of the DMN, such as the PCC, precuneus and the medial prefrontal cortex. There was no significant group difference in the within-subject average SD_{BOLD} which was subtracted during z-scoring (two sample t-test, $p = 0.195$).

SD_{BOLD} : LV1 reflects a main effect of diagnosis Figures 3.3a to 3.3c show brain and design saliences corresponding to the first significant LV ($p < 0.001$) for PLS correlation analysis of

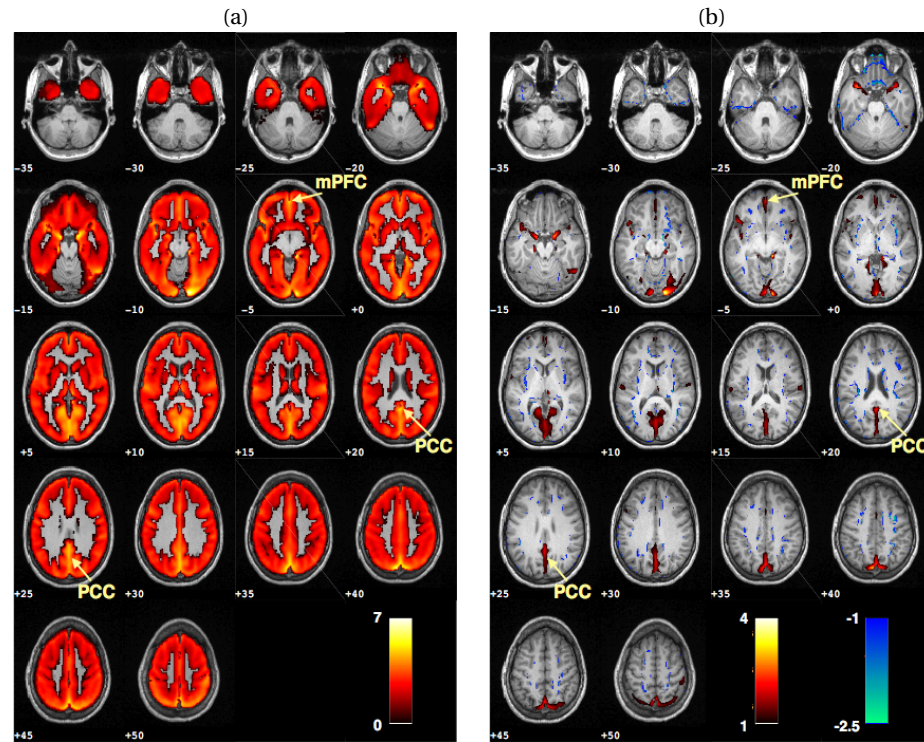


Figure 3.2 – Average SD_{BOLD} in gray matter, (a) original values (b) within-subject z-scores. mPFC - medial prefrontal cortex; PCC – posterior cingulate cortex.

SD_{BOLD} . There is a very strong effect of diagnosis (design salience 0.96 ± 0.04) a small negative effect of age (design salience -0.16 ± 0.08), as well as a negative effect of age by diagnosis interaction (design salience -0.23 ± 0.07).

Correlation plots of brain scores with age are shown on figure 3.3b. In HCs, brain scores are significantly negatively correlated with age ($\rho = -0.58$, $p = 0.001$), whereas in the patients group there is no significant correlation ($\rho = 0.09$, $p = 0.626$). This means that in brain areas with positive resp. negative bootstrap scores (red resp. blue), SD_{BOLD} is negatively resp. positively correlated with age in controls but not in patients.

Due to the high diagnosis salience, the corresponding pattern of brain salience bootstrap scores (see figure 3.3c) can be interpreted as a multivariate contrast showing areas of higher (red) and lower (blue) SD_{BOLD} in 22q11DS. Reduced SD_{BOLD} can be found in regions of the DMN such as PCC, lateral parietal and medial prefrontal cortices, as well as in the dorsal anterior cingulate and the dorso-lateral prefrontal cortices. SD_{BOLD} is bilaterally elevated in the inferior temporal cortex including parahippocampus, in the superior temporal gyrus and in caudate.

SD_{BOLD} : LV2 reflects a main effect of age Brain and design saliences of the second significant LV ($p = 0.001$) are shown on figures 3.3d to 3.3f. There are a strong age effect (design salience 0.99 ± 0.07) and a small effect of diagnosis (design salience 0.16 ± 0.09). However, no significant effect of age by diagnosis interaction appeared (design salience -0.01 ± 0.14).

Group-wise correlation analysis between brain scores and age (see figure 3.3e) shows strong correlation values in both groups, as was expected based on the high age salience without interaction salience. Overall brain scores are slightly higher in patients (small diagnosis salience).

Due to the high age salience, the corresponding pattern of brain salience bootstrap scores (see figure 3.3f) contains the voxels where SD_{BOLD} is strongly correlated with age in both patients and controls. SD_{BOLD} increases over age in the dorsal anterior cingulate cortex, superior frontal cortex, as well as parts of thalamus. Small clusters with decreasing SD_{BOLD} are located in the anterior cingulate and orbitofrontal cortices.

PCC functional connectivity

This subsection begins with the average PCC connectivity maps, followed by a description of the only significant (both diagnosis- and age-related) significant LV resulting from PLS correlation analysis of PCC connectivity.

PCC connectivity: average across all subjects Figure 3.4 shows the average PCC connectivity across all subjects. As expected regions of the DMN are strongly positively correlated with the PCC, while there is a weaker, negative correlation with regions of the frontoparietal network, consisting of lateral frontal and parietal regions. There was no significant group difference in the within-subject average connectivity which was subtracted z-scoring (two sample t-test, $p=0.959$).

PCC connectivity: LV1 reflects effects of both diagnosis and age The brain bootstrap scores as well as the corresponding design saliences for the first significant LV ($p<0.001$) are shown on figures 3.5a to 3.5c. There is a very high effect of diagnosis (design salience 0.91 ± 0.06) meaning that corresponding brain voxel saliences can be interpreted as a multivariate pattern of altered DMN connectivity in 22q11DS. Additionally, there is a moderate negative effect of age (design salience -0.38 ± 0.08) and a small interaction between age and diagnosis (design salience 0.16 ± 0.08).

As already indicated by the design saliences, group-wise correlation of brain scores with age (see figure 3.5b) shows that brain scores are significantly negatively correlated with age in both groups, but the negative correlation is stronger in patients (small interaction effect).

Due to the high diagnosis salience value, the corresponding pattern of brain salience bootstrap scores (see figure 3.5c) can be interpreted as a multivariate contrast showing areas of higher (red) and lower (blue) PCC connectivity in 22q11DS. The negative age salience indicates that PCC connectivity in the brain salience pattern is furthermore negatively (red) and positively (blue) correlated with age.

Regions of elevated PCC connectivity in patients include the middle frontal and inferior parietal cortices, regions of the frontoparietal or central executive network which is in fact negatively correlated with the DMN. Thus, we can derive that the anti-correlation between the PCC and the frontoparietal network is weaker in 22q11DS.

Reduced PCC connectivity can be observed in the medial prefrontal cortex, confirming

3.1. Journal Article: Disentangling BOLD variability and PCC functional connectivity

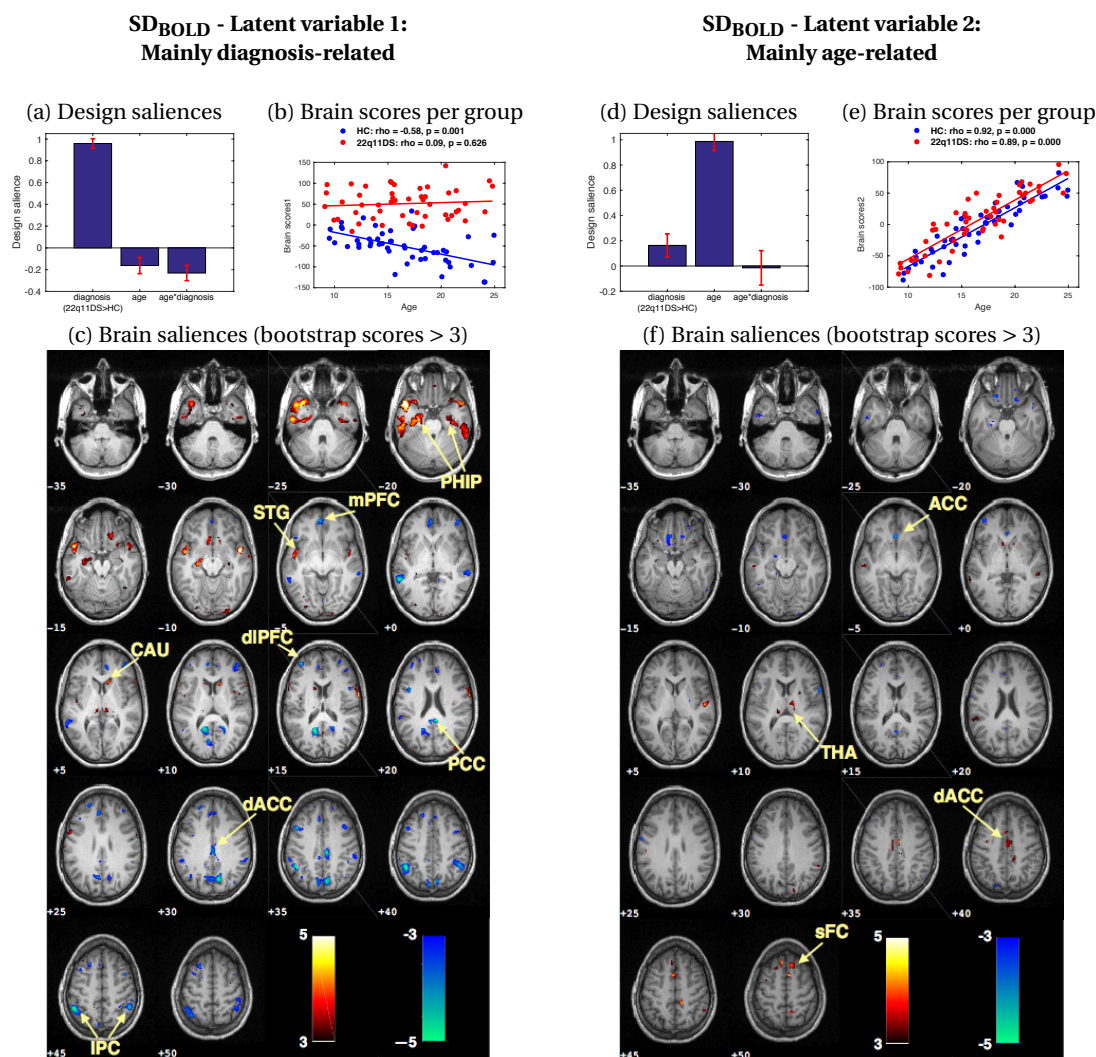


Figure 3.3 – SD_{BOLD}: PLS correlation analysis results in two significant LVs. Left column: (a) The design saliences of the first LV reveal a strong effect of diagnosis, almost no age effect and a negative age by diagnosis effect. (b) Separate correlation of brain scores with age in every group gives an alternative view of those results: Brain scores are higher in 22q11DS (diagnosis-effect) and are negatively correlated with age in HCs but not in 22q11DS (negative age- and interaction-effects). (c) The first pattern of brain saliences can thus be interpreted as multivariate contrast. Areas with robustly lower SD_{BOLD} in 22q11DS (blue) are mainly part of the DMN (PCC, IPC, mPFC), and also include medial (dACC) and lateral prefrontal (dlPFC) regions. Clusters with robustly higher SD_{BOLD} (red) are located in the inferior temporal lobes including PHIP, as well as in the STG and CAU. Right column: (d) The design saliences of the second LV reveal a strong age-effect across all subject, as well as a small effect of diagnosis, but no interaction. (e) Separate correlation between brain scores and age in every group shows again the strong relationship with age in both controls and patients. Brain scores are slightly higher in patients, as already indicated by the small positive diagnosis design salience. (f) The second pattern of brain saliences shows thus voxels which are robustly correlated with age in both groups. Regions with positive age-relationship (red) are located in THA, dACC and the sFC, while in a small cluster in the ACC (blue), SD_{BOLD} is negatively correlated with age. ACC - anterior cingulate cortex; CAU - caudate; dACC - dorsal ACC; dlPFC - dorso-lateral prefrontal cortex; IPC - inferior parietal cortex; mPFC - medial prefrontal cortex; PCC - posterior cingulate cortex; PHIP - parahippocampus; sFC - superior frontal cortex; STG - superior temporal gyrus; THA - thalamus.

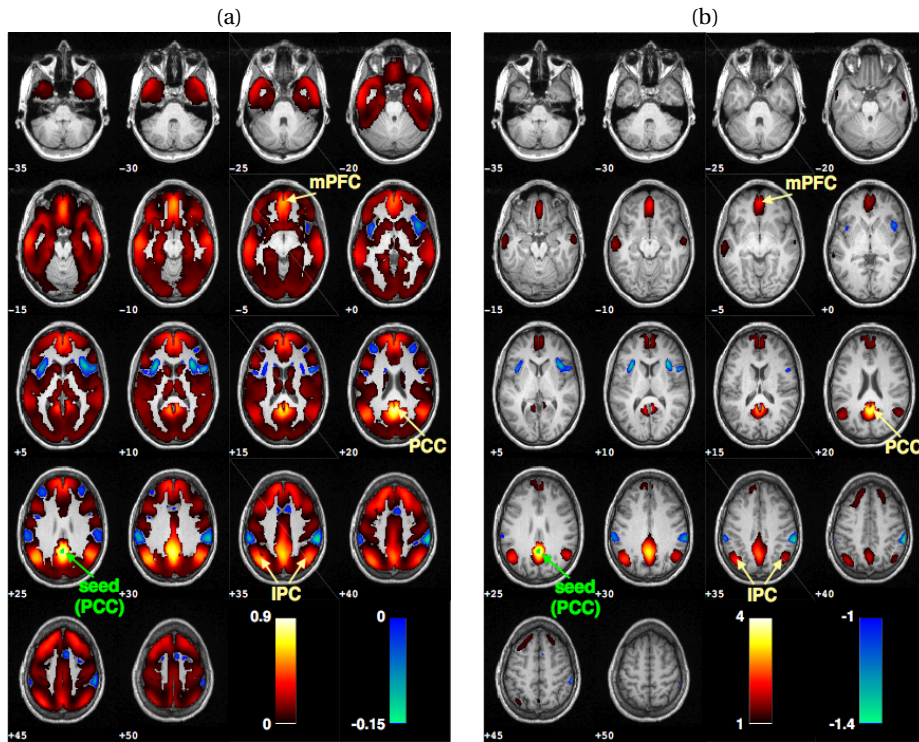


Figure 3.4 – Average PCC connectivity, (a) original values (b) within-subject z-scores. IPC - inferior parietal cortex; mPFC - medial prefrontal cortex; PCC - posterior cingulate cortex; seed - region of interest in the posterior cingulate cortex.

previous observations on long-range anterior-posterior DMN dysconnectivity (Schreiner et al., 2014; Padula et al., 2015). PCC functional connectivity towards the anterior cingulate cortex and posterior insula, areas of the salience network, is also lower in 22q11DS.

Comparison of SD_{BOLD} and PCC connectivity alterations

The first LV has a strong diagnosis salience in both SD_{BOLD} and PCC connectivity. In order to compare the two patterns of alterations in 22q11DS, we computed the joint map between the brain salience bootstrap score maps of the two measures (see figure 3.6). In some regions either only SD_{BOLD} or only PCC connectivity are altered. Most areas in the inferior temporal lobe have only higher SD_{BOLD} while PCC connectivity is not altered (red), while in the gyrus rectus only PCC connectivity is altered. In medial regions of the DMN (precuneus and medial prefrontal cortex) and in the middle temporal gyrus, both measures are reduced. Interestingly there are no areas where both measures are significantly elevated in 22q11DS. In the frontoparietal network, SD_{BOLD} is lower and PCC connectivity higher in 22q11DS (bluish green). As stated in the previous paragraph, PCC connectivity in those areas has negative values; higher connectivity thus indicates a weaker correlation. Interestingly, in most regions where both measures are altered, SD_{BOLD} is reduced. Elevated SD_{BOLD} seemingly has not driven any reductions in PCC functional connectivity.

3.1. Journal Article: Disentangling BOLD variability and PCC functional connectivity

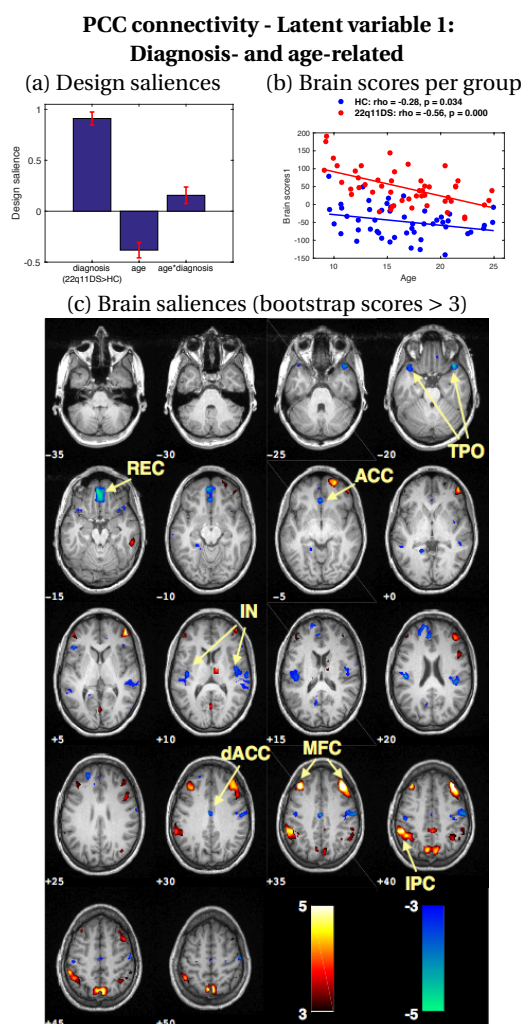


Figure 3.5 – PCC connectivity: PLS correlation analysis results in one significant LV. (a) The design saliences of the LV reveal a strong positive effect of diagnosis, as well as a moderate negative age-effect and a small positive effect of interaction. (b) Separate correlation of brain scores with age in every group gives an alternative view on those results: Brain scores are higher in 22q11DS (diagnosis-effect) and are negatively correlated with age (negative age-effect) in both groups. The correlation is stronger in patients than in controls (interaction-effect) (c) The pattern of brain saliences can thus be interpreted as areas of higher (red) and lower (blue) PCC connectivity in 22q11DS, where PCC connectivity is also negatively (red) and positively (blue) correlated with age. PCC connectivity in 22q11DS is higher (red) in the frontoparietal network (IPC and MFC). PCC connectivity in 22q11DS is lower (blue) in the posterior insula and the ACC, as well as in the TPO and REC. ACC - anterior cingulate cortex; dACC - dorsal ACC; IN - insula; IPC - inferior parietal cortex; MFC - middle frontal cortex; REC - gyrus rectus; TPO - temporal poles.

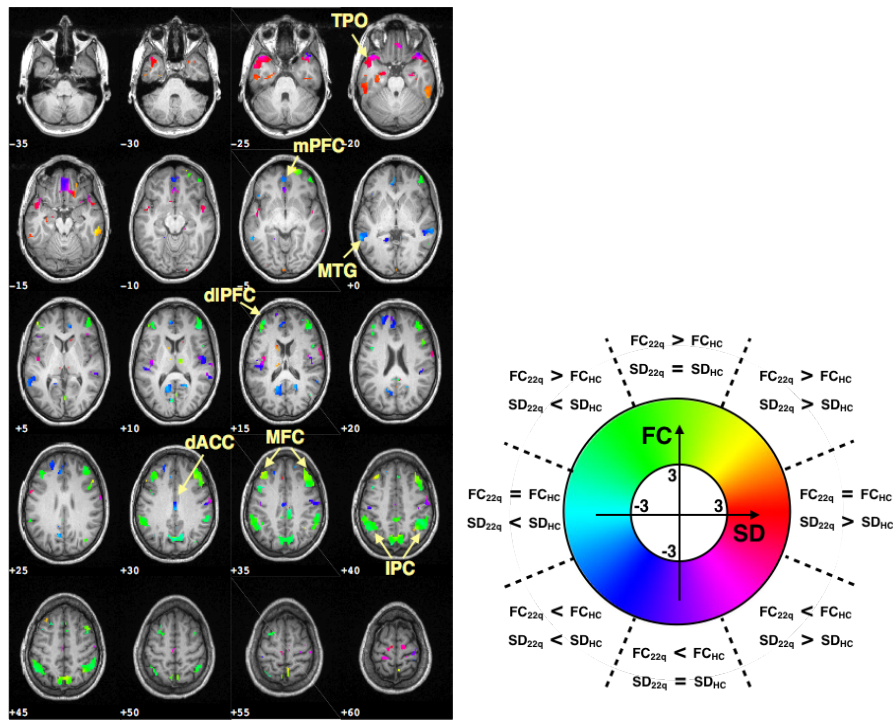


Figure 3.6 – Joint map between SD_{BOLD} LV1 bootstrap scores (see figure 3.3c) and PCC connectivity LV1 bootstrap scores (see figure 3.5c). Color codes indicated whether only one measure is altered in 22q11DS or both and in which direction. In the frontoparietal network, SD_{BOLD} is lower and PCC connectivity higher in 22q11DS (bluish green). In medial regions of the DMN (mPFC, precuneus) both are reduced. Interestingly, in areas with elevated SD_{BOLD} (inferior temporal lobe), PCC connectivity is mostly not altered. IPC - inferior parietal cortex; dACC - dorsal anterior cingulate cortex; dIPFC - dorso-lateral prefrontal cortex; MFC - middle frontal cortex; mPFC - medial prefrontal cortex; MTG - middle temporal gyrus; TPO - temporal poles; FC – functional connectivity; SD_{BOLD} – BOLD signal standard deviation.

3.1.4 Discussion

In the present study we employed multivariate PLS correlation to reveal altered brain function and age-relationship in 22q11DS. We used two different approaches to analyze resting-state BOLD signals: BOLD signal fluctuations assessed by the standard deviation of every voxel's temporal signal and seed-based functional connectivity between the PCC and the other brain voxels. With both approaches we were able to reveal multivariate patterns of altered brain function in 22q11DS. In both measures, the first significant LV was representing areas of altered brain function related to 22q11DS. In SD_{BOLD} , there was also an effect of age by diagnosis interaction in the first LV, suggesting an altered developmental trajectory of SD_{BOLD} in those areas. In SD_{BOLD} there was a second age-related brain pattern, which revealed the brain regions with the strongest age-relationship in both groups. The corresponding pattern was not overlapping with the pattern of the first LV and patients had the same developmental curve as controls in those areas. In PCC connectivity, the pattern of alterations corresponding to LV1

3.1. Journal Article: Disentangling BOLD variability and PCC functional connectivity

was also correlated with age, but PLS correlation revealed no separate age-related component as in SD_{BOLD} .

In the following, the two significant LVs for SD_{BOLD} and the only significant LV for PCC connectivity will be discussed one after another. Finally, the relationship between SD_{BOLD} and functional connectivity will be examined on the basis of the comparison between the patterns of altered brain function.

SD_{BOLD} alterations in 22q11DS

To our best knowledge, this is the first study to date analyzing moment-to-moment BOLD signal variability in 22q11DS. During our first analysis we showed that z-scored SD_{BOLD} is altered in a broad pattern, showing both elevated and reduced SD_{BOLD} in patients with 22q11DS (LV1, see figure 3.3c). SD_{BOLD} is lower in large parts of the DMN including the medial prefrontal cortex, PCC, and lateral parietal cortex. A previous study on BOLD variability during task in healthy adults found decreased variability in an elderly, low performing group compared to young adults in a very similar set of brain regions (Garrett et al., 2011). Alterations in lateral parietal regions might be implicated in visuospatial processing difficulties of patients with 22q11DS (Gothelf et al., 2008), while the PCC and precuneus have been identified as structural and functional network hubs, associated with self-referential processes and theory of mind (Van Den Heuvel et al., 2013; Spreng et al., 2008). Another cluster of reduced SD_{BOLD} is located in the dorso-lateral prefrontal cortex, a region which is known to be structurally and functionally affected in schizophrenia (Jung et al., 2010; Sun et al., 2009; Karlsgodt et al., 2014). In 22q11DS, structural MRI studies have shown relative reductions of cortical volume and thickness in the parietal cortex, the dorso-lateral prefrontal cortex and along midline structures (Schmitt et al., 2015; Gothelf et al., 2008; Jalbrzikowski et al., 2013). The similarity to the here observed pattern of BOLD variability reductions suggests a link between altered cortical volume and BOLD signal variability alterations.

Additionally, we observed a significant relationship with age in regions with altered SD_{BOLD} in HCs, but not in the 22q11DS group (see figures 3.3a and 3.3b). More specifically, brain scores decrease over age in controls whereas in patients, they are not correlated with age. This observation suggests that elevated and reduced SD_{BOLD} might be caused by altered developmental trajectories in patients with 22q11DS. Developmental alterations in 22q11DS have already been observed in several other modalities (Schaer et al., 2009; Padula et al., 2015; Gothelf et al., 2008; Shashi et al., 2012; Jalbrzikowski et al., 2013), including deviant maturation curves of cortical thickness (Schaer et al., 2009) and structural connectivity (Padula et al., 2015).

SD_{BOLD} development

We furthermore showed that, in a different set of brain regions, SD_{BOLD} is strongly correlated with age, both in 22q11DS and HCs (LV2, see figure 3.3f). More specifically, BOLD variability increases with age in most of the regions showing a robust age-effect, namely thalamus, dorsal anterior cingulate and superior frontal cortex. In those regions, older subjects of our cohort

had higher SD_{BOLD} than children. In one cluster of the anterior cingulate cortex and bilaterally in the orbitofrontal cortex, SD_{BOLD} was robustly decreasing over age. Garrett et al. (2013b) suggested that brain signal variability follows an inverted U-shaped curve over life-span, increasing from child- to young adulthood and decreasing again with higher age. In the present study, we observed mainly increasing SD_{BOLD} from child- to young adulthood, a result which is in line with the previously stated hypothesis. However, Garrett et al. based their hypothesis within the age range from child- to adulthood only on task-based EEG (McIntosh et al., 2008; Lippé et al., 2009) and MEG studies (Misić et al., 2010). Here we provide additional information to those results in our cohort using rs-fMRI. Increasing variability suggests the transition towards a system of higher dynamic complexity that has greater adaptability, efficiency and dynamic range leading to enhanced cognitive function (Misić et al., 2010; Deco et al., 2011; Ghosh et al., 2008; Garrett et al., 2013b). Interestingly, the areas showing robust relationship with age are not overlapping with the pattern of SD_{BOLD} alterations. Patients have normally developing BOLD signal variability in those areas.

PCC connectivity alterations in 22q11DS

In order to compare the effects of BOLD signal variability with conventional functional connectivity, we studied seed-based connectivity within the DMN. The DMN is one of the most studied RSNs and two studies to date explicitly studied DMN functional connectivity in 22q11DS using different seed-based approaches (Schreiner et al., 2014; Padula et al., 2015). Padula et al. (2015) found reduced connectivity between anterior-posterior nodes of the DMN, as well as between right and left parietal lobes. Schreiner et al. (2014) used a very similar approach to ours in an independent sample, analyzing voxelwise connectivity of a seed placed in the PCC. They found globally lower within-DMN connectivity and higher connectivity between the PCC and the right inferior frontal gyrus.

In the present study we were able to confirm the lower anterior-posterior connectivity within the DMN between PCC and the medial prefrontal and left superior frontal cortices (LV1, see figure 3.5c). However, thanks to our multivariate approach, we obtained a much broader pattern of altered PCC connectivity. In particular, we found lower connectivity with the temporal poles, an effect that has also been observed in schizophrenia with a relationship to self-disturbance and hallucinations (Pankow et al., 2015).

Furthermore we observed weaker anti-correlation between the PCC and the frontoparietal network, a network playing a central role in working memory and attention. It has been proposed that switching between the DMN, the frontoparietal network and the saliency network is crucial for normal brain functioning and that dysconnectivity between those networks plays a central role in multiple psychopathologies (Menon, 2011; Menon and Uddin, 2010) and schizophrenia in particular (Hasenkamp et al., 2011).

Our observation on broad dysconnectivity between the DMN and frontoparietal network in our cohort of 22q11DS patients, supports the hypothesis of a strong implication in psychiatric disorders.

To date, only one study has analyzed the development of DMN connectivity over age

3.1. Journal Article: Disentangling BOLD variability and PCC functional connectivity

in 22q11DS (Schreiner et al., 2014), reporting increased long-range connectivity within the DMN in controls and abnormally increasing PCC connectivity with regions outside the DMN in patients. Our approach in the present study is complementary, as our PLS approach optimizes for a maximum age correlation in *all* subjects, independently of the diagnosis. The age-relationship of the mainly diagnosis-related LV1 supports increasing within-DMN connectivity. However, we did not observe any effect of interaction between age and diagnosis.

PCC connectivity development

In PCC connectivity, there was no significant second LV as in the analysis of SD_{BOLD} , indicating that all developmental effects of DMN connectivity were already explained by the first LV. In the first LV, PCC connectivity was correlated with age in both groups, but stronger in patients (see figures 3.5a and 3.5b). As most studies focus only on maturation effects *within* the DMN without taking into account the whole brain (for instance Sherman et al., 2014 and Supekar et al., 2010) those results are difficult to confirm and further analysis will be necessary to get more insight in the underlying effects.

Relationship of SD_{BOLD} and functional connectivity

Overall, we showed that alterations in SD_{BOLD} might be explained by altered developmental trajectories in 22q11DS, while in PCC connectivity both groups show a strong relationship with age. Furthermore, the second significant LV in SD_{BOLD} , which represents strong age-relationship in all subjects, is absent in PCC connectivity, suggesting that SD_{BOLD} is stronger implicated in development. These findings confirm existing literature emphasizing BOLD signal variability as a promising tool for the analysis of brain development and its alterations in neurodevelopmental disorders (Garrett et al., 2013b; McIntosh et al., 2010), which is complementary to functional connectivity analysis.

Furthermore, there is a close relationship between SD_{BOLD} and functional connectivity, as the standard deviation appears in the denominator of the Pearson correlation coefficient (Garrett et al., 2013b; Zalesky et al., 2012):

$$\rho_{xy} = \frac{\sum (x - \bar{x})(y - \bar{y})}{SD_x SD_y} \quad (3.1)$$

Thus, alterations of functional connectivity might actually be driven by alterations of covariance in the numerator or by variance in the denominator. In the present study we addressed this question based on the analysis of the DMN as one exemplary RSN. We showed that lower functional connectivity of the PCC is not driven by higher SD_{BOLD} , but that in the areas where both are altered, SD_{BOLD} is also lower and thus covariance has to be lower to an even stronger extent than the correlation. Future analysis including more RSNs and whole brain functional connectivity may give further insight into this question.

3.1.5 Methodological considerations

PLS correlation analysis

We employed multivariate PLS correlation analysis to investigate diagnosis-related alterations and the age-relationship of SD_{BOLD} and functional connectivity of the DMN. We chose this approach because conventional general linear model (GLM) analysis, and also other multivariate approaches such as multivoxel pattern analysis (MVPA) (De Martino et al., 2008) or multivariate distance matrix regression (MDMR) (Zapala and Schork, 2006) have the limitation that we obtain only one brain map per included regressor, which indicates how strong that regressor is related to the response variable (here SD_{BOLD}). PLS correlation instead searches to explain the most variance as possible between distributed patterns of brain data and a *combination* of regressors. Its great advantage compared to other multivariate approaches is thus the possibility to investigate the relationship of brain data with multiple external variables at the same time. Here, this approach allowed us to investigate alterations related to 22q11DS *and* developmental characteristics *at the same time*. However, the multivariability of both brain and design saliences also introduces challenges the interpretability of the results.

SD_{BOLD} and motion

In the analysis of functional connectivity, but even more in SD_{BOLD} , motion is a known issue, as high changes in the BOLD signal might be caused by sudden motion (Power et al., 2012, 2014). Clinical populations, such as our cohort of patients with 22q11DS who present both mental and psychiatric disorders, move more than healthy subjects. This makes it especially difficult to disentangle effects which are solely driven by motion. Here, we addressed this issue by excluding extreme motion outliers during preprocessing. After motion scrubbing, the framewise displacement was significantly higher in patients compared to controls, while the mean translation and rotation parameters did not differ between the groups. As this difference in motion is inherent to the clinical population under study, it is very difficult to obtain a perfect match between patients and controls without selecting a subpopulation of patients. Even though we applied strict motion correction, this effect presents still a limitation to our study. A more detailed analysis of the association between SD_{BOLD} and motion can be found in the Supplementary Material (Appendix A.1).

3.1.6 Conclusions and outlook

In this study we showed that BOLD signal variability is broadly altered in 22q11DS, strongest in regions of the DMN. We moreover observed that SD_{BOLD} is strongly related to age in a set of mainly subcortical brain regions. The locations and comparison to studies on BOLD variability during task suggest an implication of higher BOLD signal variability for better cognitive performance. However, further targeted studies including behavioral variables and task-based fMRI will be necessary to obtain a better understanding on the relationship on BOLD signal variability and behavior. Furthermore, we note that areas showing altered BOLD signal variability are reported to be also structurally affected in 22q11DS. The direct link between BOLD variance and brain anatomy should thus be subject to further analysis.

3.1. Journal Article: Disentangling BOLD variability and PCC functional connectivity

In an attempt to study the relationship between SD_{BOLD} and functional connectivity, we analyzed functional connectivity within the DMN and identified locations where functional connectivity might be confounded by brain variability. However, as we only studied connectivity of one seed region located in the PCC, the conclusions that can be driven are limited to this particular network. Further analysis should also include other RSNs or whole-brain connectivity approaches.

3.2 Journal Article: BOLD variability in patients with 22q11DS with psychotic symptoms

Postprint version of the article published in: Schizophrenia Research 2018, 193:319–328, <https://doi.org/10.1016/j.schres.2017.08.003>

Psychotic symptoms influence the development of anterior cingulate BOLD variability in 22q11.2 deletion syndrome.

Daniela Zöllner^{1,2,3}, Maria Carmela Padula³, Corrado Sandini³, Maude Schneider³, Elisa Scariati³, Dimitri Van De Ville^{1,2}, Marie Schaer³, Stephan Eliez³

¹Medical Image Processing Laboratory, Institute of Bioengineering, École Polytechnique Fédérale de Lausanne (EPFL), Lausanne, Switzerland; ²Department of Radiology and Medical Informatics, University of Geneva, Geneva, Switzerland; ³Developmental Imaging and Psychopathology Laboratory, Office Médico-Pédagogique, Department of Psychiatry, University of Geneva, Geneva, Switzerland

Chromosome 22q11.2 deletion syndrome (22q11DS) is a neurodevelopmental disorder associated with a broad phenotype of clinical, cognitive and psychiatric features. Due to the very high prevalence of schizophrenia (30-40 %), the investigation of psychotic symptoms in the syndrome is promising to reveal biomarkers for the development of psychosis, also in the general population. Since schizophrenia is seen as a disorder of the dynamic interactions between brain networks, we here investigated brain dynamics, assessed by the variability of blood oxygenation level dependent (BOLD) signals, in patients with psychotic symptoms. We included 28 patients with 22q11DS presenting higher positive psychotic symptoms, 29 patients with lower positive psychotic symptoms and 69 healthy controls between 10 and 30 years old. To overcome limitations of mass-univariate approaches, we employed multivariate analysis, namely partial least squares correlation, combined with proper statistical testing, to analyze resting-state BOLD signal variability and its age-relationship in patients with positive psychotic symptoms. Our results revealed a missing positive age-relationship in the dorsal anterior cingulate cortex (dACC) in patients with higher positive psychotic symptoms, leading to globally lower variability in the dACC in those patients. Patients without positive psychotic symptoms and healthy controls had the same developmental trajectory in this region. Alterations of brain structure and function in the anterior cingulate cortex (ACC) have been previously reported in 22q11DS and linked to psychotic symptoms. The present results support the implication of this region in the development of psychotic symptoms and suggest aberrant BOLD signal variability development as a potential biomarker for psychosis.

3.2. Journal Article: BOLD variability in patients with 22q11DS with psychotic symptoms

3.2.1 Introduction

Chromosome 22q11.2 deletion syndrome (22q11DS) is a neurodevelopmental disorder that comes with a vast cognitive and clinical phenotype (Oskarsdóttir et al., 2004; Maeder et al., 2016; Karayiorgou et al., 2010; McDonald-McGinn et al., 2015). The prevalence of schizophrenia in adult patients with the disorder is estimated at 30 % to 40 % (Murphy et al., 1999; Lewandowski et al., 2007; Schneider et al., 2014), which makes the deletion syndrome a model for the study of neurodevelopmental markers of psychosis and schizophrenia (Bassett and Chow, 1999).

Even though the exact neural mechanisms that may underlay the pathophysiology of psychosis and schizophrenia remain uncertain, schizophrenia is commonly seen as a disorder of functional network dysconnectivity rather than regionally specific pathophysiology (Friston et al., 1996; Friston, 1998). The recently proposed triple network model (Menon, 2011) sees mental disorders as a disruption of the interaction between three large scale brain networks in particular, namely the default mode network (DMN), the central executive network (CEN) and the salience network (SN). Findings in schizophrenia confirm and emphasize this hypothesis as a model for the disorder (Nekovarova et al., 2014). More precisely, structural and functional findings in the anterior cingulate cortex and the insula, two main regions of the SN (Nekovarova et al., 2014), suggest that disruptions in the SN mediate the altered relationship between DMN and CEN.

Since alterations in schizophrenia are obviously complex and more and more research confirms the impairment of brain dynamics in the disorder (Van Den Heuvel and Fornito, 2014), the investigation of brain dynamics in psychosis seems a promising approach when searching for neural correlates of its development. One simple approach to probe into dynamic brain function is moment-to-moment blood oxygenation level dependent (BOLD) signal variability (Garrett et al., 2013b). Even though it is not commonly considered in resting-state functional magnetic resonance imaging (fMRI) studies, its implication in development and cognitive performance suggests its importance for healthy brain function (Grady and Garrett, 2014). Indeed, higher temporal signal variability reflects a higher dynamic range and network complexity, which is crucial for the function of neural systems (Deco et al., 2009, 2011; Garrett et al., 2013b; McIntosh et al., 2010). Findings in electroencephalography (EEG), magnetoencephalography (MEG) and fMRI suggest that brain variability increases from child- to adulthood (McIntosh et al., 2008; Lippé et al., 2009; Misić et al., 2010; Miskovic et al., 2016; Zöller et al., 2017) and is reduced under anesthesia (Huang et al., 2016). Furthermore higher variability has been linked to better cognitive performance (Garrett et al., 2013a, 2014), cognitive flexibility (Armbruster-Genc et al., 2016) and better pain coping (Rogachov et al., 2016).

While there are several studies relating psychosis in 22q11DS to altered brain morphology and structural connectivity (Scariati et al., 2016a), only few investigated brain function in relationship to psychosis (Debbané et al., 2012; Mattiaccio et al., 2016; Scariati et al., 2014; Padula et al., 2017b; Tomescu et al., 2014). Two resting-state fMRI studies on whole brain functional connectivity linked increased DMN activity in 22q11DS to psychotic symptoms

(Debbané et al., 2012; Mattiaccio et al., 2016). Padula et al. (2017b) investigated functional connectivity within and between DMN, CEN and SN in 22q11DS, but did not find any significant relationship with psychotic symptoms. Using a multivariate approach, another resting-state fMRI study revealed a connectivity pattern that discriminated patients presenting prodromal positive symptoms (Scariati et al., 2014). The pattern included the anterior cingulate, right inferior frontal and left superior temporal cortices. Furthermore, an EEG study in patients with 22q11DS has linked altered SN function (i.e. the over-representation of EEG microstate C) to the presence of hallucinations (Tomescu et al., 2014; Britz et al., 2010).

While we already investigated BOLD signal variability alterations and development in 22q11DS (Zöllner et al., 2017), to date no study has revealed its relationship to psychotic symptoms in 22q11DS. Here, we employed partial least squares correlation (PLSC) (Krishnan et al., 2011) as a powerful multivariate approach to reveal alterations and age-relationship of BOLD variability related to psychotic symptoms in 22q11DS. We furthermore compared BOLD variability in patients with and without psychotic symptoms to healthy controls (HCs) to evaluate alterations intrinsic to the presence of psychotic symptoms.

3.2.2 Methods

Participants

In the present study, we included 57 patients with 22q11DS aged between 10 and 30 years and 69 HCs in the same age range. HCs were recruited amongst siblings of the patients and through the Geneva state school system. Within the group of patients with the microdeletion, psychotic symptoms were assessed using the structured interview of prodromal symptoms (SIPS) (Miller et al., 2003). Patients with a score of ≥ 3 in at least one of the positive SIPS sub-scales (i.e. Unusual Thought Content, Suspiciousness, Grandiosity, Hallucinations, and Disorganised Communication) were considered as having attenuated positive symptoms aside the criteria of frequency and duration (Fusar-Poli et al., 2013). Amongst the patients with 22q11DS, 28 patients were diagnosed with at least attenuated positive symptoms (PS+), while the remaining 29 had low positive symptoms scores (≤ 2) and were included in the PS- group. In the PS+ group, five patients were diagnosed with a psychotic disorder according to DSM-IV-TR criteria (see Supplementary Table A.3). For more detailed demographic information, see table 3.3. Written informed consent was received from participants and their parents (for subjects younger than 18 years old). The research protocols were approved by the Institutional Review Board of Geneva University School of Medicine. For a summary on criteria for the exclusion of subjects from our initial cohort and information on subjects included in our previous fMRI studies refer to Supplementary Materials (appendix A.2).

Image acquisition

All MRI brain scans were acquired at the Centre d'Imagerie BioMédicale (CIBM) in Geneva on a Siemens Trio (N = 86: 53 HCs, 18 PS+, 15 PS-) and a Siemens Prisma (N = 40: 16 HCs, 10 PS+, 14 PS-) 3 Tesla scanner. Structural images were obtained with a T1-weighted sequence of $0.86 \times 0.86 \times 1.1 \text{ mm}^3$ volumetric resolution (192 slices, TR = 2500 ms, TE = 3 ms, acquisition

3.2. Journal Article: BOLD variability in patients with 22q11DS with psychotic symptoms

Table 3.3 – Demographic information.

	PS+	PS-	HCS	p-value PS+ vs. PS-	p-value PS+ vs. HCs	p-value PS- vs. HCs
Number of subjects (M/F)	28 (12/16)	29 (14/15)	69 (30/39)	0.6813	0.9554	0.6629
Age mean±SD (range)	17.93±4.50 (10.3-27.9)	17.44±4.54 (11.1-28.4)	17.60±5.22 (10.0-29.6)	0.6846	0.7651	0.8918
Right handed*	60.71 %	96.55%	78.79 %	<0.001	0.0697	0.0288
IQ**	67.25±9.82	70.21±13.71	108.86±13.47	0.3563	<0.001	<0.001
N. subjects meeting criteria for psychiatric diagnosis***	20	14	N/A			
Anxiety disorder	5	4	N/A			
Attention deficit hyperactivity disorder	1	1	N/A			
Mood disorder	2	3	N/A			
Schizophrenia spectrum disorder	2	0	N/A			
More than one psychiatric disorder	10	6	N/A			
N. subjects medicated						
Methylphenidate	1	7	0			
Antipsychotics	3	0	0			
Anticonvulsants	1	0	0			
Antidepressants	3	1	0			
More than one class of medication	2	0	0			

* Handedness was measured using the Edinburgh laterality quotient, right handedness was defined by a score of more than 50. ** IQ was measured using the Wechsler Intelligence Scale for Children–III (Wechsler, 1991) for children and the Wechsler Adult Intelligence Scale–III (Wechsler, 1997) for adults. *** The presence of psychiatric disorders was evaluated during a clinical interview with the patients using the Diagnostic Interview for Children and Adolescents Revised (DICA-R) (Reich, 2000), the psychosis supplement from the Kiddie-Schedule for Affective Disorders and Schizophrenia Present and Lifetime version (K-SADS-PL) (Kaufman et al., 1997) and the Structured Clinical Interview for DSM-IV Axis I Disorders (SCID-I) (First et al., 1996).

matrix = 224×256 , field of view = 22 cm^2 , flip angle = 8°). Resting-state fMRI data were recorded with a T2-weighted sequence of 8 minutes (voxel size = $1.84 \times 1.84 \times 3.2 \text{ mm}$, 38 slices, TR = 2400 ms, TE = 30 ms, flip angle = 85°). During the resting-state session, participants were instructed to let their minds wander and not to think of anything in particular, while fixing a cross on the screen, and not to fall asleep.

Preprocessing

In the present study, data were processed similarly as in our previous paper on BOLD variability in 22q11DS (Zöllner et al., 2017). MRI preprocessing was done using statistical parametric mapping (SPM12) (Wellcome Trust Centre for Neuroimaging, London, UK: <http://www.fil.ion.ucl.ac.uk/spm/>) and functions of the data processing assistant for resting-state fMRI (DPARSF) (Yan Chaogan, 2010) and individual brain atlases using statistical parametric mapping (IBASPM) (Aleman-Gomez et al., 2006) toolboxes. After realignment of

functional scans, we applied spatial smoothing with an isotropic Gaussian kernel of 6 mm full width half maximum (FWHM) and coregistered structural scans to the functional mean. Structural images were segmented with the SPM12 *Segmentation* algorithm (Ashburner and Friston, 2005) and a study-specific template was generated using diffeomorphic anatomical registration (DARTEL) (Ashburner, 2007). Then, the first five functional scans were excluded from the analysis, mean white matter (WM) and cerebrospinal fluid (CSF) signals were regressed from the BOLD time series, which were then filtered with a bandwidth of 0.01 Hz to 0.1 Hz. For a more extended correction of motion artifacts, we further applied motion scrubbing (Power et al., 2012), excluding frames with a framewise displacement of more than 0.5 mm, as well as one frame before and two frames after. Refer to Supplementary Table A.4 for a summary on motion characteristics of the groups before and after motion scrubbing.

BOLD signal variability

At every voxel, BOLD signal variability was defined as the BOLD signal standard deviation (SD_{BOLD}) of preprocessed time series in subject space. Afterwards, every subject's SD_{BOLD} map was spatially normalized to the study-specific DARTEL template. Spatial normalization was applied after SD_{BOLD} computation, as in this way voxel-wise variability measures such as amplitude of low-frequency fluctuations (ALFF) are less affected by spatial distortions (Wu et al., 2011). Then, SD_{BOLD} maps were thresholded in order to keep only voxels with a probability higher than 0.2 of laying inside the gray matter and spatially z-scored for every subject.

Partial least squares correlation

We employed PLSC (Krishnan et al., 2011; McIntosh and Lobaugh, 2004) to investigate multivariate alterations and age-relationship of SD_{BOLD} related to the diagnosis. Figure 3.7 shows a schematic representation of the steps for PLSC.

By extracting principal components of covariance between brain data and a set of subject-specific design variables (here: diagnosis, age and their interaction), PLSC uncovers brain patterns with the strongest multivariate correlation to the design variables. We first computed the partial correlation matrix across subjects \mathbf{R} between SD_{BOLD} data \mathbf{X} and design variables \mathbf{Y} . Brain and design data were z-scored across subjects before applying PLSC, and motion (i.e. average framewise displacement), scanner type (Trio or Prisma) and full-scale intelligence quotient (IQ) were included as nuisance regressors. Then, so called latent variables were extracted by singular value decomposition (SVD) of $\mathbf{R} = \mathbf{U}\mathbf{S}\mathbf{V}^T$. In this work, we refer to the latent variables as “correlation components”. Each of the components is associated with a singular value (diagonal elements of \mathbf{S}) indicating how much of the correlation is explained by this component. Design saliences in \mathbf{U} contain the design loadings for every component that indicate how strong each of the design variables contributes to the brain-design correlation explained by this component. Brain saliences in \mathbf{V} contain a brain pattern for every component, representing how strong every voxel contributes to the brain-design correlation explained by this component. Furthermore, so-called “brain-scores” were obtained for every subject by

3.2. Journal Article: BOLD variability in patients with 22q11DS with psychotic symptoms

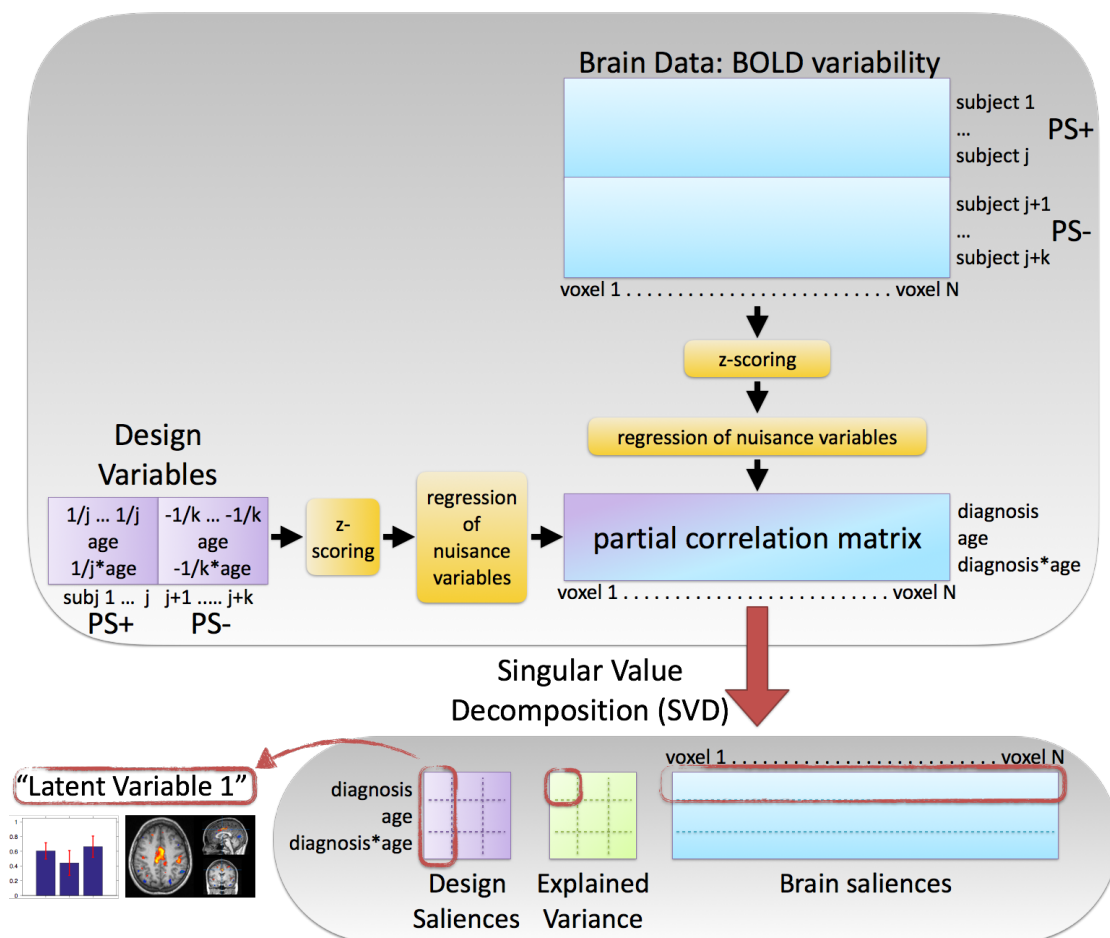


Figure 3.7 – Schematic representation of PLSC.

projecting the subject's SD_{BOLD} map (in \mathbf{X}) on the brain salience pattern (in \mathbf{V}) of the correlation components: $\mathbf{L}_X = \mathbf{XV}$. So-called "design scores" were computed similarly: $\mathbf{L}_Y = \mathbf{YU}$.

In order to evaluate how many components explain a significant amount of the correlation, we employed permutation testing. By shuffling the elements of \mathbf{Y} 1000 times while keeping the order of \mathbf{X} unchanged, we determined the null distribution of explained correlation. A component was considered significant ($p=0.05$) if its singular value was higher than 95 % of its null distribution. For the significant components, we furthermore evaluated the robustness of brain and design saliences using a bootstrapping procedure with 500 random samples with replacement. For every bootstrap sample, we recalculated design and brain saliences (\mathbf{U} and \mathbf{V}) and so obtained a typical bootstrap distribution of the salience values. Brain bootstrap ratios, calculated by dividing brain salience values by their standard deviations, indicate for every voxel its contribution to the brain-design correlation and can be interpreted similarly to z-scores (Krishnan et al., 2011).

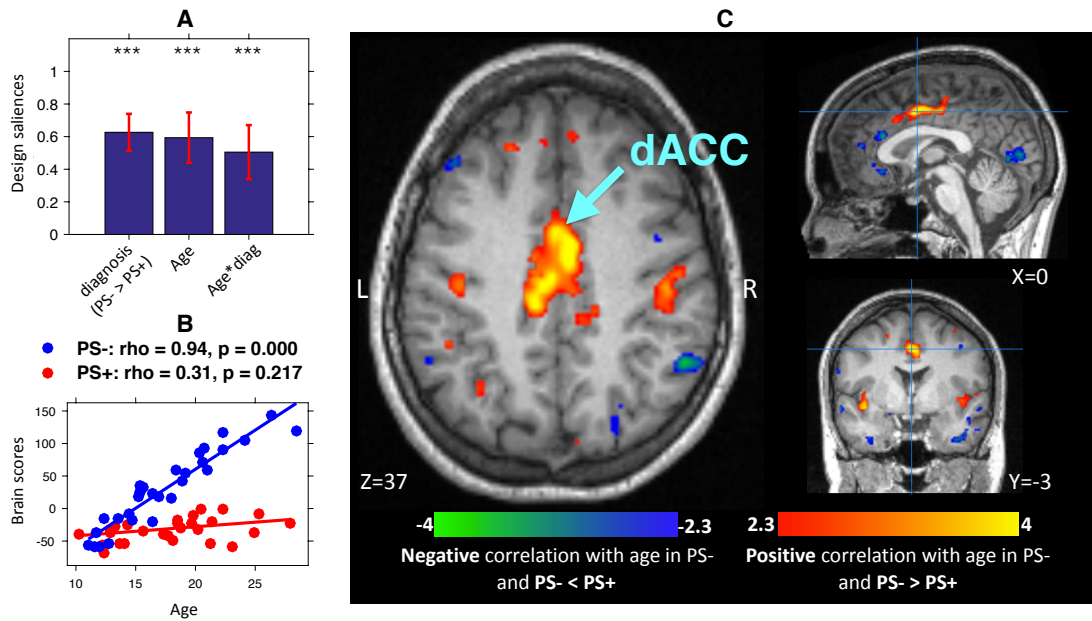


Figure 3.8 – First significant correlation component ($p=0.002$) resulting from PLSC comparing PS+ patients to PS- patients. Subfigures show design saliences with bootstrap error bars (A), brain scores as a function of age (B), and brain salience bootstrap ratios (C). The component reveals that PS- patients have increasing SD_{BOLD} in the dACC, while in PS+ patients this age-relationship is absent. dACC - dorsal anterior cingulate cortex; ** $p<0.01$; *** $p<0.001$.

3.2.3 Results

Different age-relationship in PS+ and PS- patients

Our main goal was to investigate alterations and age-relationship of SD_{BOLD} related to the presence of psychotic symptoms in patients with 22q11DS. We used PLSC with the design variables diagnosis (1 for PS+ patients, -1 for PS- patients), age and their interaction. Motion, scanner type and full-scale IQ were included as nuisance regressors. PLSC resulted in two significant correlation components.

Figure 3.8 shows the design and brain saliences for the first significant correlation component ($p=0.002$) resulting from PLSC comparing the PS+ and PS- groups. This first component represents a brain pattern where SD_{BOLD} is strongly correlated with age in PS- patients. This age-relationship, however, is not evident in the PS+ group and the average SD_{BOLD} in the pattern is lower in the PS+ group. The largest cluster of the corresponding pattern (see also Supplementary Table A.5) is located in the dorsal anterior cingulate cortex (dACC). Positive brain salience values indicate that SD_{BOLD} in PS- patients is increasing over age in this area and is globally higher in PS- patients than in PS+ patients.

Figure 3.9 shows design and brain salience of the second significant correlation component ($p=0.014$) of the comparison of PS+ and PS- patients. This component represents a brain pattern where SD_{BOLD} is correlated with age in the PS+ group, whereas PS- patients show an opposed relationship with age. The corresponding pattern (see also Supplementary Ta-

3.2. Journal Article: BOLD variability in patients with 22q11DS with psychotic symptoms

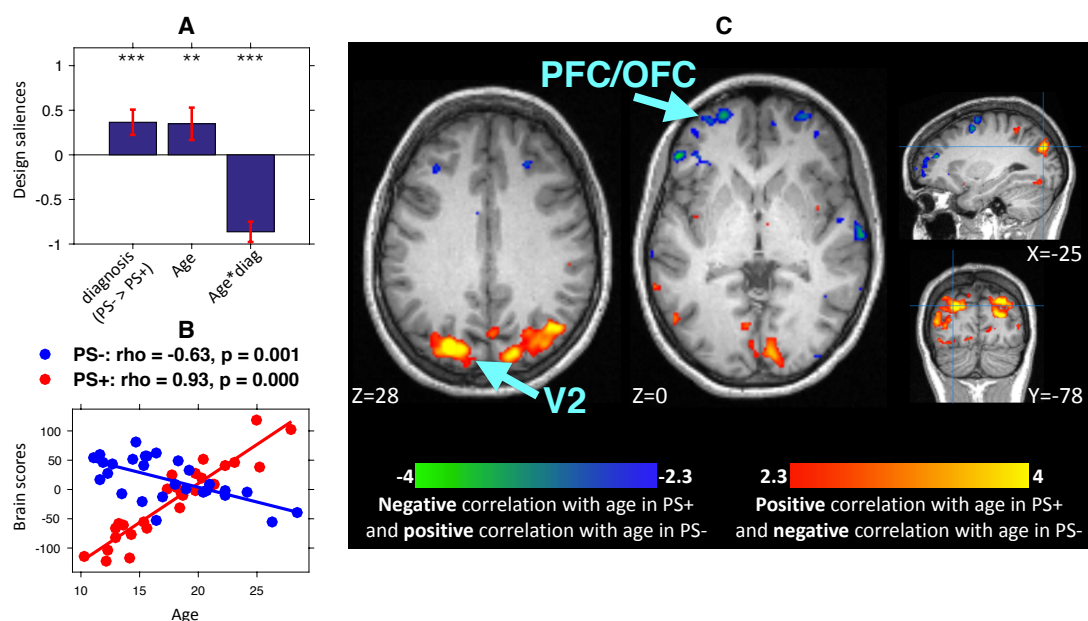


Figure 3.9 – Second significant correlation component ($p=0.014$) resulting from PLSC comparing PS+ patients to PS- patients. Subfigures show design saliences with bootstrap error bars (A), brain scores as a function of age (B), and brain salience bootstrap ratios (C). The component uncovers that in PS+ patients, SD_{BOLD} decreases over age in the PFC/OFC and increases over age in V2. In PS- patients, SD_{BOLD} in this pattern has an opposed relationship with age: increasing in the PFC/OFC and decreasing in V2. OFC - orbitofrontal cortex; PFC - prefrontal cortex; V2 - secondary visual cortex; *** $p<0.001$.

ble A.6) contains bilateral negative clusters spanning the prefrontal and orbitofrontal cortices, indicating that there, SD_{BOLD} decreases with age in PS+ patients and increases with age in PS- patients. It furthermore includes positive clusters in occipital, secondary visual regions, indicating an increase over age of SD_{BOLD} in PS+ patients, while SD_{BOLD} in PS- patients is decreasing.

Comparison of PS+ patients, PS- patients and HCs

In order to compare SD_{BOLD} in the two 22q11DS subgroups against HCs, we employed a second PLSC, this time with five design variables: the diagnosis of 22q11DS (diagnosis 1: 1 for PS+ and PS- patients, -1 for HCs); the presence of psychotic symptoms (diagnosis 2: 1 for PS+ patients, -1 for PS- patients, and 0 for HCs); age; the interaction between age and diagnosis 1, and the interaction between age and diagnosis 2. Motion and scanner type were included as nuisance regressors. IQ was not included to avoid the insensitivity to SD_{BOLD} group differences introduced by systematic group differences in full-scale IQ. Again, PLSC resulted in two significant correlation components.

Figure 3.10 shows design and brain saliences for the first significant correlation component ($p<0.0001$) resulting from the comparison of patients with 22q11DS (PS+ and PS-) to HCs. The corresponding pattern shows areas where SD_{BOLD} in patients with 22q11DS is different from

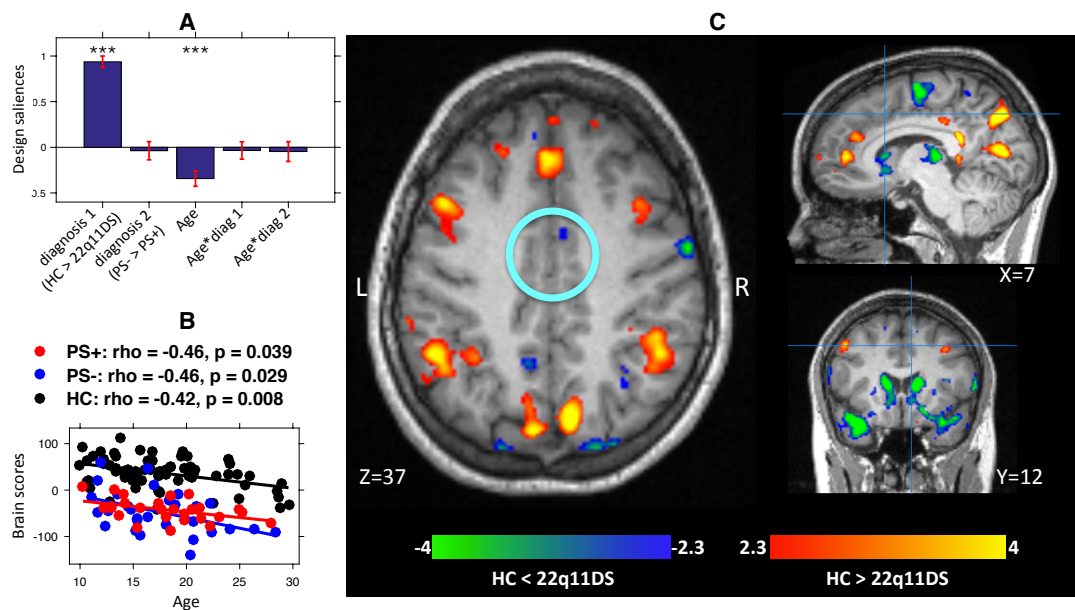


Figure 3.10 – First significant correlation component ($p < 0.0001$) resulting from PLSC comparing patients with 22q11DS to HCs. Subfigures show design saliences with bootstrap error bars (A), brain scores as a function of age (B), and brain salience bootstrap ratios (C). The component contains a pattern where SD_{BOLD} is higher (red) or lower (blue) in HCs compared to 22q11DS, with identical age-relationship in the three groups. The blue circle indicates the area in the dACC, where PS+ patients showed altered age-relationship compared to PS- patients (see section 3.2.3 and figure 3.8). This cluster is not different in 22q11DS compared to HCs. * $p < 0.05$; ** $p < 0.01$; *** $p < 0.001$.

HCs, but where patients within the 22q11DS group do not show significant differences. The corresponding brain salience pattern (see also Supplementary Table A.7) includes numerous areas distributed over the whole brain. SD_{BOLD} in cortical regions, including the CEN and parts of the DMN, is mainly reduced in 22q11DS, whereas in subcortical regions such as caudate and thalamus, SD_{BOLD} is higher in 22q11DS. Interestingly, dACC is not part of this pattern, which suggests that alterations in dACC (see section 3.2.3), specifically differentiate patients with 22q11DS with higher symptoms.

Figure 3.11 shows design and brain saliences for the second significant correlation component ($p = 0.001$). This component contains a pattern where SD_{BOLD} is correlated with age in HCs and in patients without psychotic symptoms (PS-). Patients with psychotic symptoms (PS+), however, do not show any correlation with age inside this pattern. Besides the superior motor area, caudate and amygdala, the brain pattern also includes the dACC (see also Supplementary Table A.8). An increase of SD_{BOLD} over age in these regions is thus common to PS- patients and HCs, but absent in PS+ patients.

3.2. Journal Article: BOLD variability in patients with 22q11DS with psychotic symptoms

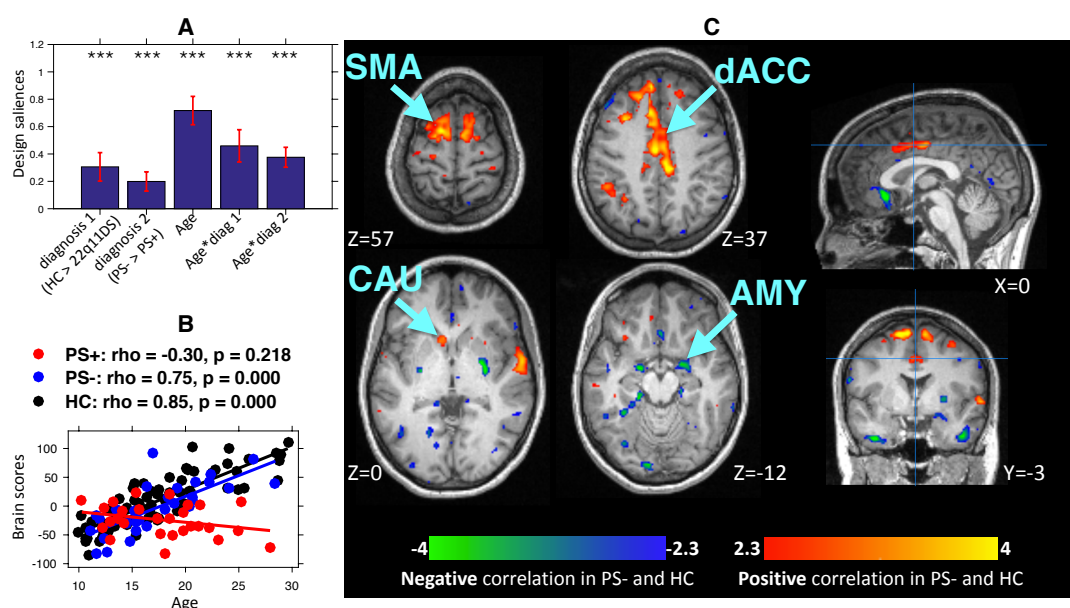


Figure 3.11 – Second significant correlation component ($p=0.001$) resulting from PLSC comparing patients with 22q11DS to HCs. Subfigures show design saliences with bootstrap error bars (A), brain scores as a function of age (B), and brain salience bootstrap scores (C). The component contains a pattern where SD_{BOLD} is increasing (red) or decreasing (blue) in PS-patients and HCs, but where in PS+ patients do not show any significant relationship with age. Amongst other areas, the pattern includes the dACC. AMY - amygdala; CAU - caudate; dACC - dorsal anterior cingulate cortex; SMA - superior motor area; * $p<0.05$; *** $p<0.001$.

Stability of the results

Exclusion of the five patients diagnosed with a psychotic disorder (see section 3.2.2 and Supplementary Table A.3) did not alter the present results besides slightly higher p-values, caused by the lower statistical power. Due to this increase, component 2 in the first analysis (see figure 3.9) was not significant anymore ($p>0.05$), but all other results remained significant with similar brain and design saliences.

Inclusion or exclusion of scanner type as covariate did not significantly alter the results.

Motion is a major concern in the analysis of BOLD variability. Supplementary Section A.2.3 outlines the correlations of the resulting brain scores with motion. There were no significant motion effects in the first analysis, and only low motion effects in brain scores of healthy controls in the second analysis.

3.2.4 Discussion

The central finding of the present study was that SD_{BOLD} in the dACC is lower in patients with higher positive psychotic symptoms than in patients with lower symptoms (section 3.2.3). We found evidence that BOLD variability in the dACC does not change over age in PS+ patients, but increases with age in PS- patients and HCs (sections 3.2.3 and 3.2.3). Furthermore, dACC was not part of a pattern where BOLD variability was altered in patients with 22q11DS compared

to HCs, independent of the presence of psychotic symptoms (section 3.2.3), indicating that alterations in dACC are intrinsic to the presence of higher psychotic symptoms in 22q11DS. Additionally, we found evidence for a pattern where only patients with psychotic symptoms show a significant relationship of BOLD variability with age (section 3.2.3).

In the following, we will discuss the relevance of alterations found in the dACC related to psychotic symptoms in 22q11DS and in the general population. We furthermore will comment on the age-relationship of BOLD variability that was evident only in PS+ patients, as well as on the BOLD variability alterations in both 22q11DS subgroups.

Our observation of altered BOLD variability in the dACC is in line with several previous findings in 22q11DS and schizophrenia. In fact, alterations in the ACC have been reported in 22q11DS (Scariati et al., 2016a; Schneider et al., 2012; Rihs et al., 2013; Schaer et al., 2010) and linked to the presence of psychotic symptoms within the syndrome using diverse modalities (Dufour et al., 2008; Scariati et al., 2014; Kates et al., 2015a; Ottet et al., 2013a; Tomescu et al., 2014). Structural MRI studies have reported gray matter volume reductions in 22q11DS which are most pronounced in the ACC (Schaer et al., 2010) and linked to the presence of psychotic symptoms in 22q11DS (Dufour et al., 2008). Furthermore, white matter dysconnectivity in cortical midline structures including the ACC has been related to psychotic symptoms in patients with the microdeletion (Kates et al., 2015a; Ottet et al., 2013a; reviewed in Scariati et al., 2016a). In a recent study conducted by our group, also structural connectivity measured by structural covariance, was found to be altered in the ACC and medial prefrontal cortex of patients with 22q11DS with psychotic symptoms (Sandini et al., 2017). Functional MRI studies in 22q11DS reported reduced resting-state functional connectivity in the ACC of patients with prodromal symptoms (Scariati et al., 2014), as well as functional hypo-activation in ACC during a self-referential task, which was correlated with the severity of positive symptoms (Schneider et al., 2012). Finally, recent EEG studies revealed a microstate C over-representation that was correlated with the presence of hallucinations in 22q11DS (Tomescu et al., 2014, 2015). This EEG microstate C has been related to fMRI activity in the ACC (Britz et al., 2010).

Also in the general population, changes of brain structure and function in the ACC have repeatedly been reported in subjects at ultra high risk for psychosis and in schizophrenia (Fornito et al., 2008, 2009; Reid et al., 2010; Jung et al., 2010; Pettersson-Yeo et al., 2011; Lord et al., 2011; Allen et al., 2010; Nekovarova et al., 2014). Alterations in the ACC have been linked to self-monitoring deficits (Allen et al., 2008) and auditory-verbal hallucinations (Allen et al., 2007).

The dACC is an area implicated in goal-directed behavior, self-related processing, and cognitive control (Shenhav et al., 2013; Sridharan et al., 2008; Uddin, 2015). It is a central hub of the SN (Menon and Uddin, 2010). Our observation of increasing BOLD variability in the SN of PS- patients and healthy controls is in line with a recent study, also showing linearly increasing resting-state BOLD variability in SN nodes (Nomi et al., 2017). Lower BOLD variability in the PS+ group may reflect a dysfunction in the attribution of salience. Such aberrant salience attribution has been suggested as mechanism for the development of psychosis and schizophrenia (Kapur, 2003). Higher BOLD variability has been suggested

3.2. Journal Article: BOLD variability in patients with 22q11DS with psychotic symptoms

to reflect optimal shifting between integrative and segregative brain states (Nomi et al., 2017; Tognoli and Kelso, 2014). Speculatively, lower BOLD variability in the dACC may thus disrupt the shifting ability of the SN, leading to a disability to correctly treat salience of external and internal stimuli.

Beyond the BOLD variability reduction in the dACC, we found that patients with psychotic symptoms have a pattern of aberrant age-relationship with increasing BOLD variability in visual regions and decreasing BOLD variability in the prefrontal and orbitofrontal cortices. Structural and functional alterations in frontal regions have been reported in psychosis and schizophrenia, including volume reductions (Jung et al., 2010), structural and functional dysconnectivity (Pettersson-Yeo et al., 2011), and increased brain signal variability (Hoptman et al., 2010; Takahashi et al., 2010). Also structural and functional alterations in the visual cortex have been observed in schizophrenia (Narr et al., 2005; Yu et al., 2014; Butler et al., 2007), and may be related to deficits in visual processing (Butler et al., 2005). Together with the altered age-relationship in the dACC, these results suggest aberrant developmental trajectories related to psychotic symptoms and point towards aberrant BOLD variability development as a potential predictor for psychosis. As these results are limited by the cross-sectional nature of the analysis, this hypothesis should be confirmed in further studies including longitudinal data.

In our previous paper (Zöller et al., 2017), we compared BOLD variability in patients with 22q11DS to HCs without differentiating patients according to psychotic symptoms. Interestingly, we here observed a weaker correlation with age in 22q11DS than in HCs. In view of the present results, this difference can be explained by the absent age-relationship in patients with psychotic symptoms, while age-relationship of BOLD variability in patients without positive symptoms is as strong as in HCs.

3.2.5 Conclusions and limitations

To our best knowledge, this is the first study investigating BOLD signal variability alterations related to psychosis in patients with 22q11DS. Firstly, we revealed reduced BOLD variability related to psychotic symptoms in the dACC, a region which is central for cognitive control and salience attribution and where alterations have been previously linked to psychotic symptoms in 22q11DS and the general population. In this region, patients without psychotic symptoms and HCs had similar levels of BOLD variability, suggesting that the reductions are intrinsic to the presence of psychotic symptoms. We furthermore retrieved a pattern of age-relationship specific to patients with psychotic symptoms, including frontal and occipital regions.

A main limitation of this study is the limited sample size over a relatively large age range. Furthermore, the cross-sectional nature of our data limits the interpretations to effects across subjects. Our results will need to be replicated in a larger sample and including longitudinal data to allow to conclude on true developmental effects.

Another confound might have been the heterogeneity in terms of symptoms severity and outcome of PS+ and PS- patients. Even though patients with positive psychotic symptoms are at higher risk to transition into psychosis, they may as well remain stable or even recover

(Schneider et al., 2016; Schultze-Lutter et al., 2015; Fusar-Poli et al., 2012). In our sample, all those patients were included in the PS+ group. Also, since there was no follow-up yet for most of the younger subjects included in the PS- group, we cannot exclude that some of those subjects might, indeed, develop symptoms at an older age. In our results, the decrease in BOLD variability in patients with psychotic symptoms only becomes evident at an age above 15, while younger individuals with and without psychotic symptoms have similar values. This effect might be driven by the aforementioned limitation in the group assignment of young subjects. Other confounds that might have driven these results are the duration of the presence of symptoms, or effects of medication.

A possible confound regarding the analysis of SD_{BOLD} may have been differences in gray matter volume between the groups. Indeed, gray matter volume is known to be globally reduced in 22q11DS (Tan et al., 2009; Gothelf et al., 2008). However, as gray matter volume in the entire cortex decreases over development (Giedd et al., 1999; Gogtay et al., 2004), including it as a confounding variable would lead to insensitivity in detecting age-dependence specific to SD_{BOLD} . Since additionally, gray matter volume and SD_{BOLD} development do not seem to be directly linked (Bray, 2017), we did not include gray matter volume as nuisance regressor.

3.3 Summary and outlook

In this chapter, we explored fMRI dynamics in terms of BOLD signal variability. In the first study, we found broad alterations in patients with 22q11DS, with lower variability in posterior occipital and parietal regions and higher variability in inferior temporal and subcortical regions, a pattern that broadly overlaps with BOLD signal variability alterations in patients with schizophrenia (Xu et al., 2015), see figure 2.7. Further, using seed-based static functional connectivity (sFC) we confirmed anterior-posterior disconnectivity of the DMN, which has been observed in several previous studies (Schreiner et al., 2014; Padula et al., 2015, 2017b). Finally, we observed that the alteration patterns of BOLD variability and DMN connectivity are not identical, which suggests that the relationship between BOLD variability and sFC is more complex and not linear. On the contrary, in overlapping alterations both measures were reduced, which may be counterintuitive as the standard deviation appears in the denominator of Pearson correlation. Importantly, while we here observed BOLD signal variability at rest, the relationship between variance and functional connectivity may vary in different task-based paradigms. In a recent article that was published after our study, Duff et al. made the intriguing observation that most correlation differences between a resting and a task condition could be explained by "Additive Signal Changes", that is a change in variance of either one or both correlated sources (Duff et al., 2018). These and our results suggest that an interpretation of shifts in functional connectivity as differences in neural coupling may be too simplistic, and multiple scenarios of changed signal variance and covariance may take place at the same time. The consideration of variance in addition to correlation may help to disentangle these effects.

In the second study, we then analyzed BOLD signal variability in patients with psychotic symptoms and found reduced variability in the dACC that was due to aberrant development in these patients. Alterations in the dACC have been suggested as a candidate biomarker for positive psychotic symptoms in 22q11DS, because they have been reported in multiple studies using a diversity of measures of brain function and anatomy (Padula et al., 2018).

Together, these results suggest that BOLD variability contains meaningful information on brain function and may provide a valuable marker for psychosis vulnerability in 22q11DS. However, one disadvantage of the measure is that it is a global measure of brain dynamics in which the entire resting-state scanning duration is summarized in one score per voxel. Critically, the exact implications of BOLD signal variability are not well understood yet and still subject to ongoing research. A recent study found that BOLD signal variability may result from higher common synchronized input from multiple other brain regions (Garrett et al., 2018). In this sense, reduced BOLD variability in dACC in patients with psychosis may be a result from a dis-synchronized interaction of dACC with other brain regions, or in other words a disrupted structure of functional brain states. It is known, that dACC is acting together with a multiplicity of brain regions, such as insula and dorso-lateral prefrontal cortex (dlPFC) for salience processing (Uddin, 2015), and the amygdala for emotion regulation and appraisal (Etkin et al., 2011). In the following chapter, we therefore used dynamic analysis of large-scale functional brain states, in order to investigate dynamics of distinct functional brain

Chapter 3. BOLD signal variability to analyze dynamic brain function

systems rather than single voxels and probe into brain activity at specific moments, rather than summarizing over the entire scanning duration.

4 Large-scale brain network dynamics

To go beyond a simple voxel-wise measure of brain dynamics, we next look into dynamics on the level of large-scale functional brain systems. Indeed, the brain during rest is known to fluctuate between multiple coherent functional brain states that are characterized by the consistent activation of sets of brain regions (Damoiseaux et al., 2006). Alterations in BOLD signal variability observed in the previous studies are likely closely linked to the altered integration with other regions of the brain (Garrett et al., 2018), which can be represented as activity of such large-scale brain states. Among the multiple approaches to decompose the fMRI signal into distinct functional components and their temporal activation (see chapter 2.1), the innovation-driven co-activation patterns (iCAPs) framework stands out as it relies on very few assumptions about the nature of the resulting components (Karahanoglu et al., 2015). Independent component analysis (ICA) for example (Calhoun et al., 2001) maximizes statistical independence in either time or space, and in the co-activation patterns (CAPs) methods (Liu and Duyn, 2013) only one brain state can be active at a time. However, functional brain states seem to be overlapping *both* in space (a region can be part of multiple brain states) *and* in time (multiple brain states can be active at one timepoint) (Karahanoglu and Van De Ville, 2017). The iCAPs approach retrieves brain states that are simultaneously transitioning, and in this way allows to recover brain states that are both temporally and spatially overlapping at the same time.

We found out, however, that the spatial dependence of brain states can introduce spurious activation in their reconstructed temporal activity. In the first article in section 4.1, we present a quantification of this problem, as well as a methodological development that we included into the iCAPs framework, which relies on transient-based constraints to avoid such spurious activations. In the second article in section 4.2, we use this improved iCAPs approach to look into altered brain function in patients with 22q11DS and into the dynamic implication of clinical risk factors for psychosis in the syndrome. Finally, the last section 4.3 will again summarize the findings of these two articles in perspective of this thesis and motivate further directions.

4.1 Journal Article: Robust recovery of temporal overlap between network activity.

Postprint version of the article published in: IEEE Transactions on Medical Imaging 2019, 38:291-302, <https://doi.org/10.1109/TMI.2018.2863944>

Robust recovery of temporal overlap between network activity using transient-informed spatio-temporal regression

Daniela Zöllner^{1,2,3}, Thomas A.W. Bolton^{1,2}, Fikret Işık Karahanoğlu^{4,5}, Stephan Eliez³, Marie Schaer³, Dimitri Van De Ville^{1,2}

¹Medical Image Processing Laboratory, Institute of Bioengineering, École Polytechnique Fédérale de Lausanne (EPFL), Lausanne, Switzerland; ²Department of Radiology and Medical Informatics, University of Geneva, Geneva, Switzerland; ³Developmental Imaging and Psychopathology Laboratory, Office Médico-Pédagogique, Department of Psychiatry, University of Geneva, Geneva, Switzerland; ⁴Athinoula A. Martinos Center for Biomedical Imaging, Charlestown, MA, United States; ⁵Department of Radiology, Massachusetts General Hospital, Harvard Medical School, Boston, MA, United States

Functional magnetic resonance imaging (fMRI) is a non-invasive tomographic imaging modality that has provided insights into systems-level brain function. New analysis methods are emerging to study the dynamic behavior of brain activity. The innovation-driven co-activation patterns (iCAPs) approach is one such approach that relies on the detection of timepoints with significant transient activity to subsequently retrieve spatially and temporally overlapping large-scale brain networks. To recover temporal profiles of the iCAPs for further time-resolved analysis, spatial patterns are fitted back to the activity-inducing signals. In this crucial step, spatial dependencies can hinder the recovery of temporal overlapping activity. To overcome this effect, we propose a novel back-projection method that optimally fits activity-inducing signals given a set of transient timepoints and spatial maps of iCAPs, thus taking into account both spatial and temporal constraints. Validation on simulated data shows that transient-based constraints improve the quality of fitted time courses. Further evaluation on experimental data demonstrates that over- and underfitting are prevented by the use of optimized spatio-temporal constraints. Spatial and temporal properties of resulting iCAPs support that brain activity is characterized by the recurrent co-activation and co-deactivation of spatially overlapping large-scale brain networks. This new approach opens new avenues to explore the brain's dynamic core.

4.1.1 Introduction

During the past two decades, investigations using resting-state functional magnetic resonance imaging (fMRI) found evidence that normal brain function is characterized by fluctuations in the activity of large-scale brain networks, that is, of distributed sets of brain regions that are

4.1. Journal Article: Robust recovery of temporal overlap between network activity.

coherently fluctuating (Damoiseaux et al., 2006; Fox et al., 2005). Functional connectivity (FC) measures statistical interdependency between two time courses, conventionally by pairwise correlation. Another widely used methodology to study networked brain activity is independent component analysis (ICA) that relies on a surrogate measure for statistical independence (McKeown et al., 1998; Calhoun et al., 2001). While FC and ICA most commonly assume stationarity over the whole resting-state run, recent findings suggest that it is meaningfully variable over time (Chang and Glover, 2010), and that the consideration of dynamic features is promising when studying brain function and its alterations in mental disorders (Christoff et al., 2016; Preti et al., 2017).

Multiple approaches exist for the retrieval and analysis of dynamic functional connectivity (dFC) networks; for extensive reviews see (Preti et al., 2017; Karahanoglu and Van De Ville, 2017; Hutchison et al., 2013a). Sliding-window approaches track dynamic changes by restraining the computation of second-order correlation to a temporal interval which is gradually shifted over time (Chang and Glover, 2010; Sakoglu et al., 2010; Leonardi et al., 2013; Allen et al., 2014). However, this approach is limited to the detection of FC changes at much slower rate than the sampling rate, whereas actual FC changes might take place at a faster rate. Several novel approaches have been proposed to go beyond sliding-window correlations and detect rapid changes in FC. Window-less ICA-based approaches propose to analyze the dynamics of independent components (ICs) using for example dictionary learning (Yaesoubi et al., 2018) or hidden Markov models (Vidaurre et al., 2017). In parallel, so-called first-order techniques were developed, which identify fMRI frames that reflect key activity patterns in a point process analysis (PPA); e.g., by the detection of significantly strong activity in a seed region (Tagliazucchi et al., 2012). An extension of this approach applies temporal clustering on the selected frames to establish whole brain co-activation patterns (CAPs) occurring during those moments defined by a single seed's time series (Liu and Duyn, 2013). This seed-driven approach has further been extended for the whole-brain by including multiple seeds (Liu et al., 2013; Tagliazucchi et al., 2016).

Yet another approach has been to incorporate a change point detector to retrieve timepoints of significant transient activity; e.g., by identifying moments of maximal brain-state changes (Cribben et al., 2012) or using derivatives (Shine et al., 2015, 2016b,a). Combining this idea with principles from CAP analysis, temporal clustering on significant transient timepoints yields innovation-driven CAPs (iCAPs) (Karahanoglu et al., 2015), which are illustrated in Fig. 4.1. These spatial patterns reminiscent for known functional networks are simultaneously *transitioning* rather than simultaneously *activating*, which provides unique advantages over other commonly used methods. ICA, for instance, imposes statistical independence either in space or in time and CAPs are per definition temporally segregated, with only one active CAP at a time. This flexibility in spatial and temporal representation makes iCAPs thus especially well suited for the investigation of the resting state where there is no prior information on timing of brain-state transitions and strong temporal overlap of functional components is likely given the hemodynamic nature of fMRI signals (Christoff et al., 2016).

To precisely detect timepoints with transient activity, fMRI signals must be deconvolved from the hemodynamic response function (HRF). For this the total activation (TA) framework

has been developed (Karahanoglu et al., 2013) (Fig. 4.1, green box), resulting into the activity-inducing signals. The derivative of activity-inducing signals, so-called innovation signals, are then temporally clustered into representative spatial patterns (Fig. 4.1, blue box). To obtain the activation time courses of the iCAPs, these spatial patterns are then fitted back to the activity-inducing signals.

Even though the possibility of spatial overlap is one of the key advantages of iCAPs, spatial dependence may hinder the recovery of temporal overlap in the regression procedure. Here, we address this issue and propose a new back-projection method to optimally fit activity-inducing signals given a set of transient timepoints and spatial maps of iCAPs. This approach takes into account both spatial and temporal constraints to retrieve iCAPs' temporal profiles, which gives access to their dynamics for further analysis.

In the following, we first briefly describe the TA and iCAPs pipeline. Then, we introduce our novel transient-informed spatio-temporal regression approach and validate the proposed method on simulated data. Finally, we evaluate it on experimental data to demonstrate the benefits of our approach.

4.1.2 Methods

Methods implementation

An open repository containing the full code for the application of processing steps including TA, iCAPs retrieval and spatio-temporal regression is available at <https://c4science.ch/source/iCAPs.git>.

Total activation and innovation-driven co-activation patterns

Total activation The TA framework uses spatio-temporal regularization to deconvolve the fMRI signal from the HRF (see Fig. 4.1, green box). The signal model explains the measured fMRI signal $y(v, t)$ as a convolution of an underlying neural signal $a(v, t)$, assumed to be block-type at the timescale of fMRI (that is seconds), with the HRF $h(t)$, and is corrupted by additive white Gaussian noise $\epsilon(v, t)$:

$$y(v, t) = (h \star a)(v, t) + \epsilon(v, t).$$

Here and throughout, the index $v \in \mathbb{N}$ indicates the voxel with $1 \leq v \leq N_v$, N_v being the total number of gray matter voxels, and index $t \in \mathbb{N}$ indicates the timepoint with $1 \leq t \leq N_t$, N_t being the total number of timepoints. Using vector notation $\mathbf{y}(v, \cdot) = [y(v, 1), \dots, y(v, N_t)]$, we write

$$\mathbf{y}(v, \cdot) = (\mathbf{h} \star \mathbf{a})(v, \cdot) + \boldsymbol{\epsilon}(v, \cdot),$$

where $\boldsymbol{\epsilon}$ is distributed as $\mathcal{N}(0, \mathbf{I}_{N_t} \sigma_v^2)$, where \mathbf{I}_{N_t} is an $N_t \times N_t$ identity matrix. We designate $\mathbf{x} = \mathbf{h} \star \mathbf{a}$ the *activity-related* signal at voxel v , and \mathbf{a} its *activity-inducing* signal. The complete data matrix of activity-related signals is denoted as $\mathbf{X} \in \mathbb{R}^{N_v \times N_t}$ and the fMRI signal matrix $\mathbf{Y} \in \mathbb{R}^{N_v \times N_t}$, see Table 4.1 for an overview of the notations.

Then, as illustrated in Fig. 4.1 (green box), the spatio-temporal regularization problem can

4.1. Journal Article: Robust recovery of temporal overlap between network activity.

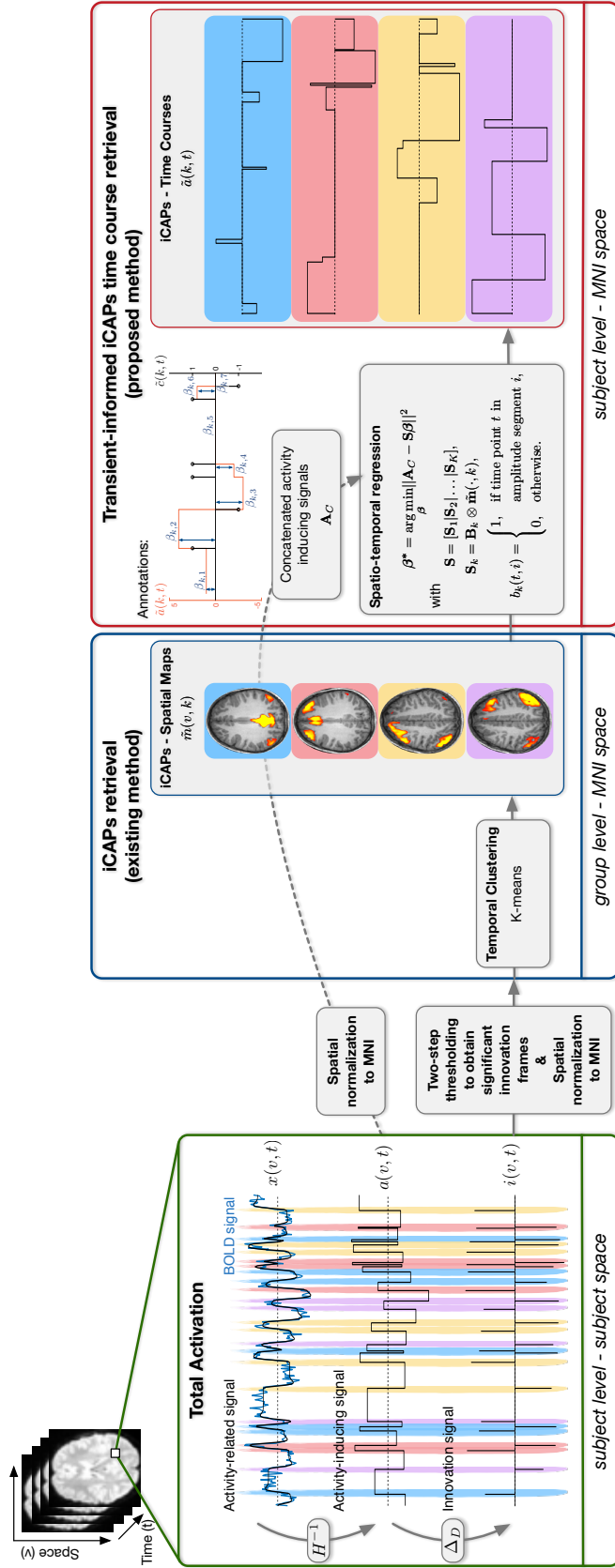


Figure 4.1 – Schematic representation of the key components related to this work. The total activation framework (green box) provides innovation signals that encode transients. Then, iCAPs are retrieved by temporal clustering (blue box). Finally, we propose to recover the iCAPs-related activity-inducing signals using a new spatio-temporal regression approach (red box).

be written as

$$\mathbf{X}^* = \arg \min_{\mathbf{X}} \frac{1}{2} \|\mathbf{Y} - \mathbf{X}\|_F^2 + \mathcal{R}_T(\mathbf{X}) + \mathcal{R}_S(\mathbf{X}),$$

where

$$\begin{aligned} \mathcal{R}_T(\mathbf{X}) &= \sum_{v=1}^{N_v} \lambda_T(v) \sum_{t=1}^{N_t} |\Delta_L \{\mathbf{x}(v, \cdot)\}[t]|, \\ \mathcal{R}_S(\mathbf{X}) &= \lambda_S \sum_{t=1}^{N_t} \sum_{v=1}^{N_v} \sqrt{\sum_{u \in \mathcal{S}(v)} (x(v, t) - x(u, t))^2}. \end{aligned}$$

Here, $\lambda_T(v)$ is the temporal regularization parameter at voxel v , and λ_S is the spatial regularization parameter, which is the same at every timepoint t . The differential operator $\Delta_L = \Delta_D H^{-1}$ combines HRF deconvolution H^{-1} and derivative Δ_D , and $\mathcal{S}(v)$ denotes the surrounding neighbors of voxel v . The temporal regularization term $\mathcal{R}_T(\mathbf{X})$ imposes sparsity on the innovation signal $\mathbf{i}(v, \cdot) = \Delta_L \{\mathbf{x}(v, \cdot)\}$; i.e., on the derivative of the activity-inducing signal, and thereby favors a piecewise-constant activity-inducing block signal $\mathbf{a}(v, \cdot)$. The spatial regularization term $\mathcal{R}_S(\mathbf{X})$ promotes localized activations that are smooth in space (Farouj et al., 2017). The HRF $h(t)$ is modeled by first-order Volterra series approximation of the balloon model (Khaldov et al., 2011; Buxton et al., 1998) and is assumed to be constant across the whole brain. For more details on the TA implementation, we refer to (Karahanoglu et al., 2011, 2013; Farouj et al., 2017).

In this study, TA was applied separately for every subject on preprocessed fMRI data in subject space.

Innovation-driven co-activation patterns After regularized deconvolution of the BOLD signal, K-means clustering is applied to innovation frames to retrieve spatial patterns of simultaneously transitioning voxels (Karahanoglu et al., 2015). First, positive and negative innovations are split into two separate frames $\mathbf{i}_P(\cdot, t)$ and $\mathbf{i}_N(\cdot, t)$, where the sign of negative innovation frames is flipped. Then, significant transient frames were determined using a two-step thresholding approach: in the first step (temporal thresholding), the null distribution of every subject's innovation signal was determined by running TA on a phase-randomized surrogate dataset, and a subject-specific threshold at a 5 %-95 % confidence interval was applied. In the second step (spatial thresholding), an innovation frame was considered significant if at least 5% of all considered voxels showed a significant innovation. With these thresholding parameters, 81.8 ± 9.1 % of positive and 79.1 ± 10.3 % of negative frames were above threshold. Overall, 99.8 ± 0.4 % of the innovation frames showed at least a significant positive or negative innovation (or both events together). After thresholding, innovation frames were spatially normalized to Montreal Neurological Institute (MNI) space using diffeomorphic anatomical registration (DARTEL) (Ashburner, 2007) (see also subsection 4.1.3).

Then, spatially normalized, significant innovation frames of all subjects were concatenated and temporal K-means clustering was applied at the group level with cosine distance as similarity measure (see Fig. 4.1, blue box). The group level spatial maps $\tilde{\mathbf{m}}(\cdot, k) =$

4.1. Journal Article: Robust recovery of temporal overlap between network activity.

Table 4.1 – Overview of notations. Signals obtained following the generation of the iCAPs are marked with a tilde.

Symbol	Description
$t \in \mathbb{N}$	timepoint (frame) index
$v \in \mathbb{N}$	voxel index
$k \in \mathbb{N}$	cluster index
$y(v, t); \mathbf{Y} \in \mathbb{R}^{N_v \times N_t}$	measured voxelwise BOLD signal
$x(v, t); \mathbf{X} \in \mathbb{R}^{N_v \times N_t}$	voxelwise activity-related signal
$a(v, t); \mathbf{A} \in \mathbb{R}^{N_v \times N_t}$	voxelwise activity-inducing signal
$\mathbf{A}_C \in \mathbb{R}^{N_t N_v \times 1}$	concatenated activity-inducing signal
$i(v, t); \mathbf{I} \in \mathbb{R}^{N_v \times N_t}$	voxelwise innovation/transient signal
$\tilde{m}(v, k); \tilde{\mathbf{M}} \in \mathbb{R}^{N_v \times K}$	iCAP spatial maps
$\tilde{a}(k, t); \tilde{\mathbf{A}} \in \mathbb{R}^{K \times N_t}$	iCAP-wise activity-inducing signal
$\tilde{c}(k, t) \in \{-1, 0, 1\}$	iCAP-wise cluster assignment

$[\tilde{m}(1, k), \dots, \tilde{m}(N_v, k)]^\top$ of each iCAP, $k \in 1, \dots, K$, were retrieved by averaging the innovation frames of every cluster, after normalizing each frame to unit Euclidean length. In what follows, signals obtained following the generation of the iCAPs are marked with a tilde.

Consensus clustering

In order to determine the best number of clusters, we employed consensus clustering (Monti et al., 2003), a resampling-based approach which applies K-means clustering on a subsample of the data and calculates the *consensus matrix* \mathcal{M} . Every element $\mathcal{M}(f_1, f_2)$ indicates the fraction of all subsamples for which two frames f_1 and f_2 are clustered together. The optimum cluster number can then be obtained by visual observation of the ordered matrix \mathcal{M} , as well as of the cumulative distribution function (CDF) of \mathcal{M} and its area under the curve (AUC) for different values of K . See (Monti et al., 2003) for more details on the methods for clustering selection. Here, we applied consensus clustering for $K \in [10, 25]$ using 10 random subsamples for every K . Each subsample included the significant innovations of 45 (80 %) randomly selected subjects, and K-means was computed for 10 random initializations. To obtain the final clustering result, we applied K-means clustering with the optimum K on the entire dataset and kept the optimal result from 50 random initializations.

Time course recovery

In what follows, subject level iCAPs' time courses are either identified with the conventional *unconstrained spatial regression* approach or with our novel *transient-informed spatio-temporal regression* approach. The former treats every timepoint independently and only depends on spatial information, while the latter incorporates both spatial and temporal information.

Unconstrained spatial regression In the conventional iCAPs framework (Karahanoğlu et al., 2015), time-dependent amplitudes $\tilde{\mathbf{a}}(\cdot, t) = [\tilde{a}(1, t), \dots, \tilde{a}(K, t)]^\top$ at timepoint t are retrieved by back-projection of the K group level spatial maps $\tilde{\mathbf{M}} \in \mathbb{R}^{N_v \times K} = [\tilde{\mathbf{m}}(\cdot, 1), \dots, \tilde{\mathbf{m}}(\cdot, K)]$ onto the activity-inducing signal $\mathbf{a}(\cdot, t)$ of each subject. Positive and negative transients are fitted

separately to minimize the effect of spatial linear dependence, and the final time courses are defined as the sum of positive and negative fitted amplitudes, \tilde{a}_P and \tilde{a}_N :

$$\tilde{a}(k, t) = \tilde{a}_P(k, t) + \tilde{a}_N(k, t),$$

with

$$\tilde{\mathbf{a}}_P^*(\cdot, t) = \underset{\tilde{\mathbf{a}}_P(\cdot, t)}{\operatorname{argmin}} \|\mathbf{a}(\cdot, t) - \tilde{\mathbf{M}}\tilde{\mathbf{a}}_P(\cdot, t)\|^2 \text{ s.t. } \tilde{a}_P(k, t) \in [0, \infty[,$$

and

$$\tilde{\mathbf{a}}_N^*(\cdot, t) = \underset{\tilde{\mathbf{a}}_N(\cdot, t)}{\operatorname{argmin}} \|\mathbf{a}(\cdot, t) - \tilde{\mathbf{M}}\tilde{\mathbf{a}}_N(\cdot, t)\|^2 \text{ s.t. } \tilde{a}_N(k, t) \in]-\infty, 0].$$

Transient-informed spatio-temporal regression As mentioned before, the unconstrained spatial regression approach for extracting the time courses of iCAPs can be contaminated by spatial dependencies of their maps, since the latter can be spatially overlapping. The main purpose of this paper is to introduce an alternative improved method, in order to overcome this problem and obtain more plausible time courses.

In principle, the method restricts changes in iCAPs time courses to moments when the iCAP in question is known to transition significantly. Information on these innovation timings is taken from the K-means clustering in the iCAPs retrieval step. Then, the design matrix for the regression problem is constructed with one regressor for each block of constant activation. In the following, we outline the detailed steps of the design matrix construction for this spatio-temporal regression method, namely (i) definition of innovation timings based on K-means information, (ii) construction of an indicator matrix $\tilde{\mathbf{C}}$ with innovation timings of all K iCAPs, (iii) construction of a temporal design matrix \mathbf{B}_k with one regressor per activity block of each iCAP $k = 1, \dots, K$, (iv) construction of the spatio-temporal design matrix \mathbf{S} that also incorporates spatial information of the iCAPs maps to group voxels, and (v) the explicit formulation of the resulting linear optimization problem. Fig. 4.2 shows the assumed model for iCAPs time courses and Fig. 4.3 shows a schematic representation of the spatio-temporal regression design.

i) Innovation timing definition: With hard cluster assignment of transient frames, only two iCAPs are allowed to transition at the same time (one positively and one negatively). In order to allow for more than one iCAP to change simultaneously, we determine innovation timings using a soft cluster assignment according to the cosine distances of each frame to the cluster center: let $d(k, t)$ be the cosine distance of innovation frame $\mathbf{i}(\cdot, t)$ to cluster $\tilde{\mathbf{m}}(\cdot, k)$. Then the frame $\mathbf{i}(\cdot, t)$ (i.e., a significant innovation at timepoint t) will be assigned to all clusters k for which

$$d(k, t) \leq \xi d_{\min}(t),$$

where $d_{\min}(t)$ is the minimum distance of frame $\mathbf{i}(\cdot, t)$ to any cluster and $\xi \geq 1$ is a tuning

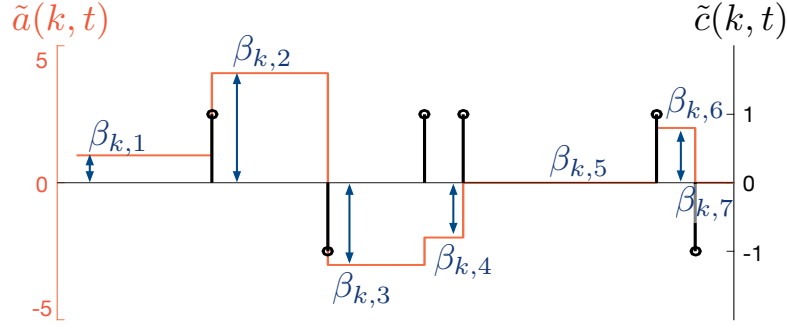


Figure 4.2 – Schematic representation of an example output iCAP time course $\tilde{\mathbf{a}}(k, \cdot)$, the corresponding innovation indicator time course $\tilde{\mathbf{c}}(k, \cdot)$, and the estimated amplitude values $\beta_{k,i}$.

parameter. Note that $\xi = 1$ corresponds to the hard cluster assignment used during K-means clustering.

ii) *Innovation timing indicator matrix*: We then define the indicator matrix $\tilde{\mathbf{C}} \in \mathbb{R}^{K \times N_t}$ denoting the timepoints t with significant innovations for each iCAP k :

$$\tilde{c}(k, t) = \begin{cases} 1, & \text{if } d_P(k, t) \leq \xi d_{P,min}(t), \\ -1, & \text{if } d_N(k, t) \leq \xi d_{N,min}(t), \\ 0, & \text{otherwise,} \end{cases}$$

where d_P and d_N designate distances to positive and negative innovation frames $\mathbf{i}_P(\cdot, t)$ and $\mathbf{i}_N(\cdot, t)$, respectively. Further, we will denote the number of innovations for iCAP k by $N_{I_k} = \sum_{t=1}^{N_t} |\tilde{c}(k, t)|$, and the total number of innovations across all networks by $N_I = \sum_{k=1}^K N_{I_k}$.

iii) *Temporal design matrix*: Our aim is to retrieve, for each iCAP k , a time course $\tilde{\mathbf{a}}(k, \cdot)$ that is piecewise constant between two nonzero values in $\tilde{\mathbf{c}}(k, \cdot)$. To do so, we must determine the optimal set of amplitudes $\beta_{k,i}$, $k = 1, \dots, K$, $i = 1, \dots, N_{I_k} + 1$ between two significant transients (see Fig. 4.2 for a schematic representation). Note that there are $N_{I_k} + 1$ coefficients to compute for each network.

For each iCAP, we construct the temporal design matrix $\mathbf{B}_k \in \mathbb{R}^{N_t \times N_{I_k} + 1}$ that contains the activation segments separated by the innovations. If

$$\phi(t, k) = 1 + \sum_{\tau=1}^t |\tilde{c}(k, \tau)|$$

expresses the index of the segment at hand at time t , the elements $b_k(t, i)$ of \mathbf{B}_k are

$$b_k(t, i) = \begin{cases} 1, & \text{if } \phi(t, k) = i, \\ 0, & \text{otherwise.} \end{cases}$$

iv) *Spatio-temporal design matrix*: Based on \mathbf{B}_k , we obtain the matrix $\mathbf{S}_k \in \mathbb{R}^{N_t N_v \times (N_{I_k} + 1)}$

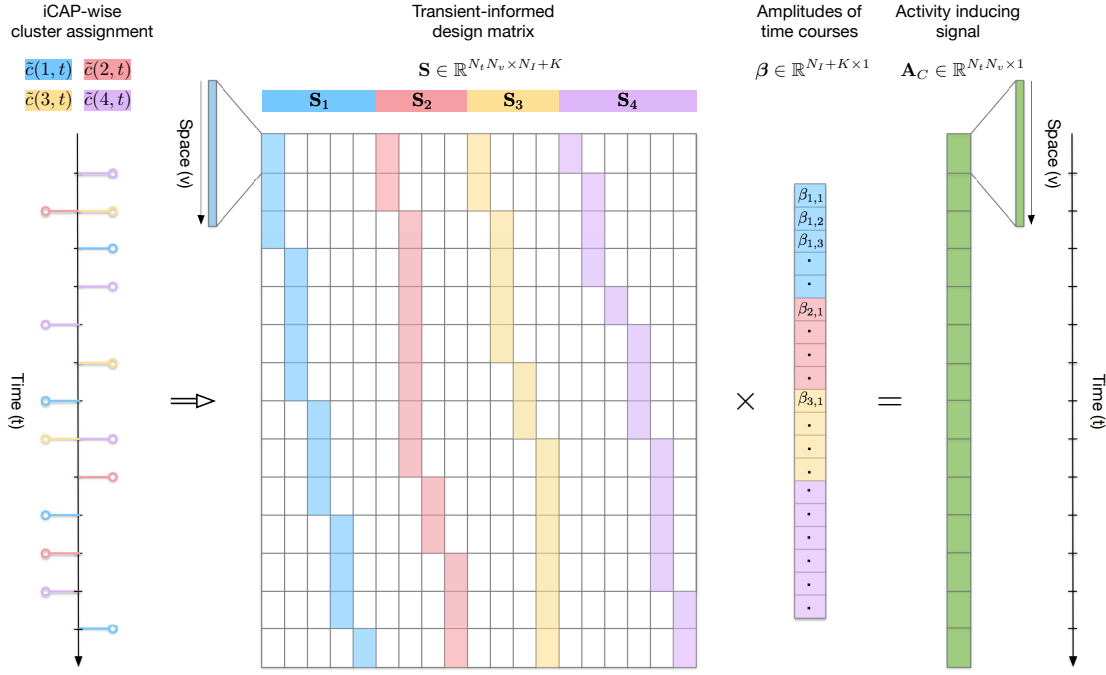


Figure 4.3 – Schematic representation of the transient-informed spatial regression optimization problem in the case of four iCAPs with $N_{I_1} = 4$, $N_{I_2} = 3$, $N_{I_3} = 3$ and $N_{I_4} = 5$ significant innovations, respectively, and $N_I = 15$ innovations in total. This example represents the most restrictive case of hard cluster assignment ($\xi = 1$) with at most two iCAPs changing simultaneously (one with positive and one with negative amplitude).

that contains the activation segments in the concatenated spatio-temporal space:

$$\mathbf{S}_k = \mathbf{B}_k \otimes \tilde{\mathbf{m}}(\cdot, k),$$

where \otimes denotes the Kronecker product. Then, the combination of all spatio-temporal matrices \mathbf{S}_k gives the final spatio-temporal design matrix $\mathbf{S} = [\mathbf{S}_1 | \mathbf{S}_2 | \dots | \mathbf{S}_K]$.

v) Optimization problem: If we then define $\mathbf{A}_C \in \mathbb{R}^{N_t N_v \times 1}$ as the concatenated activity-inducing frames (see Fig. 4.3), the optimization problem becomes

$$\boldsymbol{\beta}^* = \underset{\boldsymbol{\beta}}{\operatorname{argmin}} \|\mathbf{A}_C - \mathbf{S}\boldsymbol{\beta}\|^2,$$

with the optimal amplitudes given by $\boldsymbol{\beta} \in \mathbb{R}^{N_I + K \times 1} = [\beta_{1,1}, \beta_{1,2}, \dots, \beta_{1,N_{I_1}+1}, \beta_{2,1}, \dots, \beta_{K,N_{I_K}+1}]^T$. We then have the iCAP time course amplitudes $\tilde{a}(k, t) = \beta_{k,\phi(t,k)}$.

4.1. Journal Article: Robust recovery of temporal overlap between network activity.

4.1.3 Data description

Simulated data

In order to evaluate our transient-informed regression approach, we applied both unconstrained regression and transient-informed regression to a simulated dataset.

To be realistic, we used the iCAPs maps $\tilde{\mathbf{M}} \in \mathbb{R}^{N_v \times K}$ that were retrieved from experimental data (see next paragraph). Then, to simulate block-like iCAP time courses $\tilde{\mathbf{A}}_{sim} \in \mathbb{R}^{K \times N_t}$, we first defined transient timings by a Poisson process. We simulated data for Poisson constants of 20, 15, 10 and 5 TR, as well as for Poisson parameters as estimated from experimental data by fitting a Poisson distribution to estimated innovation timings of each iCAP. In the latter case, Poisson parameters were ranging from 7.5 for iCAP 1 to 27 for iCAP 18. Simulated time courses for this setting will be called "realistic" in the following description. The number of simultaneously transitioning iCAPs was restricted to 3 for realistic simulations and 4, 6, 8, and 10 for Poisson constants 20, 15, 10 and 5, respectively. Simulated time courses were then created by setting the segment between two simulated innovations to a random amplitude drawn from a standard normal distribution.

To obtain simulated data at the voxel level, we take the simulated iCAPs time courses $\tilde{\mathbf{A}}_{sim}$ and generate voxel-wise activity-inducing signals

$$\mathbf{A}_{sim} = \tilde{\mathbf{M}}\tilde{\mathbf{A}}_{sim} + \boldsymbol{\epsilon},$$

with additive white Gaussian noise $\boldsymbol{\epsilon}$.

Activity-inducing signals were simulated without noise and at noise levels ranging from SNR=10 dB to SNR=-10 dB. For quantitative evaluation, the root mean squared error (RMSE) between retrieved and ground truth iCAP time courses was computed, at each noise level, for 10 repetitions of the aforementioned simulation process.

Experimental data

We included resting-state fMRI scans of 56 healthy subjects with no history of neurological or psychiatric disorders (M/F=23/33, age=16.85±5.69, range: 6-29 years) who were recruited in the scope of the Geneva 22q11 deletion syndrome cohort. From our initial sample of 80 subjects within the age range, we excluded 24 subjects based on a strict criterion for motion; i.e., framewise displacement (Power et al., 2012) was computed for all frames and subjects were excluded if more than 10 % of timepoints exceeded a threshold of 0.5 mm. Written informed consent was obtained from participants and their parents for subjects younger than 18 years old. The research protocols were approved by the Institutional Review Board of Geneva University School of Medicine.

Structural and functional MRI data were acquired at the Centre d'Imagerie BioMédicale (CIBM) in Geneva on a Siemens Trio (N=42) and a Siemens Prisma (N=14) 3 Tesla scanner. Anatomical images were acquired with a T1-weighted sequence of $0.86 \times 0.86 \times 1.1 \text{ mm}^3$ volumetric resolution (192 slices, TR=2500 ms, TE=3 ms, acquisition matrix=224 × 256, field of view=22 cm², flip angle=8°), and functional images with a T2*-weighted sequence of 8 minutes

(voxel size= $1.84 \times 1.84 \times 3.2 \text{ mm}^3$, 38 slices, TR=2400 ms, TE=30 ms, flip angle=85°). For the resting-state session, participants were asked to fixate a cross projected on a screen, let their minds wander while not thinking of anything in particular and not to fall asleep.

The fMRI scans were preprocessed using statistical parametric mapping (SPM12) (Wellcome Trust Centre for Neuroimaging, London, UK: <http://www.fil.ion.ucl.ac.uk/spm/>) and functions of the data processing assistant for resting-state fMRI (DPARSF) (Yan Chaogan, 2010) and individual brain atlases using statistical parametric mapping (IBASPM) (Aleman-Gomez et al., 2006) toolboxes. The first five frames were excluded to ensure magnetization stability. Preprocessing steps included realignment, spatial smoothing with an isotropic Gaussian kernel of 6 mm full-width half-maximum, co-registration of structural scans to the functional mean and segmentation with the SPM12 *Segmentation* algorithm (Ashburner and Friston, 2005). Average signals in the white matter (WM) and cerebrospinal fluid (CSF) were regressed from the fMRI data. Then, frames with high motion were marked according to their framewise displacement (Power et al., 2012) and if exceeding a threshold of 0.5 mm, were removed and filled in by cubic spline interpolation. Interpolation of removed frames is necessary as the implementation of TA deconvolution requires a constant sampling rate; i.e., a uniformly sampled HRF representation. TA was then applied in subject space, and the activity-inducing signals were subsequently normalized to MNI space using DARTEL (Ashburner, 2007), followed by the aforementioned thresholding and clustering steps.

4.1.4 Results

Consensus clustering

We applied consensus clustering on all significant transients for cluster numbers K going from 10 to 25 (see Supplementary Fig. B.1) and evaluated the results as proposed in (Monti et al., 2003). According to the CDF and the relative increase of AUC curves, the optimum number of clusters was $K = 18$. Visual observation of the ordered consensus matrices confirmed this number, since sub-sampled frames were most stably assigned to the same cluster. In the following, we will thus investigate results for 18 clusters.

Spatial maps

Spatial maps of iCAPs that were retrieved from 56 healthy subjects are shown on Supplementary Fig. B.2. To evaluate recovered iCAPs in terms of spatial overlap, we computed the Jaccard similarity index between thresholded maps at a z -score of 1.5. The Jaccard index is defined as the intersection of two binary maps k_1 and k_2 divided by their union:

$$J_{k_1, k_2} = \frac{\sum_v [(\tilde{m}(v, k_1) > 1.5) \cap (\tilde{m}(v, k_2) > 1.5)]}{\sum_v [(\tilde{m}(v, k_1) > 1.5) \cup (\tilde{m}(v, k_2) > 1.5)]}.$$

Significant similarity values were determined by 1000 random permutations of iCAPs voxels. Fig. 4.4 shows the Jaccard similarity between the 18 iCAPs. There is significant spatial overlap between 40 out of the 153 possible combinations of iCAPs (26.14 %). Highest similarity exists

4.1. Journal Article: Robust recovery of temporal overlap between network activity.

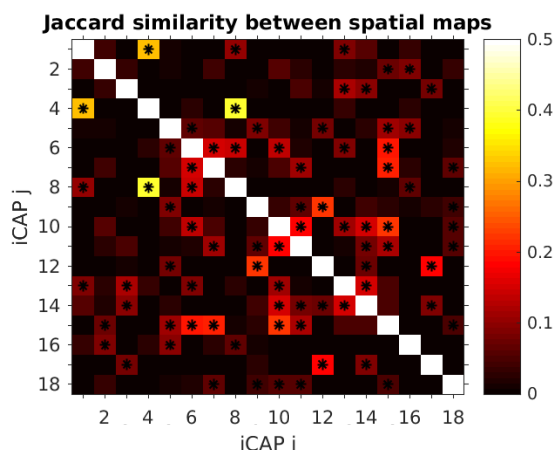


Figure 4.4 – Jaccard similarity index between spatial maps thresholded at a z -score of 1.5. Stars indicate significant values ($p < 0.01$ Bonferroni-corrected) determined with permutation testing.

between iCAP 4 (primary visual) and iCAP 8 (precuneus / visual) and between iCAP 4 and iCAP 1 (higher visual).

These results show that there is high spatial overlap between iCAPs. In the following sections, we demonstrate that this spatial overlap can introduce artifacts in time course retrieval, which can be corrected with transient-informed regression.

Simulated data: goodness of fit and temporal overlap

In order to compare unconstrained regression to transient-informed regression with known ground truth transients, we estimated time courses for different levels of noise and transient activity in the simulated data. Supplementary Table B.1 shows the quality of fit measured by the RMSE for both regression methods. RMSE values are lowest for a scenario without noise and increase with higher noise levels.

Across all assessed cases, transient-informed regression performs significantly better in retrieving block-wise time courses. Without noise, transient-informed regression with ground truth transients gives a perfect fit with RMSE close to zero. With increasing noise and with higher numbers of innovations (lower Poisson parameter), the RMSE increases slightly for transient-informed regression, but remains much lower than in unconstrained regression. Remarkably, even with very high noise and many innovations, transient-informed regression still performs more than 10 times better than unconstrained regression. We further evaluated regression with soft cluster assignment (see Supplementary Fig. B.3, first row). Here, the RMSE converges towards values between 0.02 and 0.08, which is higher than the RMSE in case of regression with ground truth innovations, but still significantly smaller than in unconstrained regression. Even the worst fit for hard cluster assignment ($\xi = 1$) gives a lower RMSE than unconstrained regression.

Fig. 4.5 shows the exemplary case of simulated time courses with SNR=0 dB and realistic

Poisson constants, which demonstrates that unconstrained regression estimates are clearly off.

Temporal overlap between iCAPs was evaluated by thresholding time courses at an absolute z -score of 1 (Karahanoglu et al., 2015). In simulated time courses, there are on average 5 to 6 simultaneously active iCAPs (see Supplementary Table B.2). Temporal overlap is consistently underestimated in unconstrained regression, while with transient-informed regression the estimated overlap is very close to the ground truth.

In simulated ground truth time courses, iCAPs appear with the same sign in 52 % to 55 % of all pairwise co-activations (i.e., either both iCAPs time courses positive or both negative, see Supplementary Table B.3). In unconstrained regression, same-signed co-activations are highly over-estimated. In fact, iCAPs appear almost always with the same sign if they are co-active (98 % to 100 %). In transient-informed regression, estimated percentages of same-signed iCAPs appearances are again very close to the ground truth.

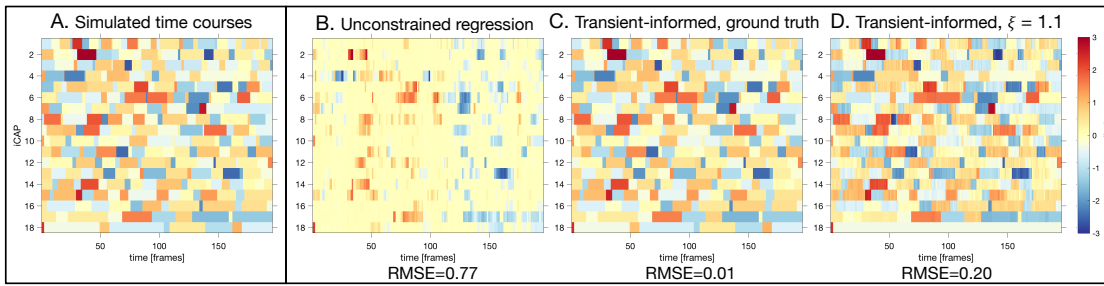


Figure 4.5 – A) Block-like time courses for transients with realistic Poisson constants from 7.5 (iCAP 1) to 27 (iCAP 18). B) to D) Time courses retrieved from activity-inducing signals, simulated with additive white Gaussian noise at SNR=0 dB B) with unconstrained regression, C) with transient-informed regression and ground truth transient timings, and D) with transient-informed regression and soft cluster assignment at $\xi = 1.1$. Unconstrained regression misses many activity blocks, while transient-informed regression manages to retrieve the ground truth time courses almost perfectly.

Experimental data: optimal soft assignment factor

Since in experimental data, the true innovations are not known, we use cluster assignments resulting from K-means to retrieve innovation timings (see subsection 4.1.2). To determine the optimum factor ξ for soft cluster assignment of innovation frames, we tested the correspondence between estimated and measured transient amplitudes. Measured amplitudes were calculated by thresholding normalized iCAPs maps at a z -score of 1.5, and for each innovation frame $\mathbf{i}(\cdot, t)$, computing the average transient amplitude within the regions part of all iCAPs showing an innovation. The measured overall amplitude was defined as the sum of average amplitudes of all transitioning iCAPs, weighted by their distance to the respective cluster centers. We then correlated these measured innovation amplitudes with the estimated innovation amplitudes, computed from iCAPs time courses $\tilde{a}(\cdot, t)$ by summing innovation

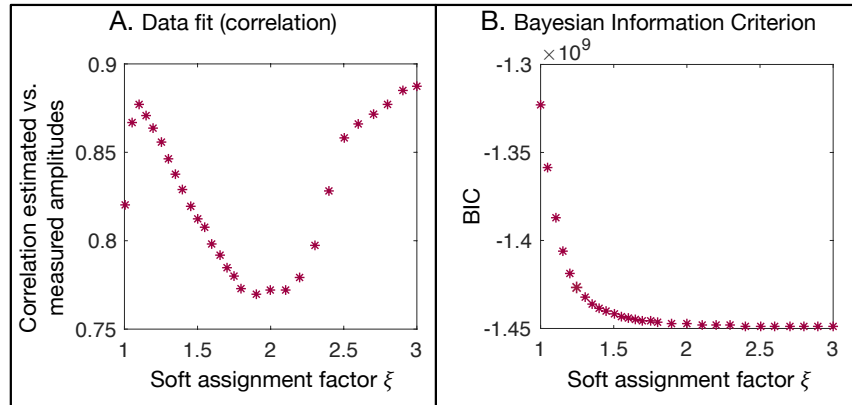


Figure 4.6 – Evaluation of soft assignment factors ξ from 1 (hard cluster assignment) to 3 (all iCAPs allowed to change at timepoints of significant transients).

amplitudes across all transitioning iCAPs, again weighted by the distance to the respective cluster centers.

Fig. 4.6 shows the correlation for different values of the soft assignment factor ξ . The correlation first increases with higher ξ , reaches a local maximum of 0.88 at $\xi = 1.1$ and then decreases again. For $\xi > 1.9$ the correlation increases again due to overfitting to noise at these high innovation numbers. For high ξ , the results approach the unconstrained regression solution, for which the correlation between measured and estimated innovations was 0.96. As an alternative, we also used the Bayesian information criterion (BIC) to evaluate different soft assignment factors. In this case, the optimum factor at the knee point of the curve was $\xi = 1.25$.

We also evaluated ξ on simulated data to validate the quality measures we used here (see Supplementary Fig. B.3). These evaluations on simulated data indicate that both correlation and BIC are good measures to estimate the optimum soft assignment factor ξ .

Experimental data: qualitative evaluation and temporal overlap

In Fig. 4.7, we show recovered time courses for one exemplary subject. In unconstrained regression results (Fig. 4.7A), there appear segments where almost all iCAPs are found active at the same time (e.g., red box). When comparing the estimated activations $\tilde{\mathbf{A}}$ with transient timings $\tilde{\mathbf{C}}_{\xi=1}$, significant differences (here represented for iCAP 9, red arrow) become evident. With transient-informed regression at $\xi = 1$ (Fig. 4.7B), time course changes are restricted to timepoints at a-priori known transient timepoints, which leads to a better correspondence between the transitions of $\tilde{\mathbf{A}}$ and $\tilde{\mathbf{C}}$. It is to note that signs of estimated transients of time courses $\tilde{\mathbf{a}}(k, \cdot)$ correspond well with the iCAP signs of $\tilde{\mathbf{c}}(k, \cdot)$, even though this was not explicitly imposed by the algorithm. However, for $\xi = 1$ activation changes are very sparse, suggesting that hard cluster assignment is a too restrictive constraint in the time course estimation. With transient-informed regression at optimum $\xi = 1.1$ (Fig. 4.7C), activations still correspond very well with transient timings, suppressing activations that are most likely wrong (as in iCAP 9,

red arrow). Yet, retrieved signals are more smooth and multiple iCAPs can change at the same time. The probably falsely detected activations retrieved during unconstrained regression may have been introduced by spatial dependence between the iCAPs (Fig. 4.7D).

To investigate differences in the whole group, we computed temporal overlap and total activity duration in every subject and compared the results for the different regression approaches. Again, time courses were thresholded at an absolute z -score of 1 to find activity timepoints. Across subjects, temporal overlap in unconstrained regression and transient-informed regression at $\xi = 1$ revealed 3.06 ± 0.36 and 3.02 ± 0.39 co-active iCAPs on average, respectively. In transient-informed regression at optimal $\xi = 1.1$, temporal overlap was significantly higher with 3.47 ± 0.44 co-active iCAPs on average.

From qualitative observation in single subjects (e.g., Fig. 4.7), we hypothesized that spatial overlap leads to an over-estimation of co-activations with the same sign in unconstrained estimates. To test for this quantitatively, we computed the percentage of co-activations with the same sign for pairwise combinations of iCAPs (Fig. 4.8) and correlated these co-activation occurrences with spatial Jaccard similarity (subsection 4.1.4). In unconstrained regression, 85.99 % of all pairwise iCAPs co-activations had the same sign, while in transient-informed regression this was only the case in 45.99 % ($\xi = 1$) and 47.56 % ($\xi = 1.1$) of co-activations. Correlation of the percentage of same-signed co-activations with Jaccard similarity was very high for unconstrained regression ($\rho = 0.54$, $p < 0.001$), almost zero ($\rho = 0.09$, $p = 0.27$) for $\xi = 1$, and in between the two previous values ($\rho = 0.31$, $p < 0.001$) for optimal $\xi = 1.1$.

As a large confound in fMRI analysis is motion, we conducted an additional analysis to verify whether the over-representation of same-signed co-activations in unconstrained regression might be related to motion artifacts. For this, we computed the overall percentage of same-signed co-activations across all pairwise iCAPs combinations for each subject and then calculated the correlation across subjects between this measure and the average framewise displacement. There was a tendency relationship in unconstrained regression ($\rho = 0.26$, $p = 0.05$) suggesting that in subjects with higher motion, there is a higher over-representation of same-signed co-activations. In transient-informed regression this relationship was entirely corrected, both for $\xi = 1$ ($\rho = -0.01$, $p = 0.93$) and for $\xi = 1.1$ ($\rho = 0.02$, $p = 0.86$).

4.1.5 Discussion

fMRI is one unique tomographic imaging modality to observe the brain at work in a non-invasive way, however, the rich structure of the data requires advanced analysis methods. The iCAPs framework combines two main ingredients: first, the TA deconvolution with regularization that drives sparse innovation signals; and, second, temporal clustering of fMRI frames with strong innovations. As temporal clustering allows for spatial overlap of the iCAPs maps, the recovery of the associated time courses from activity-inducing signals can be impeded if a timepoint-wise spatial regression is used to which we refer as unconstrained regression. We observed this effect not only qualitatively in iCAPs' activity-inducing time courses of single subjects (e.g., Fig. 4.7A, red box), but we also confirmed it quantitatively in simulated and experimental data. In particular, iCAPs appeared significantly more with the same sign

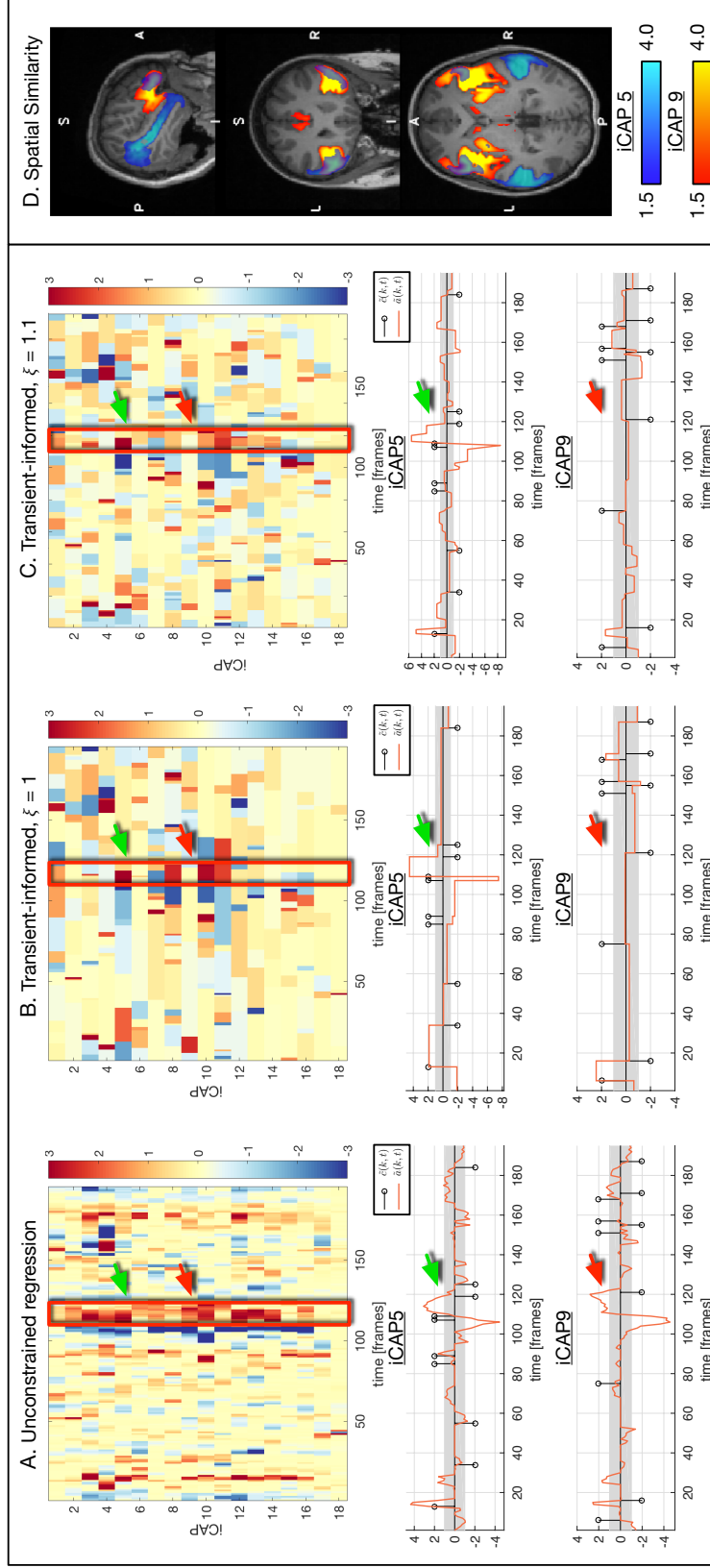


Figure 4.7 – A) Estimates from unconstrained regression for one exemplary subject. Top plots show time courses $\hat{\mathbf{a}}(\cdot, t)$ for all 18 iCAPs and bottom plots show time courses of iCAP 5 and 9 with their transient indicator functions $\tilde{\mathbf{c}}_{\xi=1}(5, \cdot)$ and $\tilde{\mathbf{c}}_{\xi=1}(9, \cdot)$. The activation threshold $z\text{-score } |1|$ is shown as gray background. $\hat{\mathbf{a}}(9, \cdot)$ contains activity which is not seen in $\tilde{\mathbf{c}}_{\xi=1}(9, \cdot)$ (red arrow). Changes in $\hat{\mathbf{a}}(5, \cdot)$ correspond better to transient locations (green arrow). B) Transient-informed regression at $\xi = 1$ yields a better correspondence between time courses $\hat{\mathbf{a}}(k, \cdot)$ and transients $\tilde{\mathbf{c}}_{\xi=1}(k, \cdot)$, but contain very sparse, biologically unlikely activations. C) Transient-informed regression at optimum $\xi = 1.1$ still suppresses unlikely activations such as in iCAP 9 (red arrow), but allows multiple iCAPs to change simultaneously and leads to smoother time courses. D) There is significant spatial overlap between iCAP 5 and iCAP 9, which may have introduced the artifacts seen in the time course of iCAP 9 using unconstrained regression.

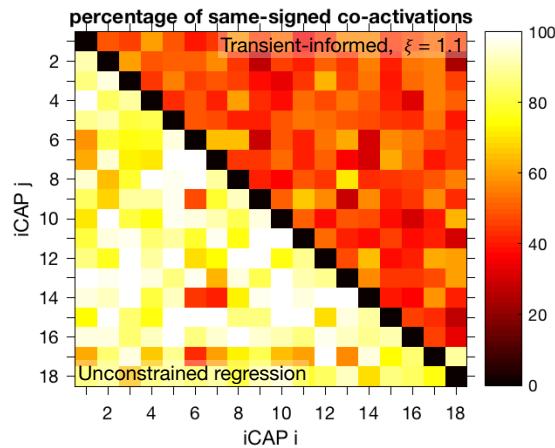


Figure 4.8 – Percentage of appearances with the same sign for pairwise co-occurrences of iCAPs in unconstrained regression (below diagonal) and in transient-informed regression with $\xi = 1.1$ (above diagonal). In unconstrained regression estimates, iCAPs appear mostly with the same sign.

(activated vs de-activated) when using the unconstrained regression. The high correlation between measures of spatial and temporal overlap further corroborates that without the use of additional constraints, temporal co-activation caused by spatial dependencies cannot be well differentiated from true underlying co-activation. The contribution of this work is to exploit the additional information that is available from the TA deconvolution procedure; i.e., innovations that encode moments of transient activity—information that can be advantageously incorporated in a spatio-temporal regression procedure for more consistent results. The recovered activity-inducing signals then play a crucial role in evaluating more general measures, for instance, iCAPs configurations of temporal overlap (Karahanoglu et al., 2015) or more advanced temporal models; e.g., hidden Markov models (Bolton et al., 2018).

Applied on simulated data with known timepoints of transient activity, the proposed approach performed significantly better in recovering block-like time courses than unconstrained regression, both in terms of estimation error and estimated temporal overlap between networks. We demonstrated that temporal overlap between networks is consistently underestimated by unconstrained regression, while there is no such systematic bias in transient-informed estimates. This bias is towards same-signed co-activations in unconstrained estimates. These results show that the new procedure exploits well the additional information (i.e., transient timepoints) that is available in the simulated setting as ground truth.

For the experimental results, we applied the iCAPs framework on a sample of 56 healthy subjects. We observed significant spatial overlap between 26 % of retrieved iCAPs maps. Higher spatial similarity was mainly observed in networks containing posterior regions (posterior cingulate and visual networks), which confirms observations by (Karahanoglu et al., 2015) of high spatial overlap mainly in posterior regions. Spatial overlap is clearly a feature of resting-state networks when allowed for. We then used soft cluster assignment of transient frames to account for the fact that ground truth transients are not known. The optimal factor for

4.1. Journal Article: Robust recovery of temporal overlap between network activity.

soft cluster assignment was of similar scale if evaluated in terms of correspondence between measured and estimated transients ($\xi = 1.1$) and in terms of BIC ($\xi = 1.25$), which was also confirmed in simulations (see Supplementary Fig. B.3). For $\xi = 1.1$, the correlation between spatial and temporal overlap was still significant, but substantially lower than in unconstrained regression. However, the estimated percentage of same-signed co-activations was only slightly higher than for the most restrictive case $\xi = 1$ and substantially lower than in the unconstrained case. Together, these results suggest that even though the interaction between spatial and temporal overlap could not be completely avoided, false temporal co-activations due to spatial dependence, as indicated by an over-representation of same-sign co-activations, could be significantly reduced. Furthermore, motion-related effects on the sign of co-activations were entirely removed in transient-informed regression.

Transient-informed regression can be related to more general nonlinear regression methods such as segmented regression, spline regression in the case of piecewise polynomial functions (Wegman and Wright, 1983), and locally weighted regression (Cleveland and Devlin, 1988; Atkeson et al., 1997). In those cases, the input space is decomposed in (usually uniformly distributed) sub-parts, and independent regressions are applied to each of them. A large body of literature also exists on the estimation of breakpoints in a segmented regression problem (e.g., Acharya et al., 2016; Yamamoto and Perron, 2013). Approaches inspired by this principle have been applied in neuroimaging; e.g., dynamic connectivity regression (DCR) (Cribben et al., 2012), which detects change points of FC by subsequently sub-dividing the time courses in windows with variable length. While segmented regression methods either assume equally spaced change points or estimate the optimum change points from the data, in the present work, change points are not estimated during regression, but taken from the transients that are revealed by the deconvolution and derivative in the previous processing steps. Further, it is to note that most segmented regression approaches apply the same change points to the whole brain while in the present work, we extract and apply change points that are *specific* to each network, which allows for a high flexibility in retrieving independent time courses for each network. In addition to change points, a second piece of information is taken from previous processing steps: the spatial information of the iCAPs maps is used to group voxels and, therefore, both spatial and temporal constraints are included in a single spatio-temporal regression. Since change points are defined based on transients and no second-order correlations need to be computed, the approach overcomes limitations related to the selection of the window size for dFC calculation. Furthermore, it allows to recover temporal overlap, which is not possible in change point detection approaches that are based on temporal subdivision into windows (Cribben et al., 2012; Xu and Lindquist, 2015) or in point process approaches that only detect co-activation of brain regions (Tagliazucchi et al., 2012; Liu and Duyn, 2013; Liu et al., 2013). We also mention the more recent use of temporal ICA (Smith et al., 2012) for fMRI data. Here, temporal statistical independence is favored, but since there is no derivative involved, temporal overlap can as well not be accounted for, and thus the method has only been deployed for fast-TR and long acquisitions.

The iCAPs approach is also closely related to other methodologies that allow networks to be temporally overlapping. The probably most widely used such methodology to date is ICA that

relies on a surrogate measure for statistical independence (Calhoun et al., 2001). Conventional ICA for fMRI deploys this criterion in the spatial domain due to the dimensionality of the data ($N_v \gg N_t$) and concatenates all subjects' data in the temporal dimension. Therefore, the estimated sources at the group level are spatial maps and the recovery of the individuals' time courses is required, for which three main approaches have emerged (Erhardt et al., 2011; Du et al., 2016). First, back-reconstruction (Calhoun et al., 2001) of temporal principal component analysis (PCA) reduced data recovers time courses by applying the inverse PCA projections. Second, the dual regression technique (Beckmann et al., 2009) uses the group-level maps as regressors on the individual complete functional data. The obtained time courses are then normalized and used on their turn as regressors to obtain individual maps. Third, spatially constrained ICA (Du et al., 2016) relies on a similar approach for time course recovery, but estimates individual maps first and then uses them as regressors on the individual blood oxygenation level dependent (BOLD) signals for each subject separately. In the latter two approaches, time courses are basically recovered by spatial regression for each timepoint, which is essentially the same procedure as in the original iCAPs framework (Karahanoglu et al., 2013) that we called "unconstrained regression" in the current paper. Similar to iCAPs, these ICA-based approaches allow to recover temporal overlap of brain networks (e.g., (Miller et al., 2016)). Contrary to ICs, iCAPs can be spatially correlated (see also Supplementary Figs. B.4 and B.5), which requires the introduction of constraints for the successful recovery of temporal overlap as proposed in the current paper. When accounted for this artifact, the iCAPs framework is unique in its ability to give access to spatially *and* temporally overlapping brain networks.

It is noteworthy that statistical dependence is not equivalent to spatial overlap; i.e., spatial ICs being uncorrelated does not necessarily mean that they cannot contain spatial overlap (Daubechies et al., 2009; Calhoun et al., 2013). However, overlapping areas in ICs mostly appear with different sign to ensure that the maps are spatially uncorrelated. In practice, ICs appear thus either spatially segregated or introduce negativity, which impedes interpretability. Additionally, ICA is based on a source separation model that does not explicitly include a noise term and consequently, ICs of interest have to be visually inspected and selected, whereas TA already includes denoising and deconvolution. With the iCAPs framework, we found multiple networks including the posterior cingulate cortex that do not only include the default mode network (DMN) (Karahanoglu et al., 2015), an observation that had never been revealed before.

From a neuroscientific perspective, the present results support the view of functional networks of distributed brain regions that co-activate with substantial temporal overlap. Our results further improve the iCAPs approach with better and more robust time course recovery. The fact that iCAPs seem to co-activate and -deactivate in approximately a balanced way corroborates recent findings using other methodologies. For instance, dominant spatial patterns of voxel-wise sliding-window dFC are characterized by roughly task-negative versus -positive networks, however, with notable subsystems of each network that change side (Preti and Van De Ville, 2017). The organization of the brain in two opposing networks has also been explained using topographic principles on the cortical surface derived from resting-state FC (Margulies et al., 2016). Similar dynamic behavior was reported by (Zalesky et al.,

4.1. Journal Article: Robust recovery of temporal overlap between network activity.

2014) using graph-based FC and measures of modular network organization. In terms of potential applications, dynamic analysis of large-scale brain networks is of high interest in the investigation of brain development with age (as demonstrated, for example, in (Hutchison and Morton, 2015; Qin et al., 2015; Hutchison and Morton, 2016; Ryali et al., 2016; Viviano et al., 2017)). In section B.1.3. Supplementary Results, we show that temporal properties of iCAPs retrieved with the method proposed here are correlated with age, which further supports the relevance of dynamic network activity for development. Other applications of interest include the investigation of the relationship between brain function and cognition (Cohen, 2018), or in the search for alterations and biomarkers in clinical populations (e.g., in patients with schizophrenia (Damaraju et al., 2014), autism (Wee et al., 2016), or Alzheimer's disease (Córdova-Palomera et al., 2017)). Finally, the proposed methodology is not restricted to the analysis of resting-state data since task-based paradigms can also be analyzed, which is of particular interest when probing into functional brain mechanisms related to cognition and behavioral performance (Cohen, 2018; Medaglia et al., 2015).

4.1.6 Conclusions and future directions

We have addressed the crucial step in the iCAPs framework of activity-inducing time course recovery, which is essential to properly quantify temporal overlap of functional brain networks. We showed that the conventional unconstrained regression approach is hindered by spatial dependencies of the iCAPs maps, which cannot be avoided as these maps are spatially overlapping and not orthogonal. We therefore have introduced a transient-informed spatio-temporal regression scheme, which incorporates knowledge on transients and finds the activity-inducing signal levels by a global fit. We validated our approach on simulated data and demonstrated its potential on experimental data.

The iCAPs framework is still a fairly new approach for large-scale network retrieval, and even though it is unique in its potential to retrieve spatially *and* temporally overlapping networks, there are still possible improvements that can be made in the framework. First, in the TA step, the HRF deconvolution using TA could possibly be improved by the consideration of a variable HRF model (Rangaprakash et al., 2018). Second, the selection of the number of clusters for retrieval of iCAPs maps is not unique. Here, we selected $K = 18$ clusters since consensus clustering showed high stability, which was not significantly improved by considering more clusters. However, clustering was also fairly stable for different K . Future work should explicitly address this question by investigating stability and consistency for different numbers of clusters.

Finally, physiological noise such as motion or spontaneous breath hold is always a confounding factor. Here, we used scrubbing and regression of WM and CSF signals to account for such artifacts. We further demonstrated that the effect of motion on erroneous time course estimation could be corrected by using transient-based constraints. However, further research should investigate whether there is a relationship between all types of physiological noise and the occurrence or co-occurrence of particular networks.

4.2 Journal Article: Dynamics of large-scale brain networks in 22q11DS.

Postprint version of the article published in: Biological Psychiatry: Cognitive Neuroscience and Neuroimaging 2019, in press, <https://doi.org/10.1016/j.bpsc.2019.04.004>

Large-scale brain network dynamics provide a measure of psychosis and anxiety in 22q11.2 deletion syndrome.

Daniela Zöllner^{1,2,3}, Corrado Sandini³, Fikret Işık Karahanoğlu^{4,5}, Maria Carmela Padula^{3,6}, Marie Schaer³, Stephan Eliez³, Dimitri Van De Ville^{1,2}

¹Medical Image Processing Laboratory, Institute of Bioengineering, École Polytechnique Fédérale de Lausanne (EPFL), Lausanne, Switzerland; ²Department of Radiology and Medical Informatics, University of Geneva, Geneva, Switzerland; ³Developmental Imaging and Psychopathology Laboratory, Office Médico-Pédagogique, Department of Psychiatry, University of Geneva, Geneva, Switzerland; ⁴Athinoula A. Martinos Center for Biomedical Imaging, Charlestown, MA, United States; ⁵Department of Radiology, Massachusetts General Hospital, Harvard Medical School, Boston, MA, United States; ⁶Friedrich Miescher Institute for Biomedical Research, Basel, Switzerland

Prodromal positive psychotic symptoms and anxiety are two strong risk factors for schizophrenia in chromosome 22q11.2 deletion syndrome (22q11DS). The analysis of large-scale brain network dynamics during rest is promising to investigate aberrant brain function and identify potentially more reliable biomarkers. We retrieved and examined dynamics of large-scale functional brain networks using innovation-driven co-activation patterns (iCAPs) and probed into functional signatures of prodromal psychotic symptoms and anxiety. Patients with 22q11DS had shorter activation in cognitive brain networks and longer activation in emotion processing networks. Functional signatures of prodromal psychotic symptoms confirmed an implication of cingulo-prefrontal salience network activation duration and coupling. Functional signatures of anxiety uncovered an implication of amygdala activation and coupling, indicating differential roles of dorsal and ventral sub-divisions of anterior cingulate and medial prefrontal cortices. These results confirm that the dynamic nature of brain network activation contains essential function to develop clinically relevant imaging markers of psychosis vulnerability.

4.2.1 Introduction

Schizophrenia is a strongly debilitating mental disorder both for affected individuals and in terms of societal cost (Insel, 2010; Gore et al., 2011). Converging evidence suggests that schizophrenia is a progressive neurodevelopmental disorder, given that in most cases, sub-clinical psychiatric and cognitive symptoms of the disorder are present several years prior to the onset of a full-blown psychotic episode (Insel, 2010; Fusar-Poli et al., 2013; Kremen et al., 2010; Marín, 2016; Rapoport et al., 2012; Yung et al., 2005). The neurodevelopmental model critically implies that earlier interventions might prove more effective in preventing

4.2. Journal Article: Dynamics of large-scale brain networks in 22q11DS.

the progression towards psychosis (Marín, 2016; Millan et al., 2016). Hence extensive research has been devoted to characterizing the prodromal disease stage, also known as psychosis High-Risk State (Fusar-Poli et al., 2013). In particular, the presence of attenuated positive psychotic symptoms, operationalized in the Ultra-High-Risk criteria (Yung et al., 2006), confers a strongly increased 30-40% risk of developing psychosis (Fusar-Poli et al., 2012). While current clinical management is based purely on clinical observation (Nelson et al., 2018; Schmidt et al., 2015), the identification of biomarkers of early psychosis could improve our understanding of the pathophysiology in its earliest disease stage (Kapur et al., 2012). In this sense, the addition of imaging markers to the existing clinical diagnostic tools could allow the establishment of more precise biomarker-informed stages in the evolution of psychosis, which would give way to more targeted therapeutic strategies and improved clinical outcomes (Insel, 2010; Millan et al., 2016; Kapur et al., 2012).

Chromosome 22q11.2 deletion syndrome (22q11DS) is a neurodevelopmental disorder coming with a highly elevated risk for schizophrenia with a 30%-40% prevalence by adulthood (Schneider et al., 2014). Most patients with 22q11DS are diagnosed already during childhood, which allows to characterize the earliest stages of schizophrenia's disease course (Insel, 2010; Bassett and Chow, 1999). Similarly to the general population the presence of attenuated psychotic symptoms strongly increases the risk of psychosis in 22q11DS pointing to a common clinical trajectory with non-syndromic schizophrenia (Schneider et al., 2016). Moreover, anxiety has emerged as another strong risk factor for psychosis in 22q11DS (Gothelf et al., 2007, 2013). These clinical findings point to the particular importance of understanding the pathophysiology and characterizing biomarkers of attenuated psychotic symptoms and anxiety in 22q11DS.

Among the tools to characterize biomarkers, resting-state functional magnetic resonance imaging (rs-fMRI) has emerged as promising (Satterthwaite and Baker, 2015). fMRI provides the unique opportunity to non-invasively observe brain function, and the resting condition is especially well-suited in clinical populations because it requires minimal compliance from participants. Most studies on rs-fMRI in psychosis to date have used static functional connectivity (sFC); i.e., the correlation between the activation in different brain regions over the whole scanning time (Van Den Heuvel and Fornito, 2014). However, a limitation of such static approaches is that they ignore the inherently dynamic nature of brain activity with potentially valuable information contained in dynamic changes of activation and connectivity (Chang and Glover, 2010; Christoff et al., 2016; Preti et al., 2017; Hutchison et al., 2013b; Karahanoglu and Van De Ville, 2017). In this perspective, dynamic approaches have the potential to identify more precise and more reliable biomarkers, and are particularly promising in schizophrenia, given the multiplicity of affected behavioral domains and brain circuits (Calhoun et al., 2014; Buckholz and Meyer-Lindenberg, 2012; Fornito et al., 2012; Van Den Heuvel et al., 2013; Van Den Heuvel and Fornito, 2014). Studies on dynamic brain function in schizophrenia point towards disrupted dynamic interaction between several brain states, in particular of subcortico-cortical connectivity (Damaraju et al., 2014) and connections of the default mode network (DMN) (Du et al., 2016; Miller et al., 2016; Su et al., 2016; Sakoglu et al., 2010). The few studies to date investigating dynamic FC (dFC) in individuals at clinical high risk found

reduced dFC of salience network (SN) and DMN (Pelletier-Baldelli et al., 2018) and stronger alterations in early schizophrenia patients than subjects at ultra high risk (Du et al., 2018), underlining the potential of dynamic brain function to improve our understanding of the pathophysiology in subjects at risk for schizophrenia.

Despite these promises of dynamic fMRI analysis, functional neuroimaging research in 22q11DS has so far mostly focused on static functional features (Debbané et al., 2012; Scariati et al., 2014; Mattiaccio et al., 2016; Schreiner et al., 2017; Mattiaccio et al., 2018), often targeting only specific networks such as the DMN (Padula et al., 2015; Schreiner et al., 2014). The studies who explicitly investigated psychotic symptoms in 22q11DS showed correlations of DMN dysconnectivity with prodromal psychotic symptoms (Debbané et al., 2012), as well as successful discrimination between patients at high vs. low risk based whole-brain rs-fMRI (Scariati et al., 2014) and hypoconnectivity of DMN, SN, anterior cingulate cortex (ACC) and fronto-parietal network (FPN) (Schreiner et al., 2017). Further, in the only two studies to date investigating a dynamic feature of brain function in 22q11DS – the variability of blood oxygenation level dependent (BOLD) signals – we found widespread reductions in brain variability in 22q11DS (Zöllner et al., 2017), and reduced variability in the dorsal ACC in patients with higher prodromal psychotic symptoms (Zöllner et al., 2018). In general, aberrant function, but also structure of the ACC has been suggested as a neuroimaging marker for the development of psychosis in 22q11DS (Padula et al., 2018) and might reflect dysfunctional self-monitoring and salience processing, possible mechanisms for the emergence of psychosis (Kapur, 2003).

Among the multiple methods to investigate dynamic fMRI (Preti et al., 2017), many have already been applied in schizophrenia as outlined above (Calhoun et al., 2014; Du et al., 2018). Sliding-window dFC tracks changes in FC by computing FC in a temporal window that is shifted over time (Chang and Glover, 2010; Sakoglu et al., 2010), but are limited by the necessity to choose the window size, and can only detect relatively slow changes in FC (Leonardi and Van De Ville, 2015). Alternatively, so-called first-order approaches rely on temporal clustering of fMRI frames to obtain “co-activation patterns” (CAPs) (Liu et al., 2016). Here, even fast changes can be traced as no minimum activation duration needs to be specified. However, only one brain state (or CAP) can be active at a time point. To overcome these limitations, the recently introduced innovation-driven co-activation patterns (iCAPs) framework detects moments of significantly *changing* brain activity to extract large-scale brain networks and their dynamic properties (Karahanoğlu et al., 2015; Karahanoğlu and Van De Ville, 2017; Zöllner et al., 2019b). Here, brain networks are retrieved from dynamic activation changes, which allows to robustly retrieve spatially *and* temporally overlapping brain networks.

In this study, we complement the existing literature on dFC in schizophrenia by using iCAPs combined with multivariate pattern analysis to identify potential biomarkers for psychosis vulnerability in 22q11DS. We detect functional fingerprints of anxiety and positive prodromal symptoms, two symptoms that have emerged as reliable predictors of psychosis in 22q11DS (Gothelf et al., 2013; Schneider et al., 2016).

4.2.2 Methods and materials

Participants

The study included 221 subjects (111 patients with 22q11DS, 110 healthy controls (HCs), both aged 8–30 years). We excluded 33 patients and 25 HCs to ensure good data quality (see Supplementary Methods). The final sample included 78 patients with 22q11DS (37 males) and 85 HCs (36 males, see Table 4.2). HCs were recruited among patients' siblings and through the Geneva state school system and had no present or past history of neurological or psychiatric disorders.

Prodromal positive psychotic symptoms in patients with 22q11DS were assessed using the structured interview of prodromal symptoms (SIPS) (Miller et al., 2003). The SIPS was not conducted in HCs. Anxiety was assessed both in HCs and patients with 22q11DS by combining the child behavioral checklist (CBCL) Anxious-Depressed scale (Achenbach, 1991), and the adult behavioral checklist (ABCL) Anxious scale in adults above 18 years old (Achenbach and Rescorla, 2003).

Participants and their parents (for minors) gave their written informed consent and the research protocols were approved by the Institutional Review Board of Geneva University School of Medicine.

Image acquisition

All MRI brain scans were acquired at the Centre d'Imagerie BioMédicale (CIBM) in Geneva on a Siemens Trio (12-channel coil; 54 HCs, 42 patients) and a Siemens Prisma (20-channel coil; 31 HCs, 36 patients) 3 Tesla scanner. Structural images were obtained with a T1-weighted sequence of $0.86 \times 0.86 \times 1.1 \text{ mm}^3$ volumetric resolution (192 coronal slices, TR = 2500 ms, TE = 3 ms, acquisition matrix = 224×256 , field of view = 22 cm^2 , flip angle = 8°). Rs-fMRI data were recorded with a T2*-weighted sequence of 8 minutes (voxel size = $1.84 \times 1.84 \times 3.2 \text{ mm}$, 38 axial slices, TR = 2400 ms, TE = 30 ms, flip angle = 85°). Subjects were instructed to fixate a cross on the screen, let their mind wander and not to fall asleep.

Preprocessing

Before applying the iCAPs pipeline, MRI scans were preprocessed using statistical parametric mapping (SPM12) (<http://www.fil.ion.ucl.ac.uk/spm/>) and functions of the data processing assistant for resting-state fMRI (DPARSF) (Yan Chaogan, 2010) and individual brain atlases using statistical parametric mapping (IBASPM) (Aleman-Gomez et al., 2006) toolboxes. After realignment of functional scans, we applied spatial smoothing with an isotropic Gaussian kernel of 6 mm full width half maximum and coregistered structural scans to the functional mean. Structural images were segmented with the SPM12 *Segmentation* algorithm (Ashburner and Friston, 2005) and a study-specific template was generated using diffeomorphic anatomical registration (DARTEL) (Ashburner, 2007). Then, the first five functional scans were excluded and average white-matter and cerebrospinal fluid (CSF) signals were regressed out from the BOLD timeseries. We applied motion scrubbing (Power et al., 2012) for correction of motion artifacts, marking frames with a framewise displacement of more than 0.5 mm. As the filters

Table 4.2 – Participants demographics. N/A = not applicable.

	HC	22q11DS	p-value
Number of subjects (M/F)	85 (36/49)	78 (37/41)	0.514 (χ^2)
Age mean \pm SD (range)	16.73 \pm 5.85 (8.1-30.0)	17.19 \pm 5.37 (8.1-29.7)	0.603
Right handed*	80.00%	77.94%	0.715 (χ^2)
IQ**	110.12 \pm 13.78	70.01 \pm 12.41	<0.001
N. subjects meeting criteria for psychiatric diagnosis	N/A	43 (55%)	
Anxiety disorder	N/A	9	
Attention deficit hyperactivity disorder	N/A	8	
Mood disorder	N/A	5	
Schizophrenia or Schizoaffective Disorder	N/A	4	
More than one psychiatric disorder	N/A	17	
N. subjects medicated			
Methylphenidate	0	9	
Antipsychotics	0	3	
Anticonvulsants	0	1	
Antidepressants	0	1	
More than one class of medication	0	3	

* Handedness was measured using the Edinburgh laterality quotient, right handedness was defined by a score of more than 50. ** IQ was measured using the Wechsler Intelligence Scale for Children–III (Wechsler, 1991) for children and the Wechsler Adult Intelligence Scale–III (Wechsler, 1997) for adults.

implemented in the iCAPs framework require a constant sampling rate, marked frames were replaced by the spline interpolation of previous and following frames. Finally, motion frames were excluded before computation of temporal characteristics (described below).

Total activation and iCAPs

We used openly available Matlab code (<https://c4science.ch/source/iCAPs/>) to apply iCAPs (Karahanoglu et al., 2015; Karahanoglu and Van De Ville, 2017; Zöllner et al., 2019b). We first employed Total Activation (Karahanoglu et al., 2011, 2013; Farouj et al., 2017), which applies hemodynamically-informed deconvolution to the fMRI timeseries through spatio-temporal regularization. Significant activation change points (i.e., transients), derived from deconvolved timeseries, were concatenated across all subjects and fed into temporal K-means clustering to obtain simultaneously transitioning brain patterns, the iCAPs. The optimum number of 17 clusters was determined by consensus clustering (Monti et al., 2003, see Supplementary Figures B.7 and B.8). Finally, time courses were obtained for all iCAPs using spatio-temporal

4.2. Journal Article: Dynamics of large-scale brain networks in 22q11DS.

transient-informed regression (Zöller et al., 2019b). A detailed description of all steps can be found in the Supplementary Methods.

Extraction of temporal properties

For computation of temporal properties, iCAPs time courses were z-scored within each subject and thresholded at a z-score $> |1|$ to determine ‘active’ timepoints (Karahanoglu et al., 2015). For each iCAP, we then computed the total duration of overall activation as percentage of the total non-motion scanning time.

Further, coupling and anti-coupling duration of two iCAPs were calculated as timepoints of same-signed or oppositely-signed co-activation measured as percentage of the total non-motion scanning time or as Jaccard score; i.e., percent joint activation time of the two respective iCAPs.

Statistical analysis

Group comparisons of iCAPs activation measures Duration and coupling measures between groups were compared using two-sample t-tests. P-values were corrected for multiple comparisons with the false discovery rate (FDR).

Partial least squares correlation To evaluate multivariate patterns of correlation between behavioral variables and iCAPs activation measures, we used behavior partial least squares correlation (PLSC) (Krishnan et al., 2011). Briefly, we first computed a correlation matrix between behavioral variables and brain variables. Group-specific correlation matrices of HCs and patients with 22q11DS were concatenated and singular value decomposition of this matrix then lead to several correlation components (CorrComps). Each CorrComp is composed of a set of “behavior weights” and “iCAPs duration/coupling weights”, which indicate how strongly each variable contributes to the multivariate brain-behavior correlation. Significance of CorrComps was determined by permutation testing (1000 permutations). Stability of brain and behavior weights was obtained using bootstrapping (500 bootstrap samples). See Supplementary Methods for a detailed outline of PLSC.

Here, we first conducted two PLSC analyses with duration of altered iCAPs as brain variables and psychotic symptoms, respectively anxiety, as behavioral variables. In four more PLSC analyses, we then investigated positive couplings and anti-couplings of one selected iCAP for each behavioral measure. Due to differences in design of each PLSC in terms of measure type and number of items, we did not correct for multiple comparisons.

Nuisance variable regression Age, gender and motion were included as nuisance regressors in group comparisons and PLSC analyses. Nuisance regressors were standardized within each group to avoid linear dependence with the effects of interest.

4.2.3 Results

Extracted spatial maps correspond to known resting-state networks

We applied the iCAPs framework to rs-fMRI scans of both HCs and patients with 22q11DS. Identified iCAPs correspond to well-known resting-state networks (see Figure 4.9 and Supplementary Table B.5). The obtained networks included sensory-related networks such as primary visual 1 (PrimVIS1), primary visual 2 (PrimVIS2), secondary visual (SecVIS), auditory / sensorimotor (AUD/SM) and sensorimotor (SM) networks. The DMN was decomposed into anterior DMN (aDMN), posterior DMN (pDMN) and precuneus / ventral DMN (PREC/vDMN). There were two attention-related iCAPs; i.e., FPN and visuospatial network (VSN). Two iCAPs included regions commonly considered as the SN: the anterior insula (aIN) and dorsal anterior cingulate cortex / dorsolateral prefrontal cortex (dACC/dlPFC). The remaining iCAPs comprised a language network (LAN), inferior temporal / fusiform (iTEMP/FUS), amygdala / hippocampus (AMY/HIP), orbitofrontal cortex (OFC) and prefrontal cortex (PFC).

Altered iCAPs' activation and coupling in 22q11DS

To probe into alterations of the identified networks' temporal properties in patients with 22q11DS, we first investigated aberrant activation duration followed by the analysis of altered network interactions; i.e., duration of positive coupling (co-activation with same sign) or anti-coupling (co-activation with opposite sign) between all pair-wise combinations of iCAPs.

Altered duration of iCAPs' activation Figure 4.10 shows duration for all 17 iCAPs in percentage of total non-motion scanning time. Median total activation time ranged from 34.36 % for LAN to 1.54 % for PFC. Patients with 22q11DS had significantly shorter activation of dACC/dlPFC, PrimVIS2, FPN, aDMN and pDMN and significantly longer activation of SM, iTEMP/FUS, AMY/HIP and OFC.

Alterations in temporal coupling of networks Figure 4.11 shows significant group differences in iCAPs' coupling. For several networks the duration of coupling was longer in patients with 22q11DS than in controls. This was true for 6 positive couplings and 13 anti-couplings. Fewer networks had shorter duration of coupling in patients with 22q11DS (1 positive coupling, 5 anti-couplings). Globally, alterations were more numerous for anti-couplings (25 in total) than for positive couplings (6 in total).

Functional signature of positive psychotic symptoms

To look into the behavioral relevance of these aberrant activation and coupling, we conducted behavior PLSC including positive symptoms.

Altered iCAPs' duration associated with psychotic symptoms A first PLSC analysis including positive SIPS items in 22q11DS and iCAPs' activation duration of the nine altered iCAPs (see figure 4.10) resulted in one significant CorrComp ($p=0.05$, see figure 4.12A). Duration of dACC/dlPFC, FPN and iTEMP/FUS was positively correlated with all five positive psychotic symptoms.

4.2. Journal Article: Dynamics of large-scale brain networks in 22q11DS.

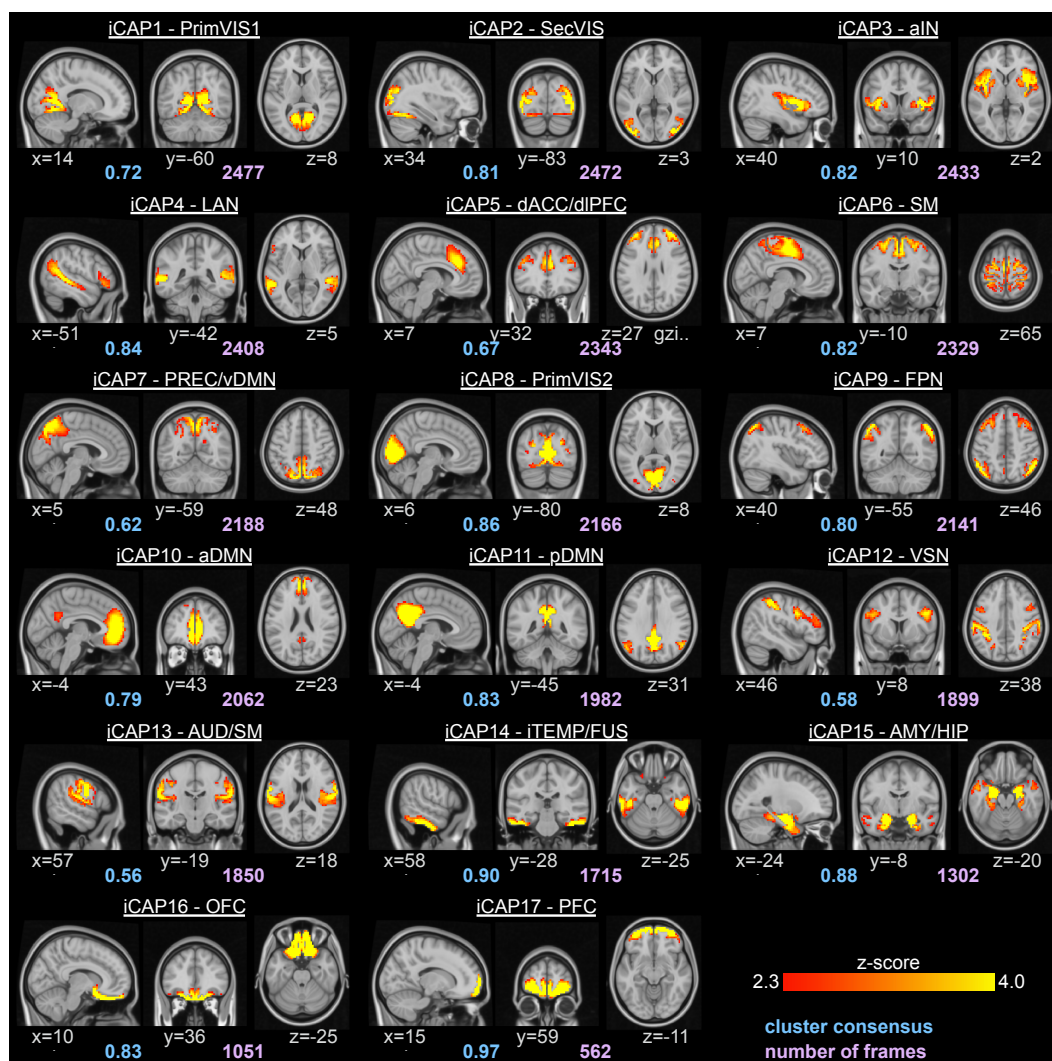


Figure 4.9 – Spatial patterns of the 17 iCAPs retrieved from all subjects, including both HCs and patients with 22q11DS. Locations denote displayed slices in MNI coordinates. Blue values denote the average consensus of each cluster, purple values indicate the total number of innovation frames that were assigned to this cluster. PrimVIS1 - primary visual 1, SecVIS - secondary visual, aIN - anterior insula, LAN - language network, dACC/dlPFC - dorsal anterior cingulate cortex/dorsolateral prefrontal cortex, SM - sensorimotor, PREC/vDMN - precuneus/ventral default mode network, PrimVIS2 - primary visual 2, FPN - fronto-parietal network, aDMN - anterior default mode network, pDMN - posterior default mode network, VSN - visuospatial network, AUD/SM - auditory/sensorimotor, iTEMP/FUS - inferior temporal/fusiform, AMY/HIP - amygdala/hippocampus, OFC - orbitofrontal cortex, PFC - prefrontal cortex.

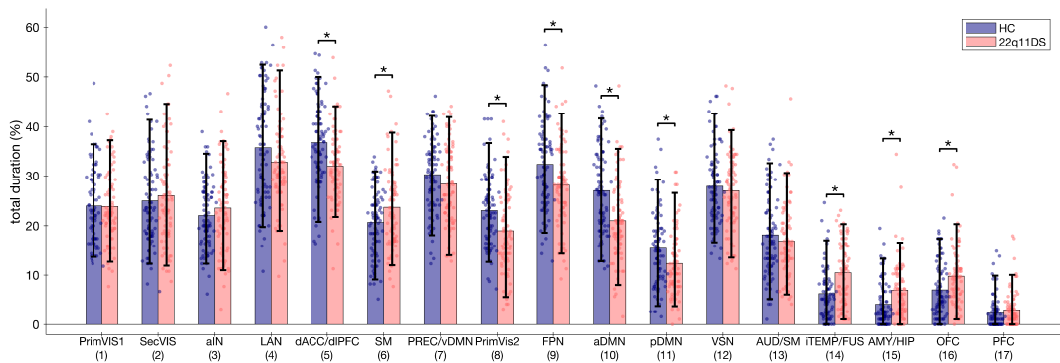


Figure 4.10 – Statistics of total temporal duration for each iCAP. P-values are FDR-corrected for the 17 multiple comparisons and age, gender and motion were included as covariates. Significant group differences ($p < 0.05$) were marked with an asterisk. Error bars indicate bootstrapping 5th to 95th percentiles. Single-subject duration measures were included as scatterplots. Corresponding test statistics (p-values, effect size) can be found in Supplementary Table B.6.

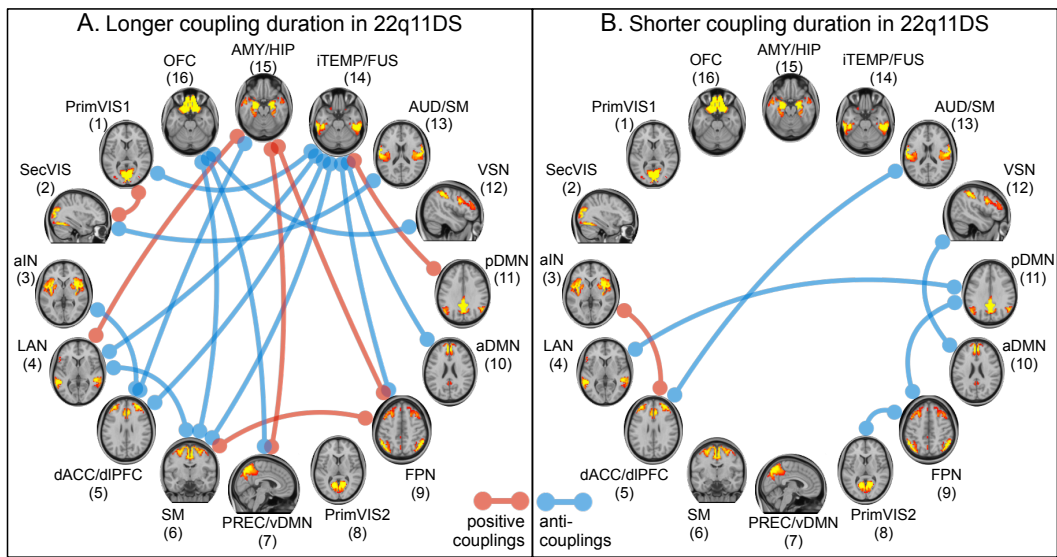


Figure 4.11 – Significant duration differences of positive couplings (red) and anti-couplings (blue) between patients with 22q11DS and HCs. A) Couplings with significantly longer duration in 22q11DS. B) Couplings with significantly shorter duration in 22q11DS. Couplings were measured in terms of percentage of total scanning time, or in percentage of the joint activation time of the two respective iCAPs (Jaccard score). We here show only differences that were significant in both coupling measures. Underlying group comparison statistics can be found in Supplementary Figure B.10 and Supplementary Table B.7.

4.2. Journal Article: Dynamics of large-scale brain networks in 22q11DS.

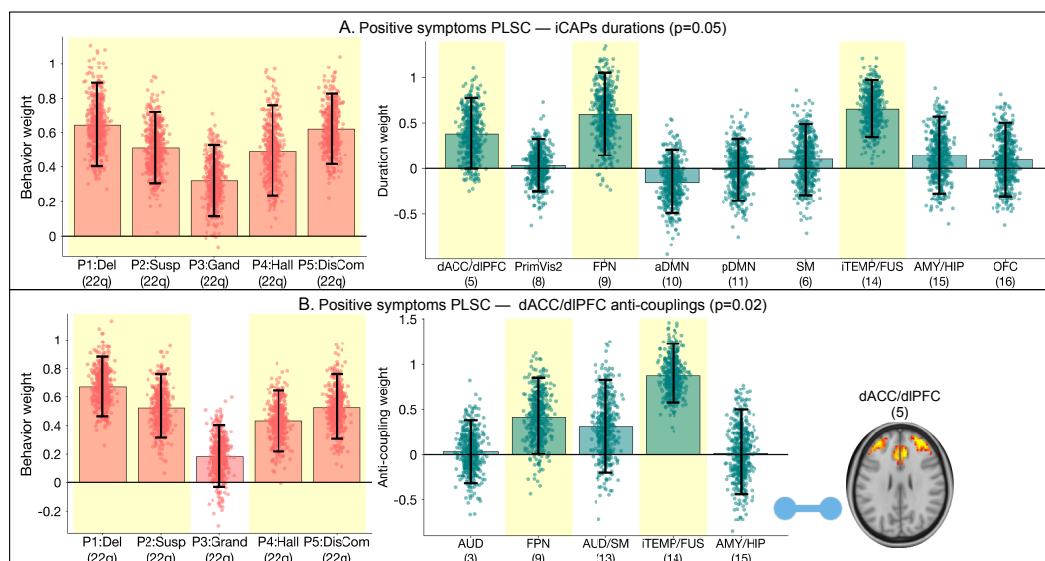


Figure 4.12 – PLSC results for positive psychotic symptoms (Five SIPS items: Delusions, Suspiciousness, Grandiosity, Hallucinations and Disorganized Communication) in patients with 22q11DS. A) Behavior weights and brain weights for PLSC including duration of nine iCAPs with altered duration in 22q11DS. There is a positive correlation of positive psychotic symptoms with duration of dACC/dlPFC, FPN and iTEMP/FUS. B) Behavior weights and brain weights for PLSC including anti-couplings of dACC/dlPFC that were altered in 22q11DS. Longer anti-coupling of dACC/dlPFC with FPN and iTEMP/FUS is associated with higher positive symptoms. Error bars indicate bootstrapping 5th to 95th percentiles, robust results were indicated by yellow background. Exact values of bootstrap mean and 5-95 percentiles are reported in Supplementary Table B.8. PLSC results for positive couplings were not significant ($p=0.6$) and are thus not reported here.

Altered couplings of dACC/dlPFC associated with psychotic symptoms Next, we investigated the relevance of couplings for psychotic symptoms. For this, we selected the dACC/dlPFC network based on its appearance in the previous analysis (see figure 4.12A), as well as literature associating ACC alterations with psychosis in 22q11DS (Padula et al., 2018). We included coupling time of dACC/dlPFC with iCAPs that had altered couplings (aIN, AUD/SM, iTEMP/FUS and AMY/HIP; see figure 4.11) and with iCAPs whose duration was significantly correlated with psychotic symptoms (FPN and iTEMP/FUS; see figure 4.12A).

A first PLSC analysis for anti-coupling time between dACC/dlPFC and these networks resulted in one significant CorrComp ($p=0.02$, see figure 4.12B) showing an association between higher positive symptoms and longer anti-coupling of dACC/dlPFC with FPN and iTEMP/FUS.

A second PLSC analysis for positive coupling time between dACC/dlPFC and these networks did not give any significant CorrComp ($p=0.58$).

Functional signature of anxiety

Finally, we conducted similar analyses to investigate dynamic brain network alterations associated with anxiety, another behavioral risk factor for psychosis in 22q11DS.

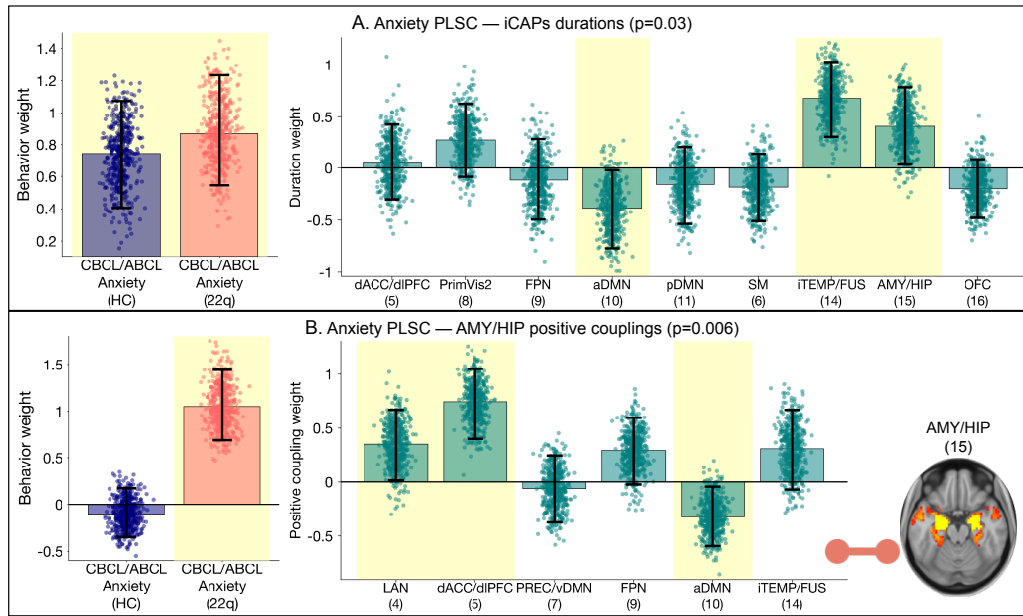


Figure 4.13 – PLSC results for anxiety scores. A) Behavior weights and brain weights for PLSC including duration of nine altered iCAPs. There is a positive correlation of anxiety with duration of iTEMP/FUS and AMY/HIP and a negative correlation with duration of aDMN. B) Behavior weights and brain weights for PLSC including positive couplings of AMY/HIP. *Longer* positive coupling of AMY/HIP with LAN and dACC/dlPFC, and *shorter* positive coupling with aDMN are associated with *higher* anxiety *only* in patients with 22q11DS. Error bars indicate bootstrapping 5th to 95th percentiles, robust results were indicated by yellow background. Exact values of bootstrap mean and 5-95 percentiles are reported in Supplementary Table B.9. PLSC results for anti-couplings were not significant ($p=0.07$) and are thus not reported here.

Altered iCAPs' duration associated with anxiety We performed PLSC analysis between CBCL/ABCL anxiety scores in 22q11DS and HCs and iCAPs' duration, again including the nine iCAPs with altered duration (see figure 4.10). There was one significant CorrComp ($p=0.03$, see figure 4.13A). Both in HCs and patients with 22q11DS, longer activation of iTEMP/FUS and AMY/HIP and shorter activation of aDMN were associated with higher anxiety.

Altered couplings of AMY/HIP are associated with anxiety in patients with 22q11DS To further investigate coupling effects related to anxiety, we selected the AMY/HIP network, because its duration was related to anxiety in the previous analysis (see figure 4.13A) and because of the well-established involvement of these brain regions in anxiety (Etkin and Wager, 2007). We included coupling time of AMY/HIP with iCAPs that had altered couplings (LAN, dACC/dlPFC, PREC/vDMN and FPN; see figure 4.11) and with iCAPs whose duration was significantly associated with anxiety (aDMN and iTEMP/FUS; see figure 4.13A).

A first PLSC analysis for anti-couplings between AMY/HIP and these networks gave no significant CorrComp ($p=0.07$).

A second PLSC analysis including positive couplings between AMY/HIP and these networks gave one significant CorrComp ($p=0.006$, see figure 4.13B). Behavior weights were

4.2. Journal Article: Dynamics of large-scale brain networks in 22q11DS.

only robust for patients with 22q11DS, indicating that the corresponding pattern of correlation weights was specific for patients. Longer positive coupling of AMY/HIP with LAN and dACC/dlPFC was positively associated with anxiety, whereas positive coupling with aDMN was negatively associated with anxiety.

4.2.4 Discussion

In this study, we investigated dynamic features of network brain activity in patients with 22q11DS, with a particular focus on the identification of functional signatures of prodromal psychotic symptoms and anxiety, two behavioral risk factors for the transition to psychosis. To the best of our knowledge, this is the first study to investigate dynamics of large-scale functional brain networks in 22q11DS. We used iCAPs to go beyond static connectivity analysis and look into precise moments of brain network activation and interaction, which is particularly promising to provide more sensitive imaging markers in schizophrenia (Calhoun et al., 2014). We detected alterations of brain networks' duration and couplings in 22q11DS and associations between these patterns of alterations with positive psychotic symptoms and anxiety.

Alterations in 22q11DS: implication of cognitive and emotional brain networks

Individuals with 22q11DS had a varied pattern of longer and shorter network activations, suggesting that they 'over-engage' in certain brain states, while 'under-engaging' in others. In particular, we found shorter activation of FPN, DMN and cingulo-prefrontal SN. According to the triple-network hypothesis, the dynamic interaction between these three networks, characterized by a shift between internally-oriented DMN and externally-oriented FPN mediated by salience-attributing SN, is central for higher cognitive functions (Menon, 2011). Conversely their dysfunction could account for several psychiatric symptoms. Here we observe reduced activation of all three networks in 22q11DS, possibly suggesting a malfunction of these basic brain dynamics, which speculatively may underlie broad impairments in higher cognitive function described both in 22q11DS and psychosis (McDonald-McGinn et al., 2015; Insel, 2010). In turn, there was longer activation in networks comprising limbic regions including amygdala, medial temporal and orbitofrontal cortices. While the dichotomy between cognitive and emotional brain is arguably artificial, longer activation in regions highly involved in emotional processing such as amygdala and orbitofrontal cortex could reflect higher emotional load during scanning in patients with 22q11DS (LeDoux, 2000; Pessoa, 2008).

The pattern of activation was significantly, but oppositely, related with age in both groups (see Supplementary Results in appendix B.2), suggesting that the atypical activation pattern observed in 22q11DS emerges with age, in accordance with the neurodevelopmental model of schizophrenia (Insel, 2010; Rapoport et al., 2012).

Besides duration of activation, the iCAPs approach allowed us to probe the pattern of aberrant coupling between networks, which was characterized by predominantly longer anti-couplings in 22q11DS, accounting for more than half (13/25) of the alterations. Longer anti-coupling is suggestive of increased segregation between brain networks and is in agreement

with evidence of increased segregation and decreased integration of structural and functional brain networks in both 22q11DS and non-syndromic psychosis (Ottet et al., 2013b; Sandini et al., 2017, 2018; Scariati et al., 2016b; Van Den Heuvel and Fornito, 2014; Váša et al., 2016). Network segregation is a central feature of brain function that is important for cognition and attention (Wig, 2017) and its alterations in 22q11DS may be reflective of cognitive disabilities on a more global level than the above mentioned alterations in triple network activation that concentrates on three core networks.

Functional signature of psychosis prodrome: aberrant salience network duration and coupling

The presence of prodromal psychotic symptoms was associated with longer activation of iTEMP/FUS, dACC/dlPFC and FPN. Increased activation of inferior temporal and fusiform gyrus has been previously reported in schizophrenia in terms of relative cerebral blood flow (Kohno et al., 2006; Malaspina et al., 1999) and BOLD variability (Li et al., 2017). Also in 22q11DS, we observed higher BOLD variability in inferior temporal and fusiform regions in a partially overlapping sample (Zöllner et al., 2017), suggesting that increased BOLD variability might reflect longer network activation. Further, prodromal psychotic symptoms were associated with longer activation of dACC/dlPFC. The dACC is considered a key node of the SN involved in attributing subjective salience to internally and externally generated events (Menon, 2011; Seeley et al., 2007). Aberrant salience attribution has been proposed as key mechanism in the emergence of positive psychotic symptoms (Kapur, 2003). Together with electroencephalography (EEG) studies in psychosis and 22q11DS that consistently reported longer representation of the EEG topography that corresponds to SN (Britz et al., 2010; Rieger et al., 2016; Tomescu et al., 2014, 2015), our findings support this hypothesis.

However, whilst duration of both dACC/dlPFC and FPN was positively correlated with psychotic symptoms, it was reduced overall in 22q11DS compared to HCs. Converging evidence from both structural and functional MRI points towards altered connectivity of the ACC in individuals with 22q11DS and psychotic symptoms (Dufour et al., 2008; Sandini et al., 2017; Scariati et al., 2014; Zöllner et al., 2018), reviewed in (Padula et al., 2018). Hence we suspected that the quality of the activations; i.e., the coupling with other networks, might be relevant for higher psychotic symptoms. Indeed, the analysis of dACC/dlPFC couplings revealed a significant relationship between higher psychotic symptoms and anti-coupling with FPN and iTEMP/FUS. Taken together, these results suggest that whilst activations of dACC/dlPFC and FPN occur less frequently in 22q11DS in general, they are more frequently anti-coupled with one another and with iTEMP/FUS in patients with higher psychotic symptoms. The triple-network model proposes that activation of the SN is instrumental in re-orienting attention by mediating the shifts between DMN and FPN (Menon, 2011). Our findings of longer anti-coupling between SN and FPN suggest that this functional role of the cingulo-prefrontal SN is disrupted in individuals with higher psychotic symptoms.

Altogether, the richness of our iCAPs approach permitted to characterize a pattern reflecting SN activations that contribute to the pathophysiology of psychotic symptoms, both in terms of duration and quality. Our findings support the key role of network dynamics in the

4.2. Journal Article: Dynamics of large-scale brain networks in 22q11DS.

ACC in higher psychosis vulnerability (Padula et al., 2018) and point towards disrupted triple network function centered on the SN, which might reflect aberrant salience processing in patients with psychotic symptoms (Menon, 2011; Kapur, 2003).

Functional signature of anxiety: aberrant amygdala & hippocampus duration and coupling

For both HCs and patients with 22q11DS anxiety was associated with a pattern of longer activation of AMY/HIP, iTEMP/FUS and shorter activation of aDMN. Evidence in animal models and humans has revealed a central role of the amygdala in fear exposure, anticipation and reaction (LeDoux, 2000; Tovote et al., 2015; Davis et al., 2010; Maren and Quirk, 2004; Etkin and Wager, 2007; Fox and Kalin, 2014). Further, increased metabolic activity in amygdala, hippocampus and inferior temporal cortex was found in rhesus monkeys with anxious temperament (Fox et al., 2012, 2008) and cerebral blood flow in amygdala and fusiform cortex has been associated with trait anxiety in humans (Kaczurkin et al., 2016). The iCAPs approach allowed us to quantify moments of network activation and confirmed that hyperactivity of AMY/HIP and iTEMP/FUS at rest could indeed represent trait markers of anxiety in both HCs and 22q11DS. Hyperactivity of AMY/HIP and iTEMP/FUS observed in 22q11DS could therefore account for increased prevalence of anxiety disorders in this population.

Importantly, the amygdala does not operate in isolation, but is part of a complex circuit involved in regulating emotional responses (Etkin et al., 2015). Indeed, in accord with the role in salience processing mentioned above, dorsal ACC and medial prefrontal cortex (mPFC) promote amygdala activity and are critical in the appraisal and expression of fear behavior (Etkin et al., 2015). Oppositely, subgenual-ACC and ventral mPFC largely dampen amygdala activity and are essential for fear extinction (Etkin et al., 2015). This functional sub-division of the frontal lobe is further supported by extensive literature on fear circuitry in rodents, where dorsal pre-limbic and ventral infra-limbic cortices are found to have opposing roles on amygdala activation, fear expression, respectively fear extinction (Tovote et al., 2015; Etkin et al., 2015; Milad and Quirk, 2002; Quirk et al., 2003; Vidal-Gonzalez et al., 2006; Corcoran and Quirk, 2007; Courtin et al., 2014; Burgos-Robles et al., 2009). Given these findings, we speculated that the modulation of AMY/HIP activity particularly by the dACC/dlPFC and aDMN network might play a crucial role in the pathophysiology of anxiety. Indeed, we showed a significant positive association between anxiety and coupling duration between AMY/HIP and dACC/dlPFC and LAN. Coupling duration between AMY/HIP and aDMN had an opposite, protective role on anxiety in accordance with the modulating role of mPFC-amygdala projections on fear expression. Of note, the effects of amygdala coupling on anxiety appeared specific to individuals with 22q11DS, which could suggest that effects of amygdala modulation are nonlinear and relate only to more severe anxiety observed in 22q11DS.

In conclusion, we observed a dynamic functional pattern characterized both by longer AMY/HIP activations and atypical prefrontal AMY/HIP modulation, which might constitute a trait maker of anxiety and contribute vulnerability to psychosis in 22q11DS.

Methodological aspects

The iCAPs framework The present study is one of the first to apply the iCAPs framework in a clinical population and, due to the flexibility of the framework, we were able to discover distinct patterns of functional activation and interaction characteristic for prodromal psychotic symptoms and anxiety. The framework is unique in its ability to detect spatially *and* temporally overlapping networks (Karahanoglu et al., 2015; Zöllner et al., 2019b), and the robustness and richness of the presented results underlines its potential. Of note, extracted spatial patterns were highly similar to previously observed iCAPs retrieved from HCs (Karahanoglu et al., 2015; Zöllner et al., 2019b), which reassures the framework's performance in a clinical population. Furthermore, the sub-division of classical resting-state networks such as DMN and SN into multiple subnetworks confirms previously observed findings (Karahanoglu et al., 2015) and suggests that different subnetworks have distinct dynamic properties, which are difficult to detect by static approaches.

While iCAPs themselves were retrieved from a purely dynamic measure (i.e., the innovations), the measure of coupling between networks is closely linked to sFC (see Supplementary Results & Discussion in appendix B.2). Activation duration, however, is a measure specific to each network which cannot be explained in terms of static connectivity.

BOLD signal analysis and motion In any fMRI study non-neural confounds are always a concern (Power et al., 2014). We have minimized the effects by taking several measures for motion correction and through additional analysis of motion (discussed in more detail in Supplementary Results & Discussion in appendix B.2). However, as motion is strongly correlated with symptoms severity, it remains a limitation of our study.

Conclusion

In summary, we here presented functional signatures of anxiety and positive psychotic symptoms in 22q11DS in terms of brain network activation and coupling. Our results confirm the implication of SN activity and connectivity in the emergence of psychotic symptoms. We further uncovered differential roles of dorsal and ventral ACC and mPFC coupling with amygdala that are relevant for anxiety. Together, these findings shed light into the pathophysiology of two clinical risk factors that might represent relevant imaging markers for psychosis vulnerability.

4.3 Summary and outlook

This chapter was dedicated to the analysis of brain dynamics in terms of large-scale brain state activation. In the first study, we presented a methodological development in the iCAPs framework for an improved estimation of temporal brain state properties. As the states are obtained from temporal clustering, they can be spatially overlapping. We discovered that this spatial overlap can lead to spurious activations in recovered time courses. To overcome this shortcoming of the framework in its previous form, we presented a novel back-projection method that is based on the introduction of spatio-temporal constraints in the time course recovery step. In the article, we demonstrated its performance both on simulated and experimental data and establish that both over- and underfitting are prevented, leading to more robust estimates and more reliable results.

Thanks to this central development, we were subsequently able to use the framework in a clinical setting. In the second study of this chapter, we have applied the iCAPs framework in patients with 22q11DS with the aim to find potential dynamic functional imaging markers for psychosis vulnerability. We looked into aberrant brain dynamics related to positive psychotic symptoms and anxiety, two strong behavioral risk factors for schizophrenia in 22q11DS (Gothelf et al., 2013; Schneider et al., 2016). Our analysis confirmed an implication of cingulo-prefrontal SN activation duration and coupling for prodromal psychotic symptoms, which is in line with our previous results on aberrant BOLD variability in the dACC. Further, we found aberrant activation and coupling of the amygdala in patients with higher anxiety, indicating differential roles of dorsal and ventral sub-divisions of ACC and mPFC. Coupling of amygdala with dorsal ACC and mPFC was promoting anxiety, whereas coupling with ventral ACC and mPFC had a protective function. Notably, this relationship corroborates the existing literature on the role of the amygdala in fear expression and regulation (Etkin et al., 2011).

Aside from the alterations in dynamic brain functions that we found so far, it is known that the brain's structural architecture is also altered in schizophrenia and 22q11DS (Scariati et al., 2016a; Váša et al., 2016). An open question remains on how these structural alterations may relate to altered functional activity such as observed in this and the previous chapter. Therefore, we next incorporate structural information in the framework and probe for a relationship between iCAPs activity and the brain's structural architecture.

5 Control energy to probe into dynamics of structural brain networks

CRITICALLY, while we hitherto focused on the brain's functional dynamics and their implications for psychosis vulnerability, the brain's underlying white matter architecture likely strongly influences such aberrant functional characteristics. However, only two studies so far have looked into multimodal functional and structural alterations in 22q11DS at the same time (Padula et al., 2015, 2017b). Both analyzed structural and functional connectivity and compared the results, but none of them explicitly investigated the structure-function relationship in these patients. To go one step further, here we were not only interested in linking static functional and structural features, but we also wanted to incorporate the brain's dynamic nature.

Recently, a myriad of approaches have been proposed in the field of structural brain network analysis to probe into the implication of structural topology for dynamic function (Breakspear et al., 2010; Mišić et al., 2015). The idea to use principles from network control theory for the investigation of brain network dynamics has been particularly promising because it allows to model not only passive, but also active dynamics (Gu et al., 2015; Betzel et al., 2016; Gu et al., 2017; Kim et al., 2018). It is based on the assumption that the brain can be described as a network defined by brain regions (the network nodes) and their white matter connectivity (the network edges). The state of this brain network is defined by the signal at all regions at a given timepoint; i.e., the spatial pattern of instantaneous activity. Given such a model, the use of network control theory aims to analyze how the brain's structural topology influences its dynamic function assuming that it is controlled from a set of regions that drive the brain from one state to another.

Essentially, the controllability of a dynamic system indicates the possibility to steer the system into a particular target state through the input of a control signal at a predefined set of controller nodes (Kalman, 1960). In the context of complex networks with a high number of nodes and edges (such as the brain), controllability has recently become a topic of investigation and is still subject to active methodological and theoretical research, as many notions from classical control theory cannot be easily applied due the high dimensionality (e.g.; Liu et al., 2011; Yuan et al., 2013; Pasqualetti et al., 2014; Gao and Liu, 2014). While the theoretical property of whether a system can be controlled or not is an interesting feature, it does not give any information on the actual effort that would be required for a specific

control task (Yan et al., 2012). Indeed, a system may be theoretically controllable, but certain states will be practically unreachable because the control energy for driving the system into that state would be (too) high. For the practical use, it is thus important to identify not only controllability per se, but to predict the optimal control trajectory and the control energy that is needed for a specific control task (Lindmark and Altafini, 2018).

In the study presented in this chapter, we combine minimum energy control (to quantify control energy of structural brain networks derived from dMRI) with iCAPs (to retrieve functional activation properties of brain states during rest). The combination of these two approaches allows us to directly compare the predicted dynamic control properties of a brain state (given its structural connectivity) with the actual temporal activation of the identical brain state as measured through fMRI. The following section 5.1 contains the unpublished manuscript presenting our methods and results, and the last section 5.2 again provides a summary in the context of this thesis.

5.1 Journal Article: Control energy of functional brain states

Preprint version of the article in preparation for submission to: Human Brain Mapping

Structural control energy of resting-state functional brain states reveals inefficient brain dynamics in psychosis vulnerability.

Daniela Zöllner^{1,2,3}, Corrado Sandini³, Marie Schaer³, Stephan Eliez³, Danielle S. Bassett^{4,5,6,7,8}, Dimitri Van De Ville^{1,2}

¹Medical Image Processing Laboratory, Institute of Bioengineering, École Polytechnique Fédérale de Lausanne (EPFL), Lausanne, Switzerland; ²Department of Radiology and Medical Informatics, University of Geneva, Geneva, Switzerland; ³Developmental Imaging and Psychopathology Laboratory, Office Médico-Pédagogique, Department of Psychiatry, University of Geneva, Geneva, Switzerland; ⁴Department of Bioengineering, University of Pennsylvania, Philadelphia, PA, United States ⁵Department of Electrical & Systems Engineering, University of Pennsylvania, Philadelphia, PA, United States ⁶Department of Neurology, University of Pennsylvania, Philadelphia, PA, United States ⁷Department of Physics & Astronomy, University of Pennsylvania, Philadelphia, PA, United States ⁸Department of Psychiatry, University of Pennsylvania, Philadelphia, PA, United States

How the brain's white-matter anatomy constrains brain activity is an open question that might give insights into the mechanisms that underlie mental disorders such as schizophrenia. Chromosome 22q11.2 deletion syndrome (22q11DS) is a neurodevelopmental disorder with an extremely high risk for psychosis providing a test case to study developmental aspects of schizophrenia. In this study, we used principles from network control theory to probe the implications of aberrant structural connectivity for the brain's functional dynamics in 22q11DS. We retrieved brain states from resting-state functional magnetic resonance images of 78 patients with 22q11DS and 85 healthy controls, and we compared them in terms of persistence control energy based on individual structural connectivity. Control energy was altered in a broad pattern of brain states including both energetically more demanding and less demanding brain states in 22q11DS. Further, we discovered that the brain minimizes energy by spending less time in energetically demanding brain states. In patients with 22q11DS, this behavior was less pronounced, suggesting a dynamic inefficiency of brain function in the disease. In summary, our results provide initial insights into the dynamic implications of altered structural connectivity in 22q11DS, which might improve our understanding of the mechanisms underlying the disease.

5.1.1 Introduction

The brain is a complex dynamic system and brain function during rest and task can be described in terms of the dynamic activation and interaction of different *brain states*: sets of brain regions that are coherently activating and deactivating (Preti et al., 2017; Karahanoglu and Van De Ville, 2017). How the brain's underlying structural backbone constrains and facilitates this dynamic behavior is an intensively studied question in the neuroscience community (Bassett and Sporns, 2017; Honey et al., 2009; Becker et al., 2018). The joint consideration of structural and functional properties is particularly promising to provide a better mechanistic explanation of the causes that underlie brain disorders such as schizophrenia (Braun et al., 2018). In recent years, approaches for the investigation of dynamic properties have proven to be particularly useful in probing brain function in health and disease (Preti et al., 2017; Karahanoglu and Van De Ville, 2017; Van Den Heuvel and Fornito, 2014). Schizophrenia, in particular, is – as an extension of the well-accepted dysconnectivity hypothesis (Stephan, 2010) – increasingly perceived as a disorder of broad alterations in large-scale brain state dynamics (Fornito et al., 2012; Du et al., 2016; Braun et al., 2016). A better insight on how alterations in the brain's structure may lead to such aberrant dynamic activation would improve our understanding of this disease to ultimately improve clinical management and patient outcomes (Braun et al., 2018).

Although initial studies of the relationship between brain structure and function used cross-modal correlations (Honey et al., 2009), more recent advances aim to describe how brain structure influences its function at a more mechanistic level (Bassett and Sporns, 2017; Braun et al., 2018). In particular, by using principles from network control theory, it is possible to analyze how the brain's structural topology influences its dynamic function (Gu et al., 2015; Betzel et al., 2016; Gu et al., 2017; Kim et al., 2018). In network control theory approaches, the brain is modeled as a graph defined by its structural connectivity, which can transition between different functional states that are given by the activation of each brain region (or network node). Under the assumption that the brain's state is controlled by a single or multiple brain regions, it is then possible to quantify how the underlying structural architecture facilitates or constrains the system's dynamic behavior. Importantly, the temporal properties are given by a (usually linear) dynamic model and are not directly measured. Initially, this framework was used to examine the controllability of the brain from a single region (Gu et al., 2015), measuring how the structural connectivity of a single region would enable it to drive the entire brain into different states that are easier to reach or more difficult to reach. This single-region approach has provided insights into the role that individual regions play in dynamic brain function. In particular, single-region controllability measures give characteristic profiles for different cognitive brain systems (Gu et al., 2015), change with development (Tang et al., 2017a), track individual differences in impulsivity (Cornblath et al., 2019), and are promising to guide target selection for neurostimulation (Muldoon et al., 2016; Khambhati et al., 2019). In patients with bipolar disorder, single-region controllability was found to be altered in subnetworks with aberrant structural connectivity (Jeganathan et al., 2018).

While it is interesting to study transition to the set of easy-to-reach states, and the set of difficult-to-reach states, the inferences are limited in the sense that we cannot say anything

about a particular transition that we might observe in the human brain. This limitation motivated recent extensions of the framework to estimate the control energy that is required for specific trajectories between a precisely defined initial state and a precisely defined target state. A simple intuitive example of such a state transition is the transition from activation of the default mode network (DMN) to activation of the fronto-parietal network (FPN) (Betz et al., 2016; Gu et al., 2017; Kim et al., 2018). Here, we define a set of brain regions that will act as controllers and we estimate the minimum control energy required to steer the brain from an initial state to a target state by formalizing the problem as an optimization problem. Thus far the method has predominantly been used to examine hypothesis-driven state transitions between cognitive brain states defined by an atlas (Gu et al., 2017; Cui et al., 2018). However, recent work extends this approach to investigate data-driven brain states retrieved from functional magnetic resonance imaging (fMRI) (Braun et al., 2019; Cornblath et al., 2018). In this way, temporal properties of functional brain states (measured using fMRI) can be directly compared to the control energy that would be needed to engage in this brain state based on structural connectivity (measured with diffusion weighted MRI (dMRI)).

Further, a disruption in this relationship between functional activity and required control energy could inform our understanding of altered mechanisms that are relevant to the pathophysiology of psychiatric disorders. Here, we tested this hypothesis in individuals with chromosome 22q11.2 deletion syndrome (22q11DS), a neurodevelopmental disorder characterized by a 30-fold increased risk for developing schizophrenia (McDonald-McGinn et al., 2015). Due to the 30-40 % prevalence of schizophrenia by adulthood (Schneider et al., 2014), the disorder is considered a model for the investigation of developmental risk factors before the onset of full-blown schizophrenia (Insel, 2010; Bassett and Chow, 1999). In 22q11DS, the white matter microstructure and connectivity has been extensively studied, mostly in terms of whole-brain or tract-based diffusivity properties (reviewed in Scariati et al., 2016a). Affected white-matter bundles mostly include long-range frontal-frontal, frontal-occipital, and fronto-parietal connections (Scariati et al., 2016a; Kikinis et al., 2016; Tylee et al., 2017; Olszewski et al., 2017; Roalf et al., 2017). Only a few studies have thus far examined the characteristics of structural whole-brain networks (Ottet et al., 2013b; Kikinis et al., 2013; Ottet et al., 2013a; Padula et al., 2017a; Váša et al., 2016; Zhan et al., 2018), also mostly reporting fronto-temporal, fronto-parietal (Ottet et al., 2013b,a; Zhan et al., 2018), and limbic dysconnectivity (Ottet et al., 2013a; Padula et al., 2015). From a topological perspective, Ottet et al. reported longer path lengths and disconnectivity of the brain's hub regions, specifically, in the frontal lobes (Ottet et al., 2013b), and Váša et al. uncovered a 'de-centralization' in 22q11DS with a rerouting of shortest network paths to circumvent an affected core that included frontal, parietal, and subcortical regions (Váša et al., 2016).

Only two studies to date have investigated structural and functional properties at the same time (Padula et al., 2015, 2017b) and none so far have attempted to examine the dynamic implications of an altered structural network architecture. In this study, we bridge this gap by combining dynamic fMRI analysis with whole-brain tractography and principles from network control theory to investigate how the brain's white matter connectivity may influence its dynamic behavior and how this relationship is affected in patients with 22q11DS. More

specifically, we extracted brain states from resting-state fMRI scans using innovation-driven co-activation patterns (iCAPs), a recently proposed approach for dynamic analysis of large-scale brain states marked by its ability to retrieve spatially and temporally overlapping states (Karahanoglu et al., 2015; Farouj et al., 2017; Zöllner et al., 2019b). Then, we calculated the control energy that is required – based on the structural connectivity of the same subjects – to engage in these specific brain states (Braun et al., 2019; Cornblath et al., 2018). In this way, we were able to explicitly investigate the relationship between the brain's structural architecture and its functional activation during rest and how this relationship is altered in patients with 22q11DS.

5.1.2 Materials and methods

Participants

fMRI analyses in this study were conducted on the identical dataset as Zöllner et al. (2019a) (see previous chapter 4.2), which included 78 patients with 22q11DS and 85 healthy controls (HCs), aged between 8 and 30 years. For structural connectivity analysis, we used dMRI scans acquired from the same subjects. One patient with 22q11DS and 7 HCs had to be excluded from dMRI analyses because no dMRI scan was recorded for them. Table 5.1 shows demographic information of the remaining 77 patients with 22q11DS and 78 HCs for which both fMRI and dMRI scans were available.

Image acquisition

MRI scans were recorded at the Centre d'Imagerie BioMédicale (CIBM) in Geneva on a Siemens Trio (12-channel head coil) and a Siemens Prisma (20-channel head coil) 3 Tesla scanner. Supplementary Table C.1 contains the number of scans that were recorded before and after the update to the Prisma scanner for each image modality, respectively. There was no significant scanner-by-group interaction. Anatomical images were acquired using a T1-weighted sequence with 192 slices (volumetric resolution = $0.86 \times 0.86 \times 1.1 \text{ mm}^3$, TR = 2500 ms, TE = 3 ms, flip angle = 8° , acquisition matrix = 256×256 , field of view = 23.5 cm). fMRI scans were recorded with an 8 minute resting-state session at a TR of 2.4 s (volumetric resolution = $1.84 \times 1.84 \times 3.2 \text{ mm}^3$, 200 frames, 38 axial slices, slice thickness 3.2 mm, TE=30 ms, 85° flip angle, acquisition matrix 94×128 , field of view 96×128). Subjects were instructed to fixate on a cross on the screen, let their minds wander, and not fall asleep. dMRI scans were acquired in 30 directions ($b = 1000 \frac{\text{s}}{\text{mm}^2}$, TR = 8300 ms to 8800 ms, TE = 82 ms, flip angle = 90° to 180° , acquisition matrix = 128×128 , field of view = 25.6 cm, 64 axial slices, slice thickness = 2 mm).

fMRI processing

We preprocessed fMRI scans identically as in Zöllner et al. (2019a) using in-house code and functions of statistical parametric mapping (SPM12) (<http://www.fil.ion.ucl.ac.uk/spm/>), data processing assistant for resting-state fMRI (DPARF) (Yan Chaogan, 2010) and individual brain atlases using statistical parametric mapping (IBASPM) (Aleman-Gomez et al., 2006). Briefly, preprocessing steps included functional realignment and spatial smoothing with a Gaussian

5.1. Journal Article: Control energy of functional brain states

Table 5.1 – Participant demographics. N/A = not applicable.

	HC	22q11DS	p-value
Number of subjects (M/F)	78 (32/46)	77 (37/40)	0.379 (χ^2)
Age mean \pm SD (range)	16.39 \pm 5.52 (8.1-30.0)	17.23 \pm 5.39 (8.1-29.7)	0.342
Right handed*	80.00%	77.61%	0.564 (χ^2)
IQ**	110.80 \pm 13.75	70.32 \pm 12.18	<0.001
Number of subjects meeting criteria for psychiatric diagnosis	N/A	42 (55%)	
Anxiety disorder	N/A	9	
Attention deficit hyperactivity disorder	N/A	8	
Mood disorder	N/A	5	
Schizophrenia or schizoaffective disorder	N/A	3	
More than one psychiatric disorder	N/A	17	
Number of subjects medicated	0	9	
Methylphenidate	0	3	
Anitpsychotics	0	1	
Anticonvulsants	0	1	
More than one class of medication	0	3	

* Handedness was measured using the Edinburgh laterality quotient, right handedness was defined by a score of more than 50. ** IQ was measured using the Wechsler Intelligence Scale for Children–III (Wechsler, 1991) for youth and the Wechsler Adult Intelligence Scale–III (Wechsler, 1997) for adults.

kernel of 6 mm full width half maximum, co-registration of the structural T1-weighted image to the functional mean, segmentation of anatomical scans using the *Segmentation* algorithm in SPM12 (Ashburner and Friston, 2005), creation of a study-specific template using diffeomorphic anatomical registration (DARTEL) (Ashburner, 2007), exclusion of the first 5 functional frames, and regression of cerebrospinal fluid (CSF) and white matter (WM) blood oxygenation level dependent (BOLD) signals. Volumes with a framewise displacement (FD) larger than 0.5 mm were replaced with the spline interpolation of previous and following frames in order to ensure the constant sampling rate required by the iCAPs implementation. After brain state extraction, motion frames were excluded for the computation of temporal characteristics (see below).

Following preprocessing, we extracted iCAPs from resting-state fMRI scans using openly available MATLAB code (<https://c4science.ch/source/iCAPs>; Karahanoglu et al., 2015; Zöller et al., 2019b). Steps included the hemodynamically-informed deconvolution of fMRI time-series using total activation (TA) (Karahanoglu et al., 2011, 2013; Farouj et al., 2017). Then, significant transients are determined with a two-step thresholding procedure following Kara-

hanoglu et al. (2015) and Zöllner et al. (2019b) (temporal threshold: 5-95 %; spatial threshold: 5% of gray matter voxels). ICAPs were determined through temporal clustering on concatenated transient frames of all subjects. According to consensus clustering (Monti et al., 2003), the optimum number of clusters was $K = 17$. Finally, a time course was estimated for each iCAP using spatio-temporal transient-informed regression with soft assignment factor $\xi = 1.3$ (Zöllner et al., 2019b), and temporal activation duration was computed from thresholded time courses (z-score $> |1|$) as a percent of the total non-motion scanning time. For a more detailed description of the methods, we refer the interested reader to (Zöllner et al., 2019a; or section 4.2 of this thesis).

dMRI processing

DMRI scans were processed using functions from the FSL library (Jenkinson et al., 2012) and from the MRtrix3 toolbox (Tournier et al., 2019). After denoising the dMRI scans (*dwidenoise* in MRtrix), eddy current and motion correction was conducted (*eddy* in FSL). Then, the skull was stripped from eddy-corrected dMRI scans (*bet* in FSL) and a white-matter mask, obtained from segmented anatomical images, was mapped to the resolution of dMRI scans (*flirt* in FSL) and dilated by one voxel (*maskfilter* in MRtrix). Then, we estimated the single-bundle response function for spherical deconvolution based on the Tournier algorithm (Tournier et al., 2013) and computed the fibre orientation distribution function for every voxel with a constrained spherical deconvolution (Tournier et al., 2007). Deterministic fibre tracking (*SD_Stream* in MRtrix) was applied to reconstruct 10×10^6 streamlines longer than 10 mm, which were subsequently filtered using spherical-deconvolution informed filtering of tractograms (SIFT) (Smith et al., 2013) to a number of 1×10^6 streamlines for each subject. The Brainnetome atlas (<http://atlas.brainnetome.org>) was warped from MNI to subject-space and down-sampled to dMRI resolution using SPM12. Finally, a structural connectivity matrix $\mathbf{A} \in \mathbb{R}^{N_{reg} \times N_{reg}}$ was reconstructed for every subject by counting the streamlines connecting each of the $N_{reg} = 234$ regions in the Brainnetome atlas.

Minimum control energy

We here used linear control theory for brain network analysis, which uses principles from control and dynamical systems theory to investigate the impact that the brain's structural topology may have on its functional dynamics (Kim and Bassett, 2019; Tang and Bassett, 2018; Lynn and Bassett, 2019). Under the assumption of a linear model of dynamics (Kim and Bassett, 2019) and control from all regions of the brain, we estimated the minimum control energy required to remain in specific functionally defined brain states. For extended reviews on the control of brain network dynamics, we refer the interested reader to (Tang and Bassett, 2018; Lynn and Bassett, 2019). In the following paragraphs, we describe the linear dynamic model used here, and outline the mathematical basis for computation of minimum control energy based on this model, as well as the way in which brain states of interest were defined.

Dynamic model In order to study how the white-matter anatomy of the brain constrains or facilitates state transitions, we modeled the brain as a continuous linear time-invariant

dynamic system following Gu et al. (2017) and Betzel et al. (2016)

$$\dot{\mathbf{x}}(t) = \mathbf{A}_s \mathbf{x}(t) + \mathbf{B} \mathbf{u}(t),$$

in which $\mathbf{x}(t) = [x_1(t), \dots, x_{N_{\text{reg}}}(t)]^\top \in \mathbb{R}^{N_{\text{reg}} \times 1}$ is the brain's functional state at timepoint t given by the activity level $x_i(t)$ in each region i . The dynamic behavior of the brain is constrained by the stabilized structural white matter connectivity matrix \mathbf{A}_s , which is derived from the original structural connectivity matrix \mathbf{A} , where each element A_{ij} is the number of streamlines connecting regions i and j . In order to ensure stability of the dynamic system, all eigenvalues of \mathbf{A}_s have to be below 0. Therefore, we stabilized the system by dividing the original structural connectivity matrix \mathbf{A} by its largest eigenvalue λ_{\max} and subtract the identity matrix \mathbf{I} : $\mathbf{A}_s = \frac{\mathbf{A}}{\|\lambda_{\max}\| + 1} - \mathbf{I}$ (Betzel et al., 2016). The diagonal matrix $\mathbf{B} \in \mathbb{R}^{N_{\text{reg}} \times N_{\text{reg}}}$ specifies the set of control nodes. Throughout this study, we assume that all regions of the brain can be controlled and therefore $\mathbf{B} = \mathbf{I}$. Finally, $\mathbf{u}(t) = [u_1(t), \dots, u_{N_{\text{reg}}}(t)]^\top \in \mathbb{R}^{N_{\text{reg}} \times 1}$ contains the control input signals $u_i(t)$ at region i and timepoint t . Notably, there are marked differences in controllability across graph models, indicating that characteristics of brain controllability are unique and potentially relevant for cognitive function (Wu-Yan et al., 2018).

Minimum persistence control energy In this study, we wished to investigate the structural control energy that is necessary to remain in a certain brain state \mathbf{x} for a duration T . Throughout this study, we compute control energy for a control horizon of $T = 1$ (Betzel et al., 2016). The optimum control input \mathbf{u}_{\min} with minimum control energy can be found by solving (Antsaklis and Michel, 2005)

$$\mathbf{u}^* = \min_{\mathbf{u}} E_{\min} = \min_{\mathbf{u}} \int_{t=0}^T \mathbf{u}(t)^\top \mathbf{u}(t) dt.$$

The analytical solution of this minimization problem is given by the minimum energy

$$E_{\min} = (\mathbf{x}(T) - e^{\mathbf{A}T} \mathbf{x}(0))^\top \mathbf{W}_r^{-1}(T) (\mathbf{x}(T) - e^{\mathbf{A}T} \mathbf{x}(0)),$$

with the *reachability Gramian*

$$\mathbf{W}_r(T) = \int_{t=0}^T e^{\mathbf{A}(T-t)} \mathbf{B} \mathbf{B}^\top e^{\mathbf{A}^\top(T-t)} dt.$$

The optimal control input with this minimum energy can be explicitly computed for each timepoint t :

$$\mathbf{u}^*(t) = \mathbf{B}^\top e^{\mathbf{A}^\top(T-t)} \mathbf{W}_r^{-1}(T) (\mathbf{x}(T) - e^{\mathbf{A}T} \mathbf{x}(0)).$$

The required control energy at every brain region is given by $E_i = \int_0^T \|u_i^*(t)\|^2 dt$ and the total control input can be computed by summing over all regions $E = \sum_{i=1}^{N_{\text{reg}}} E_i$.

Definition of brain states We wished to investigate the energy that is required to remain in a certain brain state based on the brain's structural connectivity. To compute the minimum

control energy as defined above for every functional brain state, state vectors $\mathbf{x}_k(0) = \mathbf{x}_k(T)$ were obtained by computing in each region the average normalized spatial map of every iCAPs k (see subsection *fMRI processing*). In order to minimize noise susceptibility, we thresholded the brain states at a z-score of 1.5; in other words, regions with an average z-score < 1.5 were set to zero.

Statistical analysis

Statistical group comparison and brain-behavior analysis were conducted with an identical protocol as in Zöllner et al. (2019a), or section 4.2 of this thesis.

Group comparisons of duration and persistence control energy Two-sample t-tests were used to compare functional and structural measures between patients with 22q11DS and HCs, and the false discovery rate (FDR) was used to correct for multiple comparisons.

Multivariate relationship between persistence control energy and age We used partial least squares correlation (PLSC) (Krishnan et al., 2011) to retrieve patterns of age-relationship in persistence control energy (PE) of all iCAPs. The steps of PLSC include

1. Computation of concatenated group-wise correlation matrices $\mathbf{R} = \begin{bmatrix} \mathbf{R}_{\text{HC}} \\ \mathbf{R}_{22\text{q}} \end{bmatrix} = \begin{bmatrix} \mathbf{Y}_{\text{HC}}^T \mathbf{X}_{\text{HC}} \\ \mathbf{Y}_{22\text{q}}^T \mathbf{X}_{22\text{q}} \end{bmatrix}$ between age in $\mathbf{Y} \in 1 \times N_{\text{sub}}$ and PE $\mathbf{X} \in K \times N_{\text{sub}}$ of each brain state $k = 1, \dots, K$ and subject $s = 1, \dots, N_{\text{sub}}$.
2. Singular value decomposition of $\mathbf{R} = \mathbf{U}\mathbf{S}\mathbf{V}^T$ to obtain a number of latent variables (or ‘correlation components’). Singular values on the diagonal of \mathbf{S} indicate the explained correlation by each component, age saliences (or ‘age weights’) in \mathbf{U} and brain saliences (or ‘brain weights’) in \mathbf{V} indicate how strongly the corresponding group and brain state contributes to the multivariate correlation between age and PE.
3. Permutation testing to test for significance of correlation components, where rows of \mathbf{X} were randomly permuted 1000 times, while leaving \mathbf{Y} unchanged, in order to estimate the null distribution of singular values \mathbf{S} under assumption of no significant correlation between \mathbf{Y} and \mathbf{X} .
4. Bootstrapping with 500 bootstrap samples, obtained through sampling with replacement the observations in \mathbf{Y} and \mathbf{X} , to evaluate the stability of age- and brain weights in a significant correlation component.

For a more detailed description of PLSC, we refer the interested reader to (Krishnan et al., 2011; Zöllner et al., 2017, 2018, 2019b) or sections 3.1, 3.2, or 4.2 of this thesis.

Nuisance variable regression Age and sex were included as nuisance regressors in group comparisons and only sex was used in age-PLSC analyses. Nuisance regressors were standardized within each group to avoid linear dependence with the effects of interest.

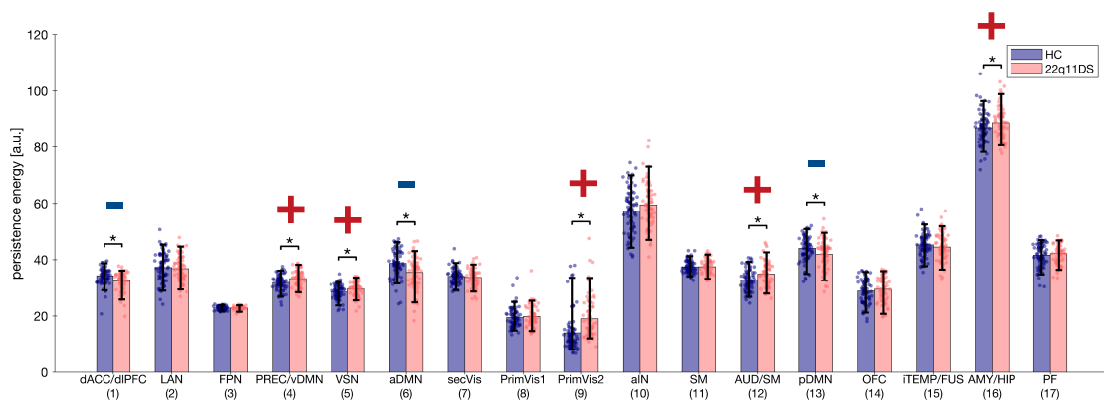


Figure 5.1 – Group differences in PE of the 17 functional brain states in patients with 22q11DS compared to HCs. P-values are FDR-corrected for the 17 multiple comparisons; age and sex were included as covariates. Significant group differences ($p < 0.05$) are marked with an asterisk, and with a + (or –) to indicate that they were higher (or lower) in patients. Error bars indicate 5th to 95th percentiles of group distributions. Single-subject duration measures are included as scatterplots. dACC/dlPFC – dorsal anterior cingulate cortex / dorsolateral prefrontal cortex, LAN – language network, FPN – fronto-parietal network, PREC/vDMN – precuneus / ventral DMN, VSN – visuospatial network, aDMN – anterior DMN, SecVIS – secondary visual, PrimVIS1 – primary visual 1, PrimVIS2 – primary visual 2, aIN – anterior insula, SM – sensorimotor, AUD/SM – auditory / sensorimotor, pDMN – posterior DMN, OFC – orbitofrontal cortex, iTEMP/FUS – inferior temporal / fusiform, AMY/HIP – amygdala / hippocampus, PFC – prefrontal cortex.

Relationship between brain state function and structure

In order to assess the relationship between resting-state fMRI activation measures and PE, we compute Pearson correlations between the two measures. First, we computed correlations across subjects for each group and each brain state, resulting in $K = 17$ correlation values per group. We then compared these 17 values between HCs and patients with 22q11DS using a paired t-test. Second, we computed correlations across the $K = 17$ brain states for each subject. We then compared the correlation values between HCs and patients with 22q11DS using a two-sample t-test.

5.1.3 Results

Spatial and temporal properties of resting-state functional states.

Using iCAPs, we extracted 17 functional brain states from the resting-state fMRI scans. The optimal number of states was determined using consensus clustering (Monti et al., 2003). Extracted networks include well-known resting-state brain states, such as DMN, fronto-parietal network (FPN), and salience network (SN) states. Supplementary figures C.1 and C.2 show the extracted states and a group comparison of their average activation duration between HCs and patients with 22q11DS, respectively. For a detailed discussion of temporal properties and

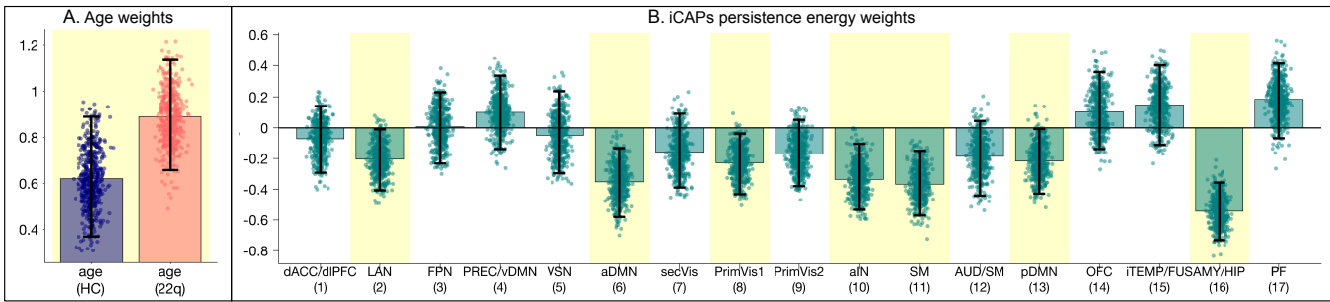


Figure 5.2 – PLSC testing for a relationship between PE and age resulted in one significant correlation component ($p < 0.001$). A) According to age weights indicating the correlation strength in each group, the age-relationship is stronger in patients with 22q11DS than in HCs. B) PE weights show that there is a significant negative relationship with age in 7 out of the 17 brain states. Error bars indicate bootstrapping 95% confidence intervals; robust results were indicated by yellow background.

their relevance for clinical symptoms in 22q11DS, we refer the interested reader to (Zöller et al., 2019a), or section 4.2 of this thesis.

Aberrant persistence control energy of functional brain states in 22q11DS.

We computed minimum PE of the 17 states for all participants based on their individual structural connectivity matrix. Figure 5.1 shows distributions of PE of every brain state in patients with 22q11DS compared to HCs.

Aberrant structural connectivity in patients with 22q11DS leads to altered PE in 8 out of the 17 brain states. PE was higher in patients with 22q11DS in brain states that involve more posterior and dorsal regions – precuneus / ventral DMN (PREC/vDMN), visuospatial network (VSN), primary visual 2 (PrimVIS2) and auditory / sensorimotor (AUD/SM) – as well as in amygdala / hippocampus (AMY/HIP). Reductions of PE on the other hand were present mainly in brain states including more anterior regions – dorsal anterior cingulate cortex / dorsolateral prefrontal cortex (dACC/dIPFC) and anterior DMN (aDMN) – and also in posterior DMN (pDMN).

Persistence control energy decreases from childhood to adulthood.

There is one significant correlation component ($p < 0.001$) resulting from PLSC analysis testing for a relationship between PE and age (see figure 5.2). PE is negatively correlated with age in 7 out of the 17 states. This correlation with age is significant for both groups, but stronger in patients with 22q11DS than in HCs. Age-related states include anterior and posterior DMN, anterior insula (aIN), sensory states (primary visual 1 (PrimVIS1) and sensorimotor (SM)), one emotional state (AMY/HIP) and the language network (LAN). The PE of states that are commonly associated with goal-directed behavior during tasks do not show any relationship with age (i.e., PREC/vDMN, which is sometimes called dorsal attention state, FPN, and VSN)

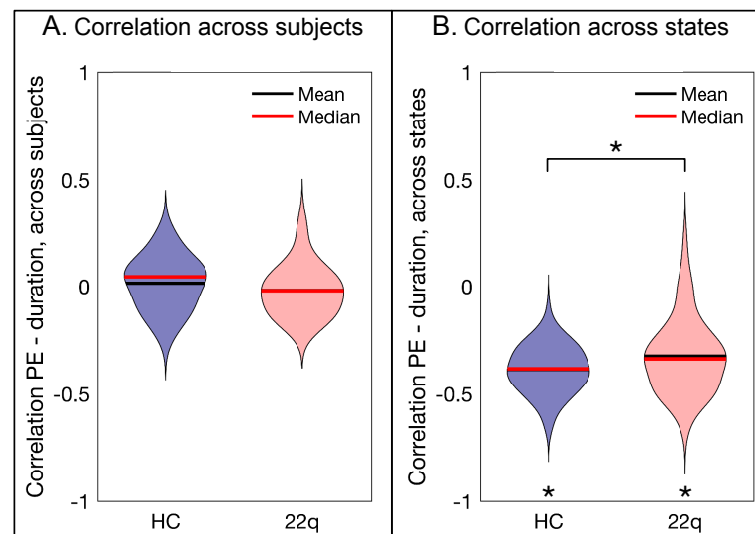


Figure 5.3 – Correlation between structural PE and resting-state activation duration. A) Across subjects there is no significant correlation, either in patients with 22q11DS or in HCs. Violin plots show the distribution of correlations for all brain states. B) Across states there is a negative correlation between the two modalities: the higher the PE, the shorter the resting-state activation duration. This correlation is significantly stronger in HCs than in patients with 22q11DS. Violin plots show the distribution of correlations for all subjects. Significant group differences ($p < 0.05$) are marked with an asterisk.

No correlation across subjects between activation duration and persistence control energy.

In order to test whether there was a relationship between the measures across subjects, we first considered between group differences. If there was a global linear relationship between structural PE and activation duration across subjects, all states would be altered in both, and always in the same or opposing direction. When comparing alterations of temporal activation and structural PE (see Supplementary Figure C.3), there is, however, no clear pattern of common alterations. While brain states with reduced PE (dACC/dlPFC, aDMN and pDMN) have all also reduced activation duration, only AMY/HIP has both increased PE and activation duration, and PrimVIS2 is even altered in different directions. Further, there are multiple brain states that are only affected in one single modality. FPN, SM, orbitofrontal cortex (OFC), inferior temporal / fusiform (iTEMP/FUS) have only aberrant activation duration, while PREC/vDMN, VSN and AUD/SM are only affected in terms of PE.

To explicitly test for a linear relationship between resting-state activation duration and structural PE in every state separately, we computed correlations between the two measures across subjects for each state. As already expected based on the observations on group differences in both modalities, there was no significant correlation between the two measures either in patients with 22q11DS or in HCs (see figure 5.3A). In other words, a subject who spends a long time in one brain state, does not have a systematically higher or lower PE of that brain state compared to other subjects.

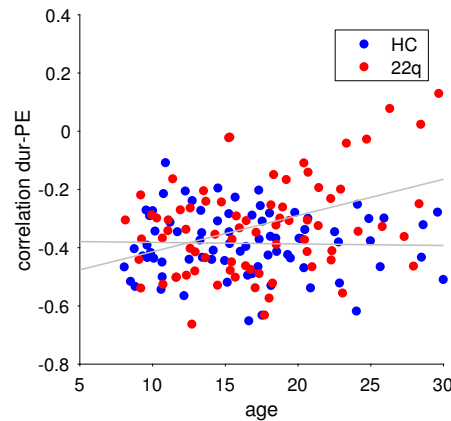


Figure 5.4 – The negative correlation between PE and activation duration is constant over age in HCs ($c=-0.04$, $p=0.73$), but significantly increasing (i.e., weakening) with higher age in patients with 22q11DS ($c=0.38$, $p<0.001$). PE – persistence control energy.

Negative correlation across states between activation duration and persistence control energy.

To test whether within each subject there was a relationship between temporal activation and structural PE, we computed across-states correlations for each subject (see figure 5.3B). There was indeed a negative correlation between activation duration and PE. In other words, all subjects tend to spend less time in brain states whose structural wiring leads to higher PE. This negative correlation was significantly stronger (lower) in HCs than in patients with 22q11DS ($p=0.01$).

Finally, we tested for a relationship with age of these negative correlation values (see figure 5.4). In HCs the energy-activation correlation did not change over age ($c=-0.04$, $p=0.73$). In patients with 22q11DS, however, the correlation became significantly weaker (higher negative values) with increasing age ($c=0.38$, $p<0.001$). In a joint model, the group-by-age interaction was significant with $p=0.002$. In other words, while at a younger age, patients showed similar energy-activation relationship as HCs, older patients have a weaker negative energy-activation correlation, indicating that the observed weakening in correlation (see previous paragraph) is emerging over age.

There was no correlation with full-scale intelligence quotient (FSIQ; HCs: $c=0.08$, $p=0.728$; 22q11DS: $c=-0.01$, $p=0.937$), positive psychotic symptoms as measured by the sum of positive SIPS scores (22q11DS: $c=-0.12$, $p=0.688$) and negative psychotic symptoms as measured by the sum of negative SIPS scores (22q11DS: $c=-0.37$, $p=0.130$).

Reported p-values were corrected for the six correlations that were computed using the false discovery rate.

5.1.4 Discussion

Here we used dynamic models to investigate the relationship between structural brain connectivity and its functional activation in 22q11DS, a population at extremely high risk for

schizophrenia. Combining fMRI activation analysis with network control energy, we probed the possible mechanistic implications of aberrant brain structure on altered functional activation (Braun et al., 2018). Functional brain states were retrieved from dynamic changes of resting-state functional activity. Then, we used network control theory to analyze how the white matter anatomy of these brain states may influence their dynamic behavior (Braun et al., 2019; Cornblath et al., 2018). We found aberrant control energy of several brain states, mainly involving anterior or posterior medial connections. Further, PE decreased from childhood to adulthood both in patients with 22q11DS and HCs. Finally, when probing for a relationship between structural control energy and functional resting-state activation, we found a negative correlation across brain states consistent with prior work (Cornblath et al., 2018), and which was less pronounced in patients with 22q11DS. However, we found no direct relationship between control energy of a brain state and its functional activation across subjects. In the following exposition, we will first discuss the alterations of PE and structure-function inefficiency in patients with 22q11DS, and then offer a tentative explanation for the absence of an across-subject relationship between control energy and functional activation.

Anterior-posterior and medial-lateral gradient of altered connectivity leads to aberrant brain control energy in 22q11DS

We analyzed persistence control energy of resting-state brain states in 22q11DS and found that aberrant structural wiring leads to a pattern of altered controllability with some brain states requiring higher energy and others requiring lower control energy. Persistence energy is mainly reduced in frontal brain states (aDMN, dACC/dlPFC) and increased in occipital (PREC/vDMN, PrimVIS2) and lateral parietal (VSN, AUD/SM) brain states. This pattern of findings confirms prior reports of aberrant anterior-posterior and medial-lateral white-matter connectivity in patients with 22q11DS (Scariati et al., 2016a; Gothelf et al., 2011; Váša et al., 2016). Our study expands upon these prior studies by probing the impact of this aberrant wiring on the dynamic behavior of the brain in terms of the energy that is needed to engage in these brain states.

In particular, we found reduced persistence control energy in DMN and cingulo-frontal SN, which are two brain systems that are known to play a central role in higher order cognition (Menon, 2011). Previous reports provide evidence that their structural and functional connectivity is altered in patients with 22q11DS (Padula et al., 2015, 2017b; Schreiner et al., 2014). In particular the dorsal anterior cingulate cortex (dACC), which is a central node of the SN, has been found to be affected in 22q11DS using different neuroimaging modalities and has been suggested as a biomarker for psychosis in the disorder (Padula et al., 2018). Of note, these states were also found to have altered resting-state activation (Zöller et al., 2019a) and even though we here did not find a linear relationship between resting-state activation duration and structural control energy, the fact that a majority of brain states is affected in both measures suggests that there may be a more complex underlying common mechanism.

Moreover, we found that persistence in the amygdala and hippocampus brain state was energetically more demanding for patients with 22q11DS, but nevertheless those same patients spent more of the resting-state scan time engaging in this state. We recently found that

higher activation and aberrant coupling of this amygdala and hippocampus brain state tracks with higher levels of anxiety (Zöller et al., 2019a) and the present results confirm that it is also affected on a structural level.

The brain gets energetically more efficient from childhood to adulthood

Aside from alterations in 22q11DS, we found that persistence control energy of many brain states (7 out of 17) is negatively correlated with age, both in patients with 22q11DS and in HCs. This finding suggests that with increasing age, the brain gets more efficiently wired to reduce the control energy required for its functional activation. In line with these findings, Tang et al. found that both average and modal controllability (which measure the general ability to steer the brain towards easy-to-reach or difficult-to-reach brain states) increase over age in a similar age range, which suggests an increasingly efficient wiring that at the same time allows a higher diversity of brain dynamics (Tang et al., 2017a). Importantly, while there are small variations in the distributions of controllability across the brain in males and females, the trend for increasing controllability with age is equally strong in both sexes (Cornblath et al., 2019). Further, Cui et al. (2018) found that control energy of atlas-based brain states calculated with a comparable approach to ours, was also decreasing from childhood to adulthood in most brain states (Cui et al., 2018). This developmental trajectory of structural brain architecture was preserved in patients, suggesting that while they present with absolute alterations of controllability properties, their overall development seems to be largely intact.

Dynamic inefficiency in patients with 22q11DS, which becomes increasingly marked with age

Finally, when investigating the relationship between functional activation and structural control energy, we found that the brain activates in a highly efficient way, spending less time in brain states that are energetically more demanding, consistent with prior evidence in a completely different cohort (Cornblath et al., 2018). In patients with 22q11DS, this relationship was significantly weaker than in HCs, which suggests that aside from the pure alteration in structure and function, the relationship between the two is also altered. In particular, patients use their brains in a less efficient way, spending more time in energetically demanding states than HCs. Additionally, this dynamic inefficiency in patients with 22q11DS became increasingly marked with greater age. Possibly, the patients' inefficient use of their brain may express in the more severe symptomatology characteristic of older patients. However, we did not find a significant correlation between our measure of dynamic efficiency and psychotic symptoms or IQ, and therefore our hypothesis should be verified in future studies with larger sample sizes.

Control energy and activation of a single state are not correlated across subjects

While we were able to detect a relationship between functional activation and structural control energy across states (pointing towards the inherent efficiency of the human brain as discussed above), we did not observe a relationship across subjects. In other words, subjects with less efficiently wired brain states (higher PE) did not spend more or less time in these

brain states compared to other subjects. A possible explanation may be that, while here we were testing for a simple relationship for each state separately, the association is likely more complex than a one-to-one linear correlation. Importantly, brain states do not act in isolation, but interact among themselves. For instance, knowing about the interaction between the DMN and the amygdala and hippocampus that we discovered in the same dataset (Zöller et al., 2019a), one could imagine that indeed alterations of controllability in the DMN may lead to increased activity of the amygdala and hippocampus. Testing for such cross-network relationships may be even more interesting, and our methodological approach offers a valuable framework to explore this complexity in future research.

Methodological considerations and limitations

Variance of structural connectivity across subjects and across regions has different scales

In the present study, structural connectivity was measured in terms of connection density; that is, with a fixed number of reconstructed streamlines. As a result, the variability of connectivity across regions is relatively high compared to the variability across subjects. Therefore, this approach supports a careful investigation into *relative* changes in connectivity, but it is less powerful in tracking *absolute* changes in connectivity. In our results, this effect can be observed in figure 5.1, where the differences in energy from one state to another are much larger than the differences in persistence energy across subjects for one single brain state. Significant differences between subjects do exist, however, they are small with respect to the differences between brain states. This effect may be a possible reason why we detected correlations with functional activation across brain states, but not across subjects.

Linear models of brain dynamics For simplicity, we here chose to use a linear model of dynamics on the structural connectivity graph (Kim and Bassett, 2019; Honey et al., 2009; Gu et al., 2015) to calculate minimum control energy (Betz et al., 2016). Even though this model is the most widely used approach for network control theory in neuroscience, it may be overly simplistic. Incorporating models of non-linear dynamics could prove useful in the future as they could potentially improve the estimation of more realistic control energy (Kim and Bassett, 2019). It is possible that an estimate based on more biologically plausible dynamic models would allow us to detect more subtle relationships between controllability and functional activation.

5.1.5 Conclusion

In this study, we investigated the control energy of functional brain states in patients with 22q11DS. This is the first study investigating the impact of aberrant structural connectivity on brain dynamics using control energy in 22q11DS. We found that altered connectivity in patients with 22q11DS leads to reduced energy impact for engaging frontal brain states, whereas more occipital and parietal brain states were energetically more demanding for patients with 22q11DS than HCs. Further, in a comparison of structural control energy with resting-state fMRI activation, we found that the brain functions in an efficient way by engaging less into energetically demanding brain states. In patients with 22q11DS the anticorrelation

between activation and control energy is weaker than in controls, suggesting a dynamic inefficiency of brain function in these patients. In summary, we contribute one of the first studies investigating a direct link between control energy and functional activation during rest and provide promising insights for a better understanding of brain alterations in 22q11DS.

5.2 Summary and outlook

In this chapter, we explored how structural connectivity of the brain may influence its dynamic behavior and whether this link is altered in patients with 22q11DS. We combined resting-state fMRI analysis for the retrieval of large-scale functional brain states with network control theory to examine how the brain's structural architecture may facilitate or impede the engagement into these functional states. We found that aberrant anterior-posterior structural connectivity in patients with 22q11DS makes it energetically more demanding to engage in occipital and parietal brain states, but energetically less demanding to engage in DMN states and the cingulo-prefrontal SN.

Of note, these alterations again include frontal areas and the ACC, similarly to the alterations we already observed in terms of BOLD signal variability and large-scale brain state activity (see chapters 3 and 4). Also the amygdala and hippocampus state, whose functional activation we found to be relevant for anxiety (see section 4.2), was altered in terms of structural control energy. Together, these results point towards relevant alterations of the amygdala in terms of structure and function, which could be a valid imaging predictor for anxiety and psychosis, and should be subject to further investigation.

Further, we found that in all subjects the brain's structure and function are linked to minimize persistence control energy, with less time spent in energetically more demanding brain states. We made the interesting observation that in patients with 22q11DS, this optimal relationship was less strong; i.e., the aberrant control energy and functional activation duration in patients lead to a rebalancing with relatively more time spent in energetically demanding brain states. This inefficiency was worse in adult patients than in children, suggesting a developmental decay.

When looking into each state separately, there was no linear relationship between control energy and functional activation, pointing towards a more complex non-linear relationship, possibly also from one state to another. Future studies should further delineate the nature of this relationship.

Methodological considerations and future avenues for brain network control theory

It is worth noting that the control theory framework in its form used here has several methodological constraints that limit the conclusions that can be drawn from it in the context of brain network analysis.

One first consideration is system stability. In the approach employed here, the structural connectivity matrix is normalized by dividing by its largest eigenvalue and subtracting the identity matrix in order to represent a stable dynamic system (see subsection 5.1.2, and Betzel et al., 2016). Also of note, due to the symmetry of structural connectivity matrices, all eigenvalues are real, and thus, only "passive", non-oscillatory eigenmodes are present. Without external control inputs, a system normalized in such way tends to decay towards a zero state ($\lim_{t \rightarrow \infty} \mathbf{x}(t) = \lim_{t \rightarrow \infty} e^{\mathbf{A}t} \mathbf{x}(0) = \mathbf{0}$). While mathematically convenient, this assumption is biologically unlikely. Indeed, it is rather difficult to say what a "zero state" would represent in the context of the brain. In the field of network control theory and its application to the

brain, there have been efforts to overcome this limitation by conceiving control schemes that stabilize the system at a specific oscillatory state, that is, in states of synchronization between specific brain regions (Menara et al., 2019). Further, theoretical developments in brain network control theory have so far been mostly validated on simulated functional data (Menara et al., 2019; Muldoon et al., 2016). The continued refinement of theoretical work, as well as the empirical validation based on measured functional activation, will be crucial to one day reach sufficiently accurate models that allow to draw conclusions on biologically valid brain dynamics. In the field of passive brain dynamics (in absence of an active control input), great efforts to conceive and validate models of large-scale nonlinear brain dynamics (reviewed in Breakspear, 2017) have shown that complex nonlinear dynamics play a central role for cortical brain function. Our study presented here is a first attempt to combine network control theory with functional activation measures, however, it is based on fairly simplistic models and that should be expanded to more complex evaluations in the future.

Secondly, as any approach modeling the brain as network of structural connectivity, the framework used here is bound by the assumptions that come with the network reconstruction based on diffusion weighted MRI. While the diffusivity that can be measured through MRI is clearly dependent on the white matter microstructure, it is still subject to ongoing research, how microstructural properties of the white matter (myelination, axonal density, etc.) translate into diffusivity (Beaulieu, 2009; Sampaio-Baptista et al., 2019). For example, higher axonal organization, but also higher myelination, would both lead to increased fractional anisotropy (Zatorre et al., 2012), but might possibly translate into different dynamic properties. Further, neither direction, nor nature (excitatory vs. inhibitory connections) of axonal connections can be reconstructed from dMRI, limiting reconstructed networks to undirected graphs with only one type of connections. However, microscale brain structure has indeed marked influence on macroscale dynamic brain function during rest (Wang et al., 2019a), and the incorporation of such microscale structural information is promising towards better models of brain dynamics. Taken together, these limitations restrict both model assumptions and possible conclusions that can be drawn from any approach that adds dynamic models on a structural connectome.

Despite these general limitations of the framework, network control theory remains nevertheless a powerful approach, as it provides an interpretation about the impact of structural brain network topology on active dynamic functional properties. The limitations mentioned here should be kept in mind to avoid an “over-interpretation” of controllability results. Further advances in the fields of network control theory, structural network reconstruction with diffusion-weighted MRI and empirical validation of dynamic models of brain function will provide continued improvement and validation of model assumptions and interpretations.

6 Summary and perspectives

This thesis was dedicated to explore dynamic properties of brain function and structure and evaluate their potential to obtain a better understanding of psychosis vulnerability. In what follows, I will summarize our main contributions and findings and explore promising future directions for methodological developments and clinical research.

6.1 Summary

BOLD signal variability We have explored the potential of measuring functional brain dynamics through blood oxygenation level dependent (BOLD) signal variability. As whole-brain BOLD signal variability maps are very high-dimensional, we have developed a partial least squares correlation (PLSC)-based approach to investigate multivariate patterns of alterations and age-relationship at the same time. Using this approach, we found that BOLD signal variability in patients with chromosome 22q11.2 deletion syndrome (22q11DS) is indeed altered in a broad pattern distributed over the entire brain. The pattern of alterations was very similar to reported BOLD signal variability alterations in schizophrenia. Further, we compared BOLD signal variability alterations with static functional connectivity (sFC) alterations of the default mode network (DMN) to test how changes in sFC may be driven by BOLD signal variability. We found that patterns of alterations are only partly overlapping, suggesting a complex non-linear relationship between sFC and BOLD signal variability. Finally, we used our multivariate PLSC-based approach to investigate BOLD variability in patients with 22q11DS with prodromal psychotic symptoms who are at higher clinical risk for converging to schizophrenia. Our results point towards developmental reductions of dynamic brain function in the dorsal anterior cingulate cortex (dACC), a central node of the salience network (SN) that is known to be implicated in salience processing and self-monitoring. These findings are in line with previous literature on brain function and structure in the psychosis prodrome in 22q11DS using non-dynamic measures.

Large-scale functional brain network dynamics In order to verify how alterations in BOLD signal variance could be explained in terms of altered activation of large-scale functional brain networks, we employed innovation-driven co-activation patterns (iCAPs). First, we discovered that in the original form of the iCAPs framework, spatial overlap in brain states can induce spurious temporal activation and co-activation of brain-states. To overcome this

limitation, we developed a novel method for the recovery of iCAPs time courses in which we exploit the information on changing functional activity that is provided by the framework. We introduced spatio-temporal constraints that integrate knowledge about the spatial distribution of all brain states, as well as temporal information on the timing of activation changes. We showed that this approach is more powerful in recovering temporal overlap of brain states than the original method. Then, we used this improved iCAPs framework to probe into aberrant temporal activation of large-scale functional brain states in 22q11DS. As previously, we were interested in patients at clinically increased risk to evolve towards schizophrenia. This time, we investigated anxiety in addition to prodromal positive psychotic symptoms and found patterns of functional alterations characteristic for both risk factors. Again, altered activation of the cingulo-prefrontal SN, which includes the dACC, was observed in patients with higher prodromal psychotic symptoms, suggesting that reduced BOLD signal variability observed previously may be explained by reduced activation of the SN. Further, we observed compelling alterations of coupling of the amygdala and hippocampus with dorsal and ventral subparts of the prefrontal cortex in patients with higher levels of anxiety. Together, these results prove the potential of studying brain dynamics in patients with 22q11DS to find clinically relevant markers for psychosis vulnerability. As this study was the first published study using iCAPs in a clinical population, it made also an important contribution by demonstrating the clinical potential of the method in providing easily interpretable measures of aberrant brain function.

Structure-function relationship through control theory Finally, in the last part of this thesis, we explored how the structural anatomy of the brain might be linked to the dynamic alterations observed so far. We proposed to combine the analysis of brain dynamics through iCAPs with principles from network control theory to explore how the brain's structural connectivity relates to its functional activation. We used iCAPs to obtain large scale functional brain states and then applied network control theory to calculate how energetically easy or difficult it is for an individual to engage in this functional brain state, given his/her structural wiring. Using this approach, we tested for alterations in patients with 22q11DS and found aberrant structural control energy in a set of brain states, which was partly overlapping with brain states that were altered in terms of functional activation. Further, we discovered that the brain operates in an intrinsically optimized way, spending less time in brain states that are energetically more demanding. While this relationship existed in patients with 22q11DS, it was weaker than in healthy subjects. We interpret this observation as a less efficient structure-function relationship, as it suggests that patients tend to spend more time in energetically more demanding brain states. This study was one of the first analyses of multimodal MRI data in patients with 22q11DS and the first probing explicitly into a relationship between structural and functional properties.

6.2 Future research directions

Linking different types of dynamic measures In chapter 3, we studied BOLD signal variability and its relationship to seed-based sFC. Our results suggest a complex non-linear relationship between the two measures that merits closer investigation. As already discussed in more

detail at the end of chapter 3, a compelling approach to probe into such a relationship is to explore different mechanistic models of changes in variance (Duff et al., 2018; Cole et al., 2016). By comparing predicted changes in functional connectivity given different models of BOLD variability with the actual functional connectivity, one can conclude on underlying mechanisms based on the model that best predicts reality. Of note, our findings on BOLD variability reported in chapter 3 partly overlap with alterations in large-scale brain state activation in chapter 4. An explicit exploration of the link between large-scale brain state activation and BOLD variability would be an interesting follow-up of our initial study on connectivity-variability relationship (section 3.1) that could provide further insights into the functional significance of BOLD variability. Importantly, here we only investigated each measure separately in terms of their alterations and correlations with clinical profiles. Nevertheless, also the relationship between functional activation, functional connectivity and BOLD signal variability may contain relevant information on noise levels and characteristic properties on how the brain engages in functional systems. Such interactions between functional measures might more reliably be linked to clinical and behavioral variables than each one on its own.

Explore further approaches to link structure and function In chapter 5, we explored the link between activation and anatomy of large-scale functional brain states by using concepts from network control theory. The advantage of this approach is that it incorporates a dynamic model to not only describe structural network topology, but also provide a prediction on the functional impact of the underlying structural connectivity. In our study we compared this prediction in terms of control energy with the actual activation during rest and uncovered that the brain seemingly operates in an inherently efficient way. We observed an alteration in this functional efficiency in patients with 22q11DS that was increasing with age, which points towards a developmental relevance that should be studied further.

Additionally, future studies could investigate the effects of different model parameters of the dynamic model on the relationship between structural connectivity and functional activation. For example, in a study on attention deficit hyperactivity disorder (ADHD), Hearne et al. compared different scenarios of regional noise variability in a generative model that predicts functional connectivity from structural connectivity (Hearne et al., 2019). The authors found that clinically relevant structure-function alterations are related to regional heterogeneity of noise levels, providing a mechanistic explanation of the observed structure-function breakdown, and proving the potential of uncovering structure-function relations to improve our understanding of aberrant mechanisms that underlie mental diseases.

Another promising approach comes from the emerging field of graph signal processing (Atasoy et al., 2016, 2017; Huang et al., 2018; Medaglia et al., 2018). Instead of simply predicting functional activation from structural connectivity, this framework allows to decompose the functional signal into harmonic components that represent differential coupling strength between functional activation and structural architecture. In this way it is possible to go beyond a pure quantification of structure-function coupling strength, by considering functional components that are coupled or decoupled with the structure, as well as the link between coupled and decoupled components. The recently introduced *structural-decoupling index* is based on

such a decomposition and uncovered a decoupling gradient from lower- to higher-level cognition with strong coupling in sensory regions, but higher decoupling in high-level cognitive regions (Preti and Van De Ville, 2019). So far, this approach has not been applied in clinical neuroscience, but the compelling findings in healthy populations underline its potential to uncover relevant alterations in structure-function integration also in clinical populations.

Neurostimulation In chapter 5, we investigated the assumption of intrinsic control through naturally changing neural activity. Another implication of control theory for brain research is the possibility for controlling aberrant brain states from the outside by means of invasive stimulation through, e.g., deep brain stimulation (Ashkan et al., 2017), or non-invasive stimulation through transcranial magnetic or electric stimulation (Polanía et al., 2018). As targets for neurostimulation have to be carefully chosen, simulations and dynamic modeling will be very useful to select brain regions and systems of interest, as well as the best stimulation procedures. Models from network control theory, such as the ones used in chapter 5 of this thesis, provide the ideal framework for this goal. In these lines, one seminal study evaluating the effects of neurostimulation based on control theory used simulations of functional connectivity to evaluate the system-wide impact of focal stimulation at different targets (Muldoon et al., 2016), and two further studies went beyond simulations by incorporating electrocorticography (ECoG) measurements before and after neurostimulation (Stiso et al., 2018; Khambhati et al., 2019). Notably, while therapy through neurostimulation is subject to active investigation, for psychiatric disorders so far no therapeutic protocol has been fully established (Temel et al., 2012; Polanía et al., 2018; Lefaucheur et al., 2017). In schizophrenia, a deeper understanding of the underlying pathophysiology will be necessary to evaluate potential targets and develop successful stimulation protocols. Future research on the pathophysiology together with further advances in the field of brain network control theory will potentially allow to translate improved knowledge of schizophrenia into most promising targets and protocols for brain stimulation.

Going beyond standard diagnostic categories While we here mainly considered symptoms and risk factors related to psychosis and schizophrenia, an emergent view is that mental disorders represent a continuum rather than discrete diagnostic categories, and that there are common mechanisms underlying different mental disorders (Buckholtz and Meyer-Lindenberg, 2012; Insel and Cuthbert, 2015). This has been conceptualized by Caspi et al. in the general psychopathology factor, or “p factor”. Comparing several factor models, the authors showed that a single factor best explains a range of psychiatric disorders, which points towards a common underlying mechanism that may explain the high comorbidity among mental diseases (Caspi et al., 2014). Given this clinical evidence, research on the pathophysiology of mental diseases should incorporate symptoms, rather than categorical diagnostic labels, and should include individuals with different diagnoses in order to delineate transdiagnostic effects of psychopathology and specific characteristics for individual diseases. In the article in section 4.2 of this thesis, we incorporated this concept by considering continuous symptoms scores of clinical risk variables rather than discrete diagnostic groups. Further research should additionally consider symptoms and clinical variables related to other mental disor-

ders such as ADHD, autism and mood disorders, which are also prevalent in patients with 22q11DS, but commonly only studied individually. In the general population, transdiagnostic symptoms-based studies investigating the common substrate of multiple psychiatric disorders have already given promising insights into the general pathophysiology of mental diseases (Goodkind et al., 2015; McTeague et al., 2017; Xia et al., 2018). For example Xia et al. mapped patterns of functional connectivity onto four cross-diagnostic dimensions of psychopathology in a large sample of youth, which points towards the existence of biological subgroups that do not map well onto clinical diagnostic categories (Xia et al., 2018). In future, larger datasets and data sharing initiatives will allow more such transdiagnostic brain imaging studies to further delineate biologically defined subtypes of psychopathology.

Integration of multimodal data beyond brain imaging Schizophrenia and mental diseases in general are complex disorders: underlying brain alterations are manifold, with multiple causes and factors leading to the final outbreak of the disease and, thus, the heterogeneity in groups of patients with the same diagnostic label is huge (Insel, 2010; Insel and Cuthbert, 2015). Therefore, an improved understanding and ultimately better diagnostics and treatment will likely only be obtained through the integration of multiple types of data. Here, we made a first attempt in that direction by considering multimodal structural and functional MRI data. However, there are important other risk factors that are for example of genetic and environmental nature and cannot be measured through brain imaging (Buckholtz and Meyer-Lindenberg, 2012). In order to successfully delineate these complex effects and mechanisms, future research in mental health will have to develop algorithms for the integration of multimodal data incorporating information on genes, behavior, and environmental factors in addition to neuroimaging data (Bzdok and Meyer-Lindenberg, 2018). In the Geneva 22q11DS cohort, future research in this direction should aim to integrate available genome sampling data, as well as metabolic data such as cortisol levels. Further, an ongoing project is currently using the “experience sampling method” to record data from subjects in the cohort. The experience sampling method is a novel smartphone-based method that asks individuals to fill in structured questionnaires at random moments during a day or week, allowing the assessment of continuous changes in everyday activity (Larson and Csikszentmihalyi, 2014). In this way, psychopathology and well-being can be assessed more directly in the moment, which increases ecological validity and specificity of the assessed symptoms compared to classical retrospective questionnaires or interviews. The integration of these experience sampling data with brain imaging bares the large potential to detect more reliable and relevant markers of psychopathology and improve the prediction of clinical outcomes.

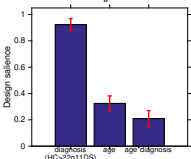
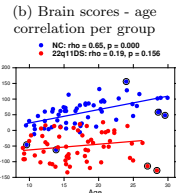
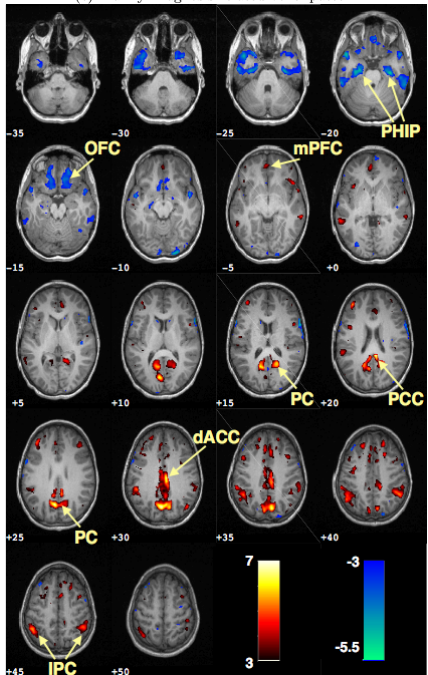
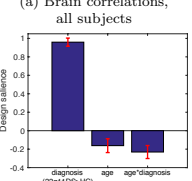
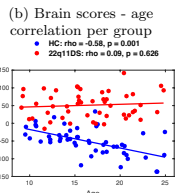
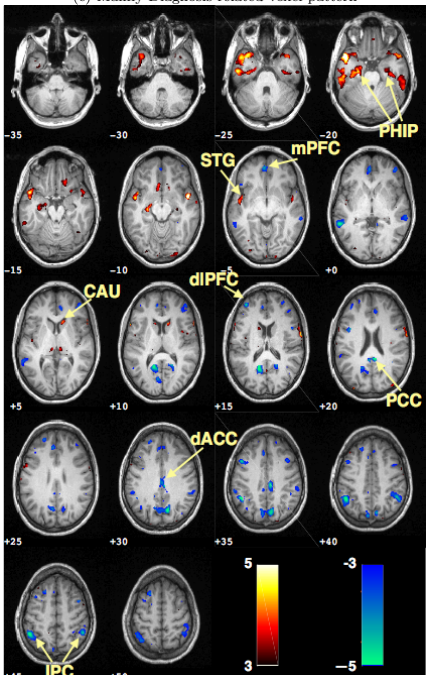
A Supplementary material for chapter 3

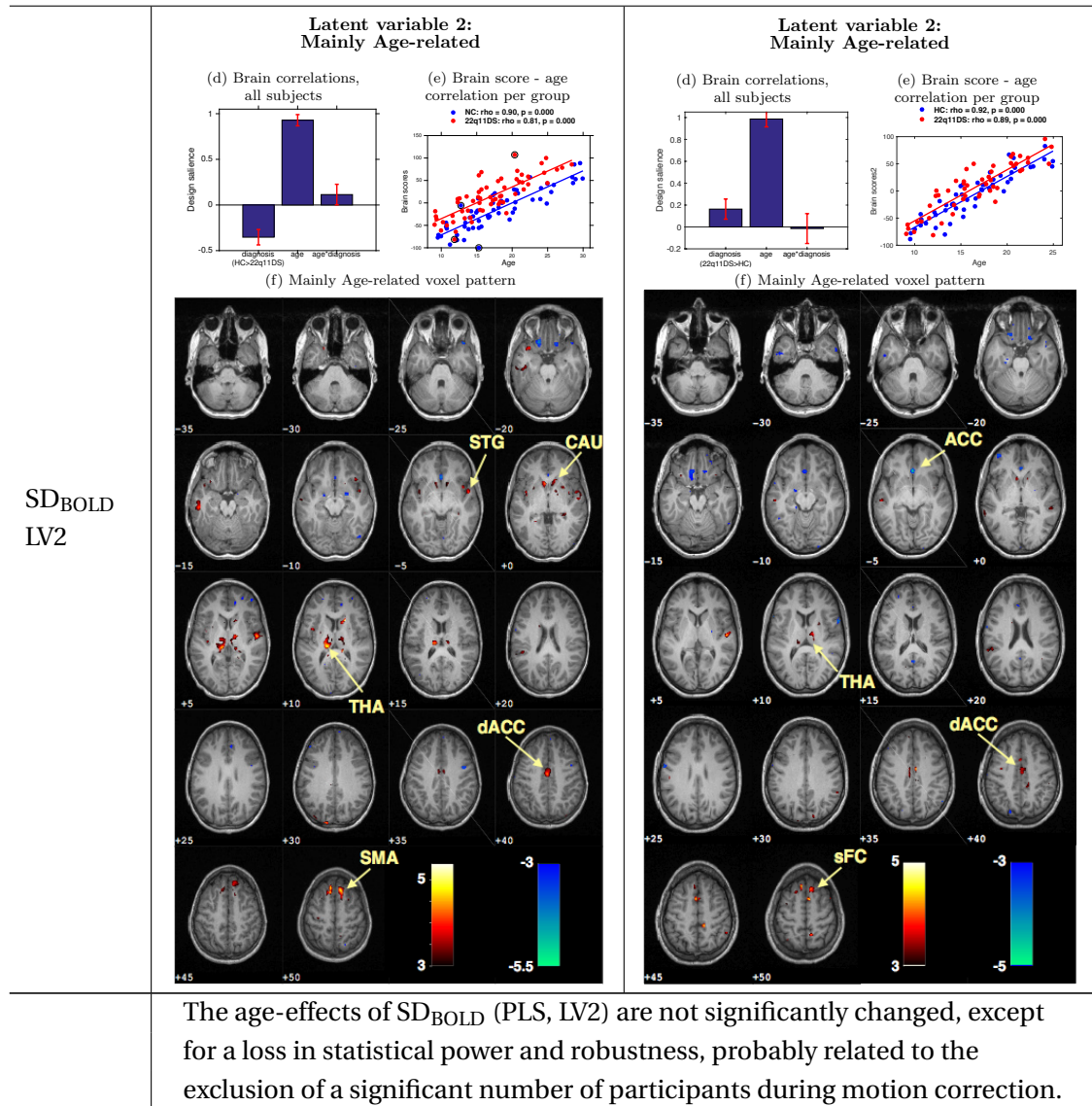
A.1 Supplementary material for section 3.1

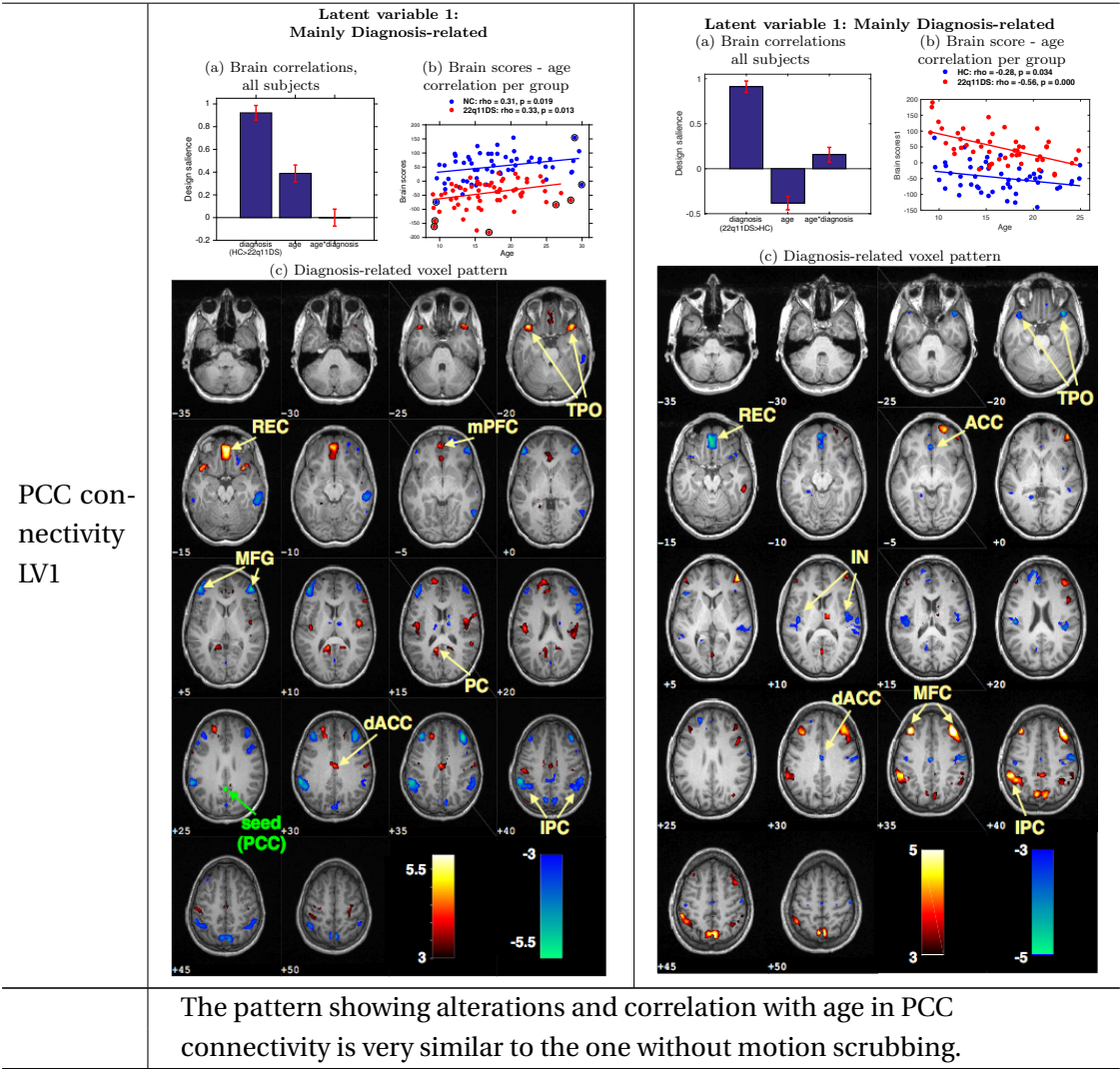
In order to study the effect of motion on our results, we conducted the same analysis without using motion scrubbing for motion correction on a dataset including the subjects which were excluded after scrubbing. Instead of motion scrubbing, we applied regression of the six motion parameters estimated during realignment.

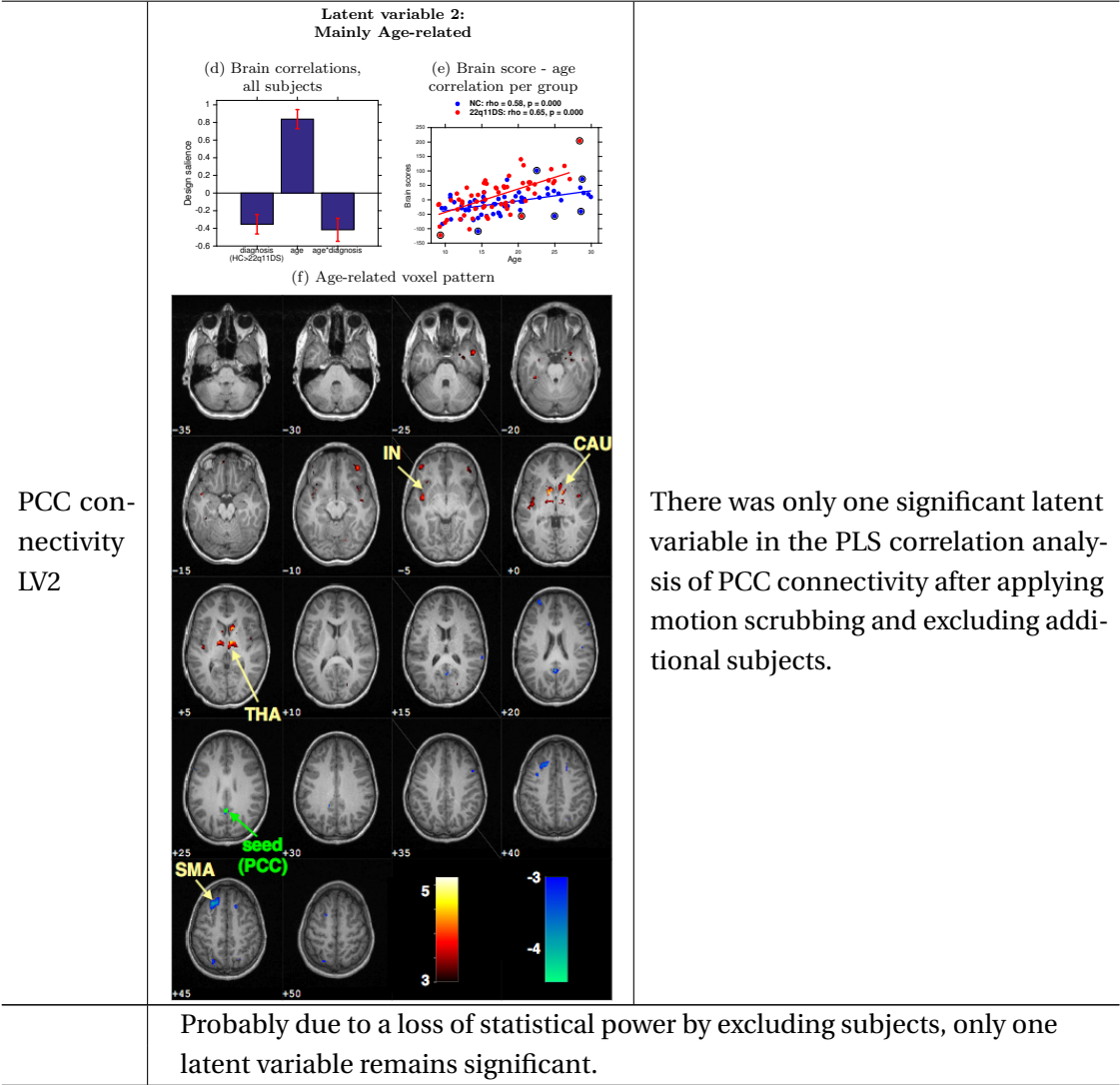
In the following table, we compare the PLS correlation results before (left column) and after applying stronger motion correction (right column, results included in the final version of the present paper) in SD_{BOLD} and PCC connectivity:

Table A.1

	Without motion scrubbing (61 patients, 59 controls)	With motion scrubbing (50 patients, 50 controls)
SD _{BOLD} LV1	<p>Latent variable 1: Mainly Diagnosis-related</p> <p>(a) Brain correlations, all subjects</p>  <p>(b) Brain scores - age correlation per group</p>  <p>(c) Mainly Diagnosis-related voxel pattern</p> 	<p>Latent variable 1: Mainly Diagnosis-related</p> <p>(a) Brain correlations, all subjects</p>  <p>(b) Brain scores - age correlation per group</p>  <p>(c) Mainly Diagnosis-related voxel pattern</p> 
	<p>The group effects in SD_{BOLD} (PLS, LV1) along midline structures mainly disappeared after stricter motion correction and those in the inferior temporal lobe were significantly reduced. In return, another set of regions appeared, including the dorso-lateral prefrontal cortex, the superior temporal gyrus and caudate.</p>	



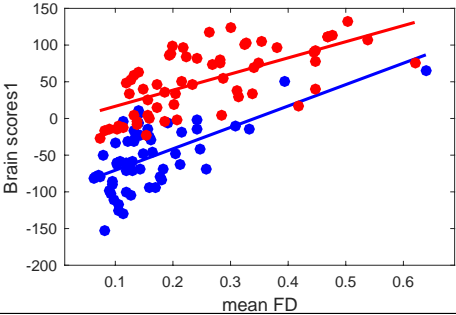
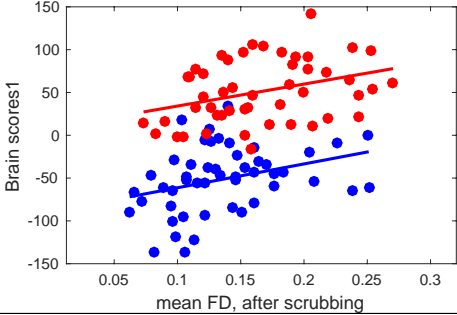
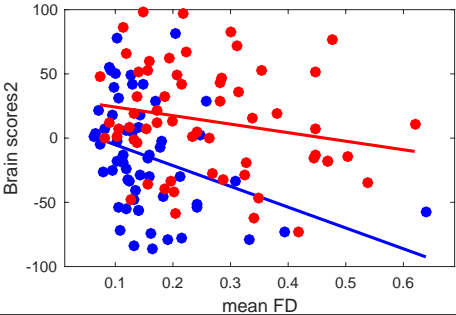
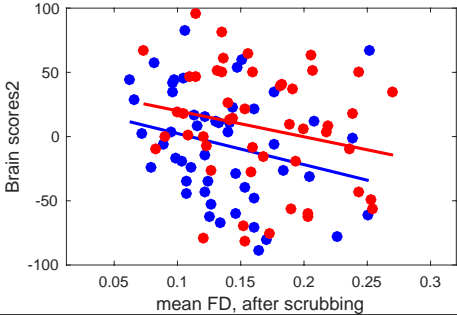




Appendix A. Supplementary material for chapter 3

To further understand the relationship between our results in SD_{BOLD} and motion, we computed the Spearman correlation coefficient between every subject's mean framewise displacement and the brain scores resulting from the PLS correlation analysis of SD_{BOLD} . The following two plots show that there is indeed a strong association with motion in both latent variables, but that after motion scrubbing this relationship was significantly reduced.

Table A.2

	Without motion scrubbing (61 patients, 59 controls)	With motion scrubbing (50 patients, 50 controls)
SD_{BOLD} LV1 (Mainly diagnosis- related)	<p>● HC: $\rho = 0.56$, $p = 0.000$ ● 22q11DS: $\rho = 0.70$, $p = 0.000$</p> 	<p>● HC: $\rho = 0.39$, $p = 0.005$ ● 22q11DS: $\rho = 0.34$, $p = 0.016$</p> 
	In the mainly diagnosis-related pattern (SD_{BOLD} , LV1), the correlation with motion is significant in both groups, but stronger in patients.	In the mainly diagnosis-related pattern (LV1, see figures 3a to 3c), the correlation with motion is still significant in both groups, but much lower than before. The correlation strength does not differ anymore between the two groups.
SD_{BOLD} LV2 (Mainly age- related)	<p>● HC: $\rho = -0.42$, $p = 0.001$ ● 22q11DS: $\rho = -0.19$, $p = 0.150$</p> 	<p>● HC: $\rho = -0.31$, $p = 0.030$ ● 22q11DS: $\rho = -0.20$, $p = 0.176$</p> 

A.1. Supplementary material for section 3.1

	In the mainly age-related pattern, only healthy controls show a significant negative correlation with motion. This effect corresponds to the negative correlation between age and motion (see main text, table 2).	In the mainly age-related pattern (see main text, figures 3d to 3f) there is still a significant correlation with motion only in healthy controls. However, the correlation magnitude is reduced and the p-value increased to $p=0.03$. The association between age and motion in healthy controls is thus less strong than before.
--	--	--

These two results show that we were able to reduce the motion effects in our results by applying motion scrubbing and excluding further subjects, even though also after scrubbing we still observe a significant relationship with motion. This correlation however is now significantly reduced and does not differ between the groups anymore. As motion is an issue, which is very difficult to address in clinical populations such as ours (see also main text, section Methodological Considerations), we think that this is the best correction we can obtain without losing too much statistical power or introducing selection bias in our data.

A.2 Supplementary material for section 3.2

Table A.3 – Demographic characteristics of the five subjects with a psychotic disorder according to DSM-IV-TR criteria.

subject	diagnosis*	age	gender	FSIQ
S1	psychosis	24.97	female	63
S2	schizoaffective disorder	23.05	male	56
S3	psychosis	18.13	female	67
S4	schizophrenia	14.09	female	46
S5	psychosis	14.28	male	68

* The presence of psychiatric disorders was evaluated during a clinical interview with the patients using the Diagnostic Interview for Children and Adolescents Revised (DICA-R; Reich, 2000), the psychosis supplement from the Kiddie-Schedule for Affective Disorders and Schizophrenia Present and Lifetime version (K-SADS-PL; Kaufman et al., 1997) and the Structured Clinical Interview for DSM-IV Axis I Disorders (SCID-I; First et al., 1996)..

A.2.1 Subjects already included in previous studies.

The cohort is partly overlapping with our previous resting-state fMRI studies: 30 subjects (8 PS+, 6 PS-, 16 HC) have been also included in Debbané et al. (2012), 51 subjects (10 PS+, 8 PS-, 33 HC) in Scariati et al. (2014), 56 subjects (10 PS+, 11 PS-, 35 HC) in Padula et al. (2015), 54 subjects (13 PS+, 9 PS-, 32 HC) in Scariati et al. (2016b), 79 subjects (16 PS+, 16 PS-, 47 HC) in Padula et al. (2017b), 83 subjects (16 PS+, 19 PS-, 48 HC) in Zöllner et al. (2017).

A.2.2 Summary on subject exclusion criteria.

From our initial sample of 97 patients and 90 HCs between 10 and 30 years old, a total of 61 participants had to be excluded to ensure the good quality of the data. 4 subjects (3 with 22q11DS, 1 HC) were excluded because they reported having fallen asleep during the scanning session. Another 31 subjects (24 with 22q11DS, 7 HC) had to be excluded due to excessive motion of more than 3 mm in translation or 3° in rotation, and the data of 20 more subjects (7 with 22q11DS, 13 HC) were not used because parts of the cortex were not captured. From the remaining dataset, 6 patients with 22q11DS were excluded after motion scrubbing (Power et al. 2012, see paragraph *Preprocessing*) as less than 100 rs-fMRI scans, corresponding to 4 min of scanning time, remained after exclusion of frames with a framewise displacement below the threshold of 0.5 mm. Supplementary Table A.4 shows a summary of motion data for the three groups.

A.2.3 Analysis of motion effects.

In fMRI analysis, in particular when investigating the standard deviation of the BOLD signal, motion is a major concern. To explicitly test for motion effects in our data, we computed

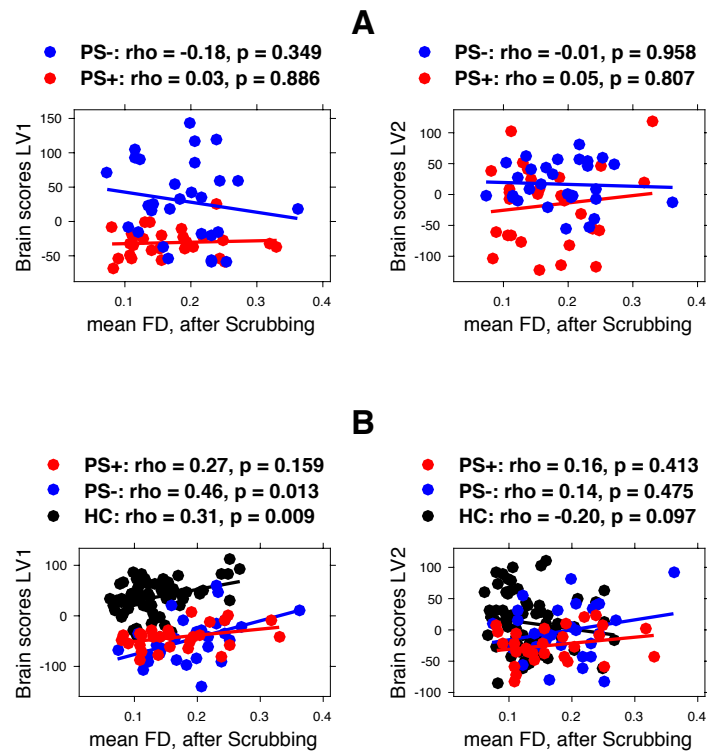


Figure A.1 – Correlation of brain scores with average framewise displacement (FD) for results comparing PS+ and PS- (A) and results comparing the two sub-groups with 22q11DS to healthy controls (B).

the correlation between brain scores and motion (i.e. the average framewise displacement). Figure A.1 shows the correlations for the four correlation components.

Appendix A. Supplementary material for chapter 3

Table A.4 – fMRI motion parameters. FD - framewise displacement.

		PS+	PS-	HC	correlation with age (p value)
Mean translation (mm)	x	0.15±0.18	0.17±0.16	0.13±0.14	0.0270 (0.7640)
	y	0.20±0.17	0.17±0.15	0.19±0.16	-0.1123 (0.2106)
	z	0.38±0.37	0.34±0.23	0.30±0.29	-0.1607 (0.0723)
Mean rotation (degree)	r_x	0.40±0.32	0.38±0.32	0.39±0.37	-0.0963 (0.2832)
	r_y	0.22±0.19	0.18±0.11	0.21±0.19	-0.0873 (0.3308)
	r_z	0.21±0.22	0.25±0.20	0.17±0.17	-0.1212 (0.1765)
Mean FD (mm), before scrubbing		0.21±0.12	0.25±0.12	0.16±0.09	-0.1711 (0.0555)
Mean FD (mm), after scrubbing		0.17±0.07	0.19±0.06	0.13±0.05	-0.1396 (0.1190)

A.2. Supplementary material for section 3.2

Table A.5 – PS+ vs. PS- first correlation component: Table of clusters in brain salience pattern (see figure 3.8C).

Cluster	cluster size (voxels)	Max	AAL Regions (% of Cluster)
1	980	5.5996	Cingulum Mid L (40.00) Cingulum Mid R (27.24)
2	356	4.8309	Precuneus L (41.57) Parietal Inf L (27.25)
3	291	4.4196	Postcentral L (51.20)
4	260	4.1516	Postcentral L (61.15)
5	239	-4.7206	Temporal Inf R (61.51)
6	174	-4.9847	Frontal Mid Orb R (72.41)
7	162	4.1728	Insula R (58.64)
8	154	4.1949	Postcentral R (86.36)
9	145	4.5537	Frontal Sup R (46.90) Supp Motor Area R (32.41)
10	134	-3.8843	Parietal Inf R (46.27) Angular R (46.27)
11	133	3.7223	Parietal Sup R (66.92)
12	124	4.5115	Insula L (70.97)
13	123	-5.0961	Frontal Inf Oper R (48.78) Rolandic Oper R (36.59)
14	123	3.3118	Postcentral R (82.93)
15	121	-4.7685	Precentral L (48.76) Frontal Inf Oper L (33.06)
16	115	3.8668	Temporal Sup L (77.39)
17	105	4.0302	Caudate R (57.14)

Appendix A. Supplementary material for chapter 3

Table A.6 – PS+ vs. PS- second correlation component: Table of clusters in brain salience pattern (see figure 3.9C).

Cluster	cluster size (voxels)	Max	AAL Regions (% of Cluster)
1	2390	5.6646	Occipital Mid L (24.98) Occipital Sup R (14.94) Occipital Mid R (12.89)
2	629	-4.9480	Frontal Mid L (34.02) Frontal Inf Tri L (17.17)
3	283	-5.4507	Frontal Sup L (37.46) Supp Motor Area L (31.80)
4	118	3.7825	Parietal Inf L (68.64)
5	114	-4.9117	Supp Motor Area R (57.89)
6	112	-4.3542	Temporal Sup R (100.00)
7	102	-6.3650	Supp Motor Area R (66.67)
8	98	4.2737	Fusiform L (69.39)

A.2. Supplementary material for section 3.2

Table A.7 – 22q11DS vs. HC first correlation component: Table of clusters in brain salience pattern (see figure 3.10C).

Cluster	cluster size (voxels)	Max	AAL Regions (% of Cluster)
1	2944	-8.4020	Temporal Inf L (21.81) Temporal Mid L (15.05) Temporal Pole Sup L (11.55) Insula L (9.78)
2	1855	-10.9609	Temporal Sup R (15.36) Temporal Pole Sup R (13.42) Caudate R (12.78) Insula R (11.70)
3	1616	7.3895	Precuneus R (20.05) Calcarine L (19.25) Calcarine R (17.57)
4	1141	5.4858	Frontal Mid R (40.14) Frontal Mid Orb R (28.66)
5	951	-5.3670	Paracentral Lobule L (22.92) Precuneus L (19.03) Supp Motor Area L (15.98)
6	854	6.6592	Parietal Inf R (43.33) Temporal Mid R (25.29)
7	688	6.5589	Parietal Inf L (69.04)
8	499	-4.5475	Temporal Inf R (45.49) Hippocampus R (22.85)
9	403	-4.6535	Occipital Mid L (45.66) Occipital Inf L (30.52)
10	379	5.8835	Frontal Mid Orb L (51.45)
11	304	4.5216	Frontal Sup Medial L (50.99)
12	293	4.5203	Precentral L (54.61)
13	284	-5.4070	Thalamus L (96.83)
14	283	7.7556	Cingulum Mid R (34.28) Cingulum Post L (22.61)
15	275	-5.7140	Supp Motor Area R (70.18)
16	258	4.9003	Frontal Mid R (46.51) Frontal Inf Oper R (29.46)
17	250	5.7538	Thalamus R (95.20)
18	235	4.6995	Occipital Mid R (59.15)
19	201	4.6118	Cingulum Ant R (37.81) Frontal Sup Orb Medial L (26.37)
20	139	-3.8166	Postcentral R (58.27)
21	131	-5.2702	Occipital Sup L (53.44)
22	127	4.8752	Frontal Mid L (54.33)
23	118	4.5912	Temporal Mid L (100.00)
24	111	4.1011	Frontal Mid L (59.46)
25	110	3.6418	Occipital Mid L (69.09)
26	108	-4.1782	Putamen R (100.00)
27	106	-4.7828	Occipital Sup R (66.04)

Appendix A. Supplementary material for chapter 3

Table A.8 – 22q11DS vs. HC second correlation component: Table of clusters in brain salience pattern (see figure 3.11C).

Cluster	cluster size (voxels)	Max	AAL Regions (% of Cluster)
1	3048	5.9324	Frontal Mid L (18.18) Supp Motor Area L (13.32) Supp Motor Area R (11.88) Frontal Sup L (10.66)
2	408	4.0058	Parietal Inf L (67.16)
3	380	-4.6755	Temporal Inf R (58.95)
4	347	-5.0529	Caudate L (17.58) Frontal Sup Orb L (15.27) Rectus L (14.41) Rectus R (12.39)
5	226	4.3457	Temporal Sup R (61.95)
6	218	-3.8788	Occipital Mid R (54.13)
7	207	-5.3421	Fusiform L (43.48) ParaHippocampal L (31.88)
8	199	-4.7324	Temporal Inf L (79.40)
9	199	-4.3567	Frontal Inf Oper L (33.17) Precentral L (29.65)
10	123	-4.9940	Frontal Inf Oper R (35.77) Rolandic Oper R (33.33)
11	123	-4.7006	Frontal Mid L (93.50)
12	119	-5.0014	Putamen R (70.59)
13	115	-5.0571	Fusiform R (52.17)
14	114	-3.9913	Cuneus L (52.63)
15	102	-3.9348	Occipital Mid L (100.00)
16	101	-3.8270	Amygdala R (53.47)
17	97	3.6622	Postcentral R (64.95)

B Supplementary material for chapter 4

B.1 Supplementary material for section 4.1

B.1.1 Supplementary tables

Table B.1 – Across noise levels and simulated transient numbers, RMSE (mean and standard deviation across 10 repetitions) between z-scored ground truth and fitted time courses with unconstrained (top values) or transient-informed (bottom values) regression. In each case, the better estimate is highlighted in bold.

RMSE		SNR					
		no noise	10 dB	5 dB	0 dB	-5 dB	-10 dB
Poisson parameter of simulated transients	<i>realistic</i>	0.79±0.03	0.79±0.03	0.79±0.03	0.79±0.03	0.79±0.02	0.79±0.02
		0.00±0.00	0.00±0.00	0.01±0.00	0.01±0.00	0.02±0.00	0.04±0.00
	20	0.80±0.03	0.80±0.03	0.80±0.03	0.80±0.03	0.80±0.03	0.80±0.03
		0.00±0.00	0.00±0.00	0.00±0.00	0.01±0.00	0.01±0.00	0.03±0.00
	15	0.79±0.03	0.79±0.03	0.79±0.03	0.79±0.03	0.79±0.03	0.79±0.03
		0.00±0.00	0.00±0.00	0.01±0.00	0.01±0.00	0.02±0.00	0.03±0.00
	10	0.77±0.04	0.77±0.04	0.77±0.04	0.77±0.04	0.77±0.04	0.77±0.04
		0.00±0.00	0.00±0.00	0.01±0.00	0.01±0.00	0.02±0.00	0.04±0.00
	5	0.78±0.02	0.78±0.02	0.78±0.02	0.78±0.02	0.78±0.02	0.78±0.02
		0.00±0.00	0.01±0.00	0.01±0.00	0.02±0.00	0.03±0.00	0.06±0.00

Appendix B. Supplementary material for chapter 4

Table B.2 – Across noise levels and simulated transient numbers, average temporal overlap in simulated ground truth and estimated time courses (mean and standard deviation across 10 repetitions) with unconstrained (top values) or transient-informed (bottom values) regression. In each case, the better estimate is highlighted in bold.

average number of co-active iCAPs		SNR						
		ground truth	no noise	10 dB	5 dB	0 dB	-5 dB	-10 dB
Poisson parameter of simulated transients	<i>realistic</i>	5.63±0.39	1.23±0.22 5.63±0.39	1.24±0.22 5.60±0.38	1.24±0.22 5.65±0.38	1.24±0.22 5.63±0.39	1.24±0.22 5.65±0.41	1.23±0.21 5.58±0.43
	20	5.87±0.50	1.35±0.23 5.87±0.50	1.36±0.23 5.89±0.47	1.36±0.23 5.88±0.51	1.36±0.24 5.88±0.49	1.37±0.24 5.89±0.49	1.37±0.24 5.93±0.48
	15	5.98±0.57	1.41±0.21 5.98±0.57	1.41±0.21 5.99±0.56	1.41±0.21 5.96±0.55	1.41±0.21 5.98±0.57	1.41±0.22 5.96±0.57	1.42±0.23 5.96±0.53
	10	5.67±0.41	1.44±0.23 5.67±0.41	1.44±0.22 5.67±0.42	1.44±0.23 5.67±0.42	1.44±0.23 5.67±0.39	1.43±0.22 5.67±0.44	1.42±0.22 5.61±0.32
	5	5.72±0.22	1.39±0.16 5.72±0.22	1.39±0.16 5.72±0.21	1.40±0.16 5.70±0.19	1.38±0.16 5.69±0.20	1.40±0.16 5.71±0.24	1.39±0.14 5.79±0.23

Table B.3 – Across noise levels and simulated transient numbers, average percentage of iCAPs appearances with the same activation sign in simulated ground truth and estimated time courses (mean and standard deviation across 10 repetitions) with unconstrained (top values) or transient-informed (bottom values) regression. In each case, the better estimate is highlighted in bold.

percentage of co-activations with same sign			SNR					
		ground truth	no noise	10 dB	5 dB	0 dB	-5 dB	-10 dB
Poisson paramete- r of simu- lated trans- ients	<i>realistic</i>	52.73±3.62	99.00±1.40 52.73±3.62	98.99±1.40 52.66±3.69	99.01±1.40 53.04±3.53	98.99±1.46 52.92±3.59	98.89±1.48 53.08±3.43	99.52±0.87 52.77±3.68
	20	54.99±3.80	99.77±0.57 54.99±3.80	99.77±0.57 54.74±4.01	99.77±0.57 54.94±3.80	99.79±0.51 55.01±3.43	99.79±0.50 54.92±3.80	99.71±0.54 55.34±3.53
	15	54.92±2.44	99.47±1.07 54.92±2.44	99.49±1.00 54.95±2.33	99.50±0.98 54.86±2.42	99.40±1.02 54.72±2.32	99.49±1.03 54.98±2.55	99.62±0.71 54.94±2.68
	10	53.53±2.84	99.33±1.36 53.53±2.84	99.33±1.36 53.48±3.01	99.34±1.35 53.35±2.70	99.35±1.24 53.45±2.68	99.25±1.06 53.31±2.75	99.68±0.68 53.22±3.11
	5	52.96±1.72	99.70±0.47 52.96±1.72	99.74±0.47 52.99±1.78	99.70±0.49 52.67±1.35	99.66±0.47 52.94±1.86	99.79±0.42 52.95±1.69	99.71±0.49 52.69±1.40

B.1.2 Supplementary figures

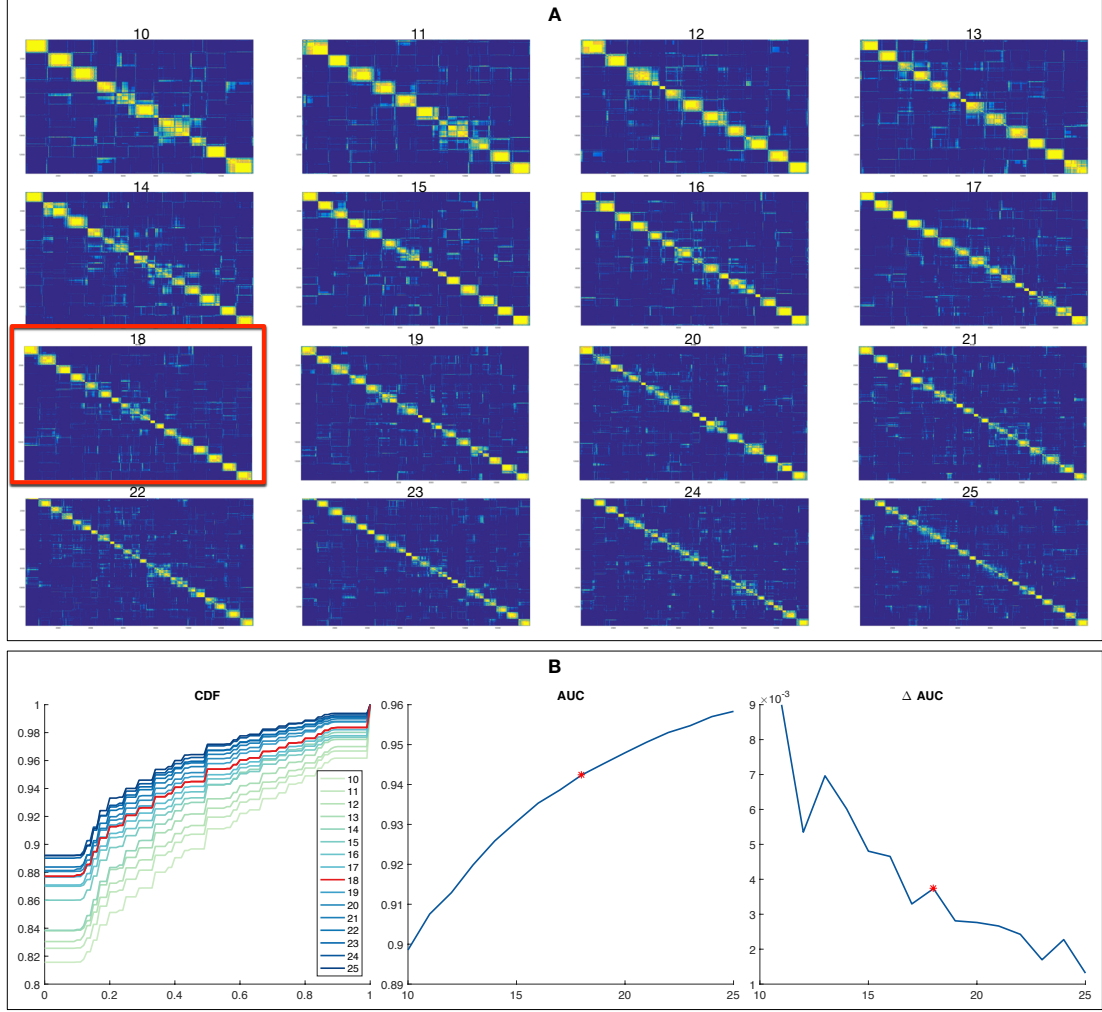


Figure B.1 – Results from consensus clustering for cluster numbers K from 10 to 25. A) Ordered consensus matrices \mathcal{M} . The consensus matrix for $K = 18$ shows the sharpest separation between values close to one on the diagonal and values close to zero on the off-diagonal of the matrix. B) CDF for tested cluster numbers K , AUC of CDF for each K and successive difference in the AUC with increasing K . The optimum number of clusters, at which the CDF has the most horizontal shape, was $K = 18$.

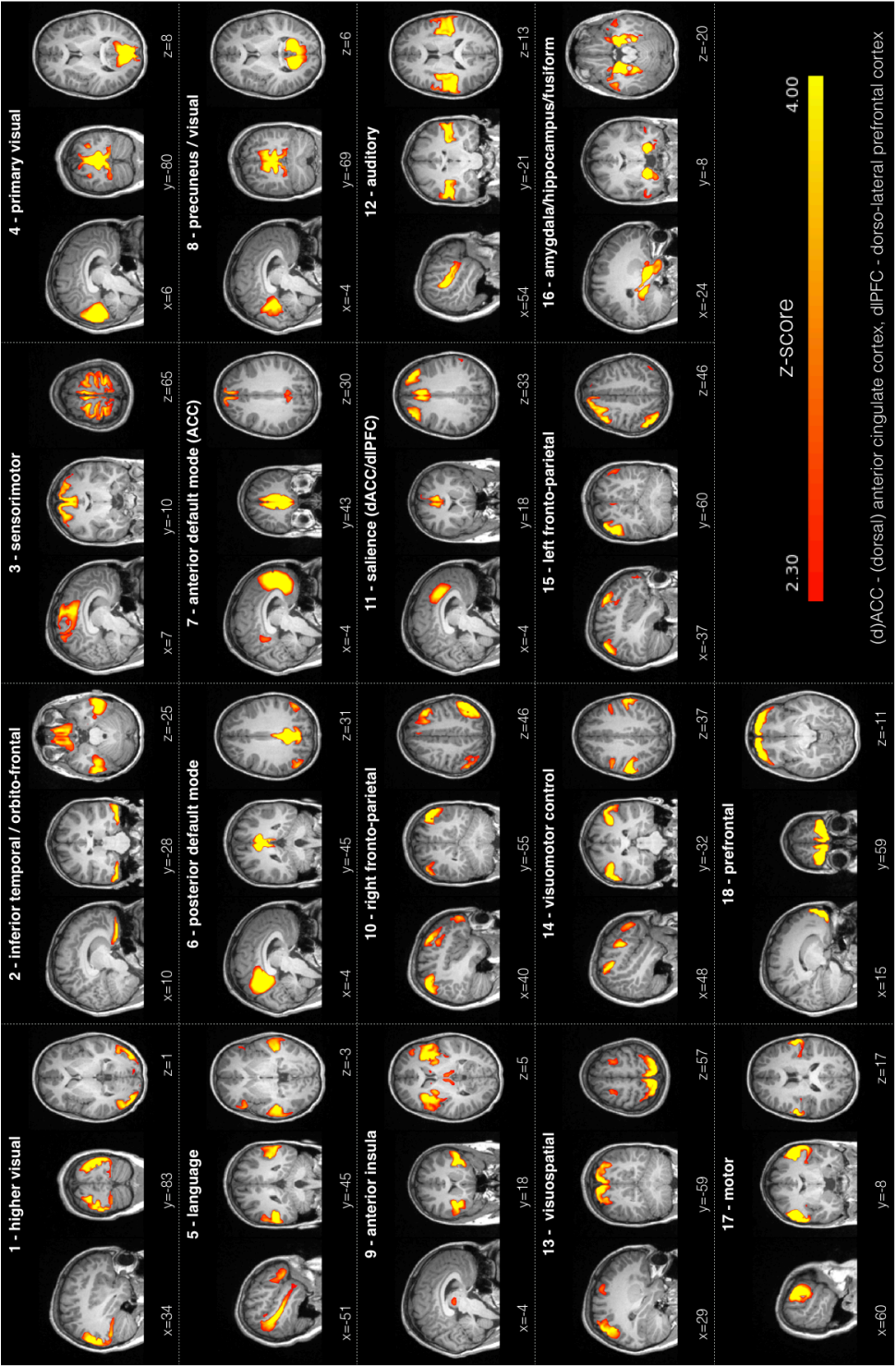


Figure B.2 – Spatial iCAPs maps $\tilde{\mathbf{M}}$ retrieved from K-means clustering (K=18). Maps are shown for z-scores > 2.3, coordinates indicate the cursor location of the shown orthogonal view.

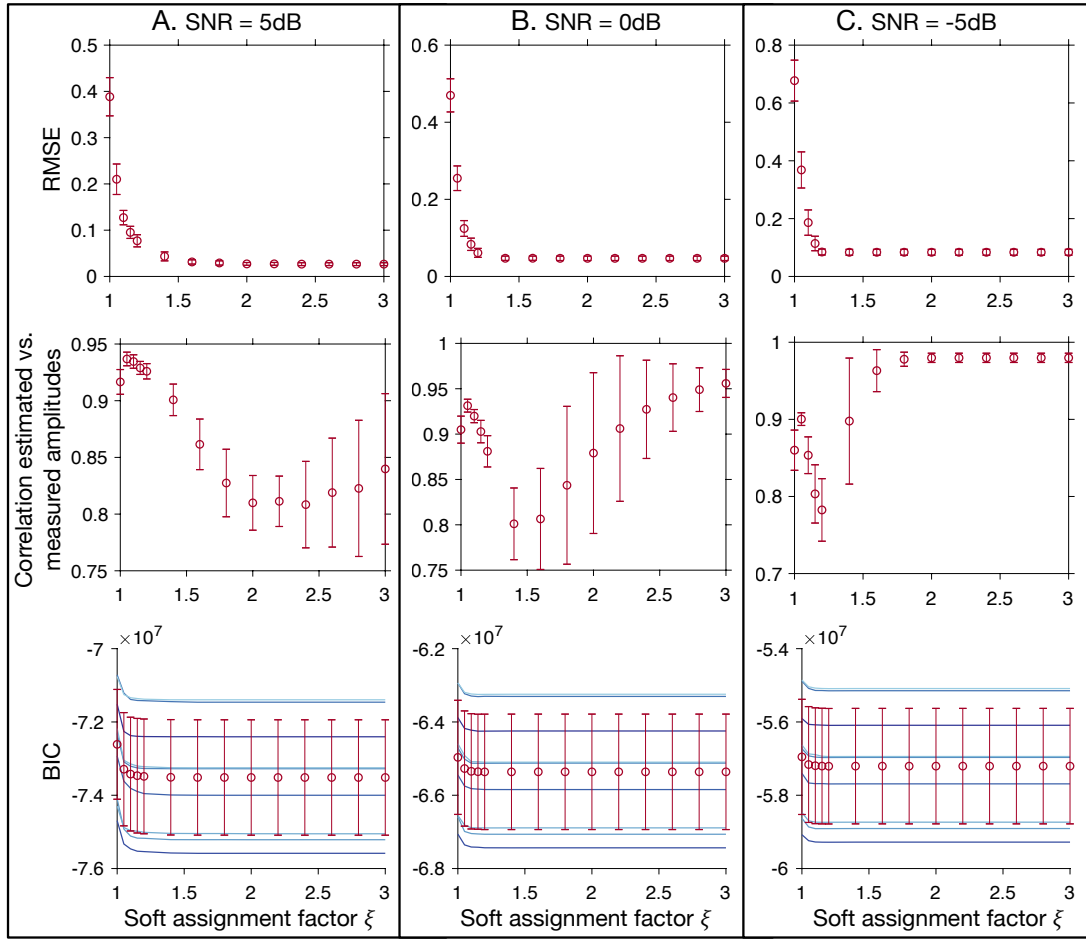


Figure B.3 – Evaluation of soft assignment factors ξ on simulated time courses with realistic Poisson constants and a) SNR=5 dB, b) SNR=0 dB and c) SNR=-5 dB. Error bars indicate mean and standard deviation for 10 repetitions of the simulations. BIC graphs show the BIC for each repetition in blue color. It can be seen that the RMSE (first line) is converging very fast for all SNR values, with a knee point at $\xi = 1.1$ for all SNR. Correlation curves (second line) all show the same shape as also observed in experimental data (see subsection IV.D and Fig. 6 of the main text), with a local maximum at around $\xi = 1.05$. The local minimum before increasing correlations that indicate strong overfitting depends on the noise level and also varies across multiple repetitions (large error bars). BIC curves (third line) show high variability between repetitions, but all have their knee point at the same value of $\xi = 1.05$. In summary, these results show that both correlation and BIC are valid criteria that properly estimate the best fit, which here was evaluated on ground truth by computing the RMSE.

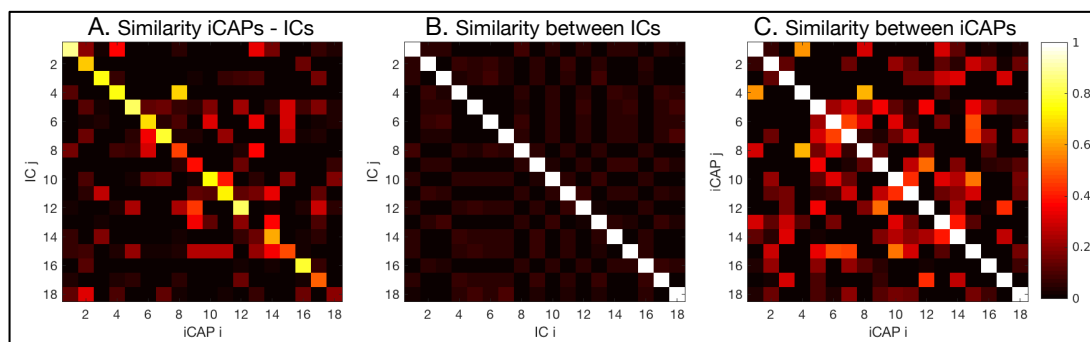


Figure B.4 – In order to demonstrate differences between iCAPs and ICA, the to date probably most commonly used approach for the analysis of networked brain activity, we applied repeated ICA (ICASSO) to our dataset and matched the 18 retrieved stable independent components (ICs) to the iCAPs with the Hungarian algorithm. A) iCAPs and ICs are very similar. B) However, since ICA is based on a criterion of independence, ICs are not correlated between themselves. C) In contrast, many iCAPs are spatially correlated.

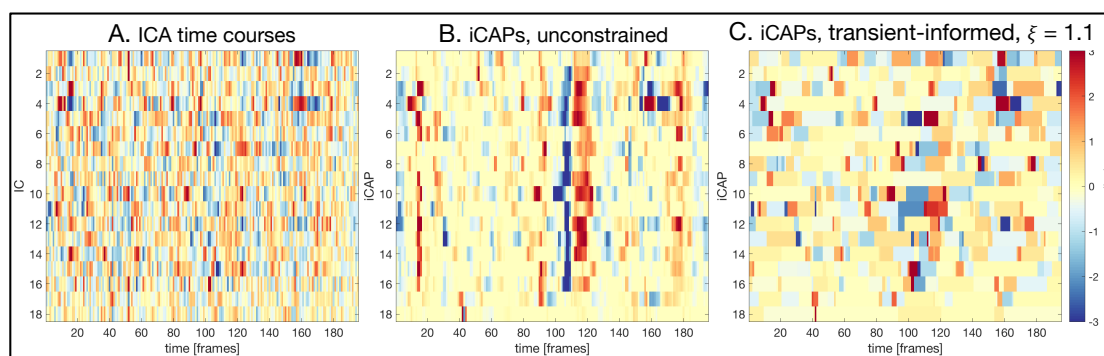


Figure B.5 – Network time courses of ICs shown in Fig. B.4 for one typical subject. A) ICA time courses are very variable and do not present the clear activation block that can be observed in iCAPs with unconstrained regression (B) or with transient-informed regression (C).

B.1.3 Supplementary results**Experimental data: effects of age and gender**

In order to test whether properties of iCAPs may be relevant for development, we computed activation and co-activation of all iCAPs for transient-informed regression with $\xi = 1.1$ and tested for effects of age and gender. Motion was included as covariate and reported p-values were Bonferroni-corrected for the 18 comparisons.

There were no significant gender differences in the total duration of any network. To test for effects of age, we fitted a linear model including age, gender and their interaction to model the total activity time of each iCAP. The duration of iCAP 4 (primary visual) increased with age ($p=0.006$), while the activation time of iCAP 16 (amygdala/hippocampus/fusiform) was lower in older subjects ($p=0.038$). We further tested for age effects in the co-activation of these two iCAPs with other networks and found a significant positive age relationship of same-signed co-activation between iCAPs 4 and 5 (language network, $p=0.047$) and iCAPs 4 and 11 (salience network, $p=0.032$). Differently-signed co-activation between iCAPs 4 and 1 (higher visual) also showed a positive age relationship ($p=0.043$). There were no age effects in the co-activation between iCAP 16 and any other network. Supplementary Fig. S6 shows scatter plots of the above-mentioned significant correlations.

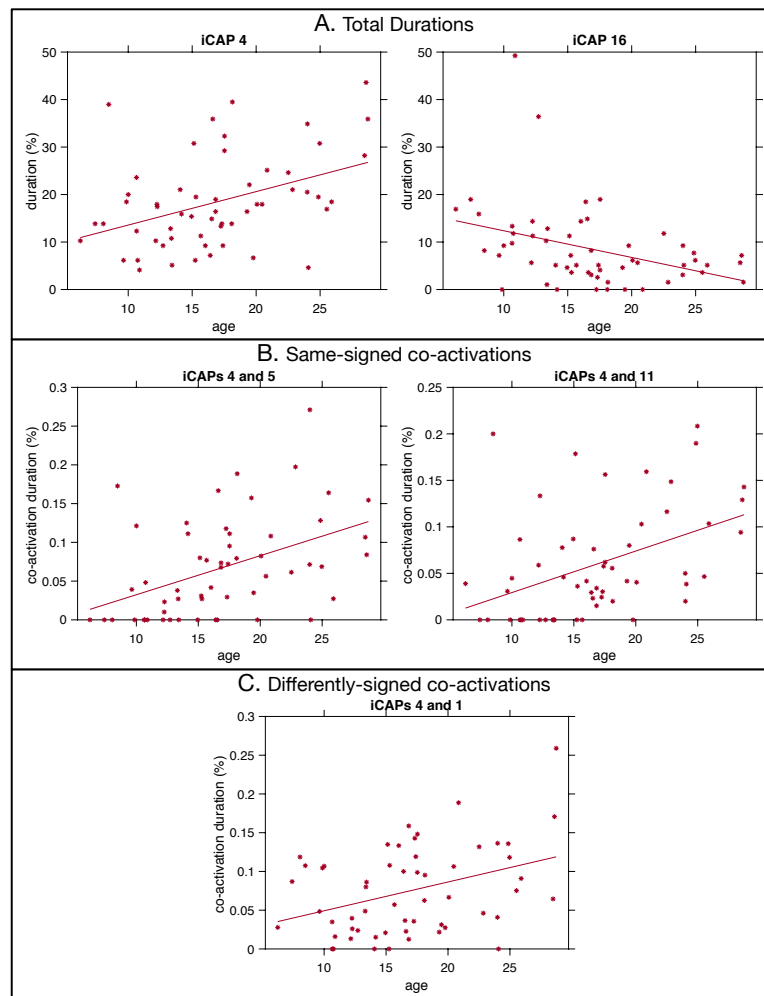


Figure B.6 – Age relationship of iCAPs duration and co-activation. A) Activation duration in percent of total scanning time was significantly correlated with age for iCAP 4 ($p=0.006$) and iCAP 16 ($p=0.038$). B) Same-signed co-activation (in percent of total duration of both iCAPs) of iCAP 4 with iCAP 5 ($p=0.047$) and with iCAP 11 ($p=0.032$) was significantly correlated with age. C) Differently-signed co-activation of iCAP 4 with iCAP 1 was also positively correlated with age ($p=0.043$). Motion, gender and their interaction were included as covariate and reported p -values were Bonferroni-corrected for the 18 comparisons.

B.2 Supplementary material for section 4.2

B.2.1 Supplementary methods

Participant exclusion criteria

From the initial sample of 221 subjects between 8 and 30 years old, we had to exclude 33 patients and 25 controls to ensure good data quality. One control and one patient were excluded from the study because they reported having fallen asleep during the resting-state scan. Another 4 subjects (3 patients) were excluded due to high motion in the anatomical T1-weighted scan, 23 subjects (15 patients) were excluded due to excessive motion of more than 3 mm in translation or 3° in rotation in the resting-state fMRI scans and scans of another 19 subjects (7 patients) were not used because part of the cortex were not captured. Finally, 10 more subjects (7 patients) were excluded from the remaining sample after motion scrubbing (Power et al., 2012) because less than 5 min of scanning time was remaining after censoring of frames with a framewise displacement higher than 0.5 mm. Motion data of the two groups is summarized in Supplementary Table B.4.

Overlapping samples

The cohort is partly overlapping with our previous resting-state fMRI studies: 31 subjects (16 patients) have been also included in Debbané et al. (2012), 57 subjects (24 patients) in Scariati et al. (2014), 62 subjects (27 patients) in Padula et al. (2015), 59 subjects (26 patients) in Scariati et al. (2016b), 94 subjects (41 patients) in Padula et al. (2017b), 91 subjects (43 patients) in Zöllner et al. (2017) and 111 subjects (47 patients) in Zöllner et al. (2018).

Total activation and iCAPs

The Total Activation (TA) and iCAPs framework is based on the detection of significant change-points in deconvolved fMRI time series. Matlab code for the application of the whole framework can be found at <https://www.c4science.ch/source/iCAPs>.

In the first step, TA was used for the regularized deconvolution of fMRI signals from the hemodynamic response function (HRF) (Karahanoglu et al., 2011, 2013; Farouj et al., 2017). In TA, the fMRI signal $\mathbf{y}(v)$ at voxel v is modeled as a block-like activity-inducing signal $\mathbf{a}(v)$ convolved with the HRF \mathbf{h} and additive white Gaussian noise $\epsilon(v)$:

$$\mathbf{y}(v) = (\mathbf{a} \star \mathbf{h})(v) + \epsilon = \mathbf{x}(v) + \epsilon$$

Then the activity-related signal matrix \mathbf{X} can be recovered by spatio-temporal regularization as follows:

$$\tilde{\mathbf{X}} = \arg \min_{\mathbf{X}} \frac{1}{2} \|\mathbf{Y} - \mathbf{X}\|_F^2 + \mathcal{R}_T(\mathbf{X}) + \mathcal{R}_S(\mathbf{X}),$$

with the temporal regularization term

$$\mathcal{R}_T(\mathbf{X}) = \sum_{v=1}^{N_v} \lambda_T(v) \sum_{t=1}^{N_t} |\Delta_L\{\mathbf{x}(v, \cdot)\}[t]|,$$

and the spatial regularization term

$$\mathcal{R}_S(\mathbf{X}) = \lambda_S \sum_{t=1}^{N_t} \sum_{v=1}^{N_v} \sqrt{\sum_{u \in \mathcal{S}(v)} (x(v, t) - x(u, t))^2}.$$

Here, $\|\cdot\|_F^2$ designates the Frobenius norm, N_v is the number of voxels, N_t is the number of time points, λ_T is the temporal regularization parameter, λ_S is the spatial regularization parameter, $\Delta_L = \Delta_D H^{-1}$ is a differential operator combining derivative Δ_D and HRF deconvolution H^{-1} and $\mathcal{S}(v)$ is the neighborhood of voxel v .

After this regularized deconvolution from the HRF, innovation signals \mathbf{i} were computed as the temporal derivative of the activity-inducing signals \mathbf{a} and significant innovations were determined by a two-step thresholding procedure (Karahanoglu et al., 2015). First, a surrogate innovation distribution was computed at every voxel, and innovations larger than 95 % and lower than 5 % of the surrogate distribution were considered significant. Second, an innovation frame was considered significant, if there was a significant innovation in at least 5 % of the gray matter voxels.

Then, K-mean clustering was applied to the significant innovation frames, resulting in K spatial maps, the iCAPs. We used consensus clustering (Monti et al., 2003) to determine the optimum number of clusters.

Finally, iCAPs time courses were computed by transient-informed spatio-temporal back-projection of the spatial maps onto the activity-inducing signals (Zöller et al., 2019b). As spatial dependence of the iCAPs maps is possible, transient-informed regression is necessary to robustly recover temporal overlap in the iCAPs time courses. In the back-projection, transients in each iCAP's time course are restricted to frames with an innovation pattern that is close to the iCAP's spatial pattern (i.e., the cosine distance $d(t)$ between the innovation frame at time t and the iCAP's spatial map has to respect $d(t) \leq \xi d_{min}(t)$ with $d_{min}(t)$ being the minimum distance of that innovation frame to any of the K iCAPs). Then the activation segments β between two iCAP transients can be found for all iCAPs simultaneously by the following linear regression

$$\tilde{\beta} = \underset{\beta}{\operatorname{argmin}} \|\mathbf{A}_C - \mathbf{S}\beta\|^2,$$

with the spatio-temporally concatenated activity-inducing signals \mathbf{A}_C , and the design matrix $\mathbf{S} = [\mathbf{S}_1 | \dots | \mathbf{S}_K]$ containing one regressor with the repeated spatial iCAP map per activation segment β . Based on the Bayesian Information Criterion, in our data the optimum tuning parameter was $\xi = 1.3$. For a more detailed discussion of this transient-informed regression scheme, please refer to (Zöller et al., 2019b).

Partial least squares correlation

Partial Least Squares Correlation (PLSC) is a well-suited method for the investigation of multi-variate relationships between behavioral measures and brain activation data (Krishnan et al., 2011; McIntosh and Lobaugh, 2004). Here, we used so-called behavior PLSC to probe into relationships between demographic or clinical variables (i.e., age or psychotic symptoms/anx-

iety) and temporal properties of iCAPs (i.e., activation duration and coupling time). In the following we outline the steps of PLSC analysis. Variable annotations are used according to (Krishnan et al., 2011). For a more detailed discussion of PLSC analysis, we refer to (Krishnan et al., 2011; McIntosh and Lobaugh, 2004).

The first step in PLSC is the computation of group-wise correlation matrices $\mathbf{R}_{\text{HC}} = \mathbf{Y}_{\text{HC}}^T \mathbf{X}_{\text{HC}} \in \mathbb{R}^{N_{\text{behav}} \times N_{\text{iCAPs}}}$ between brain network properties $\mathbf{X}_{\text{HC}} \in \mathbb{R}^{N_{\text{HC}} \times N_{\text{iCAPs}}}$ and behavioral variables $\mathbf{Y}_{\text{HC}} \in \mathbb{R}^{N_{\text{HC}} \times N_{\text{behav}}}$ of HCs and $\mathbf{R}_{22\text{q}} = \mathbf{Y}_{22\text{q}}^T \mathbf{X}_{22\text{q}} \in \mathbb{R}^{N_{\text{behav}} \times N_{\text{iCAPs}}}$ between brain network properties $\mathbf{X}_{22\text{q}} \in \mathbb{R}^{N_{22\text{q}} \times N_{\text{iCAPs}}}$ and behavioral variables $\mathbf{Y}_{22\text{q}} \in \mathbb{R}^{N_{22\text{q}} \times N_{\text{behav}}}$ of patients with 22q11DS. $N_{22\text{q}}$ is the number of patients with 22q11DS, N_{HC} is the number of HCs, N_{iCAPs} is the number of included iCAPs measures and N_{behav} is the number of included behavioral variables. $\mathbf{X}_{22\text{q}}$, \mathbf{X}_{HC} , $\mathbf{Y}_{22\text{q}}$ and \mathbf{Y}_{HC} were z-scored across subjects before calculation of $\mathbf{R}_{22\text{q}}$ and \mathbf{R}_{HC} .

The common correlation matrix \mathbf{R} is then computed by concatenating \mathbf{R}_{HC} and $\mathbf{R}_{22\text{q}}$:

$$\mathbf{R} = \begin{bmatrix} \mathbf{R}_{\text{HC}} \\ \mathbf{R}_{22\text{q}} \end{bmatrix} = \begin{bmatrix} \mathbf{Y}_{\text{HC}}^T \mathbf{X}_{\text{HC}} \\ \mathbf{Y}_{22\text{q}}^T \mathbf{X}_{22\text{q}} \end{bmatrix} \in \mathbb{R}^{2N_{\text{behav}} \times N_{\text{iCAPs}}}.$$

Finally, \mathbf{R} is decomposed into $2N_{\text{behav}}$ latent variables, or “correlation components”, using singular value composition $\mathbf{R} = \mathbf{USV}^T$. Each correlation component has a singular value (on the diagonal of \mathbf{S}) that specifies the explained correlation, as well as $2N_{\text{behav}}$ behavior saliences, or “behavior weights” (columns of \mathbf{U}), and N_{iCAPs} duration/coupling saliences, or “duration/coupling weights” (rows of \mathbf{V}^T). Behavior and brain weights indicate how strongly each variable contributes to the multivariate behavior-brain correlation in a certain correlation component. They lie between -1 and 1 and – because we normalized the data before computation of \mathbf{R}_{HC} and $\mathbf{R}_{22\text{q}}$ – can be interpreted similarly to correlation values. From the brain weights in \mathbf{V} , so called “brain scores” can be computed by projecting every subject’s brain activation data onto the respective brain weights with $\mathbf{L}_X = \mathbf{XV}$.

We used permutation testing with 1000 permutations to evaluate if any of the correlation components was significant and bootstrapping with 500 bootstrap samples to evaluate the stability of the behavior and brain weights. Significant PLSC results are reported in terms of bootstrapping mean and standard deviations.

B.2.2 Supplementary results & discussion

Relationship between age and duration of iCAPs' activation

To assess the association between age and duration of iCAPs' activation we conducted Partial Least Squares Correlation (PLSC; Krishnan et al., 2011) – a technique that provides multivariate association between variables (see Methods and Materials and Supplementary Methods). We conducted PLSC with age as behavioral variable and duration of the nine altered iCAPs (Figure 4.10) as brain variables. There was one significant correlation component ($p=0.04$) showing an opposite age-effect in HCs and patients with 22q11DS (age-weights: -0.44 ± 0.2 in HCs, 0.89 ± 0.21 in 22q11DS, see Supplementary Figure B.9). In three networks (dACC/dlPFC - 5, PrimVIS2 - 8, FPN - 9), we found declining duration with age in patients with 22q11DS, but increasing duration with age in HCs. These three iCAPs had also globally shorter activation in 22q11DS. Contrarily, two networks (iTEMP/FUS - 14, AMY/HIP - 15) had increasing duration with age in 22q11DS and declining duration with age in HCs. Both of these networks had also globally longer activation in 22q11DS. Together, these results suggest that the alterations in these five networks are emerging over age in patients with 22q11DS.

Comparison of iCAPs activation with static functional connectivity

While iCAPs themselves were retrieved from a purely dynamic measure (i.e., the innovations), the measure of coupling duration between networks is closely linked to static functional connectivity (sFC).

In order to compare our results on dynamic network activity with a conventional static approach, we conducted a supplementary sFC analysis. We computed regional averages from the preprocessed BOLD signals within each iCAP's spatial map, thresholded at a spatial z-score of 2.3. We then computed partial correlations between all pairs of iCAPs and compared the correlations between patients with 22q11DS and HCs. The results are shown in Supplementary Figure B.12B.

As expected, alterations in couplings are related to aberrant sFC (see Supplementary Figure B.12). However, while there are indeed similarities, the results are not identical, which is most likely due to the deconvolution, denoising and reconstruction of block-like time courses conducted before computing coupling duration. Further, it is of note that with conventional sFC, it is impossible to detect alterations in both coupling and anti-coupling (such as we observe for iCAPs 5 and 3), as the correlation per definition only goes in one direction.

No such direct comparison was possible for activation duration, as it is a measure specific to each network, which cannot be explained in terms of static connectivity.

BOLD signal analysis and motion

As in any fMRI study, we cannot exclude that the measured effects may have been influenced by non- neural confounds, such as heartbeat, respiration and motion (Power et al., 2014). For the current study, we addressed this issue by taking typical measures during preprocessing, such as regression of WM and CSF signals, as well as motion censoring. Further, it is of note that the regularized deconvolution from the hemodynamic response function (HRF) further

minimizes such effects, as any non-neural signals, which do not follow the HRF, are filtered out by the approach. Finally, we included group-centered average framewise displacement as nuisance regressor in all analyses to further avoid any confounding effects caused by motion in particular. To explicitly investigate whether observed group differences may have been caused by motion artifacts, we compared iCAPs activation duration in HCs with high motion versus low motion (see Supplementary Figure B.11 and Supplementary Table B.10). There were no significant differences in activation duration between these two groups, which suggests that motion was indeed not a major confound in our analysis. In patients with 22q11DS scanner motion is strongly correlated with the severity of symptoms, which makes it impossible to disentangle the two effects. Therefore, this remains a limitation of our study, despite the multiple measures we took to account for non-neural confounds.

B.2.3 Supplementary figures

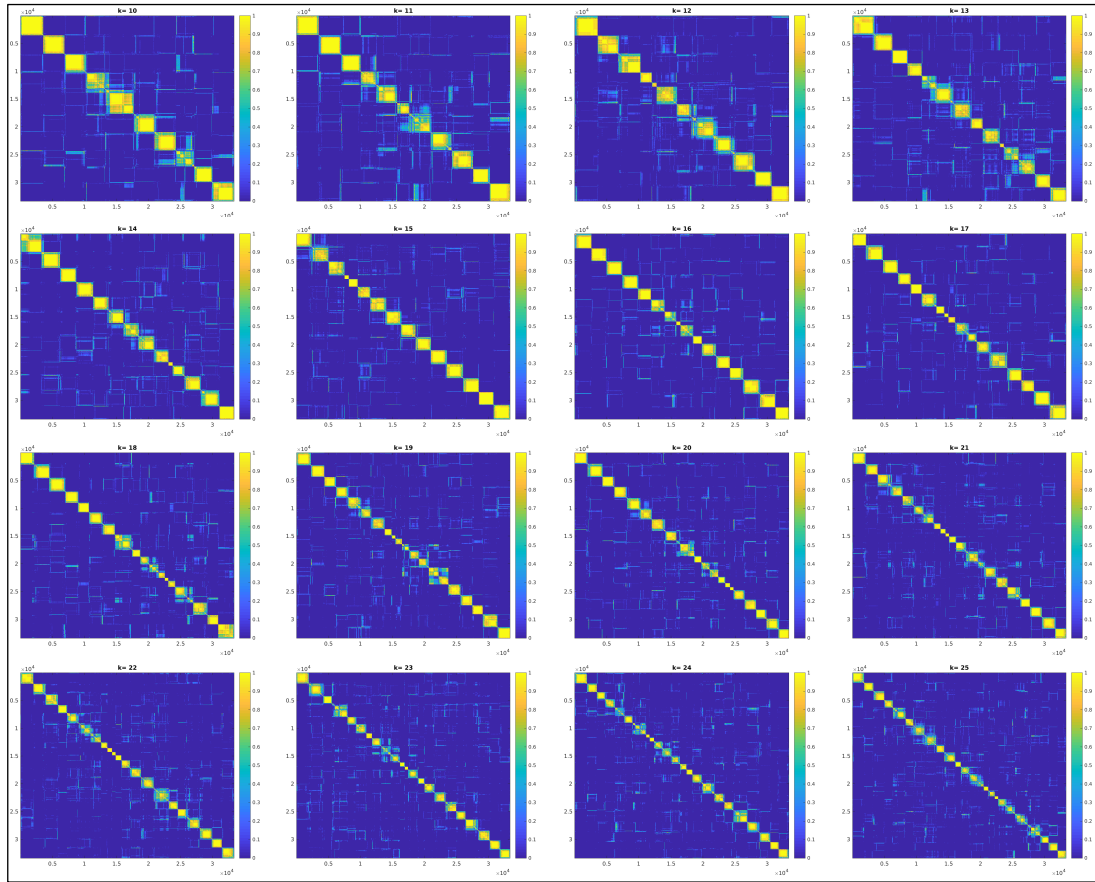


Figure B.7 – Consensus matrices for cluster numbers $K=10$ to $K=25$. The higher a value, the more often the two corresponding frames were clustered together during re-sampling. For optimum clustering, the consensus matrix should contain only zeros and ones (Monti et al., 2003). We selected to use $K = 17$ based on visual inspection of the consensus matrices and evaluation of consensus clustering quality measures (see Supplementary Figure B.8).

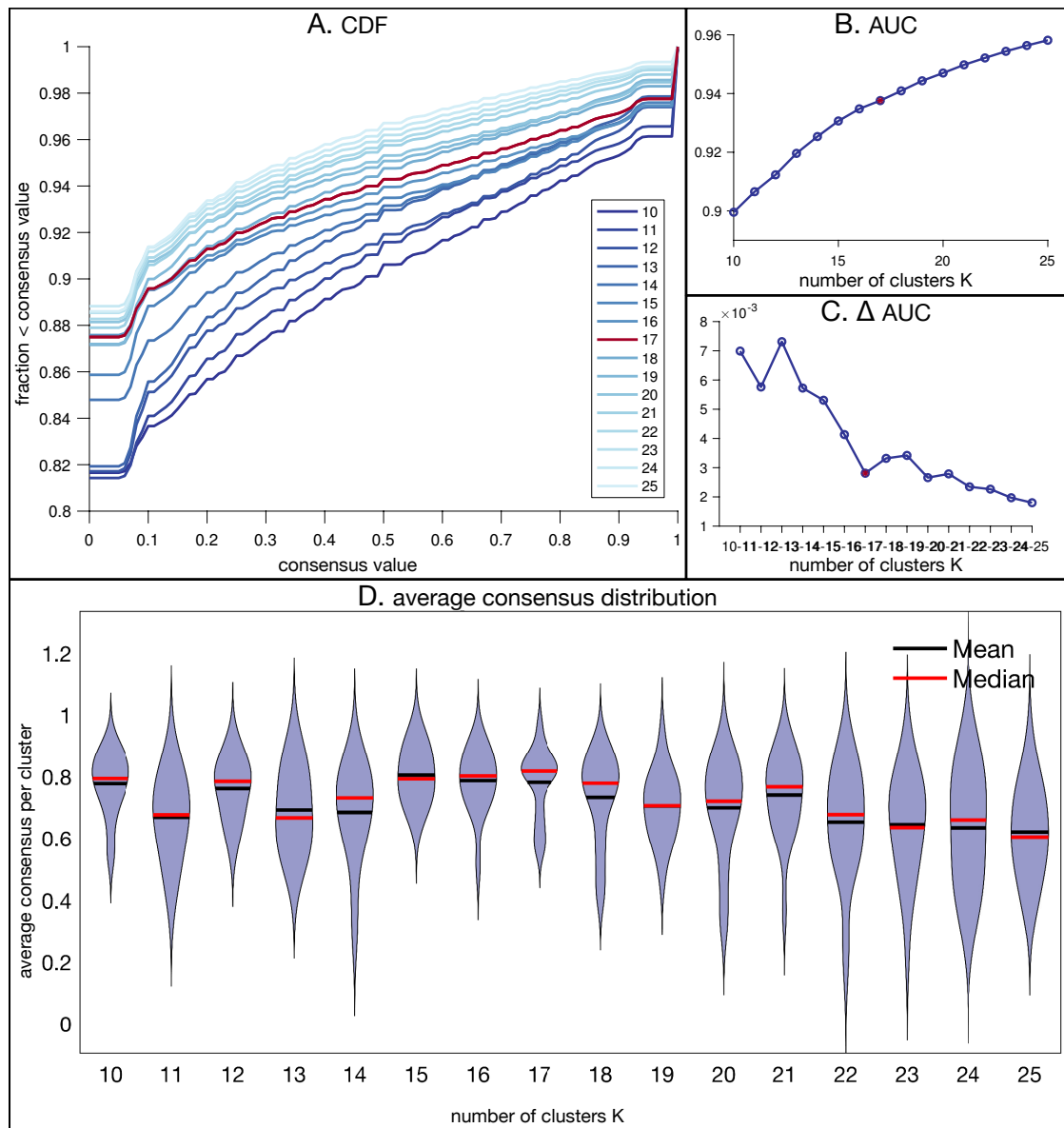


Figure B.8 – Consensus clustering quality measures for cluster numbers $K=10$ to $K=25$. A) the cumulative distribution function (CDF) of values in the respective consensus matrices (see Supplementary Figure B.7). The optimum clustering solution would have a horizontal line with only values equal to 0 (two frames are never clustered together) or 1 (two frames are always clustered together). For $K=17$, the line is flatter than for surrounding clustering values. B) Area under the CDF curve and C) increase of the area under the curve with increasing K . D) Distribution of average consensus values per cluster. Median consensus is maximal for $K=17$. We selected to use $K = 17$ based on evaluation of the consensus clustering quality measures and visual inspection of the consensus matrices.

Appendix B. Supplementary material for chapter 4

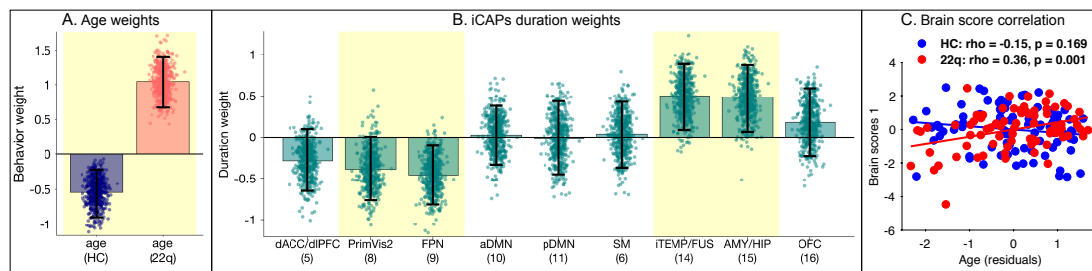


Figure B.9 – Age PLSC results ($p=0.04$). A) Age saliences indicating the strength and direction of age-relationship in HCs and patients with 22q11DS, respectively. B) iCAPs saliences indicating the strength and direction of each iCAP's duration-age-relationship. Activation of FPN (9) is shorter at higher age; activation of iTEMP/FUS (14) and AMY/HIP (15) is longer at higher age. Error bars indicate standard deviations of bootstrap distributions. C) Correlation of brain scores with age. As indicated by saliences in A, there is a positive correlation in patients with 22q11DS, and an opposite effect in HCs. Error bars indicate bootstrapping 5th to 95th percentiles, robust results were indicated by yellow background.

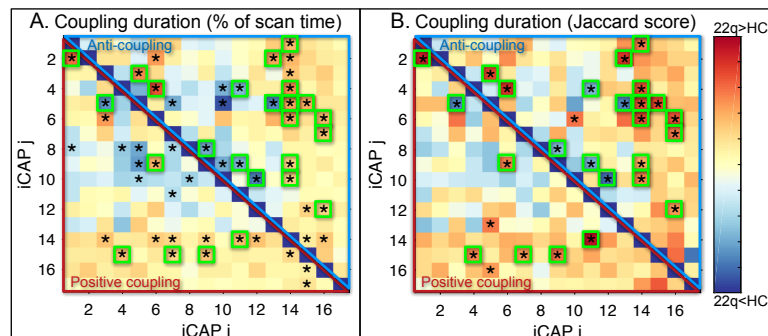


Figure B.10 – Duration differences of positive couplings (red triangles) and anti-couplings (blue triangles) between patients with 22q11DS and HCs. Corresponding test statistics (p-values, effect size) can be found in Supplementary Table B.7. A) Coupling duration measured in percentage of total scanning time. B) Coupling duration measured in percentage of the joint activation time of the two respective iCAPs (Jaccard score). Significant differences ($p < 0.05$) are marked with an asterisk (*), green boxes indicate coupling differences that are significant both in A and B. Couplings in green boxes were included in the graphical visualization in Figure 4.11 of the main manuscript. P-values are FDR-corrected for multiple comparisons and age, gender and motion were included as covariates.

B.2. Supplementary material for section 4.2

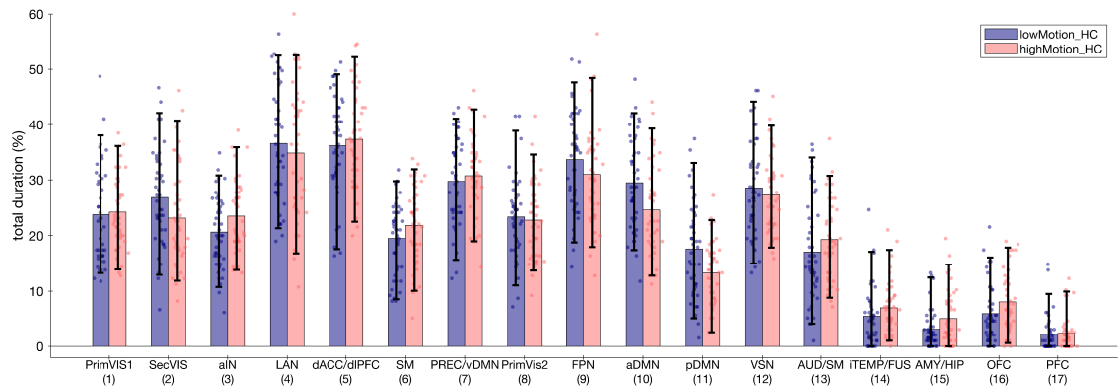


Figure B.11 – Group comparison of iCAPs' activation duration in high motion vs. low motion healthy subjects (divided by median split). There are no significant group differences between HCs with higher or lower motion. P-values are FDR-corrected for multiple comparisons and age, gender were included as covariates.

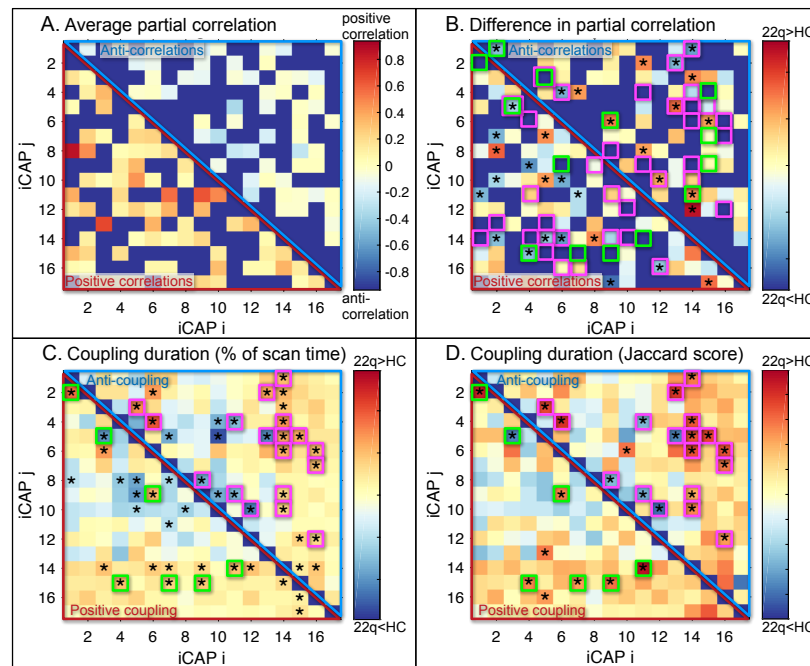


Figure B.12 – A) Average static functional connectivity (sFC) measured as partial correlations between average BOLD signals in each iCAP. The average was computed across all subjects including both patients with 22q11DS and healthy controls. B) Group differences in sFC between networks. C) Group differences in iCAPs coupling duration measured as percentage of total scan time. D) Group differences in iCAPs coupling duration measured as percentage of joint activation time (Jaccard score). Group differences in partial correlations are partially, but not entirely the same as group differences in positive couplings (green boxes) or anti-couplings (magenta boxes). The direction of alteration, if significant, is mostly the same in static FC and couplings; i.e., lower sFC corresponds to either lower positive coupling duration or higher anti-coupling (or both; e.g., iCAPs 5 and 3); higher sFC corresponds to either higher positive coupling or lower anti-coupling.

B.2.4 Supplementary tables

Table B.4 – fMRI motion data, FD - framewise displacement

	HC	22q11DS	p-value
Mean FD (mm), before scrubbing	0.15 ± 0.06	0.22 ± 0.10	<0.001
Mean FD (mm) after scrubbing	0.13 ± 0.04	0.17 ± 0.06	<0.001
N. timepoints after scrubbing	188.22 ± 12.87	178.26 ± 19.28	<0.001

B.2. Supplementary material for section 4.2

Table B.5 – iCAPs functional networks of Greicius atlas (Shirer et al., 2012) and regions in the automated anatomical labeling (AAL) atlas (Tzourio-Mazoyer et al., 2002). Percentiles indicate the fraction of voxels of a functional network or region that have a z-score > 2.3. A network/region is listed if more than 20% of the network/region is included in the iCAP.

iCAP	Greicius network (%)	AAL Lobe	AAL Region (%)	z-score	voxels
1	Primary_Visual (81.12%)	Occipital	Calcarine_R (65.97%)	3.76	221
		Occipital	Lingual_L (65.85%)	3.62	295
		Occipital	Lingual_R (61.40%)	3.73	272
		Occipital	Calcarine_L (50.45%)	3.61	224
		Occipital	Cuneus_R (23.37%)	2.98	61
		Occipital	Cuneus_L (22.86%)	2.77	56
2	Higher_Visual (75.94%)	Occipital	Occipital_Inf_L (80.47%)	3.81	136
		Occipital	Occipital_Inf_R (77.33%)	3.46	116
		Occipital	Occipital_Mid_R (65.61%)	3.63	248
		Occipital	Occipital_Mid_L (56.79%)	3.46	318
		Occipital	Fusiform_R (38.31%)	3.25	218
		Occipital	Fusiform_L (36.94%)	3.33	208
		Occipital	Occipital_Sup_R (32.39%)	2.97	57
		Occipital	Occipital_Sup_L (22.42%)	2.83	37
		Temporal	Temporal_Inf_R (20.19%)	3.48	166
3	Auditory (60.56%) Basal_Ganglia (20.13%)	Temporal	Heschl_R (83.33%)	2.88	45
		Limbic	Insula_R (80.90%)	3.58	288
		Central	Rolandic_Oper_L (77.55%)	3.00	152
		Limbic	Insula_L (74.12%)	3.35	335
		Central	Rolandic_Oper_R (71.79%)	3.05	196
		Temporal	Heschl_L (71.67%)	2.85	43
		Subcortical	Putamen_R (54.50%)	2.91	103
		Subcortical	Putamen_L (50.00%)	2.84	81
		Temporal	Temporal_Sup_L (38.04%)	2.75	167
		Subcortical	Pallidum_L (25.00%)	2.52	5
		Frontal	Frontal_Inf_Oper_L (23.56%)	2.88	41
		Frontal	Frontal_Inf_Oper_R (21.24%)	3.27	55
4	Language (78.42%)	Temporal	Temporal_Mid_L (55.49%)	3.33	551
		Temporal	Temporal_Mid_R (39.96%)	3.13	356
		Parietal	Angular_L (39.27%)	3.09	97
		Temporal	Temporal_Sup_R (36.31%)	3.22	199
5	Anterior_Salience (52.64%)	Frontal	Frontal_Mid_R (46.60%)	3.27	432
		Frontal	Frontal_Mid_L (40.14%)	3.18	334
		Limbic	Cingulum_Ant_R (28.25%)	3.13	76
		Limbic	Cingulum_Ant_L (27.40%)	3.12	77
		Limbic	Cingulum_Mid_R (21.86%)	3.33	106
6	Sensorimotor (53.69%)	Parietal	Paracentral_Lobule_L (74.15%)	3.02	109
		Parietal	Paracentral_Lobule_R (60.19%)	2.72	62
		Frontal	Supp_Motor_Area_R (59.60%)	3.32	211
		Frontal	Supp_Motor_Area_L (51.11%)	3.37	161
		Limbic	Cingulum_Mid_L (35.56%)	3.08	144
		Parietal	Postcentral_R (35.53%)	2.79	210
		Limbic	Cingulum_Mid_R (33.81%)	3.06	164
		Frontal	Precentral_L (33.20%)	3.07	172
		Frontal	Precentral_R (30.77%)	2.93	156
		Parietal	Postcentral_L (30.69%)	2.84	174

Appendix B. Supplementary material for chapter 4

iCAP	Greicius network (%)	AAL Lobe	AAL Region (%)	mean z-score	voxels
7	Precuneus (65.04%) Ventral_DMN (38.00%)	Parietal	Precuneus_R (61.35%)	3.32	319
		Parietal	Precuneus_L (51.19%)	3.39	280
		Occipital	Occipital_Sup_R (44.32%)	3.19	78
		Parietal	Parietal_Sup_L (43.09%)	3.11	134
		Parietal	Parietal_Sup_R (41.90%)	3.07	106
		Occipital	Occipital_Sup_L (40.61%)	3.09	67
		Occipital	Cuneus_R (33.33%)	2.74	87
		Occipital	Occipital_Mid_R (28.31%)	3.00	107
		Occipital	Cuneus_L (25.71%)	2.62	63
8	Primary_Visual (93.71%) Higher_Visual (22.74%)	Occipital	Calcarine_R (70.15%)	4.32	235
		Occipital	Calcarine_L (65.32%)	4.00	290
		Occipital	Cuneus_R (54.79%)	3.33	143
		Occipital	Cuneus_L (54.29%)	3.47	133
		Occipital	Lingual_R (51.47%)	3.45	228
		Occipital	Lingual_L (49.78%)	3.37	223
		Occipital	Occipital_Sup_R (44.32%)	3.05	78
		Occipital	Occipital_Sup_L (40.61%)	3.01	67
9	Left_ECN (60.21%) Right_ECN (47.88%) Precuneus (21.68%)	Parietal	Angular_L (64.37%)	3.37	159
		Parietal	Angular_R (59.64%)	3.47	201
		Parietal	Parietal_Inf_R (42.44%)	3.65	115
		Parietal	Parietal_Inf_L (34.55%)	3.46	171
		Frontal	Frontal_Mid_L (27.40%)	2.89	228
10	Dorsal_DMN (58.75%)	Limbic	Cingulum_Ant_R (73.23%)	3.93	197
		Frontal	Frontal_Sup_Orb_Medial_L (73.11%)	4.17	87
		Limbic	Cingulum_Ant_L (69.75%)	4.23	196
		Frontal	Frontal_Sup_Orb_Medial_R (69.48%)	3.87	107
		Frontal	Frontal_Sup_Medial_L (54.95%)	3.65	211
		Frontal	Frontal_Sup_Medial_R (46.30%)	3.64	169
		Limbic	Cingulum_Post_L (35.00%)	2.62	28
		Frontal	Rectus_L (34.68%)	3.17	60
		Frontal	Rectus_R (28.47%)	3.23	39
		Limbic	Cingulum_Post_R (25.00%)	2.51	8
11	Precuneus (34.73%) Dorsal_DMN (24.30%)	Limbic	Cingulum_Post_L (97.50%)	5.47	78
		Limbic	Cingulum_Post_R (96.88%)	5.55	31
		Parietal	Angular_L (61.94%)	2.94	153
		Parietal	Precuneus_R (45.77%)	4.24	238
		Parietal	Angular_R (43.92%)	2.95	148
		Parietal	Precuneus_L (39.31%)	4.47	215
12	Visuospatial (61.54%) Posterior_Salience (26.50%)	Parietal	Parietal_Inf_R (60.89%)	3.59	165
		Parietal	Parietal_Inf_L (56.77%)	3.44	281
		Frontal	Frontal_Inf_Oper_R (43.24%)	3.01	112
		Parietal	SupraMarginal_R (33.00%)	3.33	133
		Parietal	Postcentral_R (24.37%)	3.21	144
		Parietal	SupraMarginal_L (23.36%)	3.20	57
		Frontal	Frontal_Inf_Oper_L (22.99%)	2.96	40
		Frontal	Frontal_Inf_Tri_R (20.74%)	2.56	67

B.2. Supplementary material for section 4.2

iCAP	Greicius network (%)	AAL Lobe	AAL Region (%)	mean z-score	voxels
13	Auditory (46.06%) Sensorimotor (25.59%) Posterior_Salience (20.35%)	Central	Rolandic_Oper_R (76.56%)	3.26	209
		Central	Rolandic_Oper_L (63.78%)	2.99	125
		Parietal	Postcentral_L (46.56%)	3.85	264
		Parietal	Postcentral_R (37.23%)	3.93	220
		Temporal	Heschl_R (37.04%)	2.59	20
		Parietal	SupraMarginal_R (36.97%)	3.22	149
		Parietal	SupraMarginal_L (34.02%)	3.05	83
		Frontal	Precentral_R (24.46%)	3.55	124
14		Temporal	Temporal_Inf_L (55.30%)	3.87	386
		Temporal	Temporal_Inf_R (46.84%)	3.87	385
		Occipital	Fusiform_R (22.67%)	4.23	129
15		Limbic	Amygdala_L (82.76%)	3.97	48
		Limbic	Amygdala_R (79.25%)	3.54	42
		Temporal	Temporal_Pole_Mid_L (74.26%)	3.30	101
		Limbic	Hippocampus_L (70.29%)	4.56	123
		Temporal	Temporal_Pole_Mid_R (69.89%)	2.95	130
		Limbic	ParaHippocampal_L (67.46%)	3.67	114
		Limbic	ParaHippocampal_R (65.74%)	3.75	142
		Limbic	Hippocampus_R (60.37%)	4.36	99
		Occipital	Fusiform_L (30.37%)	3.04	171
		Temporal	Temporal_Pole_Sup_L (28.07%)	3.06	48
		Temporal	Temporal_Pole_Sup_R (22.91%)	2.73	41
		Occipital	Fusiform_R (21.44%)	2.87	122
16		Frontal	Rectus_R (90.51%)	4.38	124
		Frontal	Rectus_L (83.82%)	4.02	145
		Frontal	Olfactory_R (80.36%)	3.99	45
		Frontal	Olfactory_L (76.62%)	3.63	59
		Frontal	Frontal_Sup_Orb_R (53.37%)	4.80	95
		Frontal	Frontal_Sup_Orb_L (50.00%)	4.92	85
		Frontal	Frontal_Mid_Orb_L (37.71%)	3.69	66
		Frontal	Frontal_Mid_Orb_R (30.93%)	3.57	60
		Frontal	Frontal_Inf_Orb_L (25.96%)	3.68	88
		Frontal	Frontal_Inf_Orb_R (21.64%)	3.76	74
17		Frontal	Frontal_Mid_Orb_R (63.40%)	5.61	123
		Frontal	Frontal_Mid_Orb_L (57.14%)	5.21	100
		Frontal	Frontal_Sup_Orb_R (50.00%)	6.55	89
		Frontal	Frontal_Sup_Orb_L (48.82%)	7.10	83
		Frontal	Frontal_Sup_Orb_Medial_L (43.70%)	4.89	52
		Frontal	Frontal_Sup_Orb_Medial_R (35.06%)	5.91	54

Appendix B. Supplementary material for chapter 4

Table B.6 – Test statistics corresponding to Figure 4.10 of the main manuscript: Results from two-sample t-tests comparing each iCAP's activation duration between healthy controls and patients with 22q11DS. Age, gender and scanner motion (framewise displacement) were included as nuisance regressors. P-values were corrected for multiple comparisons using false discovery rate.

iCAP	t-statistic	p-value	effect size (Cohen's d)
PrimVIS1 (1)	-0.16	0.875	0.02
SecVIS (2)	0.80	0.480	-0.13
aIN (3)	1.24	0.285	-0.19
LAN (4)	-2.17	0.053	0.34
dACC/dlPFC (5)	-3.88	0.001	0.61
SM (6)	2.60	0.019	-0.41
PREC/vDMN (7)	-1.50	0.209	0.24
PrimVis2 (8)	-3.49	0.002	0.55
FPN (9)	-3.25	0.004	0.51
aDMN (10)	-4.78	0.000	0.75
pDMN (11)	-3.03	0.006	0.48
VSN (12)	-0.64	0.556	0.10
AUD/SM (13)	-1.04	0.364	0.16
iTEMP/FUS (14)	4.98	0.000	-0.78
AMY/HIP (15)	3.71	0.001	-0.58
OFC (16)	3.20	0.004	-0.50
PFC (17)	1.24	0.285	-0.19

B.2. Supplementary material for section 4.2

Table B.7 – Test statistics corresponding to Figure 4.11 and Supplementary Figure B.10: Results from two-sample t-tests comparing positive coupling time and anti-coupling time of pairwise iCAP combinations between healthy controls and patients with 22q11DS. Age, gender and scanner motion (framewise displacement) were included as nuisance regressors. P-values were corrected for multiple comparisons using false discovery rate.

	iCAP	Percentage of scan time			Jaccard score		
		t-statistic	p-value	effect size (Cohen's d)	t-statistic	p-value	effect size (Cohen's d)
positive coupling	2 - 1	3.79	0.005	-0.59	4.18	0.002	-0.65
	3 - 1	0.52	0.715	-0.08	0.12	0.942	-0.02
	4 - 1	-0.64	0.661	0.10	-0.01	0.997	0.00
	5 - 1	0.69	0.641	-0.11	1.71	0.278	-0.27
	6 - 1	0.39	0.788	-0.06	0.10	0.944	-0.02
	7 - 1	-1.75	0.208	0.28	-1.44	0.340	0.23
	8 - 1	-2.81	0.036	0.44	-2.62	0.072	0.41
	9 - 1	-1.01	0.501	0.16	-0.47	0.783	0.07
	10 - 1	-1.77	0.203	0.28	-1.00	0.501	0.16
	11 - 1	-2.59	0.049	0.41	-1.85	0.242	0.29
	12 - 1	0.73	0.630	-0.11	1.04	0.494	-0.16
	13 - 1	-1.97	0.149	0.31	-2.38	0.109	0.37
	14 - 1	2.18	0.110	-0.34	2.32	0.120	-0.36
	15 - 1	1.63	0.234	-0.25	1.51	0.333	-0.24
	16 - 1	1.66	0.233	-0.26	1.00	0.501	-0.16
	17 - 1	-0.89	0.569	0.14	-1.04	0.494	0.16
	3 - 2	0.66	0.658	-0.10	0.71	0.642	-0.11
	4 - 2	-2.08	0.124	0.33	-1.68	0.282	0.27
	5 - 2	0.96	0.530	-0.15	1.78	0.263	-0.28
	6 - 2	0.32	0.827	-0.05	-0.23	0.888	0.04
	7 - 2	-0.13	0.923	0.02	-0.37	0.810	0.06
	8 - 2	-1.36	0.349	0.21	-1.45	0.340	0.23
	9 - 2	-0.15	0.907	0.02	0.45	0.788	-0.07
	10 - 2	-1.64	0.234	0.26	-1.02	0.497	0.16
	11 - 2	0.30	0.836	-0.05	1.02	0.497	-0.16
	12 - 2	0.26	0.840	-0.04	0.10	0.944	-0.02
	13 - 2	-1.64	0.234	0.26	-1.73	0.277	0.27
	14 - 2	2.18	0.110	-0.34	1.49	0.340	-0.23
	15 - 2	1.91	0.164	-0.30	1.31	0.386	-0.21
	16 - 2	2.61	0.048	-0.41	2.13	0.168	-0.33
	17 - 2	0.89	0.568	-0.14	0.44	0.788	-0.07
	4 - 3	1.29	0.385	-0.20	1.32	0.383	-0.21
	5 - 3	-4.33	0.002	0.68	-3.99	0.003	0.63
	6 - 3	2.96	0.031	-0.46	2.46	0.093	-0.39
	7 - 3	1.81	0.194	-0.28	1.96	0.211	-0.31
	8 - 3	-0.94	0.542	0.15	-0.23	0.888	0.04
	9 - 3	-0.54	0.705	0.08	0.03	0.987	-0.00
	10 - 3	-1.62	0.241	0.25	-1.47	0.340	0.23
	11 - 3	0.07	0.958	-0.01	0.70	0.642	-0.11
	12 - 3	-0.29	0.839	0.05	-0.64	0.684	0.10
	13 - 3	1.60	0.246	-0.25	1.47	0.340	-0.23
	14 - 3	3.19	0.018	-0.50	1.78	0.263	-0.28
	15 - 3	1.92	0.162	-0.30	0.86	0.576	-0.14
	16 - 3	1.18	0.423	-0.18	0.00	0.997	-0.00
	17 - 3	0.60	0.675	-0.10	0.46	0.787	-0.07

Appendix B. Supplementary material for chapter 4

	iCAP	Percentage of scan time			Jaccard score		
		t-statistic	p-value	effect size (Cohen's d)	t-statistic	p-value	effect size (Cohen's d)
positive coupling	5 - 4	-2.22	0.107	0.35	-1.44	0.340	0.23
	6 - 4	-2.00	0.142	0.31	-1.93	0.220	0.30
	7 - 4	-1.18	0.423	0.19	-0.42	0.801	0.07
	8 - 4	-2.82	0.036	0.44	-1.99	0.202	0.31
	9 - 4	-2.39	0.074	0.38	-1.43	0.340	0.22
	10 - 4	-2.24	0.103	0.35	-1.31	0.386	0.21
	11 - 4	0.54	0.705	-0.09	1.42	0.342	-0.22
	12 - 4	-1.73	0.214	0.27	-1.04	0.494	0.16
	13 - 4	-2.60	0.049	0.41	-2.06	0.186	0.32
	14 - 4	1.27	0.388	-0.20	1.11	0.457	-0.17
	15 - 4	3.37	0.012	-0.52	3.65	0.007	-0.57
	16 - 4	1.39	0.338	-0.22	1.81	0.253	-0.28
	17 - 4	0.86	0.573	-0.13	1.34	0.377	-0.21
	6 - 5	1.19	0.423	-0.19	1.58	0.305	-0.25
	7 - 5	0.63	0.661	-0.10	1.56	0.310	-0.24
	8 - 5	-3.52	0.010	0.55	-2.51	0.088	0.39
	9 - 5	-3.60	0.008	0.57	-2.62	0.072	0.41
	10 - 5	-2.77	0.037	0.44	-1.73	0.277	0.27
	11 - 5	-1.59	0.252	0.25	-0.62	0.692	0.10
	12 - 5	0.58	0.691	-0.09	1.39	0.350	-0.22
	13 - 5	2.04	0.131	-0.32	3.09	0.030	-0.48
	14 - 5	1.28	0.385	-0.20	1.58	0.305	-0.25
	15 - 5	0.45	0.757	-0.07	0.89	0.562	-0.14
	16 - 5	2.38	0.075	-0.37	3.08	0.030	-0.48
	17 - 5	0.28	0.839	-0.04	0.40	0.809	-0.06
	7 - 6	0.63	0.661	-0.10	0.53	0.766	-0.08
	8 - 6	-0.04	0.977	0.01	0.12	0.942	-0.02
	9 - 6	2.77	0.037	-0.43	3.35	0.018	-0.52
	10 - 6	-2.21	0.107	0.35	-1.99	0.202	0.31
	11 - 6	-0.39	0.788	0.06	-0.26	0.876	0.04
	12 - 6	1.91	0.163	-0.30	1.71	0.278	-0.27
	13 - 6	-0.37	0.801	0.06	-0.23	0.888	0.04
	14 - 6	2.92	0.033	-0.45	2.10	0.170	-0.33
	15 - 6	2.01	0.139	-0.31	1.98	0.203	-0.31
	16 - 6	0.78	0.603	-0.12	0.16	0.941	-0.02
	17 - 6	1.22	0.409	-0.19	0.91	0.553	-0.14
	8 - 7	-2.73	0.040	0.43	-2.11	0.170	0.33
	9 - 7	-2.53	0.056	0.40	-1.47	0.340	0.23
	10 - 7	-2.20	0.107	0.35	-1.43	0.340	0.22
	11 - 7	-2.92	0.033	0.46	-2.10	0.170	0.33
	12 - 7	-1.11	0.460	0.17	-0.73	0.637	0.11
	13 - 7	-1.14	0.446	0.18	-0.50	0.774	0.08
	14 - 7	2.69	0.042	-0.42	2.76	0.056	-0.43
	15 - 7	4.01	0.004	-0.62	4.40	0.002	-0.68
	16 - 7	0.86	0.573	-0.14	1.02	0.497	-0.16
	17 - 7	1.21	0.416	-0.19	1.58	0.305	-0.25

B.2. Supplementary material for section 4.2

	iCAP	Percentage of scan time			Jaccard score		
		t-statistic	p-value	effect size (Cohen's d)	t-statistic	p-value	effect size (Cohen's d)
positive coupling	9 - 8	-0.69	0.641	0.11	0.47	0.783	-0.07
	10 - 8	-3.39	0.012	0.53	-2.26	0.135	0.35
	11 - 8	-0.87	0.573	0.14	0.12	0.942	-0.02
	12 - 8	-2.66	0.044	0.42	-2.39	0.109	0.38
	13 - 8	-0.27	0.839	0.04	0.14	0.941	-0.02
	14 - 8	1.23	0.408	-0.19	1.29	0.388	-0.20
	15 - 8	0.54	0.705	-0.08	0.75	0.630	-0.12
	16 - 8	-1.24	0.407	0.19	-1.25	0.401	0.20
	17 - 8	-0.48	0.742	0.07	-0.38	0.810	0.06
	10 - 9	-1.58	0.252	0.25	-0.09	0.944	0.01
	11 - 9	0.68	0.641	-0.11	1.69	0.280	-0.26
	12 - 9	-1.18	0.423	0.19	-0.39	0.810	0.06
	13 - 9	0.26	0.840	-0.04	1.58	0.305	-0.25
	14 - 9	2.90	0.033	-0.45	2.67	0.064	-0.42
	15 - 9	3.15	0.019	-0.49	3.40	0.017	-0.53
	16 - 9	1.41	0.328	-0.22	1.64	0.293	-0.26
	17 - 9	0.65	0.659	-0.10	1.12	0.457	-0.17
	11 - 10	-1.49	0.298	0.23	-0.04	0.986	0.01
	12 - 10	0.50	0.730	-0.08	1.69	0.280	-0.26
	13 - 10	-2.13	0.115	0.34	-0.70	0.642	0.11
	14 - 10	0.18	0.889	-0.03	0.46	0.787	-0.07
	15 - 10	0.74	0.625	-0.12	1.66	0.288	-0.26
	16 - 10	0.97	0.530	-0.15	1.27	0.393	-0.20
	17 - 10	-0.28	0.839	0.04	0.60	0.712	-0.09
	12 - 11	-0.68	0.641	0.11	-0.32	0.840	0.05
	13 - 11	-0.77	0.604	0.12	-0.15	0.941	0.02
	14 - 11	4.44	0.002	-0.69	4.78	0.001	-0.74
	15 - 11	1.78	0.202	-0.28	2.29	0.128	-0.35
	16 - 11	0.29	0.839	-0.05	0.71	0.638	-0.11
	17 - 11	0.80	0.590	-0.12	0.74	0.637	-0.12
	13 - 12	-0.93	0.544	0.15	-1.11	0.457	0.17
	14 - 12	3.38	0.012	-0.53	2.82	0.049	-0.44
	15 - 12	1.74	0.208	-0.27	1.83	0.250	-0.29
	16 - 12	2.04	0.131	-0.32	2.03	0.195	-0.32
	17 - 12	0.82	0.583	-0.13	0.91	0.552	-0.14
	14 - 13	2.18	0.110	-0.34	0.77	0.629	-0.12
	15 - 13	1.41	0.328	-0.22	1.35	0.374	-0.21
	16 - 13	0.72	0.633	-0.11	0.86	0.576	-0.14
	17 - 13	0.00	0.997	-0.00	0.76	0.630	-0.12
	15 - 14	2.87	0.034	-0.44	1.16	0.437	-0.18
	16 - 14	1.17	0.424	-0.18	0.58	0.718	-0.09
	17 - 14	2.11	0.118	-0.33	2.00	0.202	-0.31
	16 - 15	2.71	0.041	-0.42	1.20	0.418	-0.19
	17 - 15	2.90	0.033	-0.45	2.47	0.093	-0.38
	17 - 16	1.64	0.234	-0.26	1.51	0.333	-0.24

Appendix B. Supplementary material for chapter 4

	iCAP	Percentage of scan time			Jaccard score		
		t-statistic	p-value	effect size (Cohen's d)	t-statistic	p-value	effect size (Cohen's d)
anti-coupling	1 - 2	-1.28	0.385	0.20	-1.31	0.386	0.21
	1 - 3	0.70	0.641	-0.11	0.48	0.783	-0.08
	1 - 4	-0.33	0.827	0.05	0.10	0.944	-0.02
	1 - 5	-1.79	0.200	0.28	-1.00	0.501	0.16
	1 - 6	1.64	0.234	-0.26	1.29	0.388	-0.20
	1 - 7	1.67	0.228	-0.26	2.22	0.145	-0.35
	1 - 8	-0.85	0.573	0.13	-0.43	0.798	0.07
	1 - 9	-1.54	0.270	0.24	-1.08	0.473	0.17
	1 - 10	-1.09	0.468	0.17	-0.13	0.942	0.02
	1 - 11	-0.23	0.860	0.04	0.02	0.992	-0.00
	1 - 12	0.24	0.849	-0.04	0.48	0.783	-0.07
	1 - 13	2.17	0.111	-0.34	2.59	0.074	-0.41
	1 - 14	3.40	0.012	-0.53	3.27	0.020	-0.51
	1 - 15	1.75	0.208	-0.27	1.39	0.350	-0.22
	1 - 16	1.37	0.344	-0.21	1.17	0.433	-0.18
	1 - 17	0.51	0.723	-0.08	0.40	0.810	-0.06
	2 - 3	1.03	0.496	-0.16	0.38	0.810	-0.06
	2 - 4	0.81	0.588	-0.13	1.44	0.340	-0.23
	2 - 5	-0.94	0.542	0.15	-0.14	0.942	0.02
	2 - 6	3.18	0.018	-0.50	2.53	0.085	-0.40
	2 - 7	0.57	0.692	-0.09	0.79	0.621	-0.12
	2 - 8	-0.41	0.777	0.06	0.10	0.944	-0.02
	2 - 9	0.41	0.777	-0.07	0.94	0.536	-0.15
	2 - 10	-0.95	0.540	0.15	-0.34	0.826	0.05
	2 - 11	-0.28	0.839	0.04	-0.77	0.629	0.12
	2 - 12	0.48	0.742	-0.07	0.91	0.552	-0.14
	2 - 13	3.20	0.018	-0.50	3.65	0.007	-0.57
	2 - 14	3.45	0.011	-0.54	2.52	0.085	-0.39
	2 - 15	2.51	0.059	-0.39	1.89	0.228	-0.30
	2 - 16	1.86	0.179	-0.29	1.71	0.278	-0.27
	2 - 17	2.37	0.077	-0.37	2.19	0.149	-0.34
	3 - 4	-1.44	0.319	0.23	-1.09	0.468	0.17
	3 - 5	2.90	0.033	-0.45	3.69	0.007	-0.57
	3 - 6	1.43	0.325	-0.22	0.72	0.637	-0.11
	3 - 7	-1.13	0.450	0.18	-1.21	0.413	0.19
	3 - 8	-0.90	0.562	0.14	-0.86	0.576	0.14
	3 - 9	0.85	0.573	-0.13	1.48	0.340	-0.23
	3 - 10	-1.94	0.157	0.31	-1.45	0.340	0.23
	3 - 11	-0.84	0.575	0.13	-0.76	0.630	0.12
	3 - 12	1.35	0.352	-0.21	1.16	0.437	-0.18
	3 - 13	-0.80	0.590	0.12	-0.79	0.621	0.12
	3 - 14	3.13	0.020	-0.49	2.43	0.100	-0.38
	3 - 15	2.21	0.107	-0.34	1.68	0.282	-0.26
	3 - 16	2.48	0.062	-0.39	2.19	0.149	-0.34
	3 - 17	1.67	0.228	-0.26	1.16	0.437	-0.18

B.2. Supplementary material for section 4.2

	iCAP	Percentage of scan time			Jaccard score		
		t-statistic	p-value	effect size (Cohen's d)	t-statistic	p-value	effect size (Cohen's d)
anti-coupling	4 - 5	-2.08	0.125	0.33	-1.00	0.501	0.16
	4 - 6	3.96	0.004	-0.62	4.14	0.002	-0.64
	4 - 7	-1.05	0.488	0.16	-0.73	0.637	0.11
	4 - 8	-2.07	0.127	0.33	-1.40	0.347	0.22
	4 - 9	-0.87	0.573	0.14	0.45	0.788	-0.07
	4 - 10	-2.82	0.036	0.45	-1.29	0.388	0.20
	4 - 11	-3.67	0.007	0.58	-3.02	0.033	0.48
	4 - 12	0.57	0.691	-0.09	1.42	0.340	-0.22
	4 - 13	0.68	0.641	-0.11	1.29	0.388	-0.20
	4 - 14	4.96	0.000	-0.77	4.65	0.001	-0.72
	4 - 15	0.76	0.609	-0.12	0.72	0.637	-0.11
	4 - 16	1.94	0.157	-0.30	1.80	0.260	-0.28
	4 - 17	0.63	0.661	-0.10	0.49	0.781	-0.08
	5 - 6	0.54	0.705	-0.09	1.27	0.393	-0.20
	5 - 7	-2.81	0.036	0.44	-1.65	0.288	0.26
	5 - 8	-1.19	0.423	0.19	-0.15	0.941	0.02
	5 - 9	-0.64	0.661	0.10	1.22	0.410	-0.19
	5 - 10	-3.35	0.012	0.53	-2.19	0.149	0.34
	5 - 11	-1.75	0.208	0.28	-0.49	0.780	0.08
	5 - 12	-0.97	0.530	0.15	0.27	0.868	-0.04
	5 - 13	-3.79	0.005	0.60	-3.17	0.025	0.50
	5 - 14	3.56	0.009	-0.55	4.11	0.002	-0.64
	5 - 15	3.28	0.014	-0.51	3.75	0.007	-0.58
	5 - 16	1.23	0.408	-0.19	1.92	0.221	-0.30
	5 - 17	1.69	0.224	-0.26	2.33	0.120	-0.36
	6 - 7	0.33	0.827	-0.05	-0.10	0.944	0.02
	6 - 8	-0.44	0.765	0.07	-0.51	0.769	0.08
	6 - 9	-1.08	0.471	0.17	-0.94	0.536	0.15
	6 - 10	2.44	0.068	-0.38	3.30	0.020	-0.51
	6 - 11	0.68	0.641	-0.11	0.67	0.664	-0.11
	6 - 12	0.71	0.635	-0.11	0.35	0.821	-0.06
	6 - 13	2.66	0.044	-0.41	2.72	0.060	-0.42
	6 - 14	4.54	0.001	-0.71	3.77	0.007	-0.59
	6 - 15	2.50	0.060	-0.39	1.39	0.350	-0.22
	6 - 16	4.10	0.003	-0.64	4.20	0.002	-0.66
	6 - 17	2.13	0.115	-0.33	1.90	0.225	-0.30
	7 - 8	-2.15	0.112	0.34	-1.85	0.242	0.29
	7 - 9	0.63	0.661	-0.10	1.81	0.253	-0.28
	7 - 10	-2.15	0.112	0.34	-1.25	0.401	0.20
	7 - 11	0.06	0.963	-0.01	0.95	0.530	-0.15
	7 - 12	0.46	0.749	-0.07	0.85	0.582	-0.13
	7 - 13	0.28	0.839	-0.04	0.85	0.582	-0.13
	7 - 14	2.35	0.079	-0.37	2.71	0.060	-0.42
	7 - 15	1.41	0.328	-0.22	1.63	0.296	-0.25
	7 - 16	2.84	0.035	-0.44	3.20	0.024	-0.50
	7 - 17	1.28	0.385	-0.20	1.47	0.340	-0.23

Appendix B. Supplementary material for chapter 4

	iCAP	Percentage of scan time			Jaccard score		
		t-statistic	p-value	effect size (Cohen's d)	t-statistic	p-value	effect size (Cohen's d)
anti-coupling	8 - 9	-3.82	0.005	0.60	-2.97	0.035	0.47
	8 - 10	-2.43	0.068	0.38	-1.24	0.401	0.20
	8 - 11	-1.39	0.337	0.22	0.20	0.913	-0.03
	8 - 12	0.02	0.990	-0.00	0.42	0.798	-0.07
	8 - 13	-2.49	0.060	0.39	-1.62	0.297	0.26
	8 - 14	1.04	0.491	-0.16	1.04	0.494	-0.16
	8 - 15	0.86	0.573	-0.13	0.81	0.609	-0.13
	8 - 16	0.26	0.840	-0.04	0.38	0.810	-0.06
	8 - 17	1.05	0.490	-0.16	1.61	0.298	-0.25
	9 - 10	-4.13	0.003	0.65	-2.74	0.058	0.43
	9 - 11	-3.89	0.004	0.61	-3.01	0.033	0.47
	9 - 12	-0.02	0.990	0.00	0.64	0.684	-0.10
	9 - 13	-1.45	0.319	0.23	-0.52	0.769	0.08
	9 - 14	2.77	0.037	-0.43	2.89	0.042	-0.45
	9 - 15	1.02	0.501	-0.16	1.46	0.340	-0.23
	9 - 16	1.09	0.470	-0.17	1.72	0.278	-0.27
	9 - 17	0.13	0.923	-0.02	0.73	0.637	-0.11
	10 - 11	-0.85	0.573	0.13	0.73	0.637	-0.11
	10 - 12	-3.37	0.012	0.53	-3.27	0.020	0.51
	10 - 13	-0.32	0.829	0.05	1.00	0.501	-0.16
	10 - 14	2.68	0.042	-0.42	2.97	0.035	-0.47
	10 - 15	0.85	0.573	-0.13	1.66	0.288	-0.26
	10 - 16	-0.10	0.942	0.02	0.37	0.810	-0.06
	10 - 17	1.04	0.490	-0.16	2.02	0.199	-0.31
	11 - 12	-1.87	0.178	0.29	-1.50	0.336	0.23
	11 - 13	-1.84	0.185	0.29	-1.26	0.401	0.20
	11 - 14	-1.34	0.352	0.21	-1.23	0.403	0.19
	11 - 15	0.59	0.683	-0.09	1.59	0.305	-0.25
	11 - 16	0.36	0.804	-0.06	0.75	0.630	-0.12
	11 - 17	0.41	0.778	-0.06	1.06	0.486	-0.17
	12 - 13	-0.83	0.578	0.13	-0.31	0.846	0.05
	12 - 14	0.81	0.587	-0.13	0.39	0.810	-0.06
	12 - 15	2.77	0.037	-0.43	2.87	0.043	-0.45
	12 - 16	2.87	0.034	-0.45	3.07	0.030	-0.48
	12 - 17	2.14	0.114	-0.33	2.32	0.120	-0.36
	13 - 14	1.72	0.214	-0.27	1.12	0.457	-0.18
	13 - 15	0.80	0.590	-0.13	1.24	0.402	-0.19
	13 - 16	1.80	0.197	-0.28	1.73	0.277	-0.27
	13 - 17	0.19	0.882	-0.03	-0.19	0.913	0.03
	14 - 15	2.69	0.042	-0.42	1.77	0.267	-0.28
	14 - 16	3.00	0.029	-0.47	1.44	0.340	-0.23
	14 - 17	1.06	0.484	-0.17	0.29	0.860	-0.05
	15 - 16	2.62	0.048	-0.41	1.93	0.220	-0.30
	15 - 17	-1.38	0.339	0.22	-1.56	0.310	0.25
	16 - 17	1.71	0.218	-0.27	0.35	0.824	-0.05

B.2. Supplementary material for section 4.2

Table B.8 – Bootstrap data corresponding to Figure 4.12: PLSC results from for positive psychotic symptoms. The table shows bootstrap mean and 5 to 95 percentiles of behavior weights and brain weights.

Weights type	item	mean	5th percentile	95th percentile
Behavior: SIPS Positive Symptoms	P1:Del (22q)	0.64	0.403	0.89
	P2:Susp (22q)	0.51	0.307	0.72
	P3:Gand (22q)	0.32	0.115	0.53
	P4:Hall (22q)	0.49	0.238	0.76
	P5:DisCom (22q)	0.62	0.416	0.83
iCAPs activation duration	dACC/dlPFC (5)	0.38	-0.002	0.78
	PrimVis2 (8)	0.03	-0.246	0.33
	FPN (9)	0.59	0.144	1.05
	aDMN (10)	-0.15	-0.490	0.21
	pDMN (11)	-0.01	-0.356	0.33
	SM (6)	0.10	-0.288	0.49
	iTEMP/FUS (14)	0.66	0.347	0.97
	AMY/HIP (15)	0.14	-0.271	0.57
	OFC (16)	0.09	-0.301	0.50
Weights type	item	mean	5th percentile	95th percentile
Behavior: SIPS Positive Symptoms	P1:Del (22q)	0.69	0.468	0.90
	P2:Susp (22q)	0.54	0.318	0.76
	P3:Gand (22q)	0.18	-0.031	0.40
	P4:Hall (22q)	0.44	0.211	0.67
	P5:DisCom (22q)	0.54	0.324	0.77
anti-coupling duration with dACC/dlPFC (5)	AUD (3)	0.03	-0.320	0.38
	FPN (9)	0.41	0.005	0.86
	AUD/SM (13)	0.31	-0.193	0.83
	iTEMP/FUS (14)	0.88	0.575	1.22
	AMY/HIP (15)	0.01	-0.440	0.50

Appendix B. Supplementary material for chapter 4

Table B.9 – Bootstrap data corresponding to Figure 4.13: PLSC results from for anxiety. The table shows bootstrap mean and 5 to 95 percentiles of behavior weights and brain weights.

Weights type	item	mean	5th percentile	95th percentile
Behavior: CBCL/ABCL Anxiety	HC	0.74	0.406	1.07
	22q11DS	0.87	0.545	1.23
iCAPs activation duration	dACC/dlPFC (5)	0.05	-0.301	0.42
	PrimVis2 (8)	0.27	-0.085	0.63
	FPN (9)	-0.12	-0.494	0.28
	aDMN (10)	-0.39	-0.770	-0.02
	pDMN (11)	-0.16	-0.536	0.20
	SM (6)	-0.18	-0.510	0.14
	iTEMP/FUS (14)	0.68	0.304	1.03
	AMY/HIP (15)	0.41	0.033	0.78
	OFC (16)	-0.20	-0.479	0.08
Weights type	item	mean	5th percentile	95th percentile
Behavior: CBCL/ABCL Anxiety	HC	-0.11	-0.350	0.17
	22q11DS	1.05	0.688	1.44
Positive coupling duration with AMY/HIP (15)	LAN (4)	0.35	0.014	0.67
	dACC/dlPFC (5)	0.75	0.400	1.05
	PREC/vDMN (7)	-0.06	-0.375	0.25
	FPN (9)	0.29	-0.024	0.60
	aDMN (10)	-0.32	-0.592	-0.04
	iTEMP/FUS (14)	0.31	-0.071	0.67

B.2. Supplementary material for section 4.2

Table B.10 – Test statistics for group comparison of iCAPs' activation duration in high motion vs. low motion healthy subjects (shown in Supplementary Figure B.11). P-values are corrected for multiple comparisons using false discovery rate; age and gender were included as covariates.

iCAP	t-statistic	p-value	effect size (Cohen's d)
PrimVIS1 (1)	-0.27	0.795	0.06
SecVIS (2)	1.89	0.211	-0.41
aIN (3)	-2.01	0.205	0.44
LAN (4)	0.71	0.669	-0.15
dACC/dlPFC (5)	-0.60	0.669	0.13
SM (6)	-1.57	0.294	0.34
PREC/vDMN (7)	-0.63	0.669	0.14
PrimVis2 (8)	0.36	0.795	-0.08
FPN (9)	1.39	0.330	-0.30
aDMN (10)	2.70	0.071	-0.59
pDMN (11)	2.71	0.071	-0.59
VSN (12)	0.75	0.669	-0.16
AUD/SM (13)	-1.25	0.367	0.27
iTEMP/FUS (14)	-1.37	0.330	0.30
AMY/HIP (15)	-2.08	0.205	0.45
OFC (16)	-1.81	0.211	0.39
PFC (17)	-0.26	0.795	0.06

C Supplementary material for chapter 5

C.1 Supplementary material for section 5.1

C.1.1 Supplementary tables

Table C.1 – Number of scans recorded before and after a scanner update. There was no significant group-by-scanner interaction.

image modality	Siemens Trio scanner (22q11DS/HCs)	Siemens Prisma scanner (22q11DS/HCs)	p-value (χ^2)
fMRI	42/54	36/31	0.209
dMRI	41/49	36/29	0.227

C.1.2 Supplementary figures

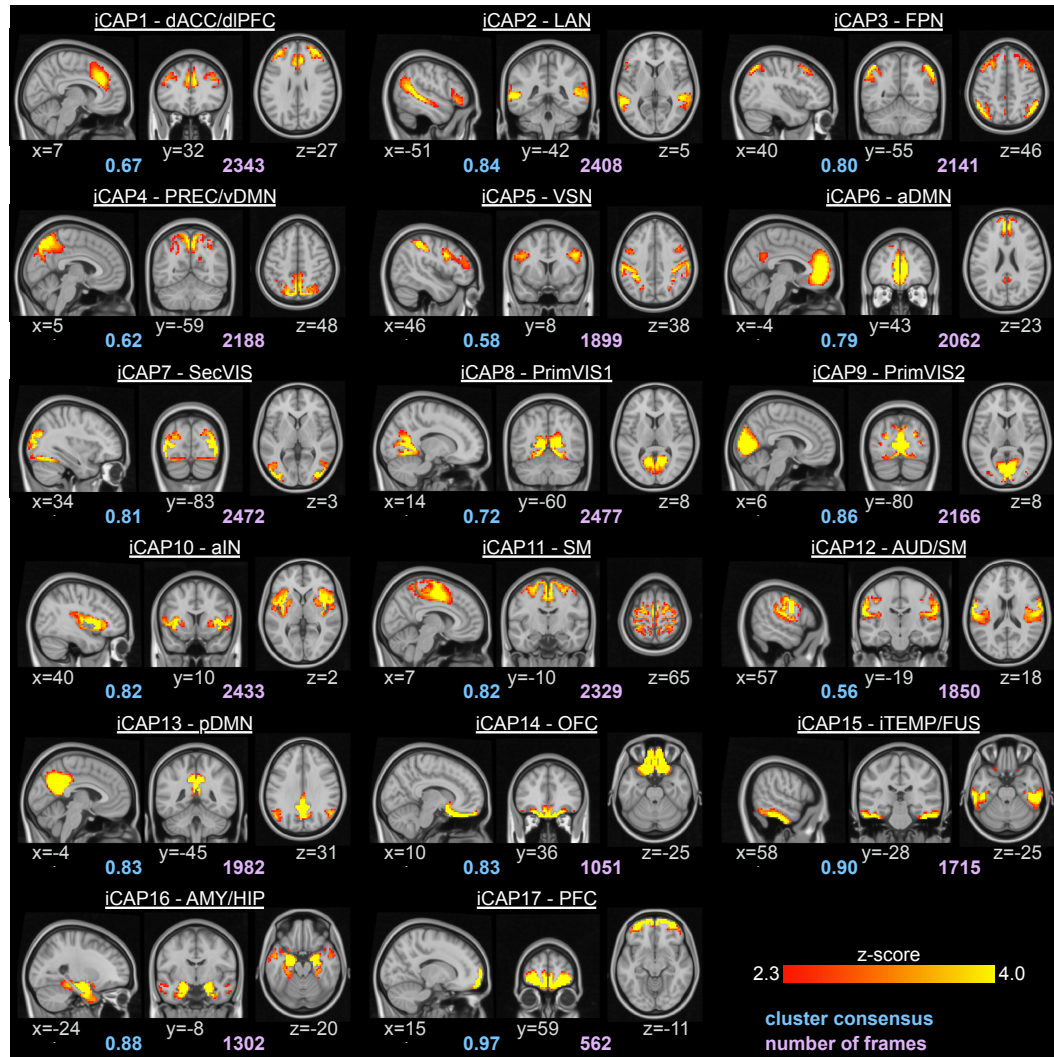


Figure C.1 – Spatial patterns of the 17 iCAPs retrieved from all subjects, including both HCs and patients with 22q11DS. The locations denote displayed slices in MNI coordinates. Blue values denote the average consensus of each cluster, purple values indicate the total number of innovation frames that were assigned to this cluster. Maps are identical to the ones in (Zöller et al., 2019a); or section 4.2 of this thesis, sorted according to the activation duration in HCs. dACC/dlPFC – dorsal anterior cingulate cortex / dorsolateral prefrontal cortex, LAN – language network, FPN – fronto-parietal network, PREC/vDMN – precuneus/ventral DMN, VSN – visuospatial network, aDMN – anterior DMN, SecVIS – secondary visual, PrimVIS1 – primary visual 1, PrimVIS2 – primary visual 2, aIN – anterior insula, SM – sensorimotor, AUD/SM – auditory/sensorimotor, pDMN – posterior DMN, OFC – orbitofrontal cortex, iTEMP/FUS – inferior temporal/fusiform, AMY/HIP – amygdala/hippocampus, PFC – prefrontal cortex.

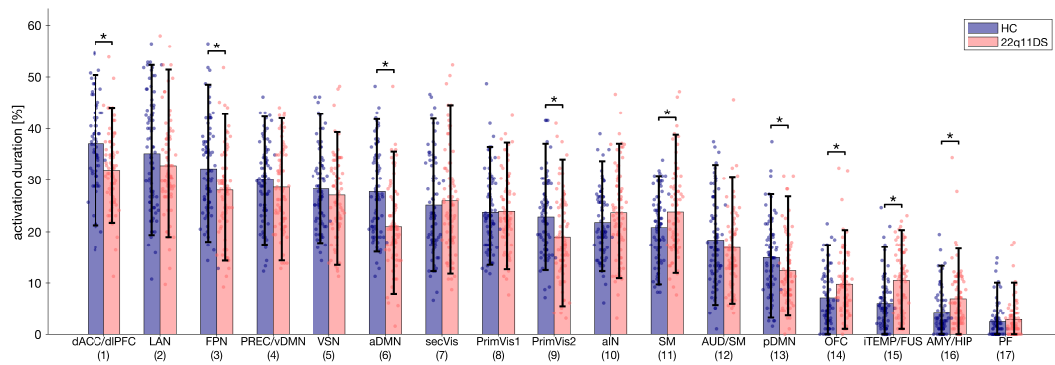


Figure C.2 – Statistics of total temporal duration for each iCAP. P-values are false discovery rate (FDR)-corrected for the 17 multiple comparisons, and both age and sex were included as covariates. Significant group differences ($p < 0.05$) were marked with an asterisk. Error bars indicate 5th to 95th percentiles of group distributions. Single-subject duration measures were included as scatterplots. Results are identical to those in (Zöller et al., 2019a); or section 4.2 of this thesis, but sorted according to the activation duration in HCs.

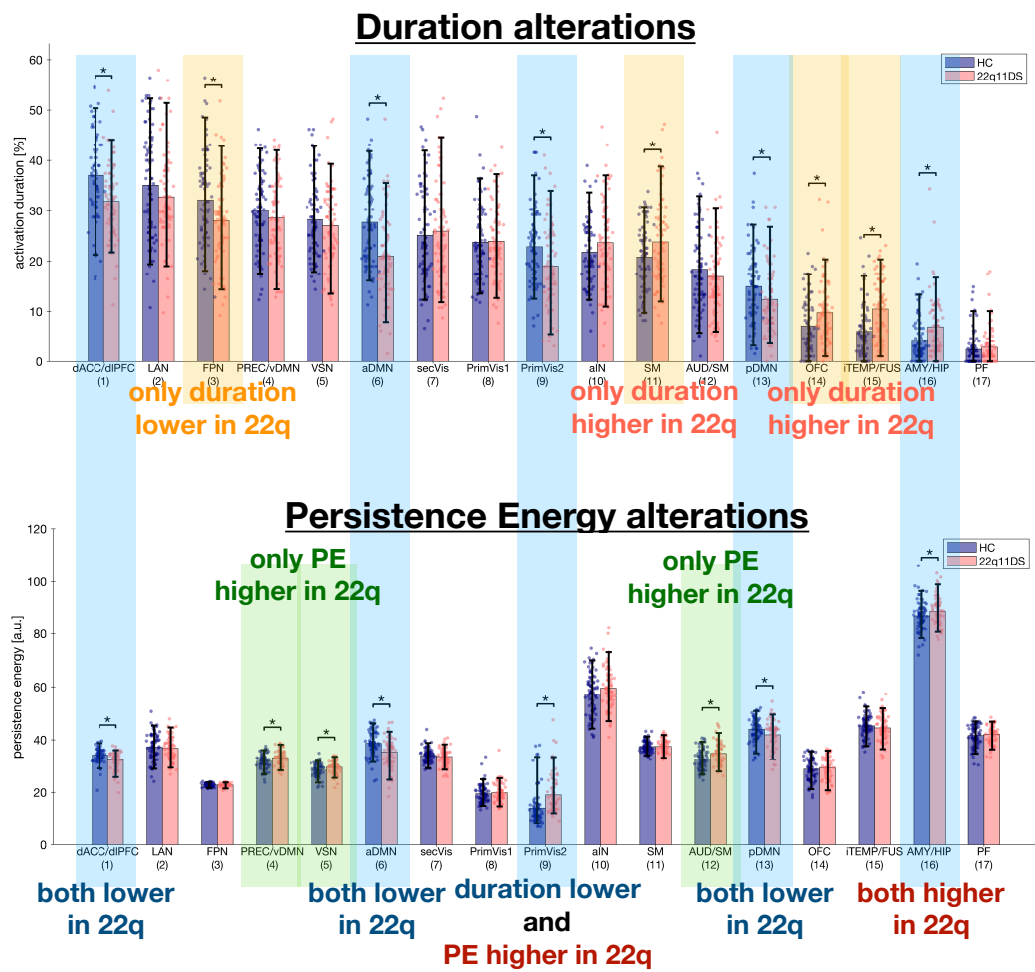


Figure C.3 – Comparison of alterations in resting-state activation duration and structural persistence control energy. While there were widespread alterations in both modalities, there was no clear pattern of common alterations. PE – persistence control energy.

Bibliography

- Acharya, J., Diakonikolas, I., Li, J., and Schmidt, L. (2016). Fast Algorithms for Segmented Regression. *Proceedings of The 33rd International Conference on Machine Learning*, 48:2878–2886.
- Achenbach, T. M. (1991). *Manual for the Child Behavior Checklist/4-18 and 1991 Profile*. Burlington, NJ: University of Vermont Department of Psychiatry.
- Achenbach, T. M. and Rescorla, L. A. (2003). *Manual for the ASEBA Adult Forms & Profiles*. Burlington, VT: University of Vermont, Research Center for Children, Youth, & Families.
- Aleman-Gomez, Y., Melie-García, L., and Valdés-Hernandez, P. (2006). IBASPM: toolbox for automatic parcellation of brain structures. In *12th Annual Meeting of the Organization for Human Brain Mapping*.
- Allen, E. A., Damaraju, E., Plis, S. M., Erhardt, E. B., Eichele, T., and Calhoun, V. D. (2014). Tracking Whole-Brain Connectivity Dynamics in the Resting State. *Cerebral Cortex*, 24(3):663–676.
- Allen, P., Aleman, A., and McGuire, P. K. (2007). Inner speech models of auditory verbal hallucinations: evidence from behavioural and neuroimaging studies. *Int Rev Psychiatry*, 19(4):407–415.
- Allen, P., Larøi, F., McGuire, P. K., and Aleman, A. (2008). The hallucinating brain: A review of structural and functional neuroimaging studies of hallucinations. *Neuroscience and Biobehavioral Reviews*, 32(1):175–191.
- Allen, P., Stephan, K. E., Mechelli, A., Day, F., Ward, N., Dalton, J., Williams, S. C., and McGuire, P. (2010). Cingulate activity and fronto-temporal connectivity in people with prodromal signs of psychosis. *NeuroImage*, 49(1):947–955.
- Alonso-Solís, A., Vives-Gilabert, Y., Portella, M. J., Rabella, M., Grasa, E. M., Roldán, A., Keymer-Gausset, A., Molins, C., Núñez-Marín, F., Gómez-Ansón, B., Alvarez, E., and Corripio, I. (2017). Altered amplitude of low frequency fluctuations in schizophrenia patients with persistent auditory verbal hallucinations. *Schizophrenia Research*, 189:97–103.
- American Psychiatric Association (2013). *Diagnostic and statistical manual of mental disorders (DSM-5®)*. American Psychiatric Pub.

Bibliography

- Antsaklis, P. J. and Michel, A. N. (2005). *Linear Systems*. Birkhäuser Boston.
- Antshel, K. M., Fremont, W., and Kates, W. R. (2008). The neurocognitive phenotype in velocardio-facial syndrome: A developmental perspective. *Developmental Disabilities Research Reviews*, 14(1):43–51.
- Armando, M., Sandini, C., Chambaz, M., Schaer, M., Schneider, M., and Eliez, S. (2018). Coping Strategies Mediate the Effect of Stressful Life Events on Schizotypal Traits and Psychotic Symptoms in 22q11.2 Deletion Syndrome. *Schizophrenia Bulletin*, pages 1–11.
- Armbruster-Genc, D. J. N., Ueltzhoffer, K., and Fiebach, C. J. (2016). Brain Signal Variability Differentially Affects Cognitive Flexibility and Cognitive Stability. *Journal of Neuroscience*, 36(14):3978–3987.
- Armitage, P. A. and Bastin, M. E. (2000). Selecting an Appropriate Anisotropy Index for. *Magnetic Resonance in Medicine*, 44:117–121.
- Ashburner, J. (2007). A fast diffeomorphic image registration algorithm. *NeuroImage*, 38(1):95–113.
- Ashburner, J. and Friston, K. J. (2005). Unified segmentation. *NeuroImage*, 26(3):839–851.
- Ashkan, K., Rogers, P., Bergman, H., and Ughratdar, I. (2017). Insights into the mechanisms of deep brain stimulation. *Nature Reviews Neurology*, 13(9):548–554.
- Atasoy, S., Donnelly, I., and Pearson, J. (2016). Human brain networks function in connectome-specific harmonic waves. *Nature Communications*, 7(1):10340.
- Atasoy, S., Roseman, L., Kaelen, M., Kringelbach, M. L., Deco, G., and Carhart-Harris, R. L. (2017). Connectome-harmonic decomposition of human brain activity reveals dynamical repertoire re-organization under LSD. *Scientific Reports*, 7(1):17661.
- Atkeson, C. G., Moore, A. W., and Schaal, S. (1997). Locally weighted learning for control. *Artificial Intelligence Review*, 11(1-5):75–113.
- Basser, P. J., Mattiello, J., and LeBihan, D. (1994). MR diffusion tensor spectroscopy and imaging. *Biophysical Journal*, 66(1):259–267.
- Bassett, A. S. and Chow, E. W. C. (1999). 22q11 deletion syndrome: A genetic subtype of schizophrenia. *Biological Psychiatry*, 46(7):882–891.
- Bassett, A. S., Costain, G., and Marshall, C. R. (2017). Neuropsychiatric aspects of 22q11.2 deletion syndrome: considerations in the prenatal setting. *Prenatal Diagnosis*, 37(1):61–69.
- Bassett, D. S. and Bullmore, E. T. (2017). Small-World Brain Networks Revisited. *Neuroscientist*, 23(5):499–516.
- Bassett, D. S. and Sporns, O. (2017). Network neuroscience. *Nature Neuroscience*, 20(3):353.

- Bassett, D. S., Xia, C. H., and Satterthwaite, T. D. (2018). Understanding the Emergence of Neuropsychiatric Disorders With Network Neuroscience. *Biological Psychiatry: Cognitive Neuroscience and Neuroimaging*, 3(9):742–753.
- Beaulieu, C. (2009). Chapter 6 - The Biological Basis of Diffusion Anisotropy. In Johansen-Berg, H. and Behrens, T. E. J., editors, *Diffusion MRI (First Edition)*, pages 105–126. Academic Press, San Diego, first edit edition.
- Becker, C. O., Pequito, S., Pappas, G. J., Miller, M. B., Grafton, S. T., Bassett, D. S., and Preciado, V. M. (2018). Spectral mapping of brain functional connectivity from diffusion imaging. *Scientific Reports*, 8(1):1–15.
- Beckmann, C. F., Mackay, C. E., Filippini, N., and Smith, S. M. (2009). Group comparison of resting-state fMRI data using multi-subject ICA and dual regression. *Neuroimage*, 47(Suppl. 1):s148.
- Betzel, R. F., Byrge, L., He, Y., Goñi, J., Zuo, X.-N., and Sporns, O. (2014). Changes in structural and functional connectivity among resting-state networks across the human lifespan. *NeuroImage*, 102:345–357.
- Betzel, R. F., Gu, S., Medaglia, J. D., Pasqualetti, F., and Bassett, D. S. (2016). Optimally controlling the human connectome: The role of network topology. *Scientific Reports*, 6:1–14.
- Bhinge, S., Mowakeaa, R., Calhoun, V. D., and Adali, T. (2019). Extraction of time-varying spatio-temporal networks using parameter-tuned constrained IVA. *IEEE Transactions on Medical Imaging*, page 1.
- Biswal, B., Yetkin, F. Z., Haughton, V. M., and Hyde, J. S. (1995). Functional connectivity in the motor cortex of resting human brain using echo-planar MRI Functional Connectivity in the Motor Cortex of Resting Human Brain Using Echo-Planar MRI. *Magnetic Resonance in Medicine*, 34(4):537–541.
- Bolton, T. A. W., Tarun, A., Sterpenich, V., Schwartz, S., and Van De Ville, D. (2018). Interactions Between Large-Scale Functional Brain Networks are Captured by Sparse Coupled HMMs. *IEEE Transactions on Medical Imaging*, 37(1):230–240.
- Braun, U., Harneit, A., Pergola, G., Merana, T., Schaefer, A., Betzel, R., Zang, Z., Schweiger, J. I., Schwartz, K., Chen, J., Blasi, G., Bertolino, A., Durstewitz, D., Pasqualetti, F., Schwarz, E., Meyer-Lindenberg, A., Bassett, D. S., and Tost, H. (2019). Brain state stability during working memory is explained by network control theory, modulated by dopamine D1/D2 receptor function, and diminished in schizophrenia. *bioRxiv preprint*, 679670.
- Braun, U., Schaefer, A., Betzel, R. F., Tost, H., Meyer-Lindenberg, A., and Bassett, D. S. (2018). From Maps to Multi-dimensional Network Mechanisms of Mental Disorders. *Neuron*, 97(1):14–31.

Bibliography

- Braun, U., Schäfer, A., Bassett, D. S., Rausch, F., Schweiger, J. I., Bilek, E., Erk, S., Romanczuk-Seiferth, N., Grimm, O., Geiger, L. S., Haddad, L., Otto, K., Mohnke, S., Heinz, A., Zink, M., Walter, H., Schwarz, E., Meyer-Lindenberg, A., and Tost, H. (2016). Dynamic brain network reconfiguration as a potential schizophrenia genetic risk mechanism modulated by NMDA receptor function. *Proceedings of the National Academy of Sciences*, 113(44):12568–12573.
- Bray, S. (2017). Age-associated patterns in gray matter volume, cerebral perfusion and BOLD oscillations in children and adolescents. *Human Brain Mapping*, 00(December 2016).
- Breakspear, M. (2017). Dynamic models of large-scale brain activity. *Nature neuroscience*, 20(3):340–352.
- Breakspear, M., Heitmann, S., and Daffertshofer, A. (2010). Generative Models of Cortical Oscillations: Neurobiological Implications of the Kuramoto Model. *Frontiers in Human Neuroscience*, 4(November):1–14.
- Britz, J., Van De Ville, D., and Michel, C. M. (2010). BOLD correlates of EEG topography reveal rapid resting-state network dynamics. *NeuroImage*, 52(4):1162–1170.
- Buckholtz, J. W. and Meyer-Lindenberg, A. (2012). Psychopathology and the Human Connectome: Toward a Transdiagnostic Model of Risk For Mental Illness. *Neuron*, 74(6):990–1004.
- Bullmore, E. and Sporns, O. (2009). Complex brain networks: graph theoretical analysis of structural and functional systems. *Nature Reviews Neuroscience*, 10(3):186–198.
- Bullmore, E. T. and Bassett, D. S. (2011). Brain Graphs: Graphical Models of the Human Brain Connectome. *Annu. Rev. Clin. Psychol.*, 7:113–40.
- Burgos-Robles, A., Vidal-Gonzalez, I., and Quirk, G. J. (2009). Sustained Conditioned Responses in Prelimbic Prefrontal Neurons Are Correlated with Fear Expression and Extinction Failure. *Journal of Neuroscience*, 29(26):8474–8482.
- Butcher, N. J., Boot, E., Lang, A. E., Andrade, D., Vorstman, J., McDonald-McGinn, D., and Bassett, A. S. (2018). Neuropsychiatric expression and catatonia in 22q11.2 deletion syndrome: An overview and case series. *American Journal of Medical Genetics Part A*, 176(10):2146–2159.
- Butler, P. D., Martinez, A., Foxe, J. J., Kim, D., Zemon, V., Silipo, G., Mahoney, J., Shpaner, M., Jalbrzikowski, M., and Javitt, D. C. (2007). Subcortical visual dysfunction in schizophrenia drives secondary cortical impairments. *Brain*, 130(2):417–430.
- Butler, P. D., Zemon, V., Schechter, I., Saperstein, A. M., Hoptman, M. J., Lim, K. O., Revheim, N., Silipo, G., and Javitt, D. C. (2005). Early-stage visual processing and cortical amplification deficits in schizophrenia. *Archives of General Psychiatry*, 62(5):495–504.
- Buxton, R. B., Wong, E. C., and Frank, L. R. (1998). Dynamics of blood flow and oxygenation changes during brain activation: the balloon model. *Magn Reson Med*, 39(17):855–864.

- Bzdok, D. and Meyer-Lindenberg, A. (2018). Machine Learning for Precision Psychiatry: Opportunities and Challenges. *Biological Psychiatry: Cognitive Neuroscience and Neuroimaging*, 3(3):223–230.
- Calhoun, V. D., Adali, T., Pearlson, G. D., and Pekar, J. J. (2001). A method for making group inferences from functional MRI data using independent component analysis. *Human brain mapping*, 14(3):140–151.
- Calhoun, V. D., Miller, R., Pearlson, G., Adali, T., and Adali, T. (2014). The Chronnectome: Time-Varying Connectivity Networks as the Next Frontier in fMRI Data Discovery. *Neuron*, 84(2):262–274.
- Calhoun, V. D., Potluru, V. K., Phlypo, R., Silva, R. F., Pearlmutter, B. A., Caprihan, A., Plis, S. M., and Adali, T. (2013). Independent Component Analysis for Brain fMRI Does Indeed Select for Maximal Independence. *PLoS ONE*, 8(8).
- Cao, M., Wang, Z., and He, Y. (2015). Connectomics in psychiatric research: advances and applications. *Neuropsychiatric Disease and Treatment*, 2015:11:2801–2810.
- Caspi, A., Houts, R. M., Belsky, D. W., Goldman-Mellor, S. J., Harrington, H., Israel, S., Meier, M. H., Ramrakha, S., Shalev, I., Poulton, R., and Moffitt, T. E. (2014). The p factor: One general psychopathology factor in the structure of psychiatric disorders? *Clinical Psychological Science*, 2(2):119–137.
- Catani, M., Howard, R. J., Pajevic, S., and Jones, D. K. (2002). Virtual in Vivo interactive dissection of white matter fasciculi in the human brain. *NeuroImage*, 17(1):77–94.
- Chang, C. and Glover, G. H. (2010). Time–frequency dynamics of resting-state brain connectivity measured with fMRI. *NeuroImage*, 50(1):81–98.
- Christoff, K., Irving, Z. C., Fox, K. C. R., Spreng, R. N., and Andrews-Hanna, J. R. (2016). Mind-wandering as spontaneous thought: a dynamic framework. *Nature Reviews Neuroscience*, 17(11):718–731.
- Cleveland, W. S. and Devlin, S. J. (1988). Locally Weighted Regression: An Approach to Regression Analysis by Local Fitting Locally Weighted Regression: An Approach to Regression Analysis by Local Fiting. *Source Journal of the American Statistical Association*, 83(403):596–610.
- Cohen, J. R. (2018). The behavioral and cognitive relevance of time-varying , dynamic changes in functional connectivity. *NeuroImage*, 180(Part B):515–525.
- Cole, M. W., Yang, G. J., Murray, J. D., Repovš, G., and Anticevic, A. (2016). Functional connectivity change as shared signal dynamics. *Journal of Neuroscience Methods*, 259:22–39.
- Collin, G., Turk, E., and Van Den Heuvel, M. P. (2016). Connectomics in Schizophrenia: From Early Pioneers to Recent Brain Network Findings. *Biological Psychiatry: Cognitive Neuroscience and Neuroimaging*, 1(3):199–208.

Bibliography

- Corcoran, K. A. and Quirk, G. J. (2007). Activity in Prelimbic Cortex Is Necessary for the Expression of Learned, But Not Innate, Fears. *Journal of Neuroscience*, 27(4):840–844.
- Córdova-Palomera, A., Kaufmann, T., Persson, K., Alnæs, D., Doan, N. T., Moberget, T., Lund, M. J., Barca, M. L., Engvig, A., Brækhus, A., Engedal, K., Andreassen, O. A., Selbæk, G., and Westlye, L. T. (2017). Disrupted global metastability and static and dynamic brain connectivity across individuals in the Alzheimer’s disease continuum. *Scientific Reports*, 7:40268.
- Cornblath, E. J., Ashourvan, A., Kim, J. Z., Betzel, R. F., Ciric, R., Baum, G. L., He, X., Ruparel, K., Moore, T. M., Gur, R. C., Gur, R. E., Shinohara, R. T., Roalf, D. R., Satterthwaite, T. D., and Bassett, D. S. (2018). Context-dependent architecture of brain state dynamics is explained by white matter connectivity and theories of network control. *bioRxiv preprint*, 412429.
- Cornblath, E. J., Tang, E., Baum, G. L., Moore, T. M., Adebimpe, A., Roalf, D. R., Gur, R. C., Gur, R. E., Pasqualetti, F., Satterthwaite, T. D., and Bassett, D. S. (2019). Sex differences in network controllability as a predictor of executive function in youth. *NeuroImage*, 188(December 2018):122–134.
- Courtin, J., Chaudun, F., Rozeske, R. R., Karalis, N., Gonzalez-Campo, C., Wurtz, H., Abdi, A., Baufreton, J., Bienvenu, T. C. M., and Herry, C. (2014). Prefrontal parvalbumin interneurons shape neuronal activity to drive fear expression. *Nature*, 505(7481):92–96.
- Cribben, I., Haraldsdottir, R., Atlas, L. Y., Wager, T. D., and Lindquist, M. A. (2012). Dynamic connectivity regression: Determining state-related changes in brain connectivity. *NeuroImage*, 61(4):907–920.
- Cui, Z., Stiso, J., Baum, G. L., Kim, J. Z., Roalf, D. R., Betzel, R. F., Gu, S., Lu, Z., Xia, C. H., Ciric, R., Moore, T. M., Shinohara, R. T., Ruparel, K., Davatzikos, C., Pasqualetti, F., Gur, R. E., Gur, R. C., Bassett, D. S., and Satterthwaite, T. D. (2018). Optimization of Energy State Transition Trajectory Supports the Development of Executive Function During Youth. *bioRxiv preprint*, 424929.
- Damadian, R., Goldsmith, M., and Minkoff, L. (1977). NMR in cancer: XVI. FONAR image of the live human body. *Physiological chemistry and physics*.
- Damaraju, E., Allen, E. A., Belger, A., Ford, J. M., McEwen, S., Mathalon, D. H., Mueller, B. A., Pearlson, G. D., Potkin, S. G., Preda, A., Turner, J. A., Vaidya, J. G., van Erp, T. G., and Calhoun, V. D. (2014). Dynamic functional connectivity analysis reveals transient states of dysconnectivity in schizophrenia. *NeuroImage: Clinical*, 5(July):298–308.
- Damoiseaux, J. S., Rombouts, S. a. R. B., Barkhof, F., Scheltens, P., Stam, C. J., Smith, S. M., and Beckmann, C. F. (2006). Consistent resting-state networks across healthy subjects. *Proceedings of the National Academy of Sciences*, 103(37):13848–13853.
- Daubechies, I., Roussos, E., Takerkart, S., Benharrosh, M., Golden, C., D’Ardenne, K., Richter, W., Cohen, J. D., and Haxby, J. (2009). Independent component analysis for brain fMRI does

- not select for independence. *Proceedings of the National Academy of Sciences of the United States of America*, 106(26):10415–10422.
- Davis, M., Walker, D. L., Miles, L., and Grillon, C. (2010). Phasic vs sustained fear in rats and humans: Role of the extended amygdala in fear vs anxiety. *Neuropsychopharmacology*, 35(1):105–135.
- Davis, T., LaRocque, K. F., Mumford, J. A., Norman, K. A., Wagner, A. D., and Poldrack, R. A. (2014). What do differences between multi-voxel and univariate analysis mean? How subject-, voxel-, and trial-level variance impact fMRI analysis. *NeuroImage*, 97:271–283.
- De Martino, F., Valente, G., Staeren, N., Ashburner, J., Goebel, R., and Formisano, E. (2008). Combining multivariate voxel selection and support vector machines for mapping and classification of fMRI spatial patterns. *NeuroImage*, 43(1):44–58.
- Debbané, M., Lazouret, M., Lagioia, A., Schneider, M., Van De Ville, D., and Eliez, S. (2012). Resting-state networks in adolescents with 22q11.2 deletion syndrome: Associations with prodromal symptoms and executive functions. *Schizophrenia Research*, 139(1-3):33–39.
- Deco, G., Jirsa, V. K., and McIntosh, A. R. (2011). Emerging concepts for the dynamical organization of resting-state activity in the brain. *Nature reviews. Neuroscience*, 12(1):43–56.
- Deco, G., Rolls, E. T., and Romo, R. (2009). Stochastic dynamics as a principle of brain function. *Progress in Neurobiology*, 88(1):1–16.
- Deng, Y., Liu, K., Cheng, D., Zhang, J., Chen, H., Chen, B., Li, Y., Wang, W., Kong, Y., and Wen, G. (2018). Ventral and dorsal visual pathways exhibit abnormalities of static and dynamic connectivities, respectively, in patients with schizophrenia. *Schizophrenia Research*.
- Di Martino, A., Yan, C.-G., Li, Q., Denio, E., Castellanos, F. X., Alaerts, K., Anderson, J. S., Assaf, M., Bookheimer, S. Y., Dapretto, M., Deen, B., Delmonte, S., Dinstein, I., Ertl-Wagner, B., Fair, D. A., Gallagher, L., Kennedy, D. P., Keown, C. L., Keyzers, C., Lainhart, J. E., Lord, C., Luna, B., Menon, V., Minshew, N. J., Monk, C. S., Mueller, S., Müller, R.-A., Nebel, M. B., Nigg, J. T., O’Hearn, K., Pelphey, K. A., Peltier, S. J., Rudie, J. D., Sunaert, S., Thioux, M., Tyszka, J. M., Uddin, L. Q., Verhoeven, J. S., Wenderoth, N., Wiggins, J. L., Mostofsky, S. H., and Milham, M. P. (2014). The autism brain imaging data exchange: towards a large-scale evaluation of the intrinsic brain architecture in autism. *Molecular Psychiatry*, 19(6):659–667.
- DiMartino, A., Fair, D. A., Kelly, C., Satterthwaite, T. D., Castellanos, F. X., Thomason, M. E., Craddock, R. C., Luna, B., Leventhal, B. L., Zuo, X. N., and Milham, M. P. (2014). Unraveling the miswired connectome: A developmental perspective. *Neuron*, 83(6):1335–1353.
- Dong, D., Duan, M., Wang, Y., Zhang, X., Jia, X., Li, Y., Xin, F., Yao, D., and Luo, C. (2018a). Reconfiguration of Dynamic Functional Connectivity in Sensory and Perceptual System in Schizophrenia. *Cerebral Cortex*.

Bibliography

- Dong, D., Wang, Y., Chang, X., Luo, C., and Yao, D. (2018b). Dysfunction of Large-Scale Brain Networks in Schizophrenia: A Meta-analysis of Resting-State Functional Connectivity. *Schizophrenia Bulletin*, 44(1):168–181.
- Du, Y., Fryer, S. L., Fu, Z., Lin, D., Sui, J., Chen, J., Damaraju, E., Mennigen, E., Stuart, B., Loewy, R. L., Mathalon, D. H., and Calhoun, V. D. (2018). Dynamic functional connectivity impairments in early schizophrenia and clinical high-risk for psychosis. *NeuroImage*, 180(Pt B):632–645.
- Du, Y., Pearlson, G. D., Yu, Q., He, H., Lin, D., Sui, J., Wu, L., and Calhoun, V. D. (2016). Interaction among subsystems within default mode network diminished in schizophrenia patients: A dynamic connectivity approach. *Schizophrenia Research*, 170(1):55–65.
- Duff, E. P., Makin, T., Smith, S. M., Woolrich, M. W., Cottaar, M., Smith, S. M., and Woolrich, M. W. (2018). Disambiguating brain functional connectivity. *NeuroImage*, 173(February):540–550.
- Dufour, F., Schaer, M., Debbané, M., Farhoumand, R., Glaser, B., and Eliez, S. (2008). Cingulate gyral reductions are related to low executive functioning and psychotic symptoms in 22q11.2 deletion syndrome. *Neuropsychologia*, 46(12):2986–2992.
- Ellison-Wright, I. and Bullmore, E. (2009). Meta-analysis of diffusion tensor imaging studies in schizophrenia. *Schizophrenia Research*, 108(1-3):3–10.
- Ered, A., Gibson, L. E., Maxwell, S. D., Cooper, S., and Ellman, L. M. (2017). Coping as a mediator of stress and psychotic-like experiences. *European Psychiatry*, 43:9–13.
- Erhardt, E. B., Rachakonda, S., Bedrick, E. J., Calhoun, V. D., and Allen, E. A. (2011). Comparison of Multi-Subject ICA Methods for Analysis of fMRI Data. *Human Brain Mapping*, 32(12):2075–2095.
- Etkin, A., Büchel, C., and Gross, J. J. (2015). The neural bases of emotion regulation. *Nature Reviews Neuroscience*, 16(11):693–700.
- Etkin, A., Egner, T., and Kalisch, R. (2011). Emotional processing in anterior cingulate and medial prefrontal cortex. *Trends in Cognitive Sciences*, 15(2):85–93.
- Etkin, A. and Wager, T. (2007). Reviews and Overviews Functional Neuroimaging of Anxiety : A Meta-Analysis of Emotional Processing in PTSD , Social Anxiety Disorder , and Specific Phobia. *The American Journal of Psychiatry*, 164(October):1476–1488.
- Fair, D. A., Cohen, A. L., Dosenbach, N. U. F., Church, J. a., Miezin, F. M., Barch, D. M., Raichle, M. E., Petersen, S. E., and Schlaggar, B. L. (2008). The maturing architecture of the brain's default network. *Proceedings of the National Academy of Sciences*, 105(10):4028–4032.
- Faisal, A. A., Selen, L. P. J., and Wolpert, D. M. (2008). Noise in the nervous system. *Nature Reviews Neuroscience*, 9(april):292–303.

- Farouj, Y., Karahanoglu, F. I., and Van De Ville, D. (2017). Regularized Spatiotemporal Deconvolution of fMRI Data Using Gray-Matter Constrained Total Variation. *Proceedings of the 14th IEEE International Symposium on Biomedical Imaging: From Nano to Macro (ISBI'17)*, pages 472–475.
- First, M., Gibbon, M., Spitzer, R., Williams, J., and Benjamin, L. (1996). Structured Clinical Interview for the DSM-IV Axis I Disorders (SCID-I). *Washington, DC: American Psychiatric Association*.
- Fornito, A., Yücel, M., Dean, B., Wood, S. J., and Pantelis, C. (2009). Anatomical abnormalities of the anterior cingulate cortex in schizophrenia: Bridging the gap between neuroimaging and neuropathology. *Schizophrenia Bulletin*, 35(5):973–993.
- Fornito, A., Yung, A. R., Wood, S. J., Phillips, L. J., Nelson, B., Cotton, S., Velakoulis, D., McGorry, P. D., Pantelis, C., and Yücel, M. (2008). Anatomic Abnormalities of the Anterior Cingulate Cortex Before Psychosis Onset: An MRI Study of Ultra-High-Risk Individuals. *Biological Psychiatry*, 64(9):758–765.
- Fornito, A., Zalesky, A., Pantelis, C., and Bullmore, E. T. (2012). Schizophrenia, neuroimaging and connectomics. *NeuroImage*, 62(4):2296–2314.
- Fox, A. S. and Kalin, N. H. (2014). A translational neuroscience approach to understanding the development of social anxiety disorder and its pathophysiology. *American Journal of Psychiatry*, 171(11):1162–1173.
- Fox, A. S., Oler, J. A., Shelton, S. E., Nanda, S. A., Davidson, R. J., Roseboom, P. H., and Kalin, N. H. (2012). Central amygdala nucleus (Ce) gene expression linked to increased trait-like Ce metabolism and anxious temperament in young primates. *Proceedings of the National Academy of Sciences*, 109(44):18108–18113.
- Fox, A. S., Shelton, S. E., Oakes, T. R., Davidson, R. J., and Kalin, N. H. (2008). Trait-like brain activity during adolescence predicts anxious temperament in primates. *PLoS ONE*, 3(7):e2570.
- Fox, M. D., Snyder, A. Z., Vincent, J. L., Corbetta, M., Van Essen, D. C., and Raichle, M. E. (2005). From The Cover: The human brain is intrinsically organized into dynamic, anticorrelated functional networks. *Proceedings of the National Academy of Sciences*, 102(27):9673–9678.
- Fox, P. T. and Lancaster, J. L. (2002). Mapping context and content: The BrainMap model. *Nature Reviews Neuroscience*, 3(4):319–321.
- Friston, K. J. (1994). Functional and effective connectivity in neuroimaging: A synthesis. *Human Brain Mapping*, 2(1-2):56–78.
- Friston, K. J. (1998). The disconnection hypothesis. *Schizophrenia Research*, 30(2):115–125.
- Friston, K. J. and Frith, C. D. (1995). Schizophrenia: A Disconnection Syndrome? *Clinical Neuroscience*, 3:89–97.

Bibliography

- Friston, K. J., Williams, S., Howard, R., Frackowiak, R. S., and Turner, R. (1996). Movement-related effects in fMRI time-series. *Magnetic resonance in medicine : official journal of the Society of Magnetic Resonance in Medicine / Society of Magnetic Resonance in Medicine*, 35(3):346–355.
- Fryer, S. L., Roach, B. J., Wiley, K., Loewy, R. L., Ford, J. M., and Mathalon, D. H. (2016). Reduced amplitude of low-frequency brain oscillations in the psychosis risk syndrome and early illness schizophrenia. *Neuropsychopharmacology*, 41(9):2388–2398.
- Fung, W. L. A., Butcher, N. J., Costain, G., Andrade, D. M., Boot, E., Chow, E. W., Chung, B., Cytrynbaum, C., Faghfoury, H., Fishman, L., García-Miñaur, S., George, S., Lang, A. E., Repetto, G., Shugar, A., Silversides, C., Swillen, A., van Amelsvoort, T., McDonald-McGinn, D. M., and Bassett, A. S. (2015). Practical guidelines for managing adults with 22q11.2 deletion syndrome. *Genetics in Medicine*, 17(8):599–609.
- Fung, W. L. A., McEvilly, R., Fong, J., Silversides, C., Chow, E., and Bassett, A. (2010). Elevated Prevalence of Generalized Anxiety Disorder in Adults With 22q11.2 Deletion Syndrome. *American Journal of Psychiatry*, 167(8):998–998.
- Fusar-Poli, P. (2017a). The Clinical High-Risk State for Psychosis (CHR-P), Version II. *Schizophrenia Bulletin*, 43(1):44–47.
- Fusar-Poli, P. (2017b). Why ultra high risk criteria for psychosis prediction do not work well outside clinical samples and what to do about it. *World Psychiatry*, 16(2):212–213.
- Fusar-Poli, P., Bonoldi, I., Yung, A. R., Borgwardt, S., Kempton, M. J., Valmaggia, L., Barale, E., Caverzasi, E., and McGuire, P. (2012). Predicting Psychosis: Meta-analysis of Transition Outcomes in Individuals at High Clinical Risk. *Archives of General Psychiatry*, 69(3):220–229.
- Fusar-Poli, P., Borgwardt, S., Bechdolf, A., Addington, J., Riecher-Rössler, A., Schultze-Lutter, E., Keshavan, M., Wood, S., Ruhrmann, S., Seidman, L. J., Valmaggia, L., Cannon, T., Velthorst, E., De Haan, L., Cornblatt, B., Bonoldi, I., Birchwood, M., McGlashan, T., Carpenter, W., McGorry, P., Klosterkötter, J., McGuire, P., and Yung, A. (2013). The Psychosis High-Risk State. *JAMA Psychiatry*, 70(1):107.
- Gao, J. and Liu, Y.-y. (2014). Target control of complex networks. *Nature Communications*, 5:5415.
- Garrett, D. D., Epp, S. M., Perry, A., and Lindenberger, U. (2018). Local temporal variability reflects functional integration in the human brain. *NeuroImage*, 183(June):776–787.
- Garrett, D. D., Kovacevic, N., McIntosh, A. R., and Grady, C. L. (2011). The Importance of Being Variable. *Journal of Neuroscience*, 31(12):4496–4503.
- Garrett, D. D., Kovacevic, N., McIntosh, A. R., and Grady, C. L. (2013a). The Modulation of BOLD Variability between Cognitive States Varies by Age and Processing Speed. *Cerebral Cortex*, 23(3):684–693.

- Garrett, D. D., McIntosh, A. R., and Grady, C. L. (2014). Brain Signal Variability is Parametrically Modifiable. *Cerebral Cortex*, 24(11):2931–2940.
- Garrett, D. D., Samanez-Larkin, G. R., MacDonald, S. W. S., Lindenberger, U., McIntosh, A. R., and Grady, C. L. (2013b). Moment-to-moment brain signal variability: A next frontier in human brain mapping? *Neuroscience and Biobehavioral Reviews*, 37(4):610–624.
- Ghosh, A., Rho, Y., McIntosh, A. R., Kötter, R., and Jirsa, V. K. (2008). Noise during rest enables the exploration of the brain's dynamic repertoire. *PLoS Computational Biology*, 4(10).
- Giedd, J. N., Blumenthal, J., Jeffries, N. O., Castellanos, F. X., Liu, H., Zijdenbos, A., Paus, T., Evans, A. C., and Rapoport, J. L. (1999). Brain development during childhood and adolescence : A longitudinal MRI study. *Nature Neuroscience*, pages 861–863.
- Gogtay, N., Giedd, J. N., Lusk, L., Hayashi, K. M., Greenstein, D., Vaituzis, A. C., Nugent III, T. F., Herman, D. H., Clasen, L. S., Toga, A. W., Rapoport, J. L., and Thompson, P. M. (2004). Dynamic mapping of human cortical development during childhood through early adulthood. *Proc.Natl.Acad.Sci.U.S.A*, 101(21):8174–8179.
- Goñi, J., van den Heuvel, M. P., Avena-Koenigsberger, A., Velez de Mendizabal, N., Betzel, R. F., Griffa, A., Hagmann, P., Corominas-Murtra, B., Thiran, J.-P., and Sporns, O. (2014). Resting-brain functional connectivity predicted by analytic measures of network communication. *Proceedings of the National Academy of Sciences*, 111(2):833–8.
- Goodkind, M., Eickhoff, S. B., Oathes, D. J., Jiang, Y., Chang, A., Jones-Hagata, L. B., Ortega, B. N., Zaiko, Y. V., Roach, E. L., Korgaonkar, M. S., Grieve, S. M., Galatzer-Levy, I., Fox, P. T., and Etkin, A. (2015). Identification of a common neurobiological substrate for mental illness. *JAMA Psychiatry*, 72(4):305–315.
- Gopal, S., Miller, R. L., Michael, A., Adali, T., Cetin, M., Rachakonda, S., Bustillo, J. R., Cahill, N., Baum, S. A., and Calhoun, V. D. (2016). Spatial Variance in Resting fMRI Networks of Schizophrenia Patients: An Independent Vector Analysis. *Schizophrenia Bulletin*, 42(1):152–160.
- Gore, F. M., Bloem, P. J., Patton, G. C., Ferguson, J., Joseph, V., Coffey, C., Sawyer, S. M., and Mathers, C. D. (2011). Global burden of disease in young people aged 10-24 years: A systematic analysis. *The Lancet*, 377(9783):2093–2102.
- Gothelf, D., Feinstein, C., Thompson, T., Gu, E., Penniman, L., Van Stone, E., Kwon, H., Eliez, S., and Reiss, A. L. (2007). Risk factors for the emergence of psychotic disorders in adolescents with 22q11.2 deletion syndrome. *American Journal of Psychiatry*, 164(4):663–669.
- Gothelf, D., Hoeft, F., Ueno, T., Sugiura, L., Lee, A. D., Thompson, P., and Reiss, A. L. (2011). Developmental changes in multivariate neuroanatomical patterns that predict risk for psychosis in 22q11.2 deletion syndrome. *Journal of Psychiatric Research*, 45(3):322–331.

Bibliography

- Gothelf, D., Schaer, M., and Eliez, S. (2008). Genes, brain development and psychiatric phenotypes in velo-cardio-facial syndrome. *Developmental disabilities research reviews*, 14(1):59–68.
- Gothelf, D., Schneider, M., Green, T., Debbané, M., Frisch, A., Glaser, B., Zilkha, H., Schaer, M., Weizman, A., and Eliez, S. (2013). Risk factors and the evolution of psychosis in 22q11.2 deletion syndrome: A longitudinal 2-site study. *Journal of the American Academy of Child and Adolescent Psychiatry*, 52(11).
- Grady, C. L. and Garrett, D. D. (2014). Understanding variability in the BOLD signal and why it matters for aging. *Brain Imaging and Behavior*, 8(2):274–283.
- Greicius, M. D., Krasnow, B., Reiss, A. L., and Menon, V. (2003). Functional connectivity in the resting brain: A network analysis of the default mode hypothesis, *Proc. Natl. Acad. Sci. U. S. A.*, 100(1):253–258.
- Gu, S., Betzel, R. F., Mattar, M. G., Cieslak, M., Delio, P. R., Grafton, S. T., Pasqualetti, F., and Bassett, D. S. (2017). Optimal trajectories of brain state transitions. *NeuroImage*, 148(January):305–317.
- Gu, S., Pasqualetti, F., Cieslak, M., Telesford, Q. K., Yu, A. B., Kahn, A. E., Medaglia, J. D., Vettel, J. M., Miller, M. B., Grafton, S. T., and Bassett, D. S. (2015). Controllability of structural brain networks. *Nature Communications*, 6:8414.
- Guo, S., Zhao, W., Tao, H., Liu, Z., and Palaniyappan, L. (2018). The instability of functional connectivity in patients with schizophrenia and their siblings: A dynamic connectivity study. *Schizophrenia Research*, 195:183–189.
- Han, Y., Wang, J., Zhao, Z., Min, B., Lu, J., Li, K., He, Y., and Jia, J. (2011). Frequency-dependent changes in the amplitude of low-frequency fluctuations in amnesic mild cognitive impairment: A resting-state fMRI study. *NeuroImage*, 55(1):287–295.
- Hart, M. G., Price, S. J., and Suckling, J. (2017). Functional connectivity networks for preoperative brain mapping in neurosurgery. *Journal of Neurosurgery*, 126(6):1747–2058.
- Hasenkamp, W., James, G. A., Boshoven, W., and Duncan, E. (2011). Altered engagement of attention and default networks during target detection in schizophrenia. *Schizophrenia Research*, 125(2-3):169–173.
- Hearne, L. J., Lin, H.-y., Sanz-leon, P., Tseng, W.-y. I., and Shur-fen, S. (2019). ADHD symptoms map onto noise-driven structure-function decoupling between hub and peripheral brain regions. *bioRxiv preprint*, 606228.
- Honey, C. J., Sporns, O., Cammoun, L., Gigandet, X., Thiran, J. P., Meuli, R., and Hagmann, P. (2009). Predicting human resting-state functional connectivity. *Proceedings of the National Academy of Sciences*, 106(6):2035–2040.

- Hoptman, M. J., Zuo, X. N., Butler, P. D., Javitt, D. C., D'Angelo, D., Mauro, C. J., and Milham, M. P. (2010). Amplitude of low-frequency oscillations in schizophrenia: A resting state fMRI study. *Schizophrenia Research*, 117(1):13–20.
- Huang, W., Bolton, T. A. W., Medaglia, J. D., Bassett, D. S., Ribeiro, A., and Van De Ville, D. (2018). A Graph Signal Processing Perspective on Functional Brain Imaging. *Proceedings of the IEEE*, 106(5):1–18.
- Huang, Z., Zhang, J., Wu, J., Qin, P., Wu, X., Wang, Z., Dai, R., Li, Y., Liang, W., Mao, Y., Yang, Z., Zhang, J., Wolff, A., and Northoff, G. (2016). Decoupled temporal variability and signal synchronization of spontaneous brain activity in loss of consciousness: An fMRI study in anesthesia. *NeuroImage*, 124:693–703.
- Huettel, S. A., Song, A. W., and McCarthy, G. (2014). Functional Magnetic Resonance Imaging, Third Edition. *Functional Magnetic Resonance Imaging, Third Edition*.
- Hutchison, R. M. and Morton, J. B. (2015). Tracking the Brain's Functional Coupling Dynamics over Development. *Journal of Neuroscience*, 35(17):6849–6859.
- Hutchison, R. M. and Morton, J. B. (2016). It's a matter of time: Reframing the development of cognitive control as a modification of the brain's temporal dynamics. *Developmental Cognitive Neuroscience*, 18:70–77.
- Hutchison, R. M., Womelsdorf, T., Allen, E. A., Bandettini, P. A., Calhoun, V. D., Corbetta, M., Della Penna, S., Duyn, J. H., Glover, G. H., Gonzalez-Castillo, J., Handwerker, D. A., Keilholz, S., Kiviniemi, V., Leopold, D. A., de Pasquale, F., Sporns, O., Walter, M., and Chang, C. (2013a). Dynamic functional connectivity: Promise, issues, and interpretations. *NeuroImage*, 80(4):360–378.
- Hutchison, R. M., Womelsdorf, T., Gati, J. S., Everling, S., and Menon, R. S. (2013b). Resting-state networks show dynamic functional connectivity in awake humans and anesthetized macaques. *Human Brain Mapping*, 34(9):2154–2177.
- Insel, T. R. (2010). Rethinking schizophrenia. *Nature*, 468(7321):187–193.
- Insel, T. R. and Cuthbert, B. N. (2015). Brain disorders? Precisely. *Science*, 348(6234):499–500.
- Jalbrzikowski, M., Jonas, R., Senturk, D., Patel, A., Chow, C., Green, M. F., and Bearden, C. E. (2013). Structural abnormalities in cortical volume, thickness, and surface area in 22q11.2 microdeletion syndrome: Relationship with psychotic symptoms. *NeuroImage: Clinical*, 3:405–415.
- Jbabdi, S., Sotiropoulos, S. N., Haber, S. N., Van Essen, D. C., and Behrens, T. E. (2015). Measuring macroscopic brain connections in vivo. *Nature Neuroscience*, 18(11):1546–1555.

Bibliography

- Jeganathan, J., Perry, A., Bassett, D. S., Roberts, G., Mitchell, P. B., and Breakspear, M. (2018). Fronto-limbic dysconnectivity leads to impaired brain network controllability in young people with bipolar disorder and those at high genetic risk. *NeuroImage: Clinical*, 19(March):71–81.
- Jenkinson, M., Beckmann, C. F., Behrens, T. E., Woolrich, M. W., and Smith, S. M. (2012). Fsl. *NeuroImage*, 62(2):782–790.
- Jung, W. H., Jang, J. H., Byun, M. S., An, S. K., and Kwon, J. S. (2010). Structural brain alterations in individuals at ultra-high risk for psychosis: A review of magnetic resonance imaging studies and future directions. *Journal of Korean Medical Science*, 25(12):1700–1709.
- Kaczurkin, A. N., Moore, T. M., Ruparel, K., Ciric, R., Calkins, M. E., Shinohara, R. T., Elliott, M. A., Hopson, R., Roalf, D. R., Vandekar, S. N., Gennatas, E. D., Wolf, D. H., Scott, J. C., Pine, D. S., Leibenluft, E., Detre, J. A., Foa, E. B., Gur, R. E., Gur, R. C., and Satterthwaite, T. D. (2016). Elevated Amygdala Perfusion Mediates Developmental Sex Differences in Trait Anxiety. *Biol Psychiatry*, 80(10):775–785.
- Kalman, R. E. (1960). A New Approach to Linear Filtering and Prediction Problems. *Journal of Basic Engineering*, 82(1):35–45.
- Kang, J., Wang, L., Yan, C., Wang, J., Liang, X., and He, Y. (2011). Characterizing dynamic functional connectivity in the resting brain using variable parameter regression and Kalman filtering approaches. *NeuroImage*, 56(3):1222–1234.
- Kapur, S. (2003). Psychosis as a state of aberrant salience: a framework linking biology, phenomenology, and pharmacology in schizophrenia. *American journal of Psychiatry*, 160(1):13–23.
- Kapur, S., Phillips, A. G., and Insel, T. R. (2012). Why has it taken so long for biological psychiatry to develop clinical tests and what to do about it. *Molecular Psychiatry*, 17(12):1174–1179.
- Karahanoglu, F. I., Bayram, I., and Van De Ville, D. (2011). A Signal Processing Approach to Generalized 1-D Total Variation. *IEEE Transactions on Signal Processing*, 59(11):5265–5274.
- Karahanoglu, F. I., Caballero-Gaudes, C., Lazeyras, F., and Van De Ville, D. (2013). Total activation: FMRI deconvolution through spatio-temporal regularization. *NeuroImage*, 73:121–134.
- Karahanoglu, F. I. and Van De Ville, D. (2017). Dynamics of Large-Scale fMRI Networks: Deconstruct Brain Activity to Build Better Models of Brain Function. *Current Opinion in Biomedical Engineering*, 3:28–36.
- Karahanoglu, F. I., Van De Ville, D., Karahanoğlu, F. I., and Van De Ville, D. (2015). Transient brain activity disentangles fMRI resting-state dynamics in terms of spatially and temporally overlapping networks. *Nature Communications*, 6:7751.

- Karayiorgou, M., Simon, T. J., and Gogos, J. A. (2010). 22q11.2 microdeletions: linking DNA structural variation to brain dysfunction and schizophrenia. *Nature reviews. Neuroscience*, 11(6):402–16.
- Karlsgodt, K. H., van Erp, T. G. M., Bearden, C. E., and Cannon, T. D. (2014). Altered relationships between age and functional brain activation in adolescents at clinical high risk for psychosis. *Psychiatry Research - Neuroimaging*, 221(1):21–29.
- Kates, W. R., Olszewski, A. K., Gnirke, M. H., Kikinis, Z., Nelson, J., Antshel, K. M., Fremont, W., Radoeva, P. D., Middleton, F. A., Shenton, M. E., and Coman, I. L. (2015a). White matter microstructural abnormalities of the cingulum bundle in youths with 22q11.2 deletion syndrome: Associations with medication, neuropsychological function, and prodromal symptoms of psychosis. *Schizophrenia Research*, 161(1):76–84.
- Kates, W. R., Russo, N., Wood, W. M., Antshel, K. M., Faraone, S. V., and Fremont, W. P. (2015b). Neurocognitive and familial moderators of psychiatric risk in velocardiofacial (22q11.2 deletion) syndrome: A longitudinal study. *Psychological Medicine*, 45(8):1629–1639.
- Kaufman, J., Birmaher, B., Brent, D., Rao, U., Flynn, C., Moreci, P., Williamson, D., and Ryan, N. (1997). Schedule for Affective Disorders and Schizophrenia for School-Age Children-Present and Lifetime Version (K-SADS-PL): Initial Reliability and Validity Data. *Journal of the American Academy of Child & Adolescent Psychiatry*, 36(7):980–988.
- Kessler, R. C., Berglund, P., Demler, O., Ma, R., Jin, M. A., Merikangas, K. R., and Walters, E. E. (2005). Lifetime Prevalence and Age-of-Onset Distributions of DSM-IV Disorders in the National Comorbidity Survey Replication. *Archives of General Psychiatry*, 62:593–602.
- Khalidov, I., Fadili, J., Lazeyras, F., Van De Ville, D., and Unser, M. (2011). Activelets: Wavelets for sparse representation of hemodynamic responses. *Signal Processing*, 91(12):2810–2821.
- Khambhati, A. N., Kahn, A. E., Costantini, J., Ezzyat, Y., Solomon, E. A., Gross, R. E., Jobst, B. C., Sheth, S. A., Zaghloul, K. A., Worrell, G., Seger, S., Lega, B. C., Weiss, S., Sperling, M. R., Gorniak, R., Das, S. R., Stein, J. M., Rizzuto, D. S., Kahana, M. J., Lucas, T. H., Davis, K. A., Tracy, J. I., and Bassett, D. S. (2019). Functional control of electrophysiological network architecture using direct neurostimulation in humans. *Network Neuroscience*, 0(ja):1–46.
- Kikinis, Z., Cho, K. I. K., Coman, I. L., Radoeva, P. D., Bouix, S., Tang, Y., Eckbo, R., Makris, N., Kwon, J. S., Kubicki, M., Antshel, K. M., Fremont, W., Shenton, M. E., and Kates, W. R. (2016). Abnormalities in brain white matter in adolescents with 22q11.2 deletion syndrome and psychotic symptoms. *Brain Imaging and Behavior*, 11(5):1353–1364.
- Kikinis, Z., Makris, N., Finn, C. T., Bouix, S., Lucia, D., Coleman, M. J., Tworog-Dube, E., Kikinis, R., Kucherlapati, R., Shenton, M. E., and Kubicki, M. (2013). Genetic contributions to changes of fiber tracts of ventral visual stream in 22q11.2 deletion syndrome. *Brain Imaging and Behavior*, 7(3):316–325.

Bibliography

- Kim, J. Z. and Bassett, D. S. (2019). Linear Dynamics & Control of Brain Networks. *arXiv preprint*, 1902.03309.
- Kim, J. Z., Soffer, J. M., Kahn, A. E., Vettel, J. M., Pasqualetti, F., and Bassett, D. S. (2018). Role of graph architecture in controlling dynamical networks with applications to neural systems. *Nature Physics*, 14(1):91–98.
- Kohno, T., Shiga, T., Kusumi, I., Matsuyama, T., Kageyama, H., Katoh, C., Koyama, T., and Tamaki, N. (2006). Left temporal perfusion associated with suspiciousness score on the Brief Psychiatric Rating Scale in schizophrenia. *Psychiatry Research - Neuroimaging*, 147(2-3):163–171.
- Kremen, W. S., Vinogradov, S., Poole, J. H., Schaefer, C. A., Deicken, R. F., Factor-Litvak, P., and Brown, A. S. (2010). Cognitive decline in schizophrenia from childhood to midlife: A 33-year longitudinal birth cohort study. *Schizophrenia Research*, 118(1-3):1–5.
- Krishnan, A., Williams, L. J., McIntosh, A. R., and Abdi, H. (2011). Partial Least Squares (PLS) methods for neuroimaging: A tutorial and review. *NeuroImage*, 56(2):455–475.
- Kucyi, A., Salomons, T. V., and Davis, K. D. (2013). Mind wandering away from pain dynamically engages antinociceptive and default mode brain networks. *Proceedings of the National Academy of Sciences*, 110(46):18692–18697.
- Lai, M. C., Lombardo, M. V., Chakrabarti, B., Sadek, S. A., Pasco, G., Wheelwright, S. J., Bullmore, E. T., Baron-Cohen, S., and Suckling, J. (2010). A shift to randomness of brain oscillations in people with autism. *Biological Psychiatry*, 68(12):1092–1099.
- Laloyaux, J., Dessart, G., Van Der Linden, M., Lemaire, M., and Larøi, F. (2016). Maladaptive emotion regulation strategies and stress sensitivity mediate the relation between adverse life events and attenuated positive psychotic symptoms. *Cognitive Neuropsychiatry*, 21(2):116–129.
- Larsen, K. M., Dzaif, I., Siebner, H. R., and Garrido, M. I. (2018). Alteration of functional brain architecture in 22q11.2 deletion syndrome – Insights into susceptibility for psychosis. *NeuroImage*, 190(September 2018):154–171.
- Larson, R. and Csikszentmihalyi, M. (2014). The experience sampling method. In *Flow and the Foundations of Positive Psychology*. Springer, Dordrecht.
- Laumann, T. O., Gordon, E. M., Adeyemo, B., Snyder, A. Z., Joo, S. J. u., Chen, M. Y., Gilmore, A. W., McDermott, K. B., Nelson, S. M., Dosenbach, N. U. F., Schlaggar, B. L., Mumford, J. A., Poldrack, R. A., and Petersen, S. E. (2015). Functional System and Areal Organization of a Highly Sampled Individual Human Brain. *Neuron*, 87(3):657–670.
- Lauterbur, P. C. (1973). Image formation by induced local interactions: Examples employing nuclear magnetic resonance. *Nature*, 242(March 16):190–191.

- Le Bihan, D. and Iima, M. (2015). Diffusion magnetic resonance imaging: What water tells us about biological tissues. *PLoS Biology*, 13(7):1–13.
- Le Bihan, D. and Johansen-Berg, H. (2012). Diffusion MRI at 25: Exploring brain tissue structure and function. *NeuroImage*, 61(2):324–341.
- LeDoux, J. E. (2000). Emotion Circuits in the Brain. *Annual Review of Neuroscience*, 23(1):155–184.
- Lee, M., Smyser, C., and Shimony, J. (2013). Resting-State fMRI: A Review of Methods and Clinical Applications. *Oxford College of Marketing*, 34(10):1866–1872.
- Lefaucheur, J. P., Antal, A., Ayache, S. S., Benninger, D. H., Brunelin, J., Cogiamanian, F., Cotelli, M., De Ridder, D., Ferrucci, R., Langguth, B., Marangolo, P., Mylius, V., Nitsche, M. A., Padberg, F., Palm, U., Poulet, E., Priori, A., Rossi, S., Schecklmann, M., Vanneste, S., Ziemann, U., Garcia-Larrea, L., and Paulus, W. (2017). Evidence-based guidelines on the therapeutic use of transcranial direct current stimulation (tDCS). *Clinical Neurophysiology*, 128(1):56–92.
- Leonardi, N., Richiardi, J., Gschwind, M., Simioni, S., Annoni, J.-M. M., Schluep, M., Vuilleumier, P., and Van De Ville, D. (2013). Principal components of functional connectivity: A new approach to study dynamic brain connectivity during rest. *NeuroImage*, 83:937–950.
- Leonardi, N. and Van De Ville, D. (2015). On spurious and real fluctuations of dynamic functional connectivity during rest. *NeuroImage*, 104:430–436.
- Lewandowski, K. E., Shashi, V., Berry, P. M., and Kwapil, T. R. (2007). Schizophrenic-like neurocognitive deficits in children and adolescents with 22q11 deletion syndrome. *American Journal of Medical Genetics, Part B: Neuropsychiatric Genetics*, 144(1):27–36.
- Li, Z., Lei, W., Deng, W., Zheng, Z., Li, M., Ma, X., Wang, Q., Huang, C., Li, N., Collier, D. A., Gong, Q., and Li, T. (2017). Aberrant spontaneous neural activity and correlation with evoked-brain potentials in first-episode, treatment-naïve patients with deficit and non-deficit schizophrenia. *Psychiatry Research - Neuroimaging*, 261(April 2016):9–19.
- Lindmark, G. and Altafini, C. (2018). Minimum energy control for complex networks. *Scientific Reports*, 8(1):1–14.
- Lippé, S., Kovacevic, N., and McIntosh, A. R. (2009). Differential maturation of brain signal complexity in the human auditory and visual system. *Frontiers in human neuroscience*, 3(November):48.
- Liu, C., Xue, Z., Palaniyappan, L., Zhou, L., Liu, H., Qi, C., Wu, G., Mwansisya, T. E., Tao, H., Chen, X., Huang, X., Liu, Z., and Pu, W. (2016). Abnormally increased and incoherent resting-state activity is shared between patients with schizophrenia and their unaffected siblings. *Schizophrenia Research*.

Bibliography

- Liu, X., Chang, C., and Duyn, J. H. (2013). Decomposition of spontaneous brain activity into distinct fMRI co-activation patterns. *Frontiers in Systems Neuroscience*, 7(December):1–11.
- Liu, X. and Duyn, J. H. (2013). Time-varying functional network information extracted from brief instances of spontaneous brain activity. *Proceedings of the National Academy of Sciences of the United States of America*, 110(11):4392–4397.
- Liu, X., Wang, S., Zhang, X., Wang, Z., Tian, X., and He, Y. (2014). Abnormal amplitude of low-frequency fluctuations of intrinsic brain activity in Alzheimer's disease. *Journal of Alzheimer's Disease*, 40(2):387–397.
- Liu, Y. Y., Slotine, J. J., and Barabási, A. L. (2011). Controllability of complex networks. *Nature*, 473(7346):167–173.
- Lord, L. D., Allen, P., Expert, P., Howes, O., Lambiotte, R., McGuire, P., Bose, S. K., Hyde, S., and Turkheimer, F. E. (2011). Characterization of the anterior cingulate's role in the at-risk mental state using graph theory. *NeuroImage*, 56(3):1531–1539.
- Lottman, K. K., Kraguljac, N. V., White, D. M., Morgan, C. J., Calhoun, V. D., Butt, A., and Lahti, A. C. (2017). Risperidone Effects on Brain Dynamic Connectivity—A Prospective Resting-State fMRI Study in Schizophrenia. *Frontiers in Psychiatry*, 8:14.
- Lynn, C. W. and Bassett, D. S. (2019). The physics of brain network structure, function and control. *Nature Reviews Physics*, 1(5):318–332.
- Maeder, J., Schneider, M., Bostelmann, M., Debbané, M., Glaser, B., Menghetti, S., Schaer, M., and Eliez, S. (2016). Developmental trajectories of executive functions in 22q11.2 deletion syndrome. *Journal of Neurodevelopmental Disorders*, 8(1):10.
- Malaspina, D., Storer, S., Furman, V., Esser, P., Printz, D., Berman, A., Lignelli, A., Gorman, J., and Van Heertum, R. (1999). SPECT study of visual fixation in schizophrenia and comparison subjects. *Biological Psychiatry*, 46(1):89–93.
- Maren, S. and Quirk, G. J. (2004). Neuronal signalling of fear memory. *Nature Reviews Neuroscience*, 5(11):844–852.
- Margulies, D. S., Ghosh, S. S., Goulas, A., Falkiewicz, M., and Huntenburg, J. M. (2016). Situating the default-mode network along a principal gradient of macroscale cortical organization. *Proceedings of the National Academy of Sciences*, 113(44):12574–12579.
- Marín, O. (2016). Developmental timing and critical windows for the treatment of psychiatric disorders. *Nature Medicine*, 22(11):1229–1238.
- Mattiaccio, L. M., Coman, I. L., Schreiner, M. J., Antshel, K. M., Fremont, W. P., Bearden, C. E., and Kates, W. R. (2016). Atypical functional connectivity in resting-state networks of individuals with 22q11.2 deletion syndrome: associations with neurocognitive and psychiatric functioning. *Journal of Neurodevelopmental Disorders*, 8(1):2.

- Mattiaccio, L. M., Coman, I. L., Thompson, C. A., Fremont, W. P., Antshel, K. M., and Kates, W. R. (2018). Frontal dysconnectivity in 22q11.2 deletion syndrome: an atlas-based functional connectivity analysis. *Behavioral and Brain Functions*, 14(1):2.
- McDonald-McGinn, D. M. and Sullivan, K. E. (2011). Chromosome 22q11.2 Deletion Syndrome (DiGeorge Syndrome/Velocardiofacial Syndrome). *Medicine*, 90(1):1–18.
- McDonald-McGinn, D. M., Sullivan, K. E., Marino, B., Philip, N., Swillen, A., Vorstman, J. A. S., Zackai, E. H., Emanuel, B. S., Vermeesch, J. R., Morrow, B. E., Scambler, P. J., and Bassett, A. S. (2015). 22q11.2 deletion syndrome. *Nature Reviews Disease Primers*, 1(November):15071.
- McIntosh, A., Chau, W., and Protzner, A. (2004). Spatiotemporal analysis of event-related fMRI data using partial least squares. *NeuroImage*, 23(2):764–775.
- McIntosh, A. R., Kovacevic, N., and Itier, R. J. (2008). Increased brain signal variability accompanies lower behavioral variability in development. *PLoS Computational Biology*, 4(7).
- McIntosh, A. R., Kovacevic, N., Lippe, S., Garrett, D., Grady, C., and Jirsa, V. (2010). The development of a noisy brain. *Archives Italiennes de Biologie*, 148(3):323–337.
- McIntosh, A. R. and Lobaugh, N. J. (2004). Partial least squares analysis of neuroimaging data: Applications and advances. *NeuroImage*, 23(SUPPL. 1):250–263.
- McKeown, M. J., Makeig, S., Brown, G. G., Jung, T., Kindermann, S. S., Bell, A. J., and Sejnowski, T. J. (1998). Analysis of fMRI data by blind separation into independent spatial components. *Human Brain Mapping*, 6(June 1997):160–188.
- McTeague, L. M., Huemer, J., Carreon, D. M., Jiang, Y., Eickhoff, S. B., and Etkin, A. (2017). Identification of common neural circuit disruptions in cognitive control across psychiatric disorders. *American Journal of Psychiatry*, 174(7):676–685.
- Medaglia, J. D., Huang, W., Karuza, E. A., Kelkar, A., Thompson-Schill, S. L., Ribeiro, A., and Bassett, D. S. (2018). Functional alignment with anatomical networks is associated with cognitive flexibility. *Nature Human Behaviour*, 2(2):156–164.
- Medaglia, J. D., Lynall, M.-E., and Bassett, D. S. (2015). Cognitive Network Neuroscience. *Journal of Cognitive Neuroscience*, 27(8):1471–1491.
- Menara, T., Baggio, G., Bassett, D. S., and Pasqualetti, F. (2019). A Framework to Control Functional Connectivity in the Human Brain. *ArXiv*, 1904.08805.
- Mennigen, E., Fryer, S. L., Rashid, B., Damaraju, E., Du, Y., Loewy, R. L., Stuart, B. K., Calhoun, V. D., and Mathalon, D. H. (2019). Transient Patterns of Functional Dysconnectivity in Clinical High Risk and Early Illness Schizophrenia Individuals Compared with Healthy Controls. *Brain Connectivity*, 9(1):60–76.

Bibliography

- Mennigen, E., Miller, R. L., Rashid, B., Fryer, S. L., Loewy, R. L., Stuart, B. K., Mathalon, D. H., and Calhoun, V. D. (2018). Reduced higher-dimensional resting state fMRI dynamism in clinical high-risk individuals for schizophrenia identified by meta-state analysis. *Schizophrenia Research*, 201:217–223.
- Menon, V. (2011). Large-scale brain networks and psychopathology: A unifying triple network model. *Trends in Cognitive Sciences*, 15(10):483–506.
- Menon, V. and Uddin, L. Q. (2010). Saliency, switching, attention and control: a network model of insula function. *Brain Structure and Function*, pages 1–13.
- Milad, M. R. and Quirk, G. J. (2002). Neurons in medial prefrontal cortex signal memory for fear extinction. *Nature*, 420(6911):70–4.
- Millan, M. J., Andrieux, A., Bartzokis, G., Cadenhead, K., Dazzan, P., Fusar-Poli, P., Gallinat, J., Giedd, J., Grayson, D. R., Heinrichs, M., Kahn, R., Krebs, M.-O., Leboyer, M., Lewis, D., Marin, O., Marin, P., Meyer-Lindenberg, A., McGorry, P., McGuire, P., Owen, M. J., Patterson, P., Sawa, A., Spedding, M., Uhlhaas, P., Vaccarino, F., Wahlestedt, C., and Weinberger, D. (2016). Altering the course of schizophrenia: progress and perspectives. *Nature reviews. Drug discovery*, 15(7):485–515.
- Miller, R. L., Yaesoubi, M., Turner, J. A., Mathalon, D., Preda, A., Pearlson, G., Adali, T., and Calhoun, V. D. (2016). Higher Dimensional Meta-State Analysis Reveals Reduced Resting fMRI Connectivity Dynamism in Schizophrenia Patients. *PLOS ONE*, 11(3):e0149849.
- Miller, T. J., Mcclashan, T. H., Rosen, J. L., Cadenhead, K., Ventura, J., Mcfarlane, W., Perkins, D. O., Pearlson, Q. D., and Woods, S. W. (2003). Prodromal Assessment With the Structured Interview for Prodromal Syndromes and the Scale of Prodromal Symptoms: Predictive Validity, Interrater Reliability, and Training to Reliability. *Schizophrenia Bulletin*, 29(4):703–715.
- Mišić, B., Betzel, R. F., Nematzadeh, A., Goñi, J., Griffa, A., Hagmann, P., Flammini, A., Ahn, Y. Y., and Sporns, O. (2015). Cooperative and Competitive Spreading Dynamics on the Human Connectome. *Neuron*, 86(6):1518–1529.
- Misić, B., Mills, T., Taylor, M. J., and McIntosh, A. R. (2010). Brain noise is task dependent and region specific. *Journal of neurophysiology*, 104(5):2667–2676.
- Miskovic, V., Owens, M., Kuntzleman, K., and Gibb, B. E. (2016). Charting moment-to-moment brain signal variability from early to late childhood. *Cortex*, 83:51–61.
- Monti, S., Tamayo, P., Mesirov, J., and Golub, T. (2003). Consensus Clustering: A Resampling-Based Method for Class Discovery and Visualization of Gene Expression Microarray Data. *Machine Learning*, 52(1):91–118.
- Muldoon, S. F., Pasqualetti, F., Gu, S., Cieslak, M., Grafton, S. T., Vettel, J. M., and Bassett, D. S. (2016). Stimulation-based control of dynamic brain networks. *PLoS Computational Biology*, 12(9):e1005076.

- Murphy, K., Jones, L., and Owen, M. (1999). High rates of schizophrenia in adults with velo-cardio-facial syndrome. *Archives of General Psychiatry*, 56(10):940–945.
- Narr, K. L., Toga, A. W., Szeszko, P., Thompson, P. M., Woods, R. P., Robinson, D., Sevy, S., Wang, Y., Schrock, K., and Bilder, R. M. (2005). Cortical thinning in cingulate and occipital cortices in first episode schizophrenia. *Biological Psychiatry*, 58(1):32–40.
- Nekovarova, T., Fajnerova, I., Horacek, J., and Spaniel, F. (2014). Bridging disparate symptoms of schizophrenia: a triple network dysfunction theory. *Frontiers in Behavioral Neuroscience*, 8(May):171.
- Nelson, B., Amminger, G. P., Yuen, H. P., Wallis, N., J. Kerr, M., Dixon, L., Carter, C., Loewy, R., Niendam, T. A., Shumway, M., Morris, S., Blasioli, J., and McGorry, P. D. (2018). Staged Treatment in Early Psychosis: A sequential multiple assignment randomised trial of interventions for ultra high risk of psychosis patients. *Early Intervention in Psychiatry*, 12(3):292–306.
- Niklasson, L. and Gillberg, C. (2010). The neuropsychology of 22q11 deletion syndrome. A neuropsychiatric study of 100 individuals. *Research in Developmental Disabilities*, 31(1):185–194.
- Nomi, J. S., Bolt, T. S., Ezie, C., Uddin, L. Q., and Heller, A. S. (2017). Moment-to-moment BOLD Signal Variability Reflects Regional Changes in Neural Flexibility Across the Lifespan. *The Journal of Neuroscience*, 37(22):3408–16.
- Ogawa, S., Lee, T. M., Kay, A. R., and Tank, D. W. (1990). Brain magnetic resonance imaging with contrast dependent on blood oxygenation. *Proceedings of the National Academy of Sciences*, 87(24):9868–9872.
- Olszewski, A. K., Kikinis, Z., Gonzalez, C. S., Coman, I. L., Makris, N., Gong, X., Rath, Y., Zhu, A., Antshel, K. M., Fremont, W., Kubicki, M. R., Bouix, S., Shenton, M. E., and Kates, W. R. (2017). The social brain network in 22q11.2 deletion syndrome: A diffusion tensor imaging study. *Behavioral and Brain Functions*, 13(1):1–17.
- Oskarsdóttir, S., Vujic, M., and Fasth, A. (2004). Incidence and prevalence of the 22q11 deletion syndrome: a population-based study in Western Sweden. *Archives of disease in childhood*, 89(2):148–151.
- Ottet, M.-C., Schaer, M., Cammoun, L., Schneider, M., Debbané, M., Thiran, J.-P., and Eliez, S. (2013a). Reduced fronto-temporal and limbic connectivity in the 22q11.2 deletion syndrome: vulnerability markers for developing schizophrenia? *PLoS One*, 8(3):e58429.
- Ottet, M.-C., Schaer, M., Debbané, M., Cammoun, L., Thiran, J.-P., and Eliez, S. (2013b). Graph theory reveals dysconnected hubs in 22q11DS and altered nodal efficiency in patients with hallucinations. *Frontiers in Human Neuroscience*, 7(September).
- Owen, M. J., Sawa, A., and Mortensen, P. B. (2016). Schizophrenia. *The Lancet*, 388:86–97.

Bibliography

- Padula, M. C., Scariati, E., Schaer, M., and Eliez, S. (2018). A Mini Review on the Contribution of the Anterior Cingulate Cortex in the Risk of Psychosis in 22q11.2 Deletion Syndrome. *Frontiers in Psychiatry*, 9(August):9–14.
- Padula, M. C., Scariati, E., Schaer, M., Sandini, C., Ottet, M. C., Schneider, M., Van De Ville, D., and Eliez, S. (2017a). Altered structural network architecture is predictive of the presence of psychotic symptoms in patients with 22q11.2 deletion syndrome. *NeuroImage: Clinical*, 16(July):142–150.
- Padula, M. C., Schaer, M., Scariati, E., Maeder, J., Schneider, M., and Eliez, S. (2017b). Multi-modal investigation of triple network connectivity in patients with 22q11DS and association with executive functions. *Human Brain Mapping*, 2189(January):2177–2189.
- Padula, M. C., Schaer, M., Scariati, E., Schneider, M., Van De Ville, D., Debbané, M., and Eliez, S. (2015). Structural and functional connectivity in the default mode network in 22q11.2 deletion syndrome. *J Neurodev Disord*, 7(1):23.
- Pankow, A., Deserno, L., Walter, M., Fydrich, T., Bermpohl, F., Schlagenhauf, F., and Heinz, A. (2015). Reduced default mode network connectivity in schizophrenia patients. *Schizophrenia Research*, 165(1):90–93.
- Pasqualetti, F., Zampieri, S., and Bullo, F. (2014). Controllability Metrics and Algorithms for Complex Networks. *Transactions on Control of Network Systems*, 1(1):40–52.
- Pelletier-Baldelli, A., Andrews-Hanna, J. R., and Mittal, V. A. (2018). Resting state connectivity dynamics in individuals at risk for psychosis. *Journal of Abnormal Psychology*, 127(3):314–325.
- Pessoa, L. (2008). On the Relationship Between Emotion and Cognition. *Nature Reviews Neuroscience*, 9(2):148–158.
- Pettersson-Yeo, W., Allen, P., Benetti, S., McGuire, P., and Mechelli, A. (2011). Dysconnectivity in schizophrenia: Where are we now? *Neuroscience and Biobehavioral Reviews*, 35(5):1110–1124.
- Polanía, R., Nitsche, M. A., and Ruff, C. C. (2018). Studying and modifying brain function with non-invasive brain stimulation. *Nature Neuroscience*, 21(2):174–187.
- Poldrack, R. A., Laumann, T. O., Koyejo, O., Gregory, B., Hover, A., Chen, M.-Y., Gorgolewski, K. J., Luci, J., Joo, S. J., Boyd, R. L., Hunicke-Smith, S., Simpson, Z. B., Caven, T., Sochat, V., Shine, J. M., Gordon, E., Snyder, A. Z., Adeyemo, B., Petersen, S. E., Glahn, D. C., Reese Mckay, D., Curran, J. E., Göring, H. H. H., Carless, M. A., Blangero, J., Dougherty, R., Leemans, A., Handwerker, D. A., Frick, L., Marcotte, E. M., and Mumford, J. A. (2015). Long-term neural and physiological phenotyping of a single human. *Nature communications*, 6:8885.
- Power, J. D., Barnes, K. A., Snyder, A. Z., Schlaggar, B. L., and Petersen, S. E. (2012). Spurious but systematic correlations in functional connectivity MRI networks arise from subject motion. *NeuroImage*, 59(3):2142–2154.

- Power, J. D., Mitra, A., Laumann, T. O., Snyder, A. Z., Schlaggar, B. L., and Petersen, S. E. (2014). Methods to detect, characterize, and remove motion artifact in resting state fMRI. *NeuroImage*, 84:320–341.
- Preti, M. G., Bolton, T. A. W., and Van De Ville, D. (2017). The dynamic functional connectome: State-of-the-art and perspectives. *NeuroImage*, 160(December):41–54.
- Preti, M. G. and Van De Ville, D. (2017). Dynamics of functional connectivity at high spatial resolution reveal long-range interactions and fine-scale organization. *Scientific Reports*, 7(1):12773.
- Preti, M. G. and Van De Ville, D. (2019). Decoupling of brain function from structure reveals regional behavioral specialization in humans. *arXiv preprint*, 1905.07813.
- Qin, J., Chen, S.-G., Hu, D., Zeng, L.-L., Fan, Y.-M., Chen, X.-P., and Shen, H. (2015). Predicting individual brain maturity using dynamic functional connectivity. *Frontiers in Human Neuroscience*, 9:418.
- Qin, P. and Northoff, G. (2011). How is our self related to midline regions and the default-mode network? *NeuroImage*, 57(3):1221–1233.
- Quirk, G. J., Likhtik, E., Pelletier, J. G., and Paré, D. (2003). Stimulation of medial prefrontal cortex decreases the responsiveness of central amygdala output neurons. *Journal of Neuroscience*, 23(25):8800–7.
- Rangaprakash, D., Wu, G.-R., Marinazzo, D., Hu, X., and Deshpande, G. (2018). Hemodynamic response function (HRF) variability confounds resting-state fMRI functional connectivity. *Magnetic Resonance in Medicine*, 80(4):1697–1713.
- Rapoport, J. L., Giedd, J. N., and Gogtay, N. (2012). Neurodevelopmental model of schizophrenia: update 2012. *Molecular Psychiatry*, 17(12):1228–1238.
- Reich, W. (2000). Diagnostic Interview for Children and Adolescents (DICA). *Journal of the American Academy of Child & Adolescent Psychiatry*, 39(1):59–66.
- Reid, M. A., Stoeckel, L. E., White, D. M., Avsar, K. B., Bolding, M. S., Akella, N. S., Knowlton, R. C., Den Hollander, J. A., and Lahti, A. C. (2010). Assessments of function and biochemistry of the anterior cingulate cortex in schizophrenia. *Biological Psychiatry*, 68(7):625–633.
- Richiardi, J., Gschwind, M., Simioni, S., Annoni, J.-M., Greco, B., Hagmann, P., Schluep, M., Vuilleumier, P., and Van De Ville, D. (2012). Classifying minimally disabled multiple sclerosis patients from resting state functional connectivity. *NeuroImage*, 62(3):2021–2033.
- Rieger, K., Hernandez, L. D., Baenninger, A., and Koenig, T. (2016). 15 years of microstate research in schizophrenia - Where are we? A meta-analysis. *Frontiers in Psychiatry*, 7(FEB):1–7.

Bibliography

- Rihs, T. A., Tomescu, M. I., Britz, J., Rochas, V., Custo, A., Schneider, M., Debbané, M., Eliez, S., and Michel, C. M. (2013). Altered auditory processing in frontal and left temporal cortex in 22q11.2 deletion syndrome: A group at high genetic risk for schizophrenia. *Psychiatry Research - Neuroimaging*, 212(2):141–149.
- Roalf, D. R., Eric Schmitt, J., Vandekar, S. N., Satterthwaite, T. D., Shinohara, R. T., Ruparel, K., Elliott, M. A., Prabhakaran, K., McDonald-McGinn, D. M., Zackai, E. H., Gur, R. C., Emanuel, B. S., and Gur, R. E. (2017). White matter microstructural deficits in 22q11.2 deletion syndrome. *Psychiatry Research: Neuroimaging*, 268(March):35–44.
- Rogachov, A., Cheng, J. C., Erpelding, N., Hemington, K. S., Crawley, A. P., and Davis, K. D. (2016). Regional brain signal variability: a novel indicator of pain sensitivity and coping. *Pain*, 2(11):1.
- Ryali, S., Supekar, K., Chen, T., Kochalka, J., Cai, W., Nicholas, J., Padmanabhan, A., and Menon, V. (2016). Temporal Dynamics and Developmental Maturation of Salience, Default and Central-Executive Network Interactions Revealed by Variational Bayes Hidden Markov Modeling. *PLOS Computational Biology*, 12(12):e1005138.
- Sakoglu, U., Pearlson, G. D., Kiehl, K. A., Wang, Y. M., Michael, A. M., Calhoun, V. D., Sakoglu, U., Pearlson, G. D., Kiehl, K. A., Wang, Y. M., Michael, A. M., and Calhoun, V. D. (2010). A method for evaluating dynamic functional network connectivity and task-modulation: application to schizophrenia. *Magnetic Resonance Materials in Physics, Biology and Medicine*, 23(5-6):351–366.
- Salvador, R., Landin-Romero, R., Anguera, M., Canales-Rodríguez, E. J., Radua, J., Guerrero-Pedraza, A., Sarró, S., Maristany, T., McKenna, P. J., and Pomarol-Clotet, E. (2017). Non redundant functional brain connectivity in schizophrenia. *Brain Imaging and Behavior*, 11(2):552–564.
- Sampaio-Baptista, C., Diosi, K., and Johansen-Berg, H. (2019). Magnetic Resonance Techniques for Imaging White Matter. In Lyons, D. A. and Kegel, L., editors, *Oligodendrocytes: Methods and Protocols*, pages 397–407. Springer New York, New York, NY.
- Sandini, C., Scariati, E., Padula, M. C., Schneider, M., Schaer, M., Van De Ville, D., and Eliez, S. (2017). Cortical Dysconnectivity Measured by Structural Covariance Is Associated With the Presence of Psychotic Symptoms in 22q11.2 Deletion Syndrome. *Biological Psychiatry: Cognitive Neuroscience and Neuroimaging*, 3(5):433–442.
- Sandini, C., Zöllner, D., Scariati, E., Padula, M. C., Schneider, M., Schaer, M., Van De Ville, D., and Eliez, S. (2018). Development of Structural Covariance From Childhood to Adolescence : A Longitudinal Study in. *Frontiers in Neuroscience*, 12(MAY):327.
- Sanfratello, L., Houck, J., and Calhoun, V. D. (2019). Dynamic Functional Network Connectivity In Schizophrenia With MEG And fMRI, Do Different Time Scales Tell A Different Story? *Brain Connectivity*, page brain.2018.0608.

- Satterthwaite, T. D. and Baker, J. T. (2015). How can studies of resting-state functional connectivity help us understand psychosis as a disorder of brain development? *Current Opinion in Neurobiology*, 30(October 2014):85–91.
- Scariati, E., Padula, M. C., Schaer, M., and Eliez, S. (2016a). Long-range dysconnectivity in frontal and midline structures is associated to psychosis in 22q11.2 deletion syndrome. *Journal of Neural Transmission*.
- Scariati, E., Schaer, M., Karahanoglu, F. I., Schneider, M., Richiardi, J., Debbané, M., Van De Ville, D., and Eliez, S. (2016b). Large-scale functional network reorganization in 22q11.2 deletion syndrome revealed by modularity analysis. *Cortex*, 2.
- Scariati, E., Schaer, M., Richiardi, J., Schneider, M., Debbané, M., Van De Ville, D., and Eliez, S. (2014). Identifying 22q11.2 deletion syndrome and psychosis using resting-state connectivity patterns. *Brain Topogr*, 27(6):808–821.
- Schaer, M., Debbané, M., Bach Cuadra, M., Ottet, M.-C., Glaser, B., Thiran, J.-P., and Eliez, S. (2009). Deviant trajectories of cortical maturation in 22q11.2 deletion syndrome (22q11DS): a cross-sectional and longitudinal study. *Schizophr Res*, 115(2-3):182–190.
- Schaer, M., Glaser, B., Ottet, M.-C., Schneider, M., Bach Cuadra, M., Debbané, M., Thiran, J.-P., and Eliez, S. (2010). Regional cortical volumes and congenital heart disease: a MRI study in 22q11.2 deletion syndrome. *Journal of Neurodevelopmental Disorders*, 2(4):224–234.
- Schleifer, C., Lin, A., Kushan, L., Ji, J. L., Yang, G., Bearden, C. E., and Anticevic, A. (2018). Dissociable Disruptions in Thalamic and Hippocampal Resting-State Functional Connectivity in Youth with 22q11.2 Deletions. *The Journal of Neuroscience*, 39(7):1301–1319.
- Schmidt, A., Crossley, N. A., Harrisberger, F., Smieskova, R., Lenz, C., Riecher-Rössler, A., Lang, U. E., McGuire, P., Fusar-Poli, P., and Borgwardt, S. (2017). Structural network disorganization in subjects at clinical high risk for psychosis. *Schizophrenia Bulletin*, 43(3):583–591.
- Schmidt, S. J., Schultze-Lutter, F., Schimmelmann, B. G., Maric, N. P., Salokangas, R. K., Riecher-Rössler, A., van der Gaag, M., Meneghelli, A., Nordentoft, M., Marshall, M., Morrison, A., Raballo, A., Klosterkötter, J., and Ruhrmann, S. (2015). EPA guidance on the early intervention in clinical high risk states of psychoses. *European Psychiatry*, 30(3):388–404.
- Schmitt, J. E., Vandekar, S., Yi, J., Calkins, M. E., Ruparel, K., Roalf, D. R., Whinna, D., Souders, M. C., Satterthwaite, T. D., Prabhakaran, K., McDonald-McGinn, D. M., Zackai, E. H., Gur, R. C., Emanuel, B. S., and Gur, R. E. (2015). Aberrant Cortical Morphometry in the 22q11.2 Deletion Syndrome. *Biological psychiatry*, 78(2):135–43.
- Schmitt, J. E., Yi, J., Calkins, M. E., Ruparel, K., Roalf, D. R., Cassidy, A., Souders, M. C., Satterthwaite, T. D., McDonald-McGinn, D. M., Zackai, E. H., Gur, R. C., Emanuel, B. S., and Gur, R. E. (2016). Disrupted anatomic networks in the 22q11.2 deletion syndrome. *NeuroImage: Clinical*, 12:420–428.

Bibliography

- Schneider, M., Armando, M., Pontillo, M., Vicari, S., Debbané, M., Schultze-Lutter, F., and Eliez, S. (2016). Ultra high risk status and transition to psychosis in 22q11.2 deletion syndrome. *World psychiatry : official journal of the World Psychiatric Association (WPA)*, 15(3):259–265.
- Schneider, M., Debbané, M., Bassett, A. S., Chow, E. W. C., Fung, W. L. A., van den Bree, M. B. M., Owen, M., Murphy, K. C., Niarchou, M., Kates, W. R., Antshel, K. M., Fremont, W., McDonald-McGinn, D. M., Gur, R. E., Zackai, E. H., Vorstman, J., Duijff, S. N., Klaassen, P. W. J., Swillen, A., Gothelf, D., Green, T., Weizman, A., Van Amelsvoort, T., Evers, L., Boot, E., Shashi, V., Hooper, S. R., Bearden, C. E., Jalbrzikowski, M., Armando, M., Vicari, S., Murphy, D. G., Ousley, O., Campbell, L. E., Simon, T. J., and Eliez, S. (2014). Psychiatric Disorders From Childhood to Adulthood in 22q11.2 Deletion Syndrome: Results From the International Consortium on Brain and Behavior in 22q11.2 Deletion Syndrome. *The American journal of psychiatry*, 171(6):627–639.
- Schneider, M., Debbané, M., Lagioia, A., Salomon, R., D'Argembeau, A., and Eliez, S. (2012). Comparing the neural bases of self-referential processing in typically developing and 22q11.2 adolescents. *Developmental Cognitive Neuroscience*, 2(2):277–289.
- Schreiner, M., Forsyth, J. K., Karlsgodt, K. H., Anderson, A. E., Hirsh, N., Kushan, L., Uddin, L. Q., Mattiaccio, L., Coman, I. L., Kates, W. R., and Bearden, C. E. (2017). Intrinsic Connectivity Network-Based Classification and Detection of Psychotic Symptoms in Youth With 22q11.2 Deletions. *Cerebral Cortex*, 27(6):3294–3306.
- Schreiner, M. J., Karlsgodt, K. H., Uddin, L. Q., Chow, C., Congdon, E., Jalbrzikowski, M., and Bearden, C. E. (2014). Default mode network connectivity and reciprocal social behavior in 22q11.2 deletion syndrome. *Social Cognitive and Affective Neuroscience*, 9(9):1261–1267.
- Schultze-Lutter, F., Michel, C., Schmidt, S. J., Schimmelmann, B. G., Maric, N. P., Salokangas, R. K., Riecher-Rössler, A., van der Gaag, M., Nordentoft, M., Raballo, A., Meneghelli, A., Marshall, M., Morrison, A., Ruhrmann, S., and Klosterkötter, J. (2015). EPA guidance on the early intervention in clinical high risk states of psychoses. *European Psychiatry*, 30(3):405–416.
- Seeley, W. W., Menon, V., Schatzberg, A. F., Keller, J., Glover, G. H., Kenna, H., Reiss, A. L., and Greicius, M. D. (2007). Dissociable Intrinsic Connectivity Networks for Salience Processing and Executive Control. *Journal of Neuroscience*, 27(9):2349–2356.
- Shashi, V., Veerapandiyan, A., Keshavan, M. S., Zapadka, M., Schoch, K., Kwapil, T. R., Hooper, S. R., and Stanley, J. A. (2012). Altered development of the dorsolateral prefrontal cortex in chromosome 22q11.2 deletion syndrome: An in vivo proton spectroscopy study. *Biological Psychiatry*, 72(8):684–691.
- Shenhav, A., Botvinick, M., and Cohen, J. (2013). The expected value of control: An integrative theory of anterior cingulate cortex function. *Neuron*, 79(2):217–240.

- Sherman, L. E., Rudie, J. D., Pfeifer, J. H., Masten, C. L., McNealy, K., and Dapretto, M. (2014). Development of the Default Mode and Central Executive Networks across early adolescence: A longitudinal study. *Developmental Cognitive Neuroscience*, 10:148–159.
- Shine, J. M., Bissett, P. G., Bell, P. T., Koyejo, O., Balsters, J. H., Gorgolewski, K. J., Moodie, C. A., and Poldrack, R. A. (2016a). The Dynamics of Functional Brain Networks: Integrated Network States during Cognitive Task Performance. *Neuron*, 92(2):544–554.
- Shine, J. M., Koyejo, O., Bell, P. T., Gorgolewski, K. J., Gilat, M., and Poldrack, R. A. (2015). Estimation of dynamic functional connectivity using Multiplication of Temporal Derivatives. *NeuroImage*, 122:399–407.
- Shine, J. M., Koyejo, O., and Poldrack, R. A. (2016b). Temporal metastates are associated with differential patterns of time-resolved connectivity, network topology, and attention. *Proceedings of the National Academy of Sciences*, 113(35):9888–9891.
- Shirer, W. R., Ryali, S., Rykhlevskaia, E., Menon, V., and Greicius, M. D. (2012). Decoding subject-driven cognitive states with whole-brain connectivity patterns. *Cerebral Cortex*, 22(1):158–165.
- Smith, R. E., Tournier, J. D., Calamante, E., and Connelly, A. (2013). SIFT: Spherical-deconvolution informed filtering of tractograms. *NeuroImage*, 67:298–312.
- Smith, S. M., Miller, K. L., Moeller, S., Xu, J., Auerbach, E. J., Woolrich, M. W., Beckmann, C. F., Jenkinson, M., Andersson, J., Glasser, M. F., Van Essen, D. C., Feinberg, D. a., Yacoub, E. S., and Ugurbil, K. (2012). Temporally-independent functional modes of spontaneous brain activity. *Proceedings of the National Academy of Sciences*, 109(8):3131–6.
- Soares, J. M., Magalhães, R., Moreira, P. S., Sousa, A., Ganz, E., Sampaio, A., Alves, V., Marques, P., and Sousa, N. (2016). A Hitchhiker’s Guide to Functional Magnetic Resonance Imaging. *Frontiers in Neuroscience*, 10(November):1–35.
- Spreng, R. N., Mar, R. A., and Kim, A. S. N. (2008). The Common Neural Basis of Autobiographical Memory, Prospection, Navigation, Theory of Mind, and the Default Mode: A Quantitative Meta-analysis. *Journal of Cognitive Neuroscience*, 21(3):489–510.
- Sridharan, D., Levitin, D. J., and Menon, V. (2008). A critical role for the right fronto-insular cortex in switching between central-executive and default-mode networks. *Proc Natl Acad Sci U S A*, 105(34):12569–12574.
- Stephan, P. E. (2010). The economics of science. *Handbook of the Economics of Innovation*, 1(1 C):217–273.
- Stiso, J., Khambhati, A. N., Menara, T., Kahn, A. E., Stein, J. M., Das, S. R., Gorniak, R., Tracy, J., Litt, B., Davis, K. A., Pasqualetti, F., Lucas, T., and Bassett, D. S. (2018). White Matter Network Architecture Guides Direct Electrical Stimulation Through Optimal State Transitions. *arXiv preprint*, 1805.01260.

Bibliography

- Su, J., Shen, H., Zeng, L.-L. L., Qin, J., Liu, Z., and Hu, D. (2016). Heredity characteristics of schizophrenia shown by dynamic functional connectivity analysis of resting-state functional MRI scans of unaffected siblings. *NeuroReport*, 27(11):843–848.
- Sun, D., Phillips, L., Velakoulis, D., Yung, A., McGorry, P. D., Wood, S. J., van Erp, T. G. M., Thompson, P. M., Toga, A. W., Cannon, T. D., and Pantelis, C. (2009). Progressive brain structural changes mapped as psychosis develops in 'at risk' individuals. *Schizophrenia Research*, 108(1-3):85–92.
- Sun, Y., Collinson, S. L., Suckling, J., and Sim, K. (2018). Dynamic Reorganization of Functional Connectivity Reveals Abnormal Temporal Efficiency in Schizophrenia. *Schizophrenia Bulletin*.
- Supekar, K., Uddin, L. Q., Prater, K., Amin, H., Greicius, M. D., and Menon, V. (2010). Development of functional and structural connectivity within the default mode network in young children. *NeuroImage*, 52(1):290–301.
- Swillen, A., Devriendt, K., Legius, E., Eyskens, B., Dumoulin, M., Gewillig, M., and Fryns, J. P. (1997). Intelligence and psychosocial adjustment in velocardiofacial syndrome: a study of 37 children and adolescents with VCFS. *Journal of Medical Genetics*, 34(3):453–458.
- Tagliazucchi, E., Balenzuela, P., Fraiman, D., and Chialvo, D. R. (2012). Criticality in Large-Scale Brain fMRI Dynamics Unveiled by a Novel Point Process Analysis. *Frontiers in Physiology*, 3(February):1–12.
- Tagliazucchi, E., Siniatchkin, M., Laufs, H., and Chialvo, D. R. (2016). The Voxel-Wise Functional Connectome Can Be Efficiently Derived from Co-activations in a Sparse Spatio-Temporal Point-Process. *Frontiers in Neuroscience*, 10:381.
- Takahashi, T., Cho, R. Y., Mizuno, T., Kikuchi, M., Murata, T., Takahashi, K., and Wada, Y. (2010). Antipsychotics reverse abnormal EEG complexity in drug-naïve schizophrenia: A multiscale entropy analysis. *NeuroImage*, 51(1):173–182.
- Tan, G. M., Arnone, D., McIntosh, A. M., and Ebmeier, K. P. (2009). Meta-analysis of magnetic resonance imaging studies in chromosome 22q11.2 deletion syndrome (velocardiofacial syndrome). *Schizophrenia Research*, 115(2-3):173–181.
- Tang, E. and Bassett, D. S. (2018). Colloquium: Control of dynamics in brain networks. *Reviews of Modern Physics*, 90(3):1–20.
- Tang, E., Giusti, C., Baum, G. L., Gu, S., Pollock, E., Kahn, A. E., Roalf, D. R., Moore, T. M., Ruparel, K., Gur, R. E. R. C. R. E., Gur, R. E. R. C. R. E., Satterthwaite, T. D., and Bassett, D. S. (2017a). Developmental increases in white matter network controllability support a growing diversity of brain dynamics. *Nature Communications*, 8(1):1252.
- Tang, S. X., Moore, T. M., Calkins, M. E., Yi, J. J., McDonald-McGinn, D. M., Zackai, E. H., Emanuel, B. S., Gur, R. C., and Gur, R. E. (2017b). Emergent, remitted and persistent

- psychosis-spectrum symptoms in 22q11.2 deletion syndrome. *Translational Psychiatry*, 7(7):e1180.
- Tang, Y., Zhou, Q., Chang, M., Chekroud, A., Gueorguieva, R., Jiang, X., Zhou, Y., He, G., Rowland, M., Wang, D., Fu, S., Yin, Z., Leng, H., Wei, S., Xu, K., Wang, F., Krystal, J. H., and Driesen, N. R. (2019). Altered functional connectivity and low-frequency signal fluctuations in early psychosis and genetic high risk. *Schizophrenia Research*.
- Temel, Y., Heschem, S. A., Jahanshahi, A., Janssen, M. L. F., Tan, S. K. H., van Overbeeke, J. J., Ackermans, L., Oosterloo, M., Duits, A., Leentjens, A. F. G., and Lim, L. (2012). Chapter Thirteen - Neuromodulation in Psychiatric Disorders. In Hamani, C. and Moro, E., editors, *Emerging Horizons in Neuromodulation*, volume 107 of *International Review of Neurobiology*, pages 283–314. Academic Press.
- Toga, A. W. and Mazziotta, J. C. (2002). *Brain mapping: the methods*. Academic press.
- Tognoli, E. and Kelso, J. A. (2014). The Metastable Brain. *Neuron*, 81(1):35–48.
- Tomescu, M. I., Rihs, T. A., Becker, R., Britz, J., Custo, A., Grouiller, F., Schneider, M., Debbané, M., Eliez, S., and Michel, C. M. (2014). Deviant dynamics of EEG resting state pattern in 22q11.2 deletion syndrome adolescents: A vulnerability marker of schizophrenia? *Schizophrenia Research*, 157(1-3):175–181.
- Tomescu, M. I., Rihs, T. A., Roinishvili, M., Karahanoglu, F. I., Schneider, M., Menghetti, S., Van De Ville, D., Brand, A., Chkonia, E., Eliez, S., Herzog, M. H., Michel, C. M., and Cappe, C. (2015). Schizophrenia patients and 22q11.2 deletion syndrome adolescents at risk express the same deviant patterns of resting state EEG microstates: A candidate endophenotype of schizophrenia. *Schizophrenia Research: Cognition*, 2(3):159–165.
- Tournier, J. D., Calamante, F., and Connelly, A. (2007). Robust determination of the fibre orientation distribution in diffusion MRI: Non-negativity constrained super-resolved spherical deconvolution. *NeuroImage*, 35(4):1459–1472.
- Tournier, J. D., Calamante, F., and Connelly, A. (2013). Determination of the appropriate b value and number of gradient directions for high-angular-resolution diffusion-weighted imaging. *NMR in Biomedicine*, 26(12):1775–1786.
- Tournier, J. D., Smith, R. E., Raffelt, D. A., Tabbara, R., Dhollander, T., Pietsch, M., Christiaens, D., Jeurissen, B., Yeh, C.-H., and Connelly, A. (2019). MRtrix3: A fast, flexible and open software framework for medical image processing and visualisation. *bioRxiv preprint*, 551739.
- Tovote, P., Fadok, J. P., and Lüthi, A. (2015). Neuronal circuits for fear and anxiety. *Nature Reviews Neuroscience*, 16(6):317–331.
- Turner, J. A., Damaraju, E., Van Erp, T. G., Mathalon, D. H., Ford, J. M., Voyvodic, J., Mueller, B. A., Belger, A., Bustillo, J., McEwen, S., Potkin, S. G., and Calhoun, V. D. (2013). A multi-site

Bibliography

- resting state fMRI study on the amplitude of low frequency fluctuations in schizophrenia. *Frontiers in Neuroscience*, 7(7 AUG):1–13.
- Tylee, D. S., Kikinis, Z., Quinn, T. P., Antshel, K. M., Fremont, W., Tahir, M. A., Zhu, A., Gong, X., Glatt, S. J., Coman, I. L., Shenton, M. E., Kates, W. R., and Makris, N. (2017). Machine-learning classification of 22q11.2 deletion syndrome: A diffusion tensor imaging study. *NeuroImage: Clinical*, 15(March):832–842.
- Tzourio-Mazoyer, N., Landeau, B., Papathanassiou, D., Crivello, F., Etard, O., Delcroix, N., Mazoyer, B., and Joliot, M. (2002). Automated Anatomical Labeling of Activations in SPM Using a Macroscopic Anatomical Parcellation of the MNI MRI Single-Subject Brain. *NeuroImage*, 15(1):273–289.
- Uddin, L. Q. (2015). Salience processing and insular cortical function and dysfunction. *Nat Rev Neurosci*, 16(1):55–61.
- Van, L., Boot, E., and Bassett, A. S. (2017). Update on the 22q11.2 deletion syndrome and its relevance to schizophrenia. *Current Opinion in Psychiatry*, page 1.
- Van Den Heuvel, M. P. and Fornito, A. (2014). Brain networks in schizophrenia. *Neuropsychology Review*, 24(1):32–48.
- van den Heuvel, M. P. and Sporns, O. (2011). Rich-Club Organization of the Human Connectome. *Journal of Neuroscience*, 31(44):15775–15786.
- van den Heuvel, M. P. and Sporns, O. (2013). Network hubs in the human brain. *Trends in Cognitive Sciences*, 17(12):683–696.
- Van Den Heuvel, M. P., Sporns, O., Collin, G., Scheewe, T., Mandl, R. C., Cahn, W., Goni, J., Pol, H. E., and Kahn, R. S. (2013). Abnormal rich club organization and functional brain dynamics in schizophrenia. *JAMA Psychiatry*, 70(8):783–792.
- Váša, F., Griffa, A., Scariati, E., Schaer, M., Urban, S., Eliez, S., and Hagmann, P. (2016). An affected core drives network integration deficits of the structural connectome in 22q11.2 deletion syndrome. *NeuroImage: Clinical*, 10:239–249.
- Viallon, M., Cuvinciuc, V., Delattre, B., Merlini, L., Barnaure-Nachbar, I., Toso-Patel, S., Becker, M., Lovblad, K.-O., and Haller, S. (2015). State-of-the-art MRI techniques in neuroradiology: principles, pitfalls, and clinical applications. *Neuroradiology*, 57(5):441–467.
- Vidal-Gonzalez, I., Vidal-Gonzalez, B., Rauch, S. L., and Quirk, G. J. (2006). Microstimulation reveals opposing influences of prelimbic and infralimbic cortex on the expression of conditioned fear. *Learning and Memory*, 13(6):728–733.
- Vidaurre, D., Quinn, A. J., Baker, A. P., Dupret, D., Tejero-Cantero, A., and Woolrich, M. W. (2016). Spectrally resolved fast transient brain states in electrophysiological data. *NeuroImage*, 126:81–95.

- Vidaurre, D., Smith, S. M., and Woolrich, M. W. (2017). Brain network dynamics are hierarchically organized in time. *Proceedings of the National Academy of Sciences*, 114(48):201705120.
- Viviano, R. P., Raz, N., Yuan, P., and Damoiseaux, J. S. (2017). Associations between dynamic functional connectivity and age, metabolic risk, and cognitive performance. *Neurobiology of Aging*, 59:135–143.
- Vorstman, J. A., Breetvelt, E. J., Duijff, S. N., Eliez, S., Schneider, M., Jalbrzikowski, M., Armando, M., Vicari, S., Shashi, V., Hooper, S. R., Chow, E. W., Fung, W. L. A., Butcher, N. J., Young, D. A., McDonald-McGinn, D. M., Vogels, A., Van Amelsvoort, T., Gothelf, D., Weinberger, R., Weizman, A., Klaassen, P. W., Koops, S., Kates, W. R., Antshel, K. M., Simon, T. J., Ousley, O. Y., Swillen, A., Gur, R. E., Bearden, C. E., Kahn, R. S., Bassett, A. S., Emanuel, B. S., Zackai, E. H., Kushan, L., Fremont, W., Schoch, K., Stoddard, J., Cubells, J., Fu, F., Campbell, L. E., Fritsch, R., Vergaelen, E., Neeleman, M., Boot, E., Debbané, M., Philip, N., Green, T., Van DenBree, M. B., Murphy, D., Canyelles, J. M., Arango, C., Murphy, K. C., and Pontillo, M. (2015). Cognitive decline preceding the onset of psychosis in patients with 22q11.2 deletion syndrome. *JAMA Psychiatry*, 72(4):377–385.
- Wang, P., Kong, R., Kong, X., Liégeois, R., Orban, C., Deco, G., Van Den Heuvel, M. P., and Yeo, B. T. (2019a). Inversion of a large-scale circuit model reveals a cortical hierarchy in the dynamic resting human brain. *Tropical and Subtropical Agroecosystems*, 21(3).
- Wang, P., Yang, J., Yin, Z., Duan, J., Zhang, R., Sun, J., Xu, Y., Liu, L., Chen, X., Li, H., Kang, J., Zhu, Y., Deng, X., Chang, M., Wei, S., Zhou, Y., Jiang, X., Wang, F., and Tang, Y. (2019b). Amplitude of low-frequency fluctuation (ALFF) may be associated with cognitive impairment in schizophrenia: a correlation study. *BMC Psychiatry*, 19(1):1–10.
- Wechsler, D. (1991). Wechsler intelligence scale for children. *San Antonio, TX: Psychological Corporation*.
- Wechsler, D. (1997). Wechsler intelligence scale for adults. *London: The Psychological Corporation*.
- Wee, C.-Y., Yap, P.-T., and Shen, D. (2016). Diagnosis of Autism Spectrum Disorders Using Temporally Distinct Resting-State Functional Connectivity Networks. *CNS Neuroscience & Therapeutics*, 22(3):212–219.
- Wegman, E. J. and Wright, I. W. (1983). Splines in statistics. *Journal of the American Statistical Association*, 78(382):351–365.
- Wig, G. S. (2017). Segregated Systems of Human Brain Networks. *Trends in Cognitive Sciences*, 21(12):981–996.
- Wu, C. W., Chen, C.-L., Liu, P.-Y., Chao, Y.-P., Biswal, B. B., and Lin, C.-P. (2011). Empirical Evaluations of Slice-Timing, Smoothing, and Normalization Effects in Seed-Based, Resting-State Functional Magnetic Resonance Imaging Analyses. *Brain Connectivity*, 1(5):401–410.

Bibliography

- Wu-Yan, E., Betzel, R. F., Tang, E., Gu, S., Pasqualetti, F., and Bassett, D. S. (2018). Benchmarking Measures of Network Controllability on Canonical Graph Models. *Journal of Nonlinear Science*, pages 1–39.
- Xi, Q., Zhao, X., Wang, P., Guo, Q., Jiang, H., Cao, X., He, Y., and Yan, C. (2012). Spontaneous brain activity in mild cognitive impairment revealed by amplitude of low-frequency fluctuation analysis: A resting-state fMRI study. *Radiologia Medica*, 117(5):865–871.
- Xia, C. H., Ma, Z., Ciric, R., Gu, S., Betzel, R. F., Kaczkurkin, A. N., Calkins, M. E., Cook, P. A., García de la Garza, A., Vandekar, S. N., Cui, Z., Moore, T. M., Roalf, D. R., Ruparel, K., Wolf, D. H., Davatzikos, C., Gur, R. C., Gur, R. E., Shinohara, R. T., Bassett, D. S., and Satterthwaite, T. D. (2018). Linked dimensions of psychopathology and connectivity in functional brain networks. *Nature Communications*, 9(1):1–14.
- Xie, W., Peng, C. K., Huang, C. C., Lin, C. P., Tsai, S. J., and Yang, A. C. (2018). Functional brain lateralization in schizophrenia based on the variability of resting-state fMRI signal. *Progress in Neuro-Psychopharmacology and Biological Psychiatry*, 86(January):114–121.
- Xu, Y. and Lindquist, M. A. (2015). Dynamic Connectivity Detection: An algorithm for determining functional connectivity change points in fMRI data. *Frontiers in Neuroscience*, 9:285.
- Xu, Y., Zhuo, C., Qin, W., Zhu, J., and Yu, C. (2015). Altered Spontaneous Brain Activity in Schizophrenia: A Meta-Analysis and a Large-Sample Study. *BioMed Research International*, 2015:1–11.
- Yaesoubi, M., Adali, T., and Calhoun, V. D. (2018). A window-less approach for capturing time-varying connectivity in fMRI data reveals the presence of states with variable rates of change. *Human Brain Mapping*, 39(4):1626–1636.
- Yamamoto, Y. and Perron, P. (2013). Estimating and testing multiple structural changes in linear models using band spectral regressions. *Econometrics Journal*, 16(3):400–429.
- Yan, G., Ren, J., Lai, Y. C., Lai, C. H., and Li, B. (2012). Controlling complex networks: How much energy is needed? *Physical Review Letters*, 108(21):1–5.
- Yan Chaogan, Z. Y. (2010). DPARSF: a MATLAB toolbox for “pipeline” data analysis of resting-state fMRI. *Frontiers in System Neuroscience*, 4:13.
- Yang, G. J., Murray, J. D., Repovs, G., Cole, M. W., Savic, A., Glasser, M. F., Pittenger, C., Krystal, J. H., Wang, X.-J., Pearlson, G. D., Glahn, D. C., and Anticevic, A. (2014). Altered global brain signal in schizophrenia. *Proceedings of the National Academy of Sciences*, 111(20):7438–7443.
- Yang, G. J., Murray, J. D., Wang, X.-J., Glahn, D. C., Pearlson, G. D., Repovs, G., Krystal, J. H., and Anticevic, A. (2015). Functional hierarchy underlies preferential connectivity disturbances in schizophrenia. *Proceedings of the National Academy of Sciences*, 113(2):E219–E228.

- Yarkoni, T., Poldrack, R. A., Nichols, T. E., Van Essen, D. C., and Wager, T. D. (2011). Large-scale automated synthesis of human functional neuroimaging data. *Nature Methods*, 8(8):665–670.
- Yu, R., Chien, Y. L., Wang, H. L. S., Liu, C. M., Liu, C. C., Hwang, T. J., Hsieh, M. H., Hwu, H. G., and Tseng, W. Y. I. (2014). Frequency-specific alternations in the amplitude of low-frequency fluctuations in schizophrenia. *Human Brain Mapping*, 35(2):627–637.
- Yuan, Z., Zhao, C., Di, Z., Wang, W. X., and Lai, Y. C. (2013). Exact controllability of complex networks. *Nature Communications*, 4:1–9.
- Yue, J.-L., Li, P., Shi, L., Lin, X., Sun, H.-Q., and Lu, L. (2018). Enhanced temporal variability of amygdala-frontal functional connectivity in patients with schizophrenia. *NeuroImage: Clinical*, 18:527–532.
- Yung, A. R., Stanford, C., Cosgrave, E., Killackey, E., Phillips, L., Nelson, B., and McGorry, P. D. (2006). Testing the Ultra High Risk (prodromal) criteria for the prediction of psychosis in a clinical sample of young people. *Schizophrenia Research*, 84(1):57–66.
- Yung, A. R., Yuen, H. P., McGorry, P. D., Phillips, L. J., Kelly, D., Dell'Olio, M., Francey, S. M., Cosgrave, E. M., Killackey, E., Stanford, C., Godfrey, K., and Buckby, J. (2005). Mapping the onset of psychosis: The Comprehensive Assessment of At-Risk Mental States. *Australian and New Zealand Journal of Psychiatry*, 39(11-12):964–971.
- Zalesky, A. and Breakspear, M. (2015). Towards a statistical test for functional connectivity dynamics. *NeuroImage*, 114:466–470.
- Zalesky, A., Fornito, A., and Bullmore, E. (2012). On the use of correlation as a measure of network connectivity. *NeuroImage*, 60(4):2096–2106.
- Zalesky, A., Fornito, A., Cocchi, L., Gollo, L. L., and Breakspear, M. (2014). Time-resolved resting-state brain networks. *Proceedings of the National Academy of Sciences*, 111(28):10341–10346.
- Zang, Y., He, Y., Zhu, C., Cao, Q., Sui, M., Liang, M., Tian, L., Jiang, T., and Wang, Y. (2007). Altered baseline brain activity in children with ADHD revealed by resting-state functional MRI. *Brain Dev*, 29(2):83–91.
- Zapala, M. and Schork, N. (2006). Multivariate regression analysis of distance matrices for testing associations between gene expression patterns and related variables. *Proceedings of the National Academy of Sciences*, 103(51).
- Zatorre, R. J., Fields, R. D., and Johansen-Berg, H. (2012). Plasticity in gray and white: neuroimaging changes in brain structure during learning. *Nature Neuroscience*, 15(4):528–536.
- Zhan, L., Jenkins, L. M., Zhang, A., Conte, G., Forbes, A., Harvey, D., Angkustsiri, K., Goodrich-Hunsaker, N. J., Durdle, C., Lee, A., Schumann, C., Carmichael, O., Kalish, K., Leow, A. D., and Simon, T. J. (2018). Baseline connectome modular abnormalities in the childhood

Bibliography

- phase of a longitudinal study on individuals with chromosome 22q11.2 deletion syndrome. *Human Brain Mapping*, 39(1):232–248.
- Zhao, Z.-L., Fan, F.-M., Lu, J., Li, H.-J., Jia, L.-F., Han, Y., and Li, K.-C. (2014). Changes of gray matter volume and amplitude of low-frequency oscillations in amnesic {MCI:} An integrative multi-modal {MRI} study. *Acta Radiol*, 56(5):614–621.
- Zöller, D., Padula, M. C., Sandini, C., Schneider, M., Scariati, E., Van De Ville, D., Schaer, M., and Eliez, S. (2018). Psychotic symptoms influence the development of anterior cingulate BOLD variability in 22q11.2 deletion syndrome. *Schizophrenia Research*, 193:319–328.
- Zöller, D., Sandini, C., Karahanoglu, F. I., Padula, M. C., Schaer, M., Eliez, S., and Van De Ville, D. (2019a). Large-scale brain network dynamics provide a measure of psychosis and anxiety in 22q11.2 deletion syndrome. *Biological Psychiatry: Cognitive Neuroscience and Neuroimaging*, in press.
- Zöller, D., Schaer, M., Scariati, E., Padula, M. C., Eliez, S., and Ville, D. V. D. (2017). Disentangling resting-state BOLD variability and PCC functional connectivity in 22q11.2 deletion syndrome. *NeuroImage*, 149:85–97.
- Zöller, D. M., Bolton, T. A., Karahanoglu, F. I., Eliez, S., Schaer, M., and Van De Ville, D. (2019b). Robust recovery of temporal overlap between network activity using transient-informed spatio-temporal regression. *IEEE Transactions on Medical Imaging*, 38(1):291–302.

Daniela M. Zöller

Rue de Saint-Jean 74
1201 Geneva, Switzerland
☎ (+41) 76 724 86 19
✉ daniela.zoller@epfl.ch

Education

10/2015–present **Ph.D. Candidate in Electrical Engineering**, *Ecole Polytechnique Fédérale de Lausanne (EPFL) and University of Geneva*, Switzerland.

Under supervision of Prof. Dr. Dimitri Van De Ville and Prof. Dr. Marie Schaefer

Thesis: "Dynamic organization of human brain function and its relevance for psychosis vulnerability."

Projects:

1. Investigation of BOLD variability in 22q11.2 deletion syndrome (22q11DS) using multivariate partial least squares correlation:
 - Linking BOLD variability and functional connectivity alterations in patients with 22q11DS.
 - Analyzing BOLD variability alterations and development in patients with 22q11DS with psychotic symptoms.
2. Analysis of functional brain network dynamics in 22q11DS using innovation-driven coactivation patterns (iCAPs):
 - Development of a transient-informed spatio-temporal regression approach for robust recovery of spatially and temporally overlapping functional networks.
 - Investigating aberrant brain network dynamics to probe into psychotic symptoms and anxiety in 22q11DS.
3. Investigation of the structural backbone shaping brain dynamics using network control theory.

07/2018–08/2018 **Research stay in the laboratory of Prof. Danielle S. Bassett**, *University of Pennsylvania*, Philadelphia, USA.

Training in network control theory for analysis of structural brain connectivity and application to diffusion MRI data in 22q11DS.

10/2009–05/2015 **Franco-German Dual-Master in Electrical Engineering and Information Technology**, *Karlsruhe Institute of Technology (KIT) and Grenoble Institute of Technology, School of Engineering in Physics, Applied Physics, Electronics and Materials Science (Grenoble INP - Phelma)*, Germany and France.

02/2013–05/2015 Master studies at KIT, GPA: 1.2 (~3.9 American GPA)

09/2011–01/2013 Engineering studies at Grenoble INP - Phelma, GPA: 15.4/20 (~4.0 American GPA)

10/2009–10/2011 Bachelor studies at KIT, GPA: 2.2 (~3.2 American GPA)

05/2015 **Master of Science (KIT) and Diplôme d'ingénieur (Grenoble INP).**

11/2012 **Bachelor's degree (Grenoble INP).**

Specializations: Control Systems (KIT) and Signal and Image Processing, Communication Systems, Multimedia (Grenoble INP - Phelma)

Master thesis: "Statistical Analysis of Propagation Patterns in Intracardiac Panoramic Mapping Data", Institute of Biomedical Engineering (IBT), KIT

Achievements

01/2019 **Best Publication Award in Human and Clinical Neuroscience by the Swiss Society for Neuroscience (SSN).**

Awarded to "Robust Recovery of Temporal Overlap Between Network Activity Using Transient-Informed Spatio-Temporal Regression", published in IEEE Transactions on Medical Imaging, CHF 1'500.

10/2018 **Selected finalist at the EPFL Engineering PhD Summit on "Data-Driven Engineering in the Life Sciences".**

Selected as one of 13 exceptional graduating PhD students from institutions worldwide to participate in a two-day workshop at the EPFL. Oral presentation on "Dynamic features of multimodal MRI data reveal functional signatures of psychosis in 22q11.2 deletion syndrome"

03/2018 **Best Poster Award in Clinical Neuroscience at the NCCR Synapsy Annual Meeting 2018.**

Poster title: "Dynamics of large-scale functional brain networks in 22q11.2 deletion syndrome", CHF 100

Oral Contributions to Conferences

- 03/2019 **Annual Meeting of NCCR Synapsy – The Synaptic Bases of Mental Diseases.**
Research Highlight Talk: "Brain network dynamics provide functional signatures of anxiety in 22q11.2 deletion syndrome"
- 01/2019 **Swiss Society for Neuroscience Early-Career Researchers Symposium.**
"Brain network dynamics provide functional signatures of anxiety in 22q11.2 deletion syndrome"
- 07/2017 **17th International Congress of ESCAP (European Society of Children and Adolescents Psychiatry).**
"Psychotic symptoms influence the development of anterior cingulate brain variability in 22q11DS"
- 02/2017 **11th Winter Conference of ESMI (European Society for Molecular Imaging): Neuroimaging – from Molecules to Networks.**
"Predicting psychotic symptoms in 22q11.2 deletion syndrome based on resting-state BOLD variability"

Teaching Experience

Training of Junior Researchers

- 09/2017–02/2019 **Training and Supervision of Laura Juan Galmès, Master Student in Neuroscience at the University of Geneva.**
◦ Project on the prediction of psychosis in 22q11DS using multimodal MRI data fusion.
- 06/2016–01/2017 **Training and Supervision of Ilia Grigoriev, Master Student in Computer Science at KIT.**
◦ Pilot project on application of innovation-driven coactivation patterns (iCAPs) in patients with 22q11DS.
◦ Evaluation of self-organizing maps for clustering in the iCAPs pipeline.

Teaching Assistance at EPFL

- Fall 2015–present **Image Processing I & Image Processing II, D. Van De Ville and M. Unser.**
Supervising and correcting student laboratory sessions.
- Spring 2016 **Signal Processing for functional Brain Imaging, D. Van De Ville.**
Organizing and teaching of exercises and laboratories accompanying the course.

Miscellaneous

Organization of Workshops

- 07/2019 **EPFL Engineering Workshop on Advances in Network Science.**
Organizing a one-day workshop to be held at EPFL in June 2019.

Knowledge Transfer

- 01/2019 **Article for Gazette of the "Office Médico-Pédagogique de Genève".**
Presenting the topic of my thesis to a general public of clinicians and administrative staff of the service.

Peer Review of Manuscripts (<https://publons.com/a/1405666>)

- 08/2018 Network Neuroscience
04/2018 Neurolmage
12/2017 Behavioral and Brain Function
11/2017 Molecular Psychiatry

Professional Experience

- 05/2014–10/2014 **Cegelec Space, Kourou, French Guiana.**
Internship in planning and project management of ground installations at the Guyana Space Center (CSG)
◦ Engineer in the Information and Communication Technologies Group.
◦ Supervising the realization of projects by subcontractors.
- 06/2012–07/2012 **Heco GmbH, Remchingen, Germany.**
Six week internship as warehouseman to get to know a working environment.

Languages

German	native
English	fluent (TOEFL iBT, 116/120)
French	fluent
Portuguese	basic
Italian	basic

Interests

Sports	Climbing, Swimming, Hiking, Snowboarding, Surfing
Art	Freelance activity as museum guide at ZKM Center for Art and Media, Karlsruhe, Germany (08/2013–09/2015)

List of Publications

2019

Zöller, D., Sandini, C., Karahanoglu, F.I., Padula, M. C., Schaer, M., Eliez, S., Van De Ville, D. (2019) *Large-scale brain network dynamics provide a measure of psychosis and anxiety in 22q11.2 deletion syndrome*. Biological Psychiatry: Cognitive Neuroscience and Neuroimaging

2018

Zöller, D., Bolton, T. A. W., Karahanoglu, F.I., Eliez, S., Schaer, M., Van De Ville, D. (2018) *Robust recovery of temporal overlap between network activity using transient-informed spatio-temporal regression*. IEEE Transactions on Medical Imaging

2018

Sandini, C., **Zöller, D.**, Scariati, E., Padula, M.C., Schneider, M., Schaer, M., Van De Ville, D., Eliez, S. (2018) *Development of Structural Covariance From Childhood to Adolescence : A Longitudinal Study*. Frontiers in Neuroscience.

2018

Franchini, M., **Zöller, D.**, Gentaz, E., Glaser, B., De Wilde, H.W., Kojovic, N., Eliez, S., Schaer, M. (2018) *Early Adaptive Functioning Trajectories in Preschoolers With Autism Spectrum Disorders*. Journal of Pediatric Psychology.

2018

Padula, M.C., Schaer, M., Armando, M., Sandini, C., **Zöller, D.**, Scariati, E., Schneider, M., Eliez, S. (2018) *Cortical morphology development in patients with 22q11.2 deletion syndrome at ultra-high risk of psychosis*. Psychological Medicine.

2017

Zöller, D., Padula, M.C., Sandini, C., Schneider, M., Scariati, E., Van De Ville, D., Schaer, M., Eliez, S. (2017) *Psychotic symptoms influence the development of anterior cingulate BOLD variability in 22q11.2 deletion syndrome*. Schizophrenia Research.

2017

Zöller, D., Schaer, M., Scariati, E., Padula, M.C., Eliez, S., Van De Ville, D. (2017) *Disentangling resting-state BOLD variability and PCC functional connectivity in 22q11.2 deletion syndrome*. Neuroimage.

2017

Padula, M.C., Schaer, M., Scariati, E., Mutlu, A.K., **Zöller, D.**, Schneider, M., Eliez, S. (2017) *Quantifying indices of short- and long-range white matter connectivity at each cortical vertex*. PLoS One 12.

2016

Emmert, K., **Zöller, D.**, Preti, M.G., Van De Ville, D., Giannakopoulos, P., Haller, S. (2016) *Influence of Vascular Variant of the Posterior Cerebral Artery (PCA) on Cerebral Blood Flow, Vascular Response to CO₂ and Static Functional Connectivity*. PLoS One 11.

